Development of fast and flow-compatible NMR diffusion methods for online reaction monitoring

Achille Marchand

DOCTORAT MATIERE BRETAGNE MOLECULES LOIRE ET MATERIAUX

Nantes Université

THESE DE DOCTORAT DE

NANTES UNIVERSITE

ECOLE DOCTORALE N° 596
Matière, Molécules, Matériaux
Spécialité : *Chimie analytique et radiochimie*

Par
Achille MARCHAND

Development of fast and flow-compatible NMR diffusion methods for online reaction monitoring.

Thèse présentée et soutenue à Nantes, le 14 décembre 2022
Unité de recherche : : Laboratoire CEISAM (UMR 6230)

Rapporteurs avant soutenance :

Ulrich HINTERMAIR Associate professor at University of Bath (UK)
Patrick BERTHAULT Directeur de recherche au CEA Paris-Saclay Gif-sur-Yvette

Composition du Jury :

Président :	Fabien FERRAGE	Directeur de recherche à L'ENS Paris
Examinateurs :	Véronique GILARD	Professeur des universités à l'Université Paul Sabatier Toulouse
Dir. de thèse :	Jean-Nicolas DUMEZ	Directeur de recherche à l'Université de Nantes

Remerciement / Acknowledgments

This work was done on the laboratory CEISAM using the NMR instrument of the CEISAM's platform. I want to thanks J.-M. Bouler director of the CEISAM, as well as P. Giraudeau director of the MIMM team.

I also want to acknowledge the member of my jury especially the rapporteurs P. Berthault and U. Hintermair as well as V. Gilard and F. Ferrage.

I cannot give enough thanks to Mr J.-N. Dumez for being my supervisor for his legendary patience and the sum of what I have learn at this contact. I will try my best to carry this to my future professional life. Now that the thesis writing is finished I admit we did not have the time for a historical part.

I want to thanks my colleague Rituraj Mishra that helped me so much understanding the math and NMR theory. His kindness and pedagogy were highly valued, I keep with me a better lifestyle with less meat-eating and I hope that a portion of his great organization skills have diffused to my nearby desk.

Warmest thanks to Arnab Dei for all the interesting discussion and NMR related meme. He managed to convince me to do some sport which is no easy task. Thanks for all the invitation, all the food shared etc.

a general thanks to all my Indian colleague at the CEISAM Assad, Shrikant, Aravind for being supportive helping me improve my English and all the laughs and tea time together. I would have never seen Mt St Michel without them. Somehow, I'm now better at filling tax.

Je voudrais remercier l'ensemble de la plateforme RMN du CEISAM, en particulier : Virginie Silvestre pour toutes les discussions passionnantes autour de l'analyse structurale et du traitement de spectre. Merci pour le soutien.

Merci à Aurélie B. pour l'aide avec les gradients la DOSY et la bonne humeur, dans les bons et moins bons moments.

Merci à Mathilde Grand sans laquelle je n'aurais pas trouvé le moindre produit chimique dans le laboratoire, ni réussi la moindre commande correctement.

Merci à Benoît Charrier, son expérience et ses conseils, sa bonne humeur ; son expertise sur les pompes et les solutions pratiques est inégalable.

Merci à mes collègues francophones :

Margherita pour toute l'aide et les bons conseils, merci d'avoir répondu à tant de questions.

Merci à Marine pour le soutien et pour avoir écouté certaines de mes angoisses. Bon courage avec le petit.

Merci à Corentin J. qui m'a quasiment appris la RMN pratique, sa pédagogie a fait de moi un meilleur scientifique, et on partait de loin.

Merci à Jonathan Farjon pour le soutien moral, les blagues et les discussions, l'aide pour trouver un post-doc. Merci pour toutes les discussions scientifiques, du premier au dernier jour de la thèse.
Merci à Clément pour son calme, mais aussi pour les discussions jeux vidéo et pop culture.
Merci à Celia d'avoir toujours gardé son calme, même lorsque je posais pour la nième fois la même question sur l'organisation d'un événement d'équipe ou l'administration.
Merci à Sophie, si elle n'avait pas passé du temps à me réexpliquer inlassablement les consignes de la soutenance, je n'aurais même pas pu soumettre un brouillon de manuscrit.
Merci à Maelys d'avoir gardé un bon sens de l'humour, et ce malgré l'utilisation d'HPLC et de mass spectrométrie (*vade retro*)
Merci à Thomas, entre autres, de ne pas m'avoir tenu rigueur pour une tentative d'assassinat peu délicate.
Merci à Benjamin pour les discussions pop culture, sur le streaming et d'autres, sur la science et les gradients à l'occasion.
La liste étant déjà si longue, désolé a ceux que j'oublie, merci à Aurore, Ilya, Estelle, Nour, Joris, Tania…
Merci à mes amis, à ma famille qui m'ont soutenu durant cette thèse, sans eux je ne serais rien, déjà qu'avec eux on ne va pas bien loin.
Pour citer le poète « je me sens si fort quand y'a ces gens qui m'portent »
Merci Kevin Vongprachahn pour la relecture du français et les discussions scientifiques, sans lui cette thèse ne serait pas ce qu'elle est. Courage pour les études, force à toi ; MAIS la chimie c'est mieux que la physique, je mourrai sur cette colline qui n'a pas de sens.
Merci à Guilhem Besson, pour être un exemple de rigueur et de travail. Tu nous as toujours soutenu, courage au meilleur sondier ici-bas. Les meilleures discussions sur la musique, demain mon prof de solfège (non). Pas merci pour m'avoir montré Elder Ring et ainsi menacé mon projet de thèse.
Merci à David pour tous les échanges depuis Lyon, les discussions électroniques et sur le taff… Un soutien de qualité. Bientôt un projet commun (c'est faux).
Merci à Alisson pour son enthousiasme continu et immarcescible, même lorsque ta maison brûle tu es moins stressée que lorsque je dois envoyer ma thèse.
Merci à Chloé, Reine de l'Albion endormi, Reine par la volonté de Titania, gouvernante d'Alfeim, etc.
Merci à Raphaël, courage pour les Beaux-Arts, les séances de Magic me manquent. J'espère que vous allez bien à Tours.
Merci à Sacha le grand thaumaturgiste, te parler me donne toujours plus de forces ; les 90-1 en versus fighting me manquent.
Merci à Richard qui m'a soutenu depuis mon stage de M2, force a lui, le vagabondage c'est dur mais les histoires qui en résultent ont un parfum de paradis.

Merci à Théo, le meilleur illustrateur pour le meilleur fond d'écran du monde, des fois je le regarde et je rêve. Merci pour Magic, sans toi à Nantes ça n'aurait pas été pareil je t'en dois une.
Merci à Thomas alias Blaise et à l'ARD, j'ai beaucoup trop ri et mon avocat me conseille de me dissocier de vos propos. Dédicace au doomer.
Merci à Charline pour les discussions scientifiques (de sociologie…) et la mauvaise humeur qui fait plaisir. Les partie d'Endless Space c'était incroyable et très cool.
Merci à Aradana, ta gentillesse et ta persévérance m'impressionnent toujours autant, merci d'être là depuis si longtemps.
Pour Heng désolé de ne pas avoir été là lorsqu'il aurait fallu, j'espère que tu as trouvé ce que tu cherchais par-delà le rêve.
Merci à Dylan du Master de Paris Descartes, ça me fait plaisir que l'on garde le contact, force à toi. Pour moi la chimie organique c'est beau quand je ne la manipule pas.
Merci à tous les autres, mais j'ai promis de pas faire plus de deux pages : Zoé, Jude, Yagaré, Maxime, Armelle, Antoine, Nas, Sarrasin, Killroy…
Merci à ma famille
Ma sœur Zoé
Mon frère joseph
Mon père et ma mère François et Carole
Romain, Marion, Hélène, Yvette, Annie, Jean…
Ça n'a pas toujours été facile mais je crois qu'on reste plus forts que ça. Merci à eux de me supporter depuis le plus longtemps, je ne sais pas comment ils font…
Un dernier merci à tous ces gens qui m'ont laissé une chance en dépit du bon sens.
Jean-Nicolas Dumez de m'avoir pris en thèse, je ne serai jamais assez reconnaissant.
Nicolas Giraud pour m'avoir pris en stage et m'avoir introduit à la RMN.
Guillaume Prestat et Mélanie Ethève-Quelquejeu pour m'avoir pris en Master après une année semi-blanche et un dossier plutôt mauvais, merci d'avoir cru en moi alors que moi-même je n'étais pas si optimiste.
L'équipe pédagogique de chimie du CNAM de paris notamment Marc Port et Zacharias Amara pour m'avoir aidé a trouvé un Master et me remettre sur les rails de la science.
Je pourrais continuer plus loin mais voici déjà des remerciements bien longs.

Résumé en français

La spectroscopie RMN est une technique d'analyse particulièrement utilisée dans le domaine de la chimie. Elle est couramment utilisée pour la caractérisation de molécules organiques pour différentes raisons. Parmi les plus importantes figurent notamment l'innocuité de cette technique d'analyse, mais encore sa grande capacité à résoudre les énigmes structurelles et à donner des spectres riches en informations sur la structure des molécules étudiées. Notons enfin que les noyaux sensibles à la RMN, et en particulier le proton, sont extrêmement courant. Compte tenu de ces faits, cet outil se révèle utile pour le suivi de réactions chimiques.

En l'occurrence pour ce dernier usage, la RMN a aussi ces limites. En effet, l'utilisation du contenant habituel de la RMN, un tube fin de 5 mm de diamètre généralement, ainsi que l'inaccessibilité du milieu réactionnel une fois dans le spectromètre, constituent un exemple de ces limites. Une manière alternative de prélever le milieu réactionnel de façon avantageuse est le flux. De la même manière, les expériences analytiques les plus riches sont souvent plus longues, notamment en ce qui concerne la RMN 2D, ce qui peut être contraignant dans le cadre de l'analyse d'un milieu qui évolue et impose donc ses propres contraintes de temps.

Nous nous proposons de nous concentrer sur un type d'expérience RMN, appelée DOSY, et d'en faire un outil de suivi réactionnel. Cette expérience s'intéresse au phénomène de diffusion au sein d'un liquide, que nous pourrions résumer en un ensemble de mouvements subtils des molécules et particules qui le constituent. Nous ajoutons à cela la possibilité d'étudier le milieu en flux afin de travailler avec une méthode qui nous rapproche des conditions de paillasse.

Durant ce travail, nous avons étudié les moyens permettant d'arriver à faire de la DOSY en flux. Notre méthode, basée sur l'utilisation de plusieurs axes de gradient de champ magnétique, a été développée pour l'observation du mouvement subtil de la diffusion, le milieu étant lui-même entrepris du mouvement de flux, moins subtil. Nous verrons aussi comment nous avons accéléré les expériences DOSY à l'aide de champs magnétiques pulsés, utilisés à des fins de sélection de cohérence.

Bibliographie

Tout d'abord, nous nous proposons d'expliquer le nécessaire sur la diffusion en solution et de la définir. Il s'agit d'un mouvement aléatoire des particules constituantes d'un liquide résultant de leur mouvement brownien dû à leur agitation thermique. Dans ce contexte, ce que nous appellerions intuitivement « vitesse des particules », nous l'appelons « coefficient de diffusion », dont la valeur dépend de la taille des molécules analysées et de la température ambiante.

Afin d'expliquer notre choix, pas forcément évident, d'étudier la DOSY à des fins de suivi réactionnel, nous avons développé un premier chapitre sur les utilisations diverses de la DOSY dans la

littérature. Nous y détaillons tout d'abord les méthodes de RMN diffusionnelle que nous utilisons, notamment la méthode STE. Pour la décrire brièvement, l'utilisation de gradients de champ magnétique permet d'encoder la diffusion. Le gradient permet d'organiser les spins de l'échantillon en fonction de leur position dans l'espace, et cette organisation prend la forme d'une hélice qui devrait être refocalisée par le gradient final de décodage de la diffusion. Du fait de la diffusion durant le temps qui sépare ces deux gradients, un mouvement moléculaire va avoir lieu, déformant l'hélice et rendant incomplète sa refocalisation. La perte de signal liée à l'imparfaite refocalisation est comparée au modèle théorique de la diffusion décrit par l'équation de Stejskal-Tanner, dont l'adéquation permet de retrouver le coefficient de diffusion.

Nous nous proposons également un état de l'art par l'étude de plusieurs exemples. Nous ne nous concentrerons pas tant sur les méthodes d'acquisition de la diffusion, mais plutôt sur l'intérêt de l'information de diffusion. En effet, en fonction de la diffusion des molécules, il est possible de remonter à des informations de taille, de longueur de chaîne voire de masse moléculaire. D'autres informations, concernant notamment les interactions entre les molécules ou des molécules avec le solvant, peuvent également être récupérées. La taille de des molécules considérées est appelée plus rigoureusement dans notre cas le « rayon hydrodynamique ».

On trouvera également une utilisation, non pas basée sur l'intérêt du coefficient de diffusion en soi, mais davantage sur sa capacité à différencier des molécules dans un mélange. Permettant ainsi une séparation par la taille des molécules au sein du mélange. Cette séparation virtuelle au sein du spectre est à rapprocher des méthodes de séparation physique, souvent fondées sur la taille des objets à séparer. C'est cette dernière utilisation couplée aux autres qui nous motive le plus à étudier la DOSY, afin d'avoir des méthodes de caractérisation, mais aussi de séparation au sein d'un mélange complexe, ceci sans interférer avec ledit mélange.

Nous étudions également la littérature afin de motiver notre choix du suivi en flux, notamment dans une méthode dite en ligne (online) de suivis réactionnels. Pour ce faire, nous discutons d'exemples d'intérêt et des limitations de plusieurs méthodes répandues qui permettent l'échantillonnage du milieu réactionnel.

Enfin, dans le cadre du projet qui vise à une méthode de suivi en ligne de milieux réactionnels par RMN diffusionnelle, nous étudions les possibilités présentes dans la littérature autour de l'accélération et d'alternatives aux méthodes de type STE.

Évaluer et accélérer l'expérience RMN

Après cet état de l'art, nous nous intéressons au cœur de ce travail, à savoir la DOSY. Les méthodes DOSY, bien que très utilisées dans divers domaines, ne sont pas les plus standardisées dans le monde de la RMN. Nous présentons donc rapidement le graphe représentant la DOSY et ses particularités.

Nous nous intéressons plus particulièrement à l'intérêt en termes de séparation virtuelle qu'offre ce graphe.

En effet, le graphe DOSY donne une séparation par l'attribution à des pics de leurs coefficients de diffusion respectifs. Ceci permet de savoir quels pics appartiennent à quelles molécules au sein du mélange et communique de premières informations sur la taille relative des molécules dans le mélange. À cette fin, le graphe DOSY donne des points de corrélation à chaque pic choisi par l'utilisateur. En abscisses sont donnés les déplacements chimiques, l'unité classique de la RMN ; en ordonnées sont représentés les coefficients de diffusion. Ainsi, les pics appartenant à la même molécule sont alignés ensemble, ce qui nous permet de commencer à parler de séparation. La diffusion étant issue de rapports d'adéquation entre une équation modèle et le signal détecté, deux informations sont présentes au niveau du point de corrélation : la coordonnée qui donne le déplacement chimique et la diffusion, et la largeur verticale de la tâche qui en donne l'erreur d'adéquation, ou incertitude, entre le modèle et les points expérimentaux. Néanmoins, pour réellement parler de séparation, il y a la nécessité d'une concordance. Ainsi, les points d'une même molécule doivent être fins et alignés, donc être le plus précis possible, et avoir des coefficients de diffusion proches, si ce n'est identique.

Nous montrons un système fait pour l'occasion qui utilise l'écart-type entre les valeurs de diffusion de coefficient des pics d'une même molécule afin d'évaluer l'alignement, puis nous utilisons la moyenne quadratique des écarts-types liée à l'incertitude, ceci afin d'avoir une idée de la précision. Nous nous retrouvons avec un système de coordonnées bidimensionnel où les points les plus proches de l'origine témoignent d'une qualité de séparation, et il y a perte en qualité à mesure que l'on s'éloigne de l'origine.

Avec ce système, nous procédons au test de plusieurs méthodes d'accélération de la DOSY en utilisant des gradients afin d'avoir une sélection de cohérences alternatives. En effet, classiquement, la sélection de cohérence se fait par le cyclage de phase qui rallonge l'analyse en imposant un nombre minimum de scans. L'utilisation de gradients orthogonaux ou parallèles permettrait de réduire ce minimum et d'accélérer significativement l'expérience. Il s'avère que la méthode utilisant des gradients orthogonaux marche significativement mieux et a été adoptée comme méthode d'accélération.

RMN diffusionnelle en flux

Afin d'atteindre le suivi de réaction en ligne comme nous le souhaitons, nous devons être doté d'un appareil capable de fonctionner en flux. Nous avons choisi le package insightMR par Bruker, parfois appelé flowtube. Il est constitué en trois parties, d'abord, une partie régulation de température à l'aide d'une pompe, d'un liquide thermique et une enveloppe ne rentrant jamais en contact direct avec le

spectromètre et/ou le milieu étudié. Un liquide thermique et une enveloppe qui ne rentre jamais en contact direct avec le spectromètre et/ou le milieu étudié. Ensuite, nous avons la partie qui transporte le milieu. Comprenant un tube en verre, similaire à un tube classiquement utilisé en RMN, des capillaires prélevant la solution à analyser puis l'amènent dans ledit tube qui se remplit, et un autre capillaire renvoie le trop-plein dans la solution mère, créant ainsi une boucle continue sans perte. Enfin, nous avons la pompe servant à donner le flux et conditionnant sa vitesse : c'est un appareil clef qui peut être changé selon les besoins.

Nous avons utilisé deux pompes : la pompe par défaut recommandée par le constructeur du flowtube, ainsi qu'une pompe HPLC Azura à bi-piston. Cette dernière, bien que performante en théorie, n'a pas donné pleine satisfaction. En effet, il semble qu'elle n'est pas faite pour pomper des liquides complexes, amenant à de nombreux problèmes et blocages.

Nous avons également utilisé la pompe Vapourtec à mouvement péristaltique. Un mouvement de ce type est, semble-t-il, bien plus adapté pour pomper des liquides divers, pouvant même pomper des gaz ou des solides en cas de problème. L'utilisation de cette pompe a permis de rendre plus simple l'étude en flux, elle a ainsi été choisie pour devenir la nouvelle pompe par défaut.

Toujours dans le but de pouvoir suivre une réaction à l'aide de RMN diffusionelle en flux, et donc d'en chercher les méthodes en amont, nous avons trouvé qu'il existe un type de séquence DSTE faite pour « compenser les effets de vélocité constants ». Bien que conçue à l'origine pour compenser les effets de convection, autre mouvement lié à la différence de température, les caractéristiques et propriétés de cette séquence RMN semblent toutes indiquées pour compenser l'effet d'un flux laminaire.

Nous comparons ainsi l'effet du flux à plusieurs vitesses de 1 à 3 mL/min sur les DOSY de type DSTE et constatons une augmentation des coefficients de diffusion avec la vitesse du flux. Cette augmentation s'accompagne de problèmes tels que l'augmentation de l'incertitude (la largeur des taches), rendant les spectres finalement peu exploitables pour un quelconque usage. L'utilisation de la DSTE dans des conditions un peu particulières, où l'utilisation des gradients d'encodage de la diffusion ne se fait non pas parallèlement mais perpendiculairement à la direction du flux, donne des résultats significativement meilleurs. Nous arrivons finalement à une erreur maximum de ~4% entre la référence (hors flux) et l'expérience en flux, ce qui est correct. En particulier et surtout, ni la valeur du coefficient de diffusion, ni l'incertitude associée ne semblent être liées à la vitesse du flux.

Le suivi d'une réaction

Armés de ces outils que sont l'accélération de séquence, l'appareillage permettant le suivi en ligne, et des séquences de RMN diffusionnelle compatible avec le flux, nous décidons d'effectuer des essais. La réaction que nous étudions est la double imitation du p-phenylènediamine par l'acétaldéhyde dans

l'acétonitrile. Une réaction simple et bien connue, mais intéressante en cela que les produits sont structurellement proches et suffisamment fragiles pour ne pas permettre une isolation ou séparation par des moyens physiques.

Le suivi de la réaction dure environ 5h durant lesquelles nous pouvons faire une expérience par minute, ce qui garantit un nombre de points conséquent. Nous discutons des limites de cette méthode de suivi qui se manifestent notamment autour de l'impossibilité d'utiliser le « lock », un système permettant de corriger de nombreuses perturbations grâce au deutérium habituellement présent dans les échantillons RMN. Du fait de son coût et de l'augmentation de volume, il n'est pas souhaitable d'utiliser des solvants deutérés. La perte ou dégradation de l'homogénéité du champ, le décalage des spectres lié à un changement de température ainsi que la dérive du champ magnétique de l'aimant sont les problèmes les plus importants que nous avons rencontré. Malgré ces préoccupations, ceux-ci restent mineurs et n'empêchent pas de mener à bien l'expérience.

Le suivi à proprement parler montre de bons résultats, notamment en ce qui concerne la stabilité dans le temps des coefficients de diffusion, qui ne semblent pas ou peu impactés par l'effet du flux. Relevons également l'effet du changement de concentration, compensé par une méthode appelée « permutation aléatoire de gradient » (p-DOSY). L'une des difficultés est la sensibilité : nous estimons qu'un minimum de ~200 en signal sur bruit est nécessaire afin que la diffusion puisse être estimée correctement. Enfin, la DOSY permet de récupérer l'information de concentration relative similairement à des méthodes classiques de RMN 1D, ce qui est appréciable.

Conclusion résumée

Pour résumer, nous avons essayé d'expliquer les fondations de la RMN diffusionelle ou DOSY, de montrer son intérêt dans le suivi réactionnel en ligne, notamment grâce à ses capacités de séparation virtuelle. Nous avons montré comment évaluer la DOSY selon ces critères, et essayé d'accélérer celle-ci par des méthodes faisant usage des gradients orthogonaux à l'encodage de la diffusion. Finalement, nous avons développé une approche permettant de compenser l'effet du flux, en combinant l'utilisation d'une séquence DSTE avec l'encodage de la diffusion selon un axe orthogonal au flux. Avec ceci, nous avons pu suivre une réaction en ligne de manière satisfaisante.

Nous espérons qu'arrivera un jour où notre méthode permettra d'aller plus loin dans le suivi de réaction et qu'elle sera accessible à des chimistes de tous bords, en dehors des spécialistes de la RMN. Nous pensons que cela constituerait un outil intéressant et efficace. Pour cette raison, nous travaillons sur de nouvelles améliorations telles que l'utilisation d'analyses multivariées qui rendent l'analyse spectrale plus simple.

Table of content

Notation et abbreviation

1D: one dimension

2D: two dimensions

NMR: nuclear magnetic resonance

DOSY: diffusion ordered spectroscopy

MRI: magnetic resonance imagery/imaging

RF: radiofrequency

STE: stimulated echoes

DSTE: double stimulated echoes

LED: longitudinal eddy current delay

SEC: size exclusion chromatography

D: Diffusion coefficient

DFT: density functional theory

DNA: deoxyribonucleic acid

PFG: pulsed field gradient

PTFE: polytetrafluoroethylene

PEEK: polyether ether ketone

CTP: coherence transfer pathway

BW: band width

DECRA: Direct Exponential Curve Resolution Algorithm

EPSI: Echo-Planar Spectrocopic Imaging

FID: free induction decay

FOV: Field Of View

FT: Fourier Transformation

SW: Spectral Width

UF: UltraFast

SPEN: SPatially ENcoded

SCORE: Speedy Component Resolution.

NUS: non uniform sampling

p-DOSY: permutated DOSY

TMS: tetramethylsillane

Introduction

Nuclear magnetic resonance spectroscopy is a powerful analytical tool with a large range of applications. For high-resolution solution-state NMR of small molecules, these notably include the analysis of organic compounds, especially their structures, the study of molecular interactions, and the analysis of mixtures, which will be the focus of the present work.

While there are many methods to study mixtures of chemicals, few have the non-disruptive nature of NMR. It is often a requirement to first separate the components of a mixture and analyse them afterwards. There are some cases, however, when this is not possible or would have an unwanted impact. One of those cases is the monitoring of chemical reactions. Chemical reactions are mixtures for which the components interact and cannot by definition be physically separated without impairing their properties. Many pieces of information are of interest for reacting mixtures: what is the outcome of the reaction? How is this outcome reached? Can it be controlled? Real-time reaction monitoring is a powerful approach to help answering these questions, and NMR spectroscopy has many advantages for that.

Diffusion NMR makes it possible to achieve virtual separation of components in a mixture, through the measurements of translational diffusion coefficients for a mixture's components. Diffusion is the subtle random motion of particles or molecules within a sample, that results from Brownian motion. Since translational diffusion depends on the size and shape of the diffusing object, if all the analytes have sufficiently distinct sizes and/or shapes then diffusion NMR can be used to separate their 1D NMR spectra. Diffusion NMR is also referred to as diffusion-ordered spectroscopy (DOSY), which originally described a specific data representation. Diffusion NMR is very useful for mixture analysis in general, and for reaction monitoring in particular.

Real-time reaction monitoring by NMR is most often achieved using a classical 5 mm tube, which is rather different form a typical flask in organic chemical synthesis. Notably, sample stirring is absent from the NMR tube, the sample volume is different, and so is the accessibility of the medium for, e.g., light irradiation or the progressive addition of a reactant. Those elements have pushed chemists towards new ways to monitor reactions. One such method is online monitoring by flow NMR, which consists of flowing the reacting medium from its typical flask toward the spectrometer and back. Flow NMR is being increasingly used for reaction monitoring. However, several key NMR methods are not directly applicable in continuous flow. In the case of diffusion NMR, it may appear as difficult to measure the subtle motion of diffusion, and use it for virtual separation, while the medium undergoes a not-so-subtle motion that is flow.

In this work, we have characterised the impact of sample flow on diffusion NMR experiments, and developed methods for accurate diffusion NMR in continuous flow. These rely on the use of a

diffusion encoding axis that is orthogonal to the main direction of the flow, and of a double stimulated echo pulse sequence. For reaction monitoring, the duration of NMR experiments is also a key consideration; fast experiments are useful to adapt to a large array of possible reactions. We have developed fast diffusion NMR methods that rely on gradient-based coherence pathway selection, and are also applicable in continuous flow. We have also assessed the resulting methodology with the monitoring of a model organic chemical reactions. In order to achieve these goals, we found it necessary to propose an approach for the quantitative comparison of diffusion NMR experiments. Overall, the resulting methodology should be useful for a broad range of reaction monitoring applications.

Part A bibliographic and theory work

1. Diffusion in NMR

1.1. Diffusion by NMR

1.1.1. What are diffusion, self-diffusion and restricted diffusion.

Diffusion is a physical phenomenon that can take several forms. It is important to give the definition we will be using throughout this whole document. In this work we will consider translational diffusion, and use the term "diffusion" to refer to self-diffusion, which is different from mutual diffusion. We will focus on this motion within liquids.

Diffusion is a passive motion of the molecules, and is the result of Brownian motion, the random motion of particle in a fluid. This random motion was a major discovery back in 1827 when it was first described by the botanist Robert Brown.[1,2] It was the topic of one of the first theoretical work of Albert Einstein[3] in 1905 and it was demonstrated experimentally in 1908 by Jean Perrin (Nobel prize 1926). Diffusion is quantified through the diffusion coefficient. Consider particles that diffuse during a time Δ, the diffusion length (D_l) of the particles in n dimensions, measured as their mean square displacement will be:

$$D_l = \sqrt{2nD\Delta} \qquad 1\text{-}1$$

Where D is the diffusion coefficient.

Just like Brownian motion, the diffusion coefficient is a function of temperature. It is an intrinsic property of a solute in a given solvent at a given temperature and this will be the main reason why we want to discuss and study diffusion.

The principles of diffusion were first described for microscopic particles, i.e., particles that were visible under the microscope but several order of magnitudes larger than molecules. It was shown that the diffusion coefficient in this case is described by the Stokes-Einstein equation:

$$D = \frac{k_b T}{6\pi\eta r} \qquad 1\text{-}2$$

where k_b is the Boltzmann constant, linked to Brownian motion. T is the temperature, η is dynamic viscosity, r is the radius of the molecule. The Stokes-Einstein equation is in principles only valid for hard and perfect-bead shaped particles that are far from each other (no mutual collision) and much larger than the solvent molecules. It can therefore only be applied in sufficient dilution condition to molecules with relatively simple interaction with the solvent. One can find it a bit surprising that we consider the size rather than the weight, not following classic inertial laws. Indeed Stokes, a major contributor in the field of fluid mechanic toward the end of the 19th century, has given his name to a law that allow to retrieve the drag force exerted on a sphere in a viscous fluid. This apply to individual

molecules which mass is negligible in regard of this drag. The dependence on the temperature captures the effect of thermal agitation, which can be seen as a random motion of molecules.

The Stokes-Einstein molecules is not generally valid in the situation encountered in typical diffusion NMR experiments, in which several of its assumptions are not verified. Still, it can provide a useful guide to analyse diffusion NMR data. The radius "r" will change depending on the kind of molecule/solute and its specific interaction with different solvent,[4,5] it is sometimes noted R_h for hydrodynamic radius.

While this work, and the majority of NMR-based studies of diffusion, focus on self-diffusion, it is interesting to consider its relation with mutual diffusion. Diffusion is also the process through which, in a closed space, through their random motion, molecules will homogenously fill the space given enough time. It was originally described by Fick.[6] Fick's second law describes the propagation of the solute within the solvent, in the presence of a concentration gradient:

$$\frac{\delta\phi(x,t)}{\delta t} = D\frac{\delta^2\phi(x,t)}{\delta x^2} \qquad 1\text{-}3$$

Where D is the diffusion coefficient, ϕ is concentration. This diffusion law governs local concentrations and describe how a solute spread into a solvent. It explains how a local increase of solute concentration lead, even if undisturbed to an homogenic concentration.

1.1.1.1. Mutual diffusion

Mutual diffusion, in contrast with self-diffusion, is not the motion of a particle seen as alone in a matrix-like inert solvent but rather the relative motion of solute and solvent particle.[7] The mutual and self-diffusion coefficient are only different in that the mutual diffusion take thermodynamic forces and solvent back flow into account, knowing that a corrected mutual diffusion coefficient $\widetilde{D}$ exist

$$\widetilde{D} \equiv D_m/[\left(\frac{M}{RT}\right)\left(\frac{\partial\Pi}{\partial c}\right)(1-\bar{\nu}c)] \qquad 1\text{-}4$$

Where M, c and $\bar{\nu}$ are respectively molecular mass, concentration, partial specific volume of the solute, R is the gas constant, T the absolute temperature, Π the osmotic pressure and D_m the mutual diffusion coefficient. The effects of the thermodynamic force and the solvent back flow are taken into account by the factors $\left(\frac{M}{RT}\right)\left(\frac{\partial\Pi}{\partial c}\right)$and $(1-\bar{\nu}c)$, respectively.[8]

The problem of equivalence between mutual ($\widetilde{D}$) and self-diffusion (D) coefficients is an important topic as mutual diffusion is measured by light scattering while self-diffusion is more often taken from NMR data. It seems that from the general stand, globular macromolecules and rigid polymer have a good equivalence between the two Ds but flexible or entangled polymer seems to behave otherwise.[8,9] As mutual diffusion is much more complex to study for small molecules and is not the outcome that NMR methods yield, we will mostly set it aside during this work. Nonetheless it is a

good reminder that concentration and diffusion are linked therefore we will consider that solutions we look at are always homogeneously concentrated and there is no gradient of concentration.

Diverting a bit from the subject we will briefly discus of a special case in diffusion studies, named restricted diffusion. The term is used when the duration needed by a diffusing molecule to travel the length of its enclosure is comparable to the diffusion time for its analysis. In this case it is possible to retrieve the size of the enclosure.[10] Restricted diffusion is a term mostly used in the MRI/NMR field, and refers to measurement method as well as the actual motion. One usually speaks about restricted diffusion in either droplets, pores or any other small enclosure.

Restricted diffusion was first characterised using NMR by Tanner and Stejskal[11] for colloid and size determination of droplets. It was then used in the field of geology for the determination of pores sizes in rocks.[12] This usage to determine porosity will be decisive as it is used for determination of cellular porosity[13] and generally to study water in confined biological environment.[14] In an important yet somewhat controversial paper for MRI[15] it is also used for diagnostic purposes. The attentive reader may have noticed that this part on restricted diffusion, mix diffusion focused study and relaxation focus studies. It is not uncommon in this field, as interaction with the enclosure's walls generates changes in relaxation that can help retrieve the relevant information. Indeed, nowadays porosity of the cells is a key point in diagnostic by MRI and rely mostly on relaxation far more than diffusion.

1.1.1.2. Flick law and chemical potential

So far, we have described diffusion as a phenomenon consequence of Brownian motion and thermal motion. Other ways to describe this phenomenon exist, in our case of reaction monitoring, the chemical potential aspect is interesting.

Chemical potential is Gibbs free energy at constant temperature and pressure when moles are considered to count particles. In a description that lies on chemical potential the drive for diffusion is not thermal motion but rather lowering G or chemical potential of the solution. In a solution at thermal equilibrium i.e. homogenous and non-reacting the Gibbs energy and chemical potential is a its minimum. Yet, diffusion still happen and diffusion rate can still be measured the difference is that they will not be defined as a flux but rather as a passive motion.

To use and describe diffusion with chemical potential one would use the diffusion flux defined in Fick laws. A flux that goes in the direction of the concentration gradient, from most concentrated to low concentrated area. This is illustrated by the Fick law of diffusion $J = -D\frac{dc(x)}{dx}$ with D the diffusion coefficient, J the diffusion flux, c the concentration and x the position.

The main interest for us, that work on homogenously concentrated solution, is about the change of Gibbs energy that could happen with the reactant/product. Let's describe a molecule that need energy E to move at a certain rate.

$$Rate \propto e^{-(E_c^0 - E_{1)}^0/RT} - e^{(E_c^0 - E_2^0)/RT} \quad 1\text{-}5$$

With E_c^0 is the 0 point of energy for the transition step, $E_1^0$for the initial step and E_2^0 for the final step. Rate is therefore a measure of the energy needed to start from a point E_1 and go to E_2 by passing in E_c. So, $G^a = E_c^0 - E_1^0$ with G^a the activation energy, and $\Delta G = E_2^0 - E_1^0$ with ΔG the change in internal energy. Henceforth we have

$$Rate \propto e^{-G^a/RT}\{1 - e^{\Delta G/RT}\} \quad 1\text{-}6$$

From this we can obtain the Arrhenius rate equation for kinetically controlled process. We can also extract 1-7 in the case of $|\Delta G| \ll RT$, which correspond to a thermo controlled process.

$$Rate \propto e^{-G^a/RT}\left|\frac{\Delta G}{RT}\right| \quad 1\text{-}7$$

We have now the tool to understand what link Flick's law to Gibbs energy and chemical potential. Let's imagine two compartment such as x the most concentrated one and x+a the less concentrated one. We are in a case such that the concentration is the driving force of the chemical potential μ and only μ contribute to ΔG. This will be the simplest case possible. In a reaction contribution to μ are mainly concentration and ΔG can be more complex. Yet for reaction to happen molecules need to encounter each other and so need to move, so the simplest step is a motion that decrease chemical potential, diffusion.

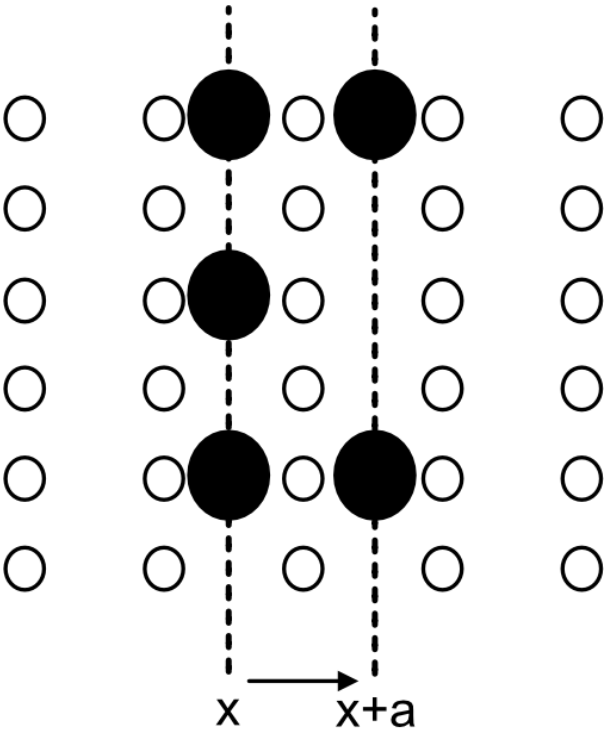

Figure 1.1 illustration of diffusion from a position x to x+a. Diffusion here is from the most concentrated to the low concentrated, henceforth go for the reduction of the chemical potential. This part and figure are strongly inspired from the lectures of Pr L. Zang of Utah university available online.

We can now define Γ the number of jumps like step a, with ν the vibrational frequency.

$$\Gamma = \nu \times e^{-\Delta G^a/RT} \quad 1\text{-}8$$

Therefore, in a 3-dimensional space with 6 equivalent direction (±x, ±y, ±z) we get

$$\Gamma = \frac{\nu}{6} \times e^{-\Delta G^a/RT} \quad \text{1-9}$$

Which lead to a rate of this form

$$rate = \frac{\nu}{6} \times e^{-\frac{\Delta G^a}{RT}}\left(-\frac{a}{RT} \times \frac{d\mu}{dx}\right) \quad \text{1-10}$$

Assuming $\frac{d\mu}{dx}$<0 which is the situation illustrated in figure 1.1. We can use this to define a flux J that will be depending on the concentration at x, $c(x)$ and the length of the displacement along x, named a.

$$J = rate \times \left(a \times c(x)\right) \quad \text{1-11}$$

$$J = -\frac{a^2\nu}{6} \times e^{-\frac{\Delta G^a}{RT}} \times \frac{c(x)}{RT} \times \frac{d\mu}{dx} \quad \text{1-11'}$$

By definition the chemical potential driven by concentration can be written as such

$$\mu(x) = \mu^0 + RTln\gamma c(x) \quad \text{1-12}$$

With γ the activity coefficient constant. We can deduct from 1-12

$$\frac{d\mu}{dx} = \frac{RT}{c(x)} \times \frac{dc}{dx} \quad \text{1-13}$$

Injecting 1-13 into 1-11' we get

$$J = -\frac{a^2\nu}{6} \times e^{-\frac{\Delta G^a}{RT}} \times \frac{dc(x)}{dx} \quad \text{1-14}$$

By having D the diffusion coefficient in the from

$$D = \frac{a^2\nu}{6} \times e^{-\frac{\Delta G^a}{RT}} \quad \text{1-15}$$

We can change 1-14 into

$$J = -D \times \frac{dc(x)}{dx} \quad \text{1-16}$$

1-16 is the Fick law of diffusion that link concentration/chemical potential to the diffusion. As we have seen it is best to describe two compartment that have different concentration, a case that we will not encounter in our studies. It is also useful as it uses notion of Gibbs energy that are key in reactivity. This links the motion of diffusion with the idea of diffusion as the motion necessary for the compound to encounter each other.

It happens that recently a controversy in the NMR diffusion community[16,17] centred about a possible acceleration of diffusion in reaction setting. The acceleration is theorized to be linked to chemical potential and chemical activity. They discuss the possible energy transfer from the reaction solvent molecule that would enhance molecular mobility.[16] Yet, the controversy in the NMR communities showed that the evidence for such boosted mobility is coming from artefact in measurement.[18] Therefore, it seems that there is no acceleration or change of speed coming from reaction. Thus, the two descriptions by either Einstein-Stokes that lie on the Brownian motion or the Fick's law and Gibbs function are seemingly equivalent. Reactions that have complex setting such as polymer's growth and increase medium viscosity, reduce molecular mobility. It could be relevant to use Fick's law and chemical potential related descriptions.

Note that very recently a new paper continued the controversy by defending boosted diffusion so the debate is still relevant.[19]

1.1.2. Measuring diffusion by NMR

1.1.2.1. Self-Diffusion and diffusion coefficient

In the previous section we have discussed about diffusion at large, here we propose to focus on how this phenomenon is analysed by NMR. We are going to focus on self-diffusion, and on the main ways we used diffusion NMR in this work. Diffusion analysis by NMR relies heavily on magnetic-field gradients and relatively simple pulse sequences. It often works by incrementing a gradient amplitude or a delay within the sequence. Unlike most 2D NMR experiment (COSY, HSQC, NOESY…), it does not rely on 2D FT and other so-called indirect dimension. It usually uses only one dimension of frequency (chemical shift or spectral dimension) and the second dimension will be the diffusion coefficient.

To understand what is happening we will describe the stimulated echo pulse sequence, shown in figure 1.1, which consists of 3 90° RF pulses and 2 gradients pulses. From there on, the word "gradient" will be used to refer to a magnetic-field gradient unless stated otherwise. Consider the equilibrium magnetization of an ensemble of uncoupled spins, which may be described by a vector aligned along the B_0 field direction. To simplify we will not consider the effects of precession, diffusion and relaxation.

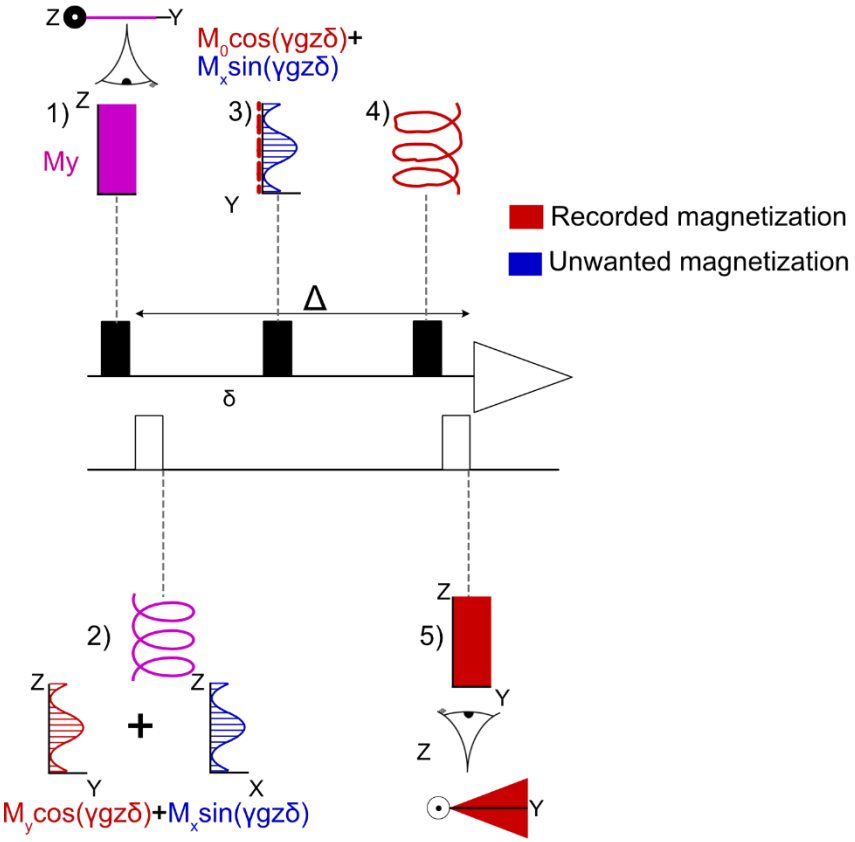

Figure 1.2: Stimulated echo (STE) sequence with monopolar gradient pulses. At each important step the magnetization is drawn. According to RGB additive colour model, red and blue make purple. Step 1) after the 90°_{x}pulse, the magnetization is along Y. Step 2) after the first gradient pulse, the magnetisation forms a helix. Step 3) The 2nd 90°_{x} pulse returns the Y component of the magnetization to the Z axis, while the X component stays and will be discarded by other means. Step 4) The 3rd 90°_{x} RF pulse rotates the Z magnetization back to the transverse plane. 5) The gradient refocuses a helix by unwrapping it. In the presence of diffusion, the resulting magnetization is imperfectly refocused due to the helix being disturbed. The spread of magnetization causes a loss of signal.

In the STE pulse sequence, a first 90° pulse is applied to rotate the magnetization to the transverse plane, orthogonal to the B_0 field (step 1 in figure 1.2). Then, a first gradient pulse is applied. When a gradient is applied, the sample is no longer in a spatially homogenous magnetic field. The magnetic field experienced by the sample is that of the main homogeneous field (B_0) and a small additional spatial variation coming from the gradient coil:

$$B_{tot} = B_0 + gz \qquad 1\text{-}17$$

Where z is the position and g is the gradient amplitude. As a result, the precession frequency of the magnetisation is no longer identical everywhere and it becomes

$$\omega(z) = -\gamma B_0 - \gamma gz \qquad 1\text{-}18$$

Where γ is the gyromagnetic ratio. If the gradient is applied during a time δ, the precession of the magnetisation will be of an angle of $\gamma gz\delta$, in the rotating frame, resulting in:

$$M_{\vec{y}} \xrightarrow{\gamma gz\delta} M_{\vec{y}} \cos(\gamma gz\delta) + M_{\vec{x}} \sin(\gamma gz\delta) \qquad 1\text{-}19$$

With such change of their phase depending on the position z, the magnetisation vectors form a helix,[20] as illustrated in step 2 of Figure 1.2. This helix pattern depends on the strength and duration of the

gradient which will modify its pitch $\Lambda = \frac{2\pi}{\gamma g \delta}$, the number of turns $NT = \frac{L}{\Lambda}$, L being the length of the sample.[5]

As soon as the gradient pulse allows the helix to complete enough turns the magnetization averages to zero over the length of the sample and there would be no detectable signal. As it is, it seems we have just described a way to kill the signal (which in itself can be useful), yet this helix-gradient concept is key in what will follow.

In the STE pulse sequence, once the first gradient pulse is applied, a second RF pulse is applied to return the magnetization along the longitudinal axis. This is important to avoid T_2 relaxation and J-modulation during the rather long diffusion delay. The RF pulse transforms the y-component of the magnetization into a z-component leaving only the x-component in the transverse plan, as see in step 3 figure 1.1. The remaining transverse magnetization (shown in blue in Figure 1.1) will be supressed, either using a gradient pulse that will make another helix that gives no signal, or using phase cycling. The magnetisation of the second RF pulse can then be written:

$$M_{\vec{y}} \cos(\gamma g z \delta) \xrightarrow{\pi/2} M_{\vec{z}} \cos(\gamma g z \delta) \qquad 1$$

The third RF pulse returns the magnetization to the transverse plan, giving:

$$M_{\vec{z}} \cos(\gamma g z \delta) \xrightarrow{\pi/2} M_{\vec{y}} \cos(\gamma g z \delta) \qquad 1\text{-}21$$

If we rewrite the above equation differently using Euler formula we have:

$$M_{\vec{z}} \cos(\gamma g z \delta) \xrightarrow{\frac{\pi}{2}} M_{\vec{y}} \frac{exp(i\gamma g z \delta) + exp(-i\gamma g z \delta)}{2} \qquad 1\text{-}22$$

Which can be seen as the sum of two helices of opposite signs.

The second gradient pulse is applied which refocuses the helix by cancelling out its now reversed phase,

$$M_{\vec{y}} \cos(\gamma g z \delta) \xrightarrow{\gamma g z \delta} [M_{\vec{y}} \cos(\gamma g z \delta) + M_{\vec{x}} \sin(\gamma g z \delta)] \cos(\gamma g z \delta) \qquad 1\text{-}23$$

Using Euler formula, we got :

$$[M_{\vec{y}} \frac{\exp(i\gamma g z \delta) + \exp(-i\gamma g z \delta)}{2} + M_{\vec{x}} \frac{\exp(i\gamma g z \delta) - \exp(-i\gamma g z \delta)}{2i}] \frac{\exp(i\gamma g z \delta) + \exp(-i\gamma g z \delta)}{2} \qquad 1\text{-}24$$

Which after some steps give

$$\frac{M_{\vec{y}}}{2} + M_{\vec{y}} \frac{\exp(2i\gamma g z \delta) + \exp(-2i\gamma g z \delta)}{4} + M_{\vec{x}} \frac{\exp(2i\gamma g z \delta) - \exp(-2i\gamma g z \delta)}{4i} \qquad 1\text{-}25$$

If we use Euler formula again in the other direction we have the blue part that is a double helix as such,

$$\frac{M_{\vec{y}} \cos(2i\gamma g z \delta)}{2} + \frac{M_{\vec{x}} \sin(2i\gamma g z \delta)}{2} \qquad 1\text{-}26$$

which signal is null while the recordable magnetisation in red have been divided by two.

In summary the first gradient pulse creates a spatial organization of the magnetisation, which forms a helix. After being stored as an amplitude modulation, this organization is refocused by using a second gradient pulse.

We have introduced a spatial dependency along z within the helix thus it is sensitive to motion along its main axe. The motion will come from diffusion that makes molecules (and their respective spin) move in a stochastic way. As we are interested in the z dependency the spin can be illustrated as moving from one slice to another. The result is that upon refocusing, there will be an additional loss as not all the spin will undergo the right refocusing because they are not in their initial slice. Without diffusion or motion the slice are expected to refocus and finish in the same state as they started, see step 1) figure 1.2. Instead, due to diffusion, some of the spins have changed slice, those will then be under a different gradient strength than they were initially encoded with. Instead of properly refocusing each slice will have a residual phase shift. The result is a phase spread of the magnetization. The consequence is the loss of signal. A random undirected motion such as diffusion induce a loss that is proportional to the level of organization. The tighter the helix, the more significant the loss. The original model of what was discussed here can be found in Ref.[21] together with an analytical description of the effect of diffusion using the Torrey-Bloch equation[22] a deeper and more mathematical definition of this can be found in ref.[21–25]

Solving the Torrey-Bloch equation for the STE pulses sequence gives a signal dependency in the form,

$$S = S_0 e^{-(Dg^2\gamma^2\delta^2\Delta')} \qquad 1\text{-}27$$

where δ is the time of the gradient pulse, g is the power of the gradient, Δ' is the main delay when diffusion happen, corrected to account for the finite width of the gradient pulses, S is the resulting signal, S_0 is the signal in the absence of diffusion, and D is the diffusion coefficient. Eq 1-27 is called the Stejskal-Tanner equation, and describes the attenuation of NMR signals under the effect of diffusion, for a pair of gradient pulses separated by a delay.

In practice, diffusion coefficients are measured by acquiring a series of 1D spectra for different degrees of diffusion attenuation. The data is then fitted with Eq 1-27, by non-linear least square optimization. Three parameters may in principle be varied to record experiments with different degree of diffusion attenuation, the power of the gradient, the pulse duration and the storage delay. In this whole work we mostly made the power vary as it is simpler on our hardware and has less consequence in the sequence.

1.1.2.2. Diffusion editing

The principle of diffusion NMR are also used for methods named diffusion-filtered NMR. Their purpose is not to retrieve information on diffusion coefficients but rather to have 1D spectra where small (fast diffusing) molecules are filtered out. This can also be used as a fast method to have a qualitative idea

on the size of molecules or on their binding abilities. This method uses the same kind of sequence and principle as regular diffusion-NMR but usually do not require increments, as no data fitting is performed. Diffusion weighting is also sometimes used to improve solvent suppression.[26] Solvent molecules being most of the time small and fast diffusing, the solvent signal can be strongly attenuated by using diffusion encoding gradients. It is mostly used in metabolomics and other fields that study biological fluids or extract.[27–31] Another use of this technic is for screening or rapid determination of binding interaction between a slow-diffusing molecule and a fast-diffusing one. It is used in the pharmaceutical field and in study of protein.[32–35]

Two examples of such uses from the literature are shown below. Figure 1.3a) and b) shows two spectra of 1 mg of strychnine in a mixture of d_6-DMSO and water. Here diffusion is used as a mean to supress the fast-moving molecules of solvent[29] and is an interesting alternative to solvent suppression. It can supress the solvent and the other small molecules present (here water) with it and do not require much knowledge on how to create special multi-signals RF pulses.

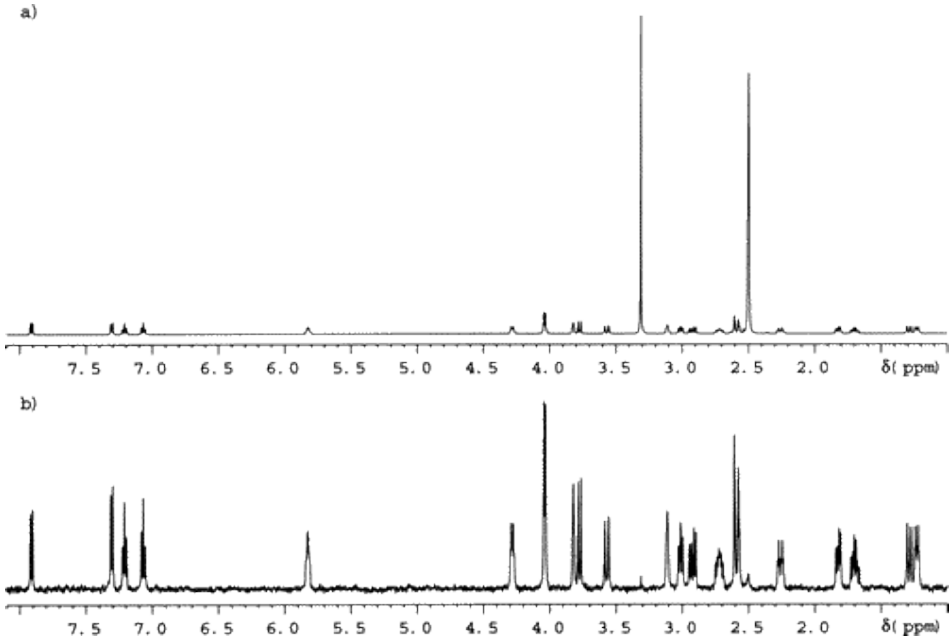

Figure 1.3. The 500-MHz ^{1}H spectra of 1 mg of **1** [strychnine] in DMSO-d_6. (a) Conventional spectrum acquired with 16 transients and (b) diffusion-filtered using the BPPLED sequence with a gradient length of 3.61 ms acquired with 512 transients. The signal-to-noise ratios are (a) 2183 and (b) 25. Reprinted with permission from Esturau et Espinosa[29] Copyright © 2006, American Chemical Society

In figure 1.4 the authors[32] are interested in a mixture of compounds and their potential interactions with hydroquinine 9-phenantryl ether. The mixture of 9 compounds including the hydroquinine is shown in figure 1.4a). Figure 1.4b) shows a diffusion edited spectrum in the absence of the hydroquinine there is no signal left and figure 1.4c) the same diffusion-edition conditions but with the hydroquinine. Results are quite striking and allows to quickly identify which compound has binding interactions with the hydroquinine and which has none. The reduction of mobility due to the

association is a rapid mean to show that there are interactions between the molecules and can be used to screen a whole mixture rather than testing each molecules two-by-two.

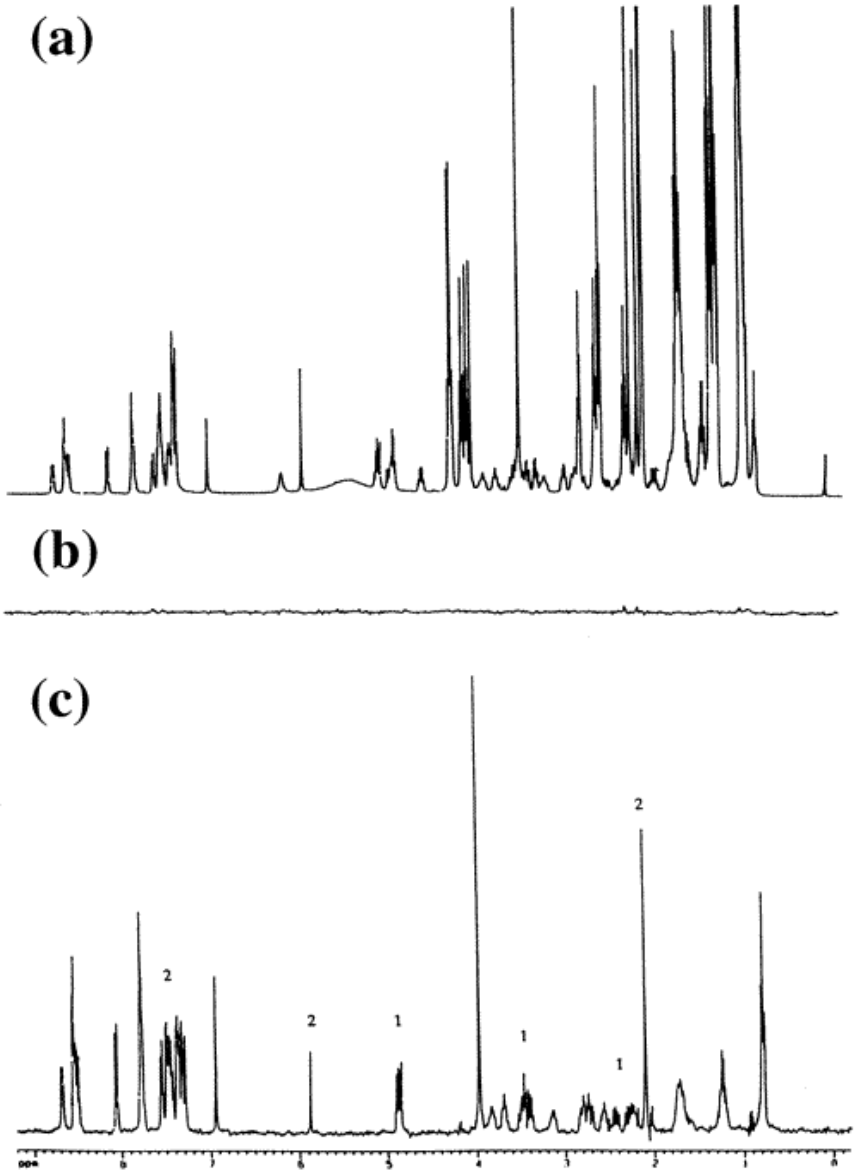

Figure 1.4 (a) 1D 400 MHz ^{1}H NMR spectrum of the nine-component mixture in $CDCl_3$. The concentration of each component is 10 mM. Components: (**1**) dl-isocitric lactone, (**2**) (*S*)-(+)-*O*-acetylmandelic acid, (**3**) dl-*N*-acetylhomocysteine thiolactone, (**4**) (±)-*sec*-butyl acetate, (**5**) propyl acetate, (**6**) isopropyl butyrate, (**7**) ethyl butyrylacetate, (**8**) butyl levulinate, (**9**) hydroquinine 9-phenanthryl ether. (b) 1D PFG ^{1}H NMR spectrum of the mixture without hydroquinine 9-phenanthryl ether using LED sequence. (c) 1D PFG ^{1}H NMR spectrum of the nine-component mixture. Chemical shifts arising from compounds **1** and **2** are labeled. All other shifts are from compound **9**. The PFG conditions were the same as in the middle spectrum. Reprinted with permission from Bleicher et al.[32] Copyright © 1998, American Chemical Society

1.1.2.3. SEC (Size Exclusion Chromatography) and DOSY for molecular size determination

The gold standard for measuring molecular size and weight in solution, especially for polymers, at this time is chromatography using SEC rather than NMR. It is especially powerful in analysing different polymers, because of its ability to determine weight distribution. Yet, it seems to be less repeatable for getting average or absolute mass determination. It also needs to be coupled with detection method

such as multi-angle laser light scattering to do so. The operative cost in terms of diversity of columns and solvent as well as pumps can also be summoned as a limitation but NMR also suffer akin cost and solvents limitations. At last, compatibility with certain kind of polymer can be limited[36] which is rarer for NMR and organic polymers. The SEC capability for mass determination is highly dependent on prior calibration, usually done with polystyrene polymers of know size and weight.

This dependence to polystyrene standards is problematic as accurate calibration with polystyrene is not so easy to get and small difference between experiments and results yield poor inter-lab repeatability. The work of P.-J. Voorter et al.[37] propose a method to make universal calibration corrected for the solvent viscosity using DOSY NMR methods for polymer weight determination.[37] Using the empirical Rouse–Zimmmodel model they can use Stoke-Einstein equation to link average molecular weight and hydrodynamic radii, $D = b'M^{-v}$. Where b' is an empirical factor and v an arbitrary shape parameter. Another way to write this equation is

$$\log(\mathrm{D})+\log(\eta)=\log(\mathrm{c})-\mathrm{v}\times\log(\mathrm{M}) \qquad \text{1-17}$$

With η the viscosity and c the new proportionality parameter. Knowing the viscosity of the various deuterated solvents and the factor v for polystyrene, they can make calibration curve using DOSY. Those curves are expected to give accurate result independent of the labs, apparatus and solvent viscosity. As shown in figure 1.5 once corrected for viscosity molecular weight are very close in all solvents even in those deemed “a bad solvent for polymer" such as acetone.[37] This can be used to create a double calibration system. The first SEC calibration done with polystyrene can be corrected to match the result of the DOSY (using same standard) thus limiting the actual problem of inter-lab lack of repeatability. They conclude that a few tests should be done in various lab to assess the claim of improving inter-lab repeatability but this is expected to work as NMR usually does not suffer from repeatability troubles.

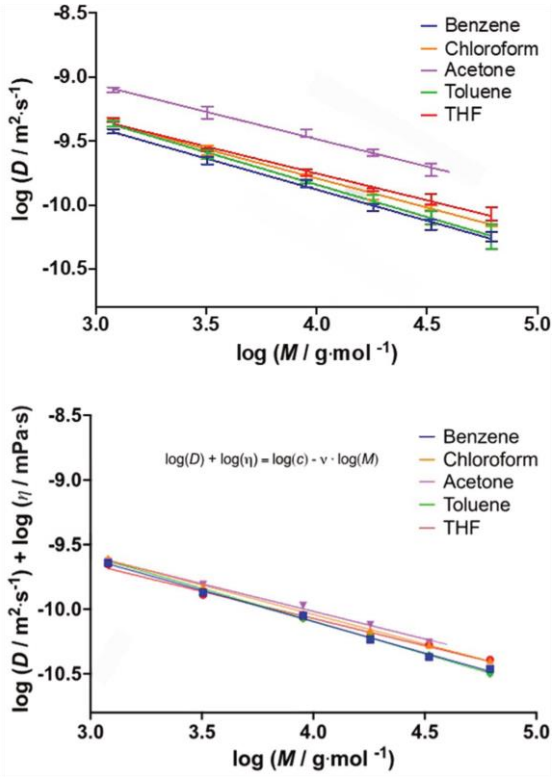

Figure 1.5 Diffusion coefficients determined via DOSY for polystyrene standards in a series of solvents (top) and viscosity-corrected data for the same measurements (bottom). Reprinted with permission from Voorter et al.[37] Copyright © 2021 Wiley-VCH GmbH

1.1.3. Review of relevant methods

In the previous section we have described the monopolar STE pulse sequence as it is the basis for most of the diffusion experiments in high-resolution NMR. Historically, the first method described for diffusion studies is the Hahn or spin echo. It consists of a 90° pulse followed by a 180° pulse, both RF pulses being followed by a gradient pulse. In this work we did not use spin-echo based pulse sequences. We will now review extensions of the monopolar STE pulse sequence that are important for diffusion NMR and especially to understand the work reported here.

1.1.3.1. Eddy/Foucault currents

Eddy currents (also called Foucault current) are electric currents created within electrical conductors by changes of an external magnetic field. Those electric currents in turn generate a magnetic field, that is usually opposite to that of the perturbation. In NMR spectroscopy such currents can happen in the probe when a gradient pulse is applied. Currents inside the coil are created and oppose the shutting down of the gradients. They can have different effects, overall negative, on the quality of the signal. The main effect is the apparition of a residual gradient field that will extend the duration and decrease the quality of the gradient pulse[38,39]. Those effect depend highly and the kind of hardware that is used.

Several methods have been described to counter the effect of eddy currents in diffusion NMR. The most used is called LED, for “longitudinal eddy current delay”. It consists of two 90° pulses with a

delay in between. The idea is to avoid that the residual gradient extends during the acquisition when it could be very harmful to the signal. The LED block stores the magnetization along the longitudinal axis during a time Te, during which the residual gradient dispels. Once this delay is over the second 90° pulse puts back the magnetization in the transverse plan where it can be recorded. A representation of LED block within a STE is shown in figure 1.6.

Putting the magnetization along the longitudinal axis is often a problem. If the longitudinal storing happens for too long *T*1 relaxation can happen thus reducing the signal strength. Small errors in calibration of the Rf pulse will also lead to artefact as all the magnetization may not be put on the longitudinal axis. Sometimes a gradient is put in-between the LED block to limit this. It remains a bit counter-intuitive to add more gradient to a sequence's part made to avoid unwanted gradients effects. Nowadays modern hardware is very well shielded and LED is less mandatory than it used to be.

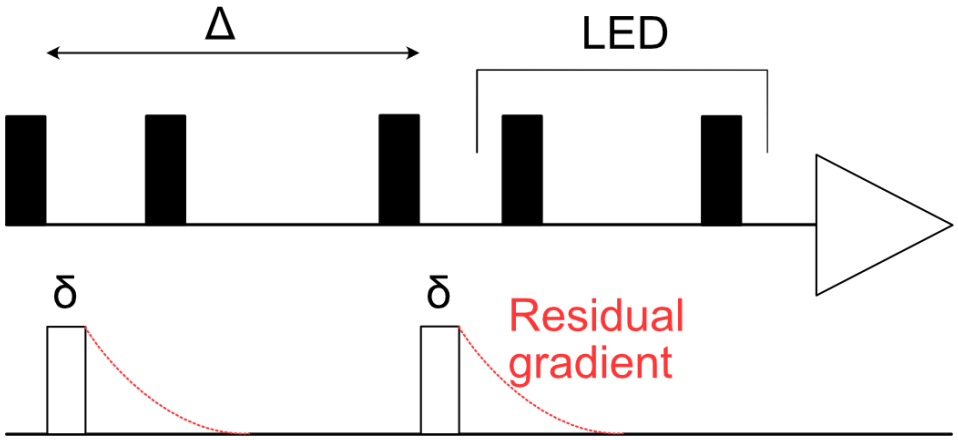

Figure 1.6 : the STE mono-pulse with the LED. The red curve after gradient pulses shows the possible eddy current induced gradient.

1.1.3.2. Bipolar gradient pulses

This method consists of using bipolar gradient pulses instead of monopolar ones. To do so and keep the same effect as with a monopolar gradient pulse, a 180° RF pulse is inserted between the two halves of the bipolar gradient pulse. In analogy with what is explained in 1.1.2.1, and as explained in Ref. [21]; the 180° pulse inverts the magnetisation helix, such that the second half of the gradient pulse, of opposite polarity, further tightens the helix. The total dephasing is equivalent to that obtained with two consecutive pulses of the same polarity. The sequence is illustrated in figure 1.7. There are several reasons to use bipolar gradient pulses.

A first reason is again eddy/Foucault currents. The effect of those residual currents will be reduced due to the opposite polarity of the bipolar gradient pulses, which compensate each other. A second reason is the stability of the lock signal. Most NMR systems use locking systems. It consists of a continuous-wave NMR system that focuses on the frequency of another nucleus than the one of interest, mostly ^{19}F or ^{2}H. The lock system makes it possible to monitor changes of the main magnetic

field and continuously compensate them. It includes the field value, its homogeneity, and outside interference (Rf signal and vibration). It is very important for spectrometer stability.

Locking is a key aspect of NMR spectroscopy, and is required to achieve good repeatability and for the automation of any experiments. The problem is that when gradients are used, unlike RF pulses, they are not selective of a nucleus. It happens that gradients will defocus the signal of any nuclei inside the sample including those that are used to lock the signal. Gradients pulses will disrupt the signal for the time of the experiment making the experiment more sensitive to outside nuisances.

Bipolar gradient pulses make it possible to avoid this problem. The 180° pulse does not affect the locked nuclei and in this case the two gradients effectively cancel out for the locked nuclei and not for the analysed one. It greatly helps to keep experiments running smoothly. Interestingly, in the standard sequence provided by the manufacturer on our system, the benefit of this effect is lost, because spoiler gradients are uncompensated.

The main drawback of using bipolar gradient pulses is that the additional RF pulses increase the complexity of the sequence. 180° pulses are more susceptible to mis-calibration and RF inhomogeneity issues, and the selection of the relevant coherence transfer pathway only has to be ensured.

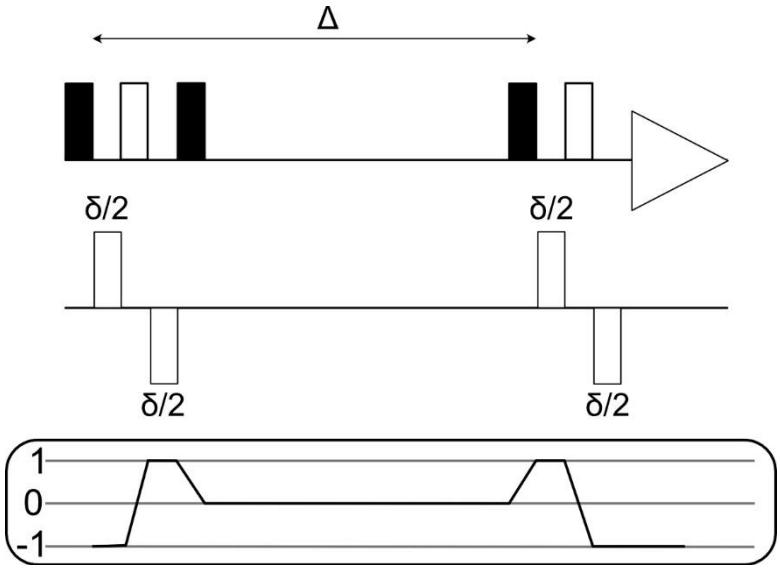

Figure 1.7 : the STE pulse sequence with the bipolar pulse strategy. Black rectangle in the upper axis are 90° RF pulse, white ones are 180°. The lower axis white pulse are gradients pulses.

1.1.3.3 Double Stimulated Echo (DSTE)

Diffusion results from molecular motion on a small scale, and its analysis by NMR lies on the fact that this motion disturbs the organization of the spin's magnetisation created by the magnetic-field gradient. For this to occur, the sample ideally needs to be steady. No unwanted motion should be present, no gradient of concentration nor inhomogeneity. One type of motion that is difficult to avoid in NMR experiments is convection.[40] It appears in any liquid when there is a gradient of temperature, which results in a convection cell. Convection cells are usually characterized by motion of cold denser fluid moving below a portion of warm lighter fluid. Convection is particularly a problem in low-viscosity

fluids like most organic solvents, and in the presence of a strong temperature gradients. Such temperature gradients are supposed to be avoided by the temperature regulation system of NMR probes, but in low viscosity solvent convection is nearly unavoidable.[41] Convection is very detrimental to the diffusion analysis as it will disrupt magnetisation helices, adding its effect to that of diffusion and leading to overestimated diffusion coefficient.

To remove this effect a sequence was proposed in 1997[42] and is still very much used nowadays. The double stimulated echo (DSTE) pulse sequence relies on the fact that the disruption by convection is not random like diffusion. Instead, it results in the coherent acquisition of a supplementary phase by the magnetisation. In the DSTE pulse sequence one performs two diffusion-encoding steps with opposite coherence pathways, so that the phase is added during the first part and subtracted during the second. This DSTE sequence is a useful method to have reliable results in solvents such as chloroform or acetonitrile (two very low viscosity solvent). The sequence is represented in figure 1.8.

One major drawback is that the storage along the longitudinal axis reduces the sensitivity by a factor 2 so doing it twice reduces sensitivity by a factor 4. This and the effect of gradient that already lessen the sensitivity make DSTE a sequence difficult to use for low concentration samples or if time constrain does not allow to accumulate enough scan/signal.

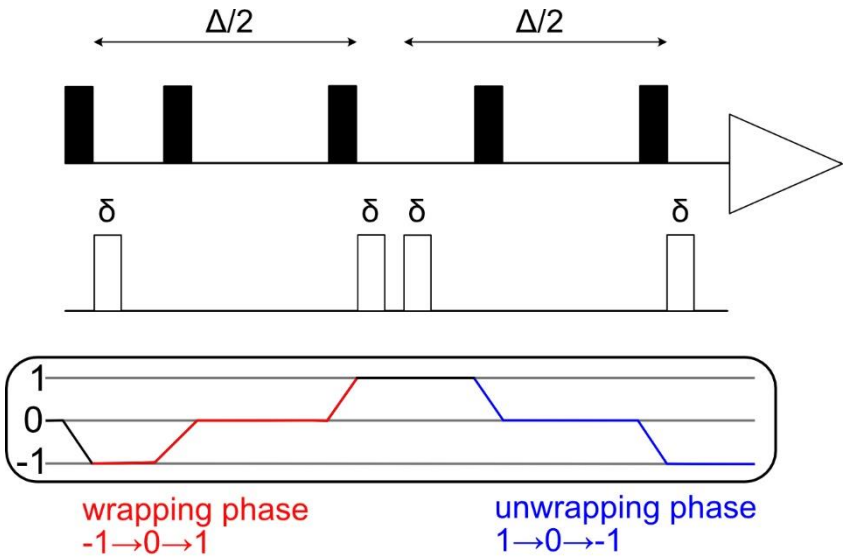

Figure 1.8 : DSTE sequence with coherence pathway.

1.2. Selected examples of application

Our work focuses on methods development. It aims to give tools and methods that may be applied to interesting topics/mixture/medium/sample. In this section we will show the diversity of research areas and uses for which diffusion NMR and DOSY are relevant.

1.2.1. Polymer

The polymer field is mostly interested in two pieces of information that DOSY experiments can provide, molecular weights and polydispersity. Let us consider first polydispersity. Until now we have focused on the classical diffusion model for NMR with monoexponential decay, yet it is not the only one. In case of polydispersity, a very common occurrence for polymers, this model fails to describe the data.[43] Multiexponential decay is far more difficult to characterize, and requires inverse Laplace transformation (ILP). Such transformations are not as straightforward as Fourier transform and require complex algorithms. To our knowledge the most commonly used algorithm in the context of diffusion NMR is CONTIN[44,45] (general purpose constrained regularization program for inverting noisy linear algebraic and integral equations). Other algorithms such as NLREG (nonlinear regularization) can be found.[46,47] The main problem is that the ILT is an ill-posed problem. Those ILT methods are often used in routine, yet they appear to be very sensitive to SNR as well as any other perturbations that could occurs.

Polydispersity is an important information, with the PolyDisperse Index (PDI) being an interesting data to obtain in a polymer sample. To get this information different models for multi-exponential decay can be used. The models used often derivate from either the log-normal models[48] used in size-exclusion chromatography (SEC) and NMR or the gamma distribution model.[49] Using those models gives gaussian distributions (or gaussian-like) results and from the shape and width of the gaussian one can extract the molecular weight distribution[50,51] and thus polydispersity. These methods have a large range of different applications that will depend on the different properties of the polymer.[43,52,53] It is to be noted that simpler analyses can sometimes be successfully used for polymer samples. For example, if the different parts of the chain (the core and the extremities) can be well resolved then comparing the spread and the coefficient diffusion of each part can allow to retrieve polydispersity.[54]

Diffusion NMR is not the reference method for size determination or polydispersity, it is rather SEC that predominates especially for commercially available polymers. For research purposes NMR and diffusion-NMR are rising due to their high reliability and reproducibility. It gives similar result as SEC[51] and timewise it is comparable if not faster. SEC needs to be coupled with a detector and like diffusion NMR, only gives information relating to hydrodynamic radius rather than mass. Polydispersity is not always easy to access and can ask for a great deal of various columns and mathematical models, for this reason diffusion NMR for polymer seems to be good alternative/complement despite its drawbacks.

Let us now consider what can be learnt on the molecular weight of polymers using diffusion NMR. Molecular weight for a polymer is directly linked to the number of monomers that are attached

together and is likely to be linked to the size of the polymer and thus to its hydrodynamic radius. As explained in section 1.1, the diffusion coefficient is linked to this radius. The determination of molecular weight from diffusion NMR data is then straightforward, using multiple monodisperse samples of known masses to make a calibration curve. This calibration curve then allows to place the diffusion coefficient of an unknown sample and access its molecular weight.[44,55]

For weight determination to work the polymer needs to verify a number of criteria. The form of the polymer in solution is important as the hydrodynamic radius is defined for mostly globular molecules (or bead shaped). Polymer being macromolecules different effects can intervene such as folding to minimize interaction with solvent or linearization to maximize it. Other phenomena such as aggregation, binding, reticulation can happen and make the model not so relevant. Thus, it is important to monitor the dilution condition[44] and sometimes it is necessary to have more complex models to describe the polymer. One relation often seen in diffusion NMR for polymer is $M \propto D^{-df}$ where df is the fractal dimension, a measure that help understand how the polymer extend in solution.[56]

Consider Ref.[44] as an example. The authors aim at using diffusion NMR and DOSY to determine the molecular weight of a special family of polymers called conjugated polymers. The team explains that such polymers are hard to characterize using SEC, the standard and most general method for polymer size characterization, hence the need for another way. They use multiple equations and different known models to describe such kind of polymer. We are not going into the detailed equation, briefly they use different information such as chain rigidity, persistence length and the chain shape. Those models are necessary to understand if the polymer fit the condition in which self-diffusion law apply (see part 1.1.1).

Using this they can have two numbers to describe the elongation per monomer. One depends on weight-average molecular weight (Mw in the text) a value suited for polydisperse sample. Another metric, absolute number-average molecular weight (Mn in the text) is suited for low-molecular weight polymers with no polydispersity. Those allow them to make the curve one can see in figure 1.7. The first row shows the Stejskal–Tanner plot obtained with different attenuation in different length of polymers. It shows the quality of the plot and the relation between number of monomer and size-related attenuation of the signal. The diffusion analysis is then shown with each diffusion coefficient and its spread, which is a function of polydispersity. Finally, the last row shows how using the diffusion coefficient, they can retrieve the Mw. They show two different polymers, poly(3-hexylthiophene-2,5-diyl) known as P3HP the model, andpoly[4-(4,4-dihexadecyl-4*H*-cyclopenta[1,2-*b*:5,4-*b*']dithiophen-2-yl)-*alt*-[1,2,5]thiadiazolo-[3,4-*c*]pyridine] known as PCDTPT used for the validation test. They manage to give molecular weight for different sample of different polymer length and polydispersity. They compare it with the standard method: Mw distribution (the spread) is assessed by SEC and its absolute value by NMR end-group analysis (another NMR method to measure Mn that does not use diffusion).[57]

This is rather interesting as it shows that weight can be accessed using size. Yet the distribution obtained using DOSY is much lesser than expected using SEC, resulting in much narrower curve. The team blame the ILT and the limited number of points for that, nonetheless the Mw obtained from DOSY are satisfactory and there is a good qualitative agreement between the two methods. Note that those kinds of plots are common in the field of polymer studies when diffusion NMR is used albeit extracted from DOSY data the DOSY classical display is not always shown or used.

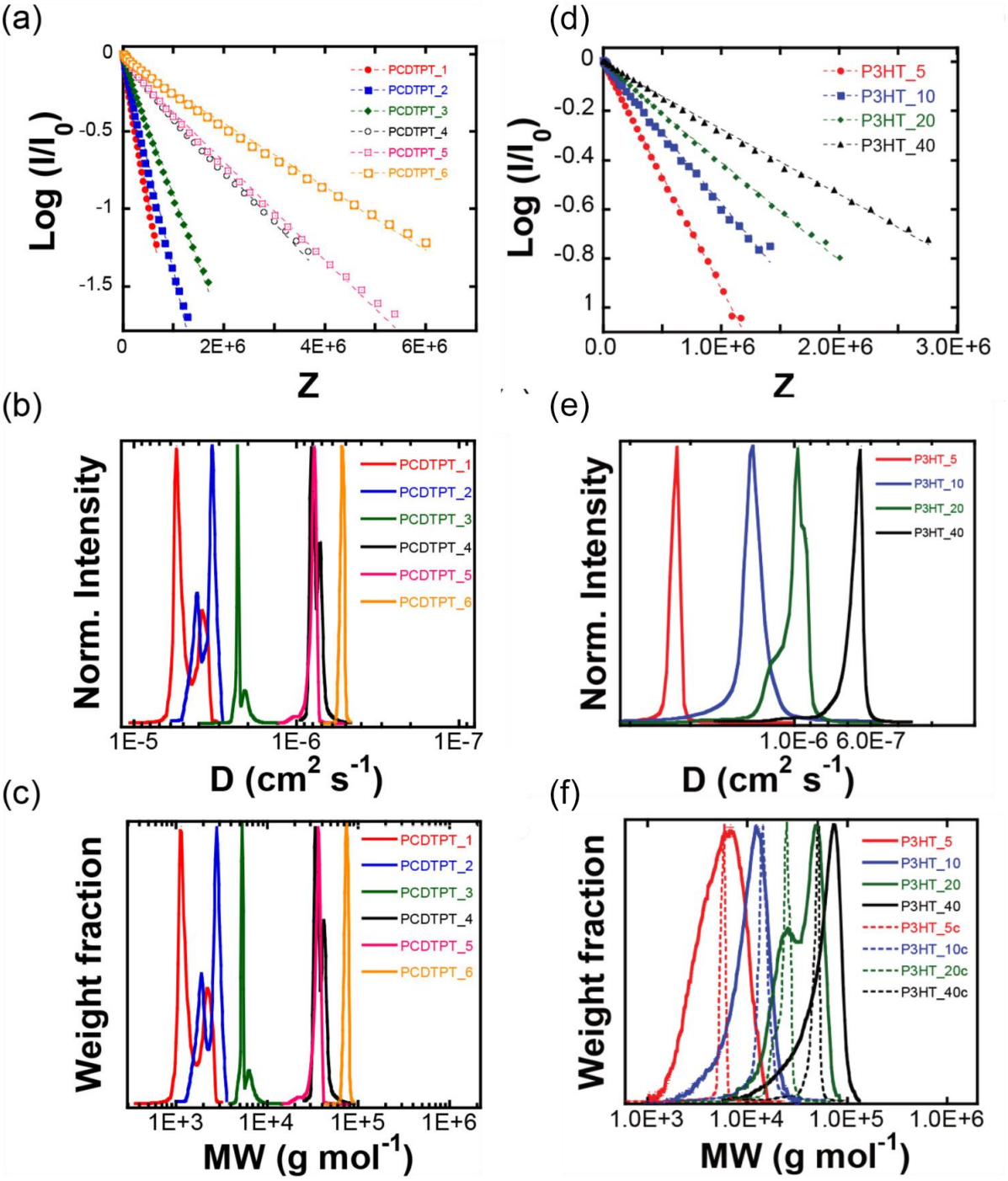

Figure 1.8 Left column (a-c) is for the polymer used for validation PCDTPT. Right column (d-e) are for the test polymer P3HT. (a) Stejskal–Tanner plot of intensity signal attenuation integrated over δ = 0.5–1 ppm and (b) diffusion coefficient distributions obtained from DOSY analysis for the six batches of PCDTPT, PCDTPT_1 through PCDTPT_6. (c) P3HT-equivalent molecular weight distributions of the six batches of PCDTPT, calculated from the respective diffusion coefficient distributions with the power-law relationship in eq 3 (original text). (d) Stejskal–Tanner plot of intensity signal attenuation at δ = 0.91 ppm of the four batches of P3HT in CDCl3. (e) Absolute weight-average molecular weight of P3HT as a function of diffusion coefficient. (f) Diffusion coefficient distributions obtained from DOSY analysis. (g) Absolute molecular weight distributions (solid lines) and calculated distributions from DOSY analysis (dotted lines) for the four batches of P3HT. adapted with permission from Gu et al.[44] Copyright © 2018, American Chemical Society.

1.2.2. Mixture virtual separation

Mixtures are ubiquitous, and important in many fields such as natural products and formulation. The analysis of mixtures often requires physical separation of the components. Diffusion NMR is sometimes used for "virtual separation "and compared to chromatography, indeed one can even find it labelled as NMR chromatography.[58] This analogy originates from one of the very first use of diffusion-NMR[59], to resolve components in a mixture. Diffusion coefficients are an information of interest, in particular through their relation with size and mass, but they can also be used just as a mean to separate components in a mixture. If we follow the analogy with chromatography the interest is not the interaction with grafted silica but rather the separation of compounds in a mixture by said interaction. DOSY can work with the same principle: as a way to identify different compounds in a mixture, using the relative value of their diffusion coefficients.

Translational diffusion occurs for molecules as a whole, thus the diffusion coefficient measured for every site of a given molecule should be the same. This means that in a diffusion NMR experiment each peak of the same molecule will decay at the same rate. Just like molecular weight, or retention time, diffusion coefficients are unlikely to be exactly the same in two different molecules. Combining all this together makes diffusion NMR a virtual separation method, which gives insight into which peak belong to which molecule, and also on the relative sizes of the molecules.

DOSY NMR is often present in the area where chromatography and Mass Spectroscopy (MS) are present, such as the analysis of natural products.[60] The information provided by diffusion NMR is analogous to the provided benefit of chromatography coupled with MS. NMR has its own disadvantages such as sensitivity and time requirement but it also has its strength, the non-destructivity and the ubiquity of NMR compatible nuclei. The use of DOSY for identification of molecules in mixture using database is fairly new[61,62] but seems promising. It shows both the rises of DOSY methods as well as its capability to give handy tool for identification of complex mixture.

Let us consider an example from the literature. You *et al.* have used DOSY to analyse alkaloid extracts.[63] Alkaloids are one of the most ubiquitous classes of molecules in natural extracts, and they have many different uses from medicine such as morphine and vincristine or in food such as piperine and are often used as platform for complex synthesis like indoles.[64] The main method for their separation is usually chromatography but it happens that because of the basic nitrogen present in their chemical structure, different interactions may rise with the silica particles as well as a strong impact of the pH, which can deteriorate the sample or worsen the separation.

DOSY NMR seems to be an interesting alternative. The spectra of the sample used in this work is quite crowded and poorly resolved because of the complexity of the mixture, and this is a recurrent problem in natural mixtures. The DOSY analysis itself is known to be sensitive to peak overlap, and

limited in terms of the range of diffusion coefficients that can be analysed in a single experiment. There are also limitations on the resolution that can be achieved in the diffusion dimension. The natural extract of *Alstonia Mairei* studied seems to have both problems, as can be seen in figure 1.9 (a) . Since DOSY alone gave unsatisfactory results, the authors decided to use a surfactant capable of making micelles (SDS for sodium dodecyl sulphate) to make a "matrix-assisted" resolution of the extract. This makes it possible to increase the resolution in the chemical shift dimension as well as in the diffusion dimension, as seen in part (b) of the figure. The probable reason being that formation of micelles will change diffusion of the molecules depending on various binding ability. Micelle might also change solubility and chemical environment explaining the change of resolution in the chemical-shift dimension. The matrix-assisted DOSY analysis can be used in conjunction with known alkaloid databases to identify the alkaloids. This example is interesting as it mixes different possibilities opened by DOSY. It also gives perspectives for identification and quantification of less known natural samples. This use of matrix and surfactant is commonly found in the world of natural extract separation[63,65,66] and relies on closely related principle than the use of DOSY in supramolecular chemistry.

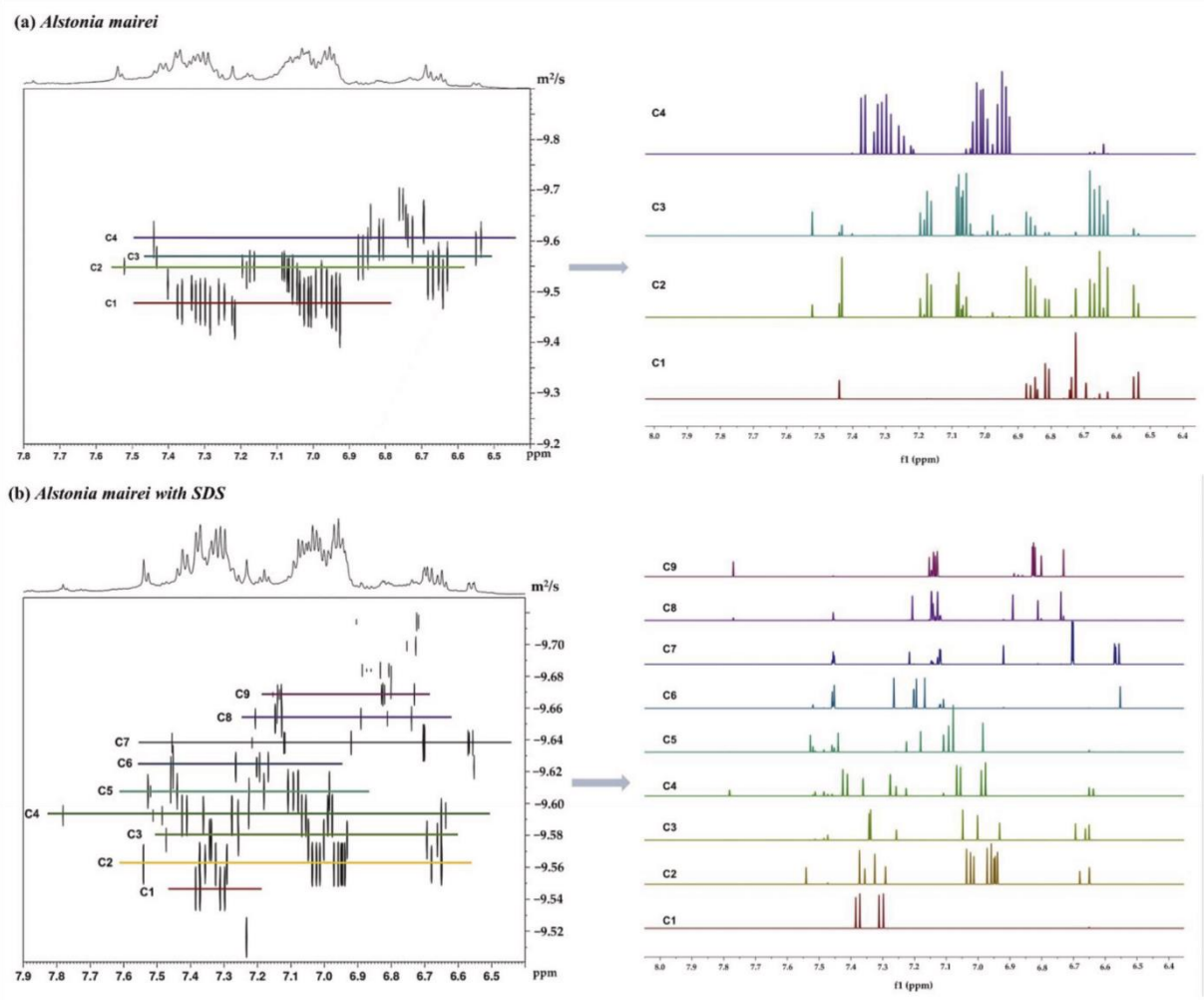

Figure 1.9 : taken from. DOSY spectra of a mixture of the real total alkaloid extract (20 mg) before (a, upper) and after (b, lower) the addition of SDS (10 mg) in DMSO-d6 (600 µL). Experimental temperature was 298K. reprinted from You et al.[63] © 2021 by the authors. Licensee MDPI, Basel, Switzerland. (open access CC BY license).

Formulation is a rather wide term that we will use here to describe mixtures that are finished commercial products. Such products can range from food to medicine, and this underlines the fact that all the things that we use and buy are often mixtures.

One application of diffusion NMR is the characterization of emulsions.[67,68] To do so technics a bit different from the classic DOSY are used yet relying in diffusion NMR. This size determination relies on the principle we have talked about in the part I.2.2.1 under the name restricted diffusion. We don't go in the details as it usually involves a lot of complex theoretical models and algorithms that are more common in the imaging field. Just to mention it they use diffusion into the small enclosure that is the droplet to determine their size. It is interesting as it allows to characterize the emulsion without disturbing it. Alternatively in such mixtures that have a high content of fat or big molecules the diffusion-filter explained in the part I.2.2.2 can be used.[69]

Fraud detection is also very important in formulation and often chromatography is the most common way to separate compounds in a formulation and check if they match the original product or a forgery. DOSY having close capability is also used for such investigation in medicine formulation[70,71], it can also be used in the same kind of compounds for quality control.[72]

1.2.3. Supramolecular chemistry

Supramolecular chemistry can be defined as a field that focuses on supramolecular interactions between molecules and the resulting molecular assemblies. More specifically on relatively weak interactions (compared to covalent bonding) between molecules, such as coordination bonds, ionic bonds, hydrogen bonds, etc. Those bonding can lead to assemblies of molecules that can take complex shape and undergo dynamic processes. One of the most studied processes is the encapsulation of molecules, in this case the host-guest paradigm is used. The host being the cage and the guest what resides inside it. Diffusion NMR is a very interesting tool for such assemblies as the nature of supramolecular bonds is weak and often sensitive to many parameters (temperature, solvent, salt…), NMR takes advantage of its capability to study such fragile objects without interfering whilst in solution.

Cohen and coworkers.[73,74] have written several reviews about diffusion NMR and cavities/cages, stressing the information that diffusion NMR can bring. To illustrate a typical use of DOSY in the field of molecular cages we are going to take an example from another review of Anna J. McConnel[75]. The work focuses on supramolecular cages that use metal centers, and here the metal is gallium. The cage formula is $[Ga_4L_6]^{12-}$ with L = 1,5-bis(2,3-dihydroxybenzamido)naphthalene, represented in the figure 1.10. The study itself focuses on the stability of the cage and its mobility with different counter-cation.[76] On figure 1.10 we can see the DOSY spectra of this cage with its guest NEt_4^+ and we see that they are able to differentiate two populations of the guest, exterior and interior. The team take

advantages of the chemical shift separation that is common in such assembly as the chemical environment is different in the cage and free in the solvent. The diffusion of the cage components and the guest being at the same diffusion rate is characteristic of a stable host-guest complex.[73,75] In the paper the team also investigates using diffusion NMR complex interactions with counter-cation, and the rate of diffusion of the complex, to learn about the inclusion mechanism.

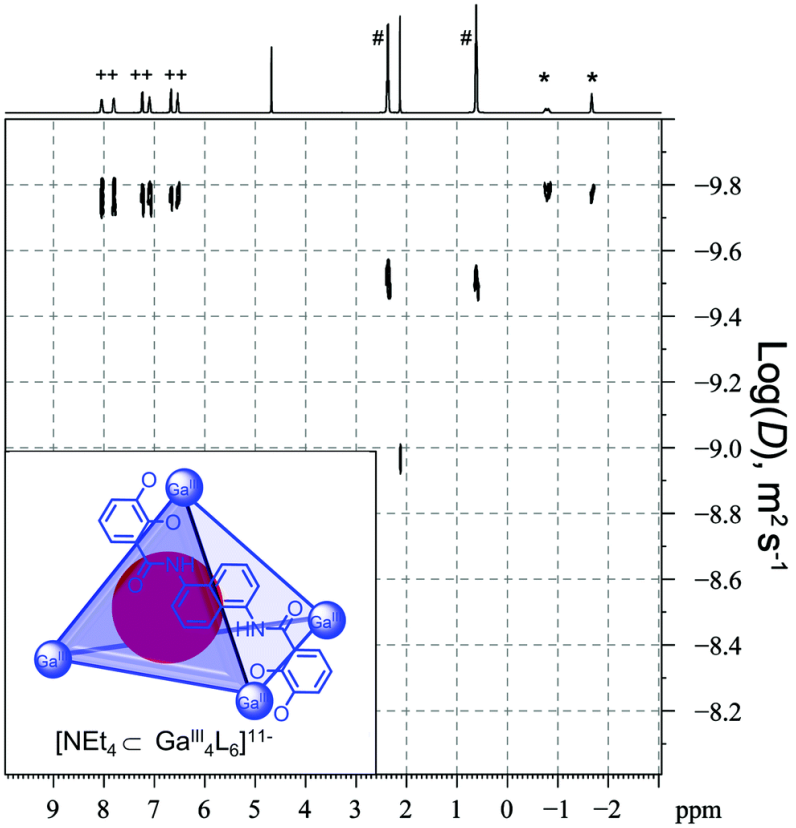

Figure 1.10 : ^{1}H and DOSY spectra of Raymond's $[NEt_4CGa^{III}_4L_6]^{11-}$ host-guest complex where the encapsulated NEt_4^+ guest is in slow exchange with ''free'' NEt_4^+. Signals marked with + correspond to the cage, * the encapsulated NEt_4^+ guest and # the ''free'' NEt_4^+. Adapted with permission from Pluth et al.[76] Copyright 2008 American Chemical Society.

NMR is particularly efficient at studying dynamical and/or weak interactions in solution. Diffusion NMR was used to determine the size, elongation and overall bulkiness of complex structures like helicates.[59] Many of the supramolecular assemblies show dynamic equilibrium that will be dependent on the concentration of the species in solution. Those species are often crystallised and studied by X-ray to have the first insight of the shape in solid-state. Diffusion NMR is one of the rare technics that allows some determination of size and shape in solution. Merget et al.[77] report a usually large molecular cage that self-assemblies from macrocycle monomers. Figure 1.11 shows a comparison of the evolution of diffusion coefficients as a function the concentration of the monomers. It shows the rapid decrease of diffusion as the monomer is added as well as the diminution of the hexamer's coefficient (figure 1.11b). This hints at a mechanism of self-assembly and exchange between the monomer and the hexameric cages, especially at low concentration where the hexamer is effectively

absent. On figure 1.11c) the quicker diminution of the hexamer's diffusion coefficient compared to other known macrocycle, that are also known to hexamerise, hint at it being much larger. Those kinds of assemblies are often very dependent on the solvent and thus NMR analysis within their medium show that diffusion-NMR can give information on complex equilibrium in solution.

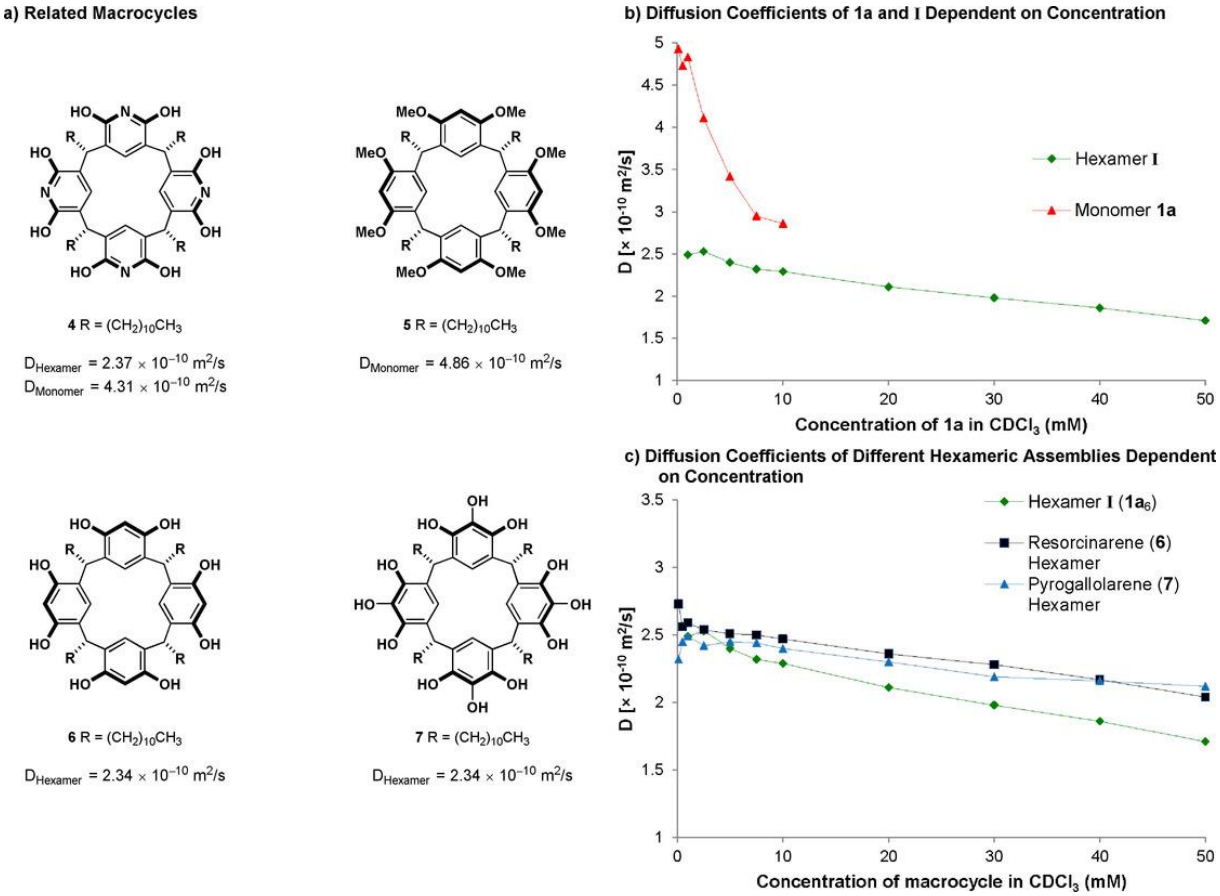

Figure 1.11 : a) Related macrocycles: pyridinearene 4, octamethylated resorcinarene derivative 5, resorcinarene 6 and pyrogallarene 7, and their respective diffusion coefficients in $CDCl_3$. b) Concentration dependence of the diffusion coefficients of the monomeric species 1a and the hexameric species I (1 mM −50 mM in $CDCl_3$). c) Comparison of the diffusion coefficients of the related hexameric assemblies based on macrocycles 1a, 6 and 7 at different concentrations(1 mM −50 mM in $CDCl_3$). Reprinted with permission from Merget et al.[77] © 2020 Wiley-VCH GmbH

Diffusion NMR is a powerful tool for supramolecular chemistry. Here we have focused on cages as the applications of diffusion NMR to those kinds of assemblies are particularly striking. Other kind of assemblies can be studied by NMR. We can mention gelators[61], ionic pairs[62] and various shaped complex.[73–75,78]

1.3.4 Aggregates

Aggregates could also be defined as supramolecular entities, they share the weak bonds that is the core of their nature. We decided to make a separate part for them because they are found in very different contexts.

The use of catalysts is very common in modern chemistry and many key-steps in modern reactions involve different kinds of interactions between the catalyst and its substrate. Diffusion NMR

can be useful in the case of reactive intermediates. As we have seen it can access the size of those intermediates and thus give information on their stoichiometries and shape. Unfortunately, those intermediates are often too short-lived to appear on the spectra and do not build-up sufficient concentration to be seen by NMR. If one aims to see those steps, it is needed to trap the intermediate species. This species might get weakly bonded to the catalyst thus forming a reactive aggregate that could be analysed by NMR.

Reducing the temperature is often an efficient way to trap transients species. For example, Qiao et al.[79] have used this approach. They used ^{1}H and ^{19}F NMR and diffusion-NMR to characterize intermediates aggregates at low temperature, -55°C. They used ^{19}F DOSY to avoid the overcrowding of the spectra, typical of glycochemistry. DOSY experiments allows two things, to observe that the catalyst is indeed bound to the reactant of interest, and to validate their hypothesis on the kind of aggregates by comparison between diffusion coefficients recorded and predicted. They conclude on different intermediates/reactive pathway depending on the catalyst used which allow them to propose a new catalyst.[79]

Other ways to stabilize intermediate aggregates can be found, such as trapping them by chemical means[80] or using a test-solution to recreate the conditions of the reaction with a more stable aggregate. Such is the work of Matador et al.[81] The reaction they are interested in is summarized in Fig. 1.12. The thiourea is the reactant of interest while the benzoic acid is the catalyst, in the reaction it is present in catalytic quantity. To understand better the mechanism the two are added here in equal molarity. As one can see on figure 1.13, this led to the formation of an aggregate with NMR signal of both species present in the spectral dimension, albeit slightly shifted and larger typical for the formation of an aggregate. The two compound signals correlate at the same coefficient diffusion. This resulting coefficient is smaller than that the two reactants it is made of, which strongly hints at an aggregate formation. This rules that the active catalytic specie is the ion-pair Ia/$PhCOO^{-}$. Its weak bond allows to be temporally broken to let the substrate enter (see figure 1.12) and is strong enough to resume its initial paired state and continue the catalytic cycle. The DOSY analysis is an important step in the catalytic cycle unravelling process, it is part of a package of methods that includes DFT calculation and X-ray, which is relevant with aggregates and weakly bounded molecules as well as any mechanistical study.

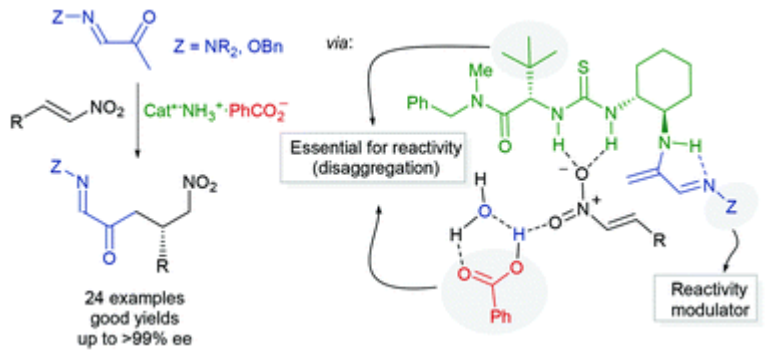

Figure 1.12. The reaction of interest. Reproduced from Matador et al.[81] with permission from the Chinese Chemical Society (CCS), Shanghai Institute of Organic Chemistry (SIOC), and the Royal Society of Chemistry.

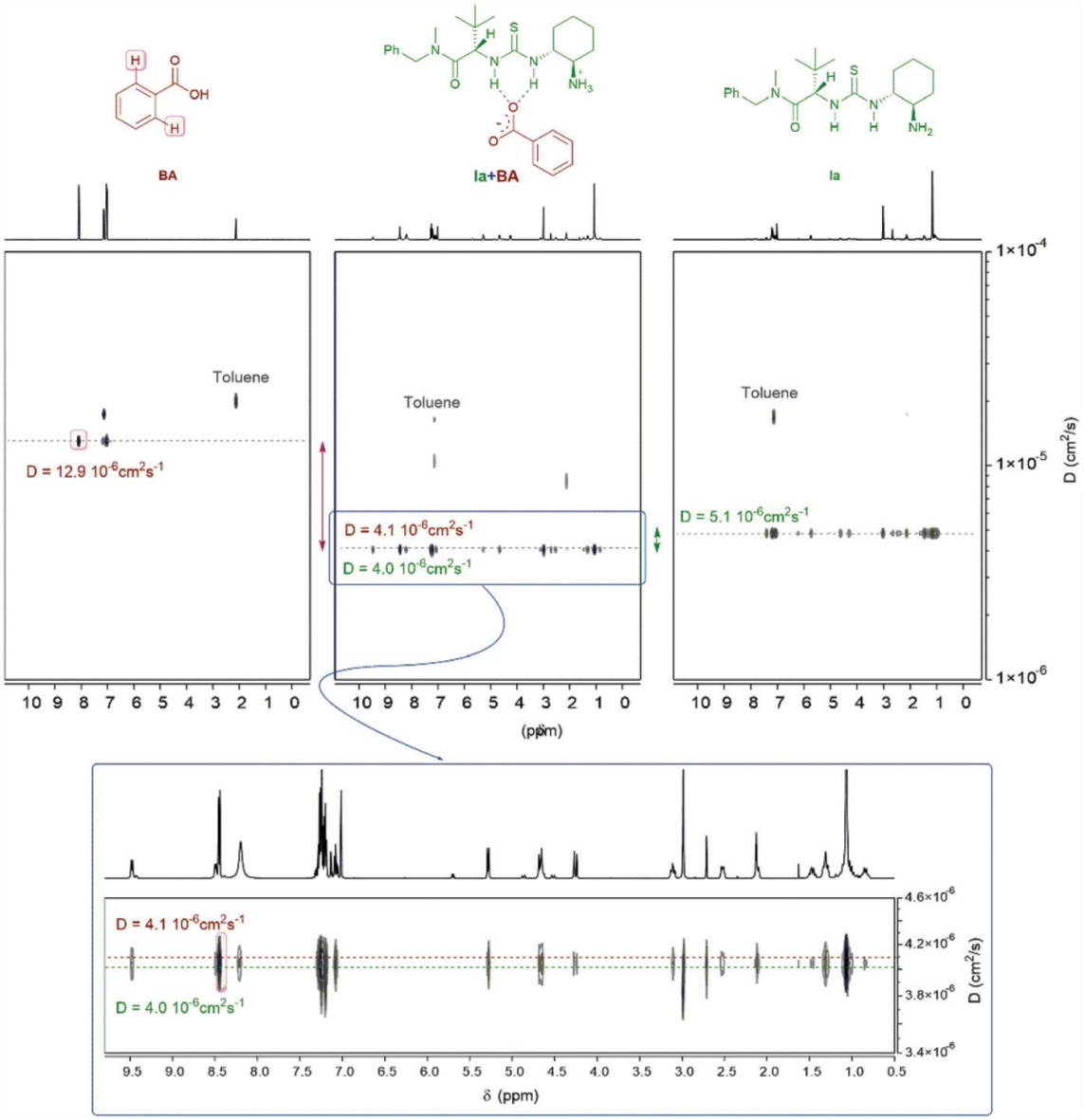

Figure 1.13. ^{1}H DOSY NMR (500 MHz, 0.2 M, toluene-d_8) of benzoic acid (left), thiourea Ia (right) and Ia/PhCOOH 1 : 1 mixture (middle). Reproduced from Matador et al.[81] with permission from the Chinese Chemical Society (CCS), Shanghai Institute of Organic Chemistry (SIOC), and the Royal Society of Chemistry.

We have seen intermediate-aggregates in the course of a reaction. Another kind of reactive aggregates exists, those for which the aggregation state can plays a role as intermediate but also in

their initial state, on their availability as reactive species. This is mostly the case for very reactive species with difficult storage. In particular, diffusion NMR has been extensively used to characterize various form of lithium aggregate. Those compounds are known for their extreme reactivity even in mild conditions.[82] Studies on lithium aggregates can focus on a range of questions, such as availability in solution,[83] basicity,[84] impact on selectivity[85,86] (chiral and chemio-), and one of the most hot topic battery and electrolyte.[87,88] Note that some of those studies take full advantage of the fact that ^{6}Li or ^{7}Li are both active NMR nucleus, yet when lithium is used with organic compounds most study rather study ^{1}H proton NMR as it is more convenient.

Another interesting consequence of aggregation is found in the study of biological molecules. Indeed, it happen that quite a few health issues come from aggregation of chemicals endogen or exogen[74] that once aggregated cannot be removed/metabolized.[89,90] MRI and solid NMR are out of our scope but they are often used to study such assemblies.

They are multiple examples of aggregation studies in the living, common topic includes, understanding aggregation in amyloid fiber formation[91,92] and allosteric protein.[93] An interesting example is this review[94] by Dehner and Kessler that showcase examples of interest for DOSY and diffusion-NMR in the study of the protein p53. They are interested in folding and aggregation in the p53 protein using diffusion NMR. They illustrate the binding ability of different DNA-binding domains for variants of p53 with its associated consensus-DNA (con2x25). This consensus-DNA is expected to link with the p53 Wild-Type (WT on the figure 1.14) protein through those DNA-binding sites. As we have seen in previous parts a strong association lead to an aggregate with a reduced diffusion coefficient. Using simulations, they can estimate that a reduction of 33% of the coefficient hint at a strong association while a reduction of 18% is a single-site association. The results are shown in figure 1.14 It allows to study binding ability of several mutated domain versus wild-type, as well as its possible binding mechanism. By changing amino-acid of the protein they can identify which amino-acid does have an impact of this bounding here hinting at importance of the pair E-R (glutamine-asparagine) in the protein at 180/181.

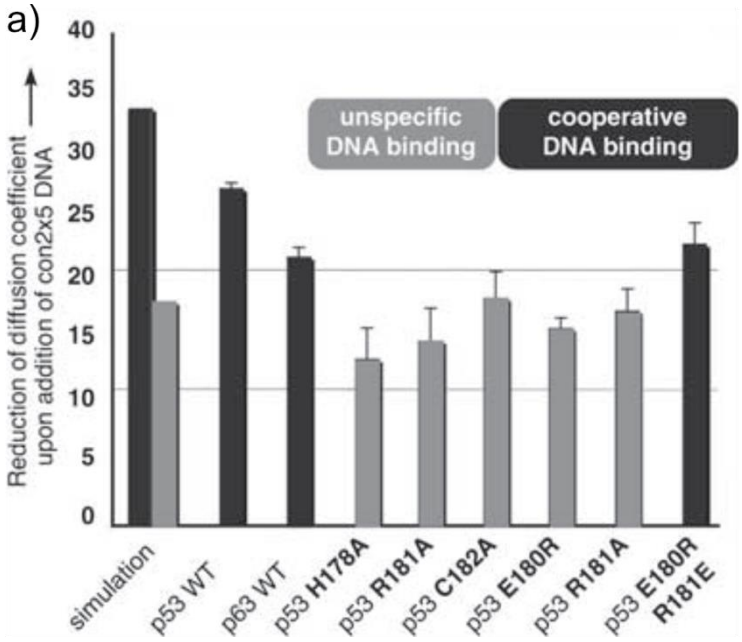

Figure 1.14 Reduction of the diffusion coefficients of p53 DBD, p63 DBD, and the p53 DBD dimerization mutants upon complexation with consensus DNA, as measured by pulsed-field gradient NMR spectroscopy. Hydrodynamic simulations with a cooperative p53 DBD–DNA model predict a theoretical re-duction of 33 %, while a single-site binding of DNA should result in 18 % reduction. Adapted with permission from Dehner et Kessler[94] Copyright © 2005 WILEY-VCH Verlag GmbH & Co. KGaA, Weinheim

2. Reaction monitoring by NMR

There are many different spectroscopic methods to monitor reactions, such as Raman,[95] Infrared[55], NMR, UV-vis spectroscopy, and mass spectrometry.[96] Those methods have different pro and cons. NMR is a very powerful method for structure elucidation, often mandatory to characterize any new product (NMR characterization is actually mandatory to report new structures). If NMR is so common, it is for the great amount of information it can provide from molecular dynamics to structural studies. The fact that NMR relies on a ubiquitous probe (nuclear spins), as well as its non-destructive nature make it a great technique for many kinds of analyses. A monitoring analysis should be able to provide extensive information on a system in an innocuous and reproducible way. It should not impact the reaction and it should be usable in variety of experimental conditions. NMR seems to fit all those criteria. It may therefore seem straightforward to characterize species as they appear.

Despite all of these advantages, NMR monitoring is not as common as it could be. The reasons for this are multiple. They include limited sensitivity, and cost of operation and other more specific reasons that we will describe this chapter.

2.1. The sampling methods

NMR seems a very well-suited spectrometric method for monitoring, thanks to the innocuity of analysis and its large array of obtainable information. Yet a number of challenges arise when monitoring is the focus.[97,98] One of those questions is how to observe the reaction medium without disturbing it. This question is not specific to NMR. Yet the NMR environment with a magnetic field, a need for homogeneity (of magnetic-field and medium), motion dependency, etc. creates specific challenges. It is hard to be exhaustive as each reaction can call for its own specificities. In this part we will describe the sampling methods for NMR analysis rather than the NMR analysis itself.

2.1.1. Aliquoting

Aliquoting a reactive medium is a common strategy, which is not specific to NMR.[99,100] It is relatively straightforward to implement. It consists of taking small samples (aliquots) of the reactive medium as the reaction progresses, and analysing them. Yet nowadays to our knowledge and by looking at the recent literature it seems this method is not very widespread, at least in NMR field. It seems to be restricted to matters that specifically needs such methodology because they might not be compatible with another.

Examples can be found in polymer chemistry, which sometimes require very specific reactors that, e.g., are very tight to prevent oxygen to enter, or are able to sustain various temperatures and

pressures that play a role in the degree of wanted polymerization.[101,102] In such cases, it is hard or meaningless to try the reaction elsewhere, and aliquoting make sense.

Aliquoting poses multiple problems. First getting the aliquot out of the medium can be an issue. If pressure is highly controlled or oxygen/air exposition is an issue, getting an aliquot can be hard and pose a significant risk of disturbing the reaction. Another problem can be that the reaction may continue in the aliquot. To have a perfect snapshot at the right moment of the reaction, one need a non-evolving sample of the reaction medium. The aliquot can be quenched,[103] and for that many different means can be used. A drop in temperature such as using liquid nitrogen or cold-water bath can be used to freeze the solution and stop the reaction.[97] Adding large amount of solvent,[104] the same solvent as the reaction or another where the reagents are less soluble than the product, is also a possibility. In NMR it is an especially good solution as it can serve as well to add deuterated solvent, whilst the reagent will be in too low concentration to react at any meaningful rate. Finally, another approach can be to use an active chemical, for example a base that will counter the acid that makes the medium react, or an oxidant/reducer, this kind of quenching is for example seen in polymer chemistry where radical traps are sometimes used.[105]

From the NMR point of view, aliquoting is a labour-intensive option. Every aliquot needs to be transferred into an NMR tube and the spectrometer needs to be calibrated for each tube (shimming, tuning and matching, pulse calibration…) which can be long. Assuming the reaction is not so long, it can play a huge role on the maximum number of aliquots that can be taken, as they should not be stored for too long. For this reason and the others, this method is also used to check the initial and final condition by taking only two aliquots.[105]

Understandably all those manipulations of the sample are unwanted. They try to be as neutral to the main interest but any modification of the sample even as simple as change of volume, can be unwanted. The perfect monitoring should be like a picture whereas aliquoting is more like taking sample of an historic site in order to rememorate it better. It can directly impact the subject and can give information of a flawed system.

2.1.2. In-situ

To our knowledge the most common way of monitoring by NMR is “in-situ monitoring”, meaning that the reagents are put into the NMR tube and the reaction happens in the spectrometer. The NMR magnet is usually seen as a reasonable place for reactions to take place, since most spectrometers provide temperature regulation, and the in-situ analysis is non-destructive as well as non-invasive. However, NMR tubes are in fact not ideal chemical reactors. Some of the main reasons include: incompatibility with solid and precipitate, need for homogeneity (droplets or multiple phases are best avoided), problems with highly exothermic reactions, lack of agitation/stirring, small reactive volume,

etc. Foley et al.[98] did an extensive work on the difference of kinetics between *in situ* NMR and the insightMR flowtube they helped to develop. Showing meaningful differences between the kinetic profiles on the tube and online, they even tried a method to stir the tube, by inverting it twice at regular intervals, and still see major differences.

Despite all this, *in situ* monitoring is fairly used, and the main reason is the simplicity to do it. It does not require anything more than what a routine analysis would require. There are countless examples of its use and it is the default monitoring technic with NMR. In this section, we are going to discuss three publications and what *in situ* monitoring allowed them to do. We chose mostly exotic examples that extend the reach of *in situ* NMR. We also have chosen them because they focus on both the NMR apparatus and the system studied.

Sollogoub and coworker[106] in a relatively simple *in situ* monitoring setting, studied the capabilities of a new metallo-pocket molecule for catalysis. They created, from cyclodextrin, a cavity with a metal center. This approach aims at creating new catalyst for known reactions. Those new catalysts would show better selectivity for their ligand. The cavity or pocket size and interactions within it govern which substrate can enter and react in an enzyme-mimetic fashion.[107] The reaction being relatively fast (~35 min), ^{1}H 1D NMR seems a good way to monitor it. They can integrate the peaks of interest with good resolution and obtain the results shown in figure 2.1 and figure 2.2 that give the concentrations based on a reference in the tube. In figure 2.1 they monitor the cycloisomerization with their catalyst (β-ICyD)AuCl. They can determine an initial rate of $1.2\ 10^{-6}$ mol L^{-1} s^{-1}. Figure 2.2 shows the same information but with the conventional catalyst. The rate is higher for the conventional one, which is expected as the cyclodextrine-based one is bulkier, yet the cyclodextrine-based one gives same product at the same concentration with turnover rate and relative stability of the same order.[106] NMR allows to have a straightforward method of monitoring that does not ask for specialized NMR knowledge or settings, an easy way to setup a monitoring that give information on a complex system. This is an example of the classic way for *in situ* monitoring, we will now look at more exotic setups, to show the large range of possibilities with such methods.

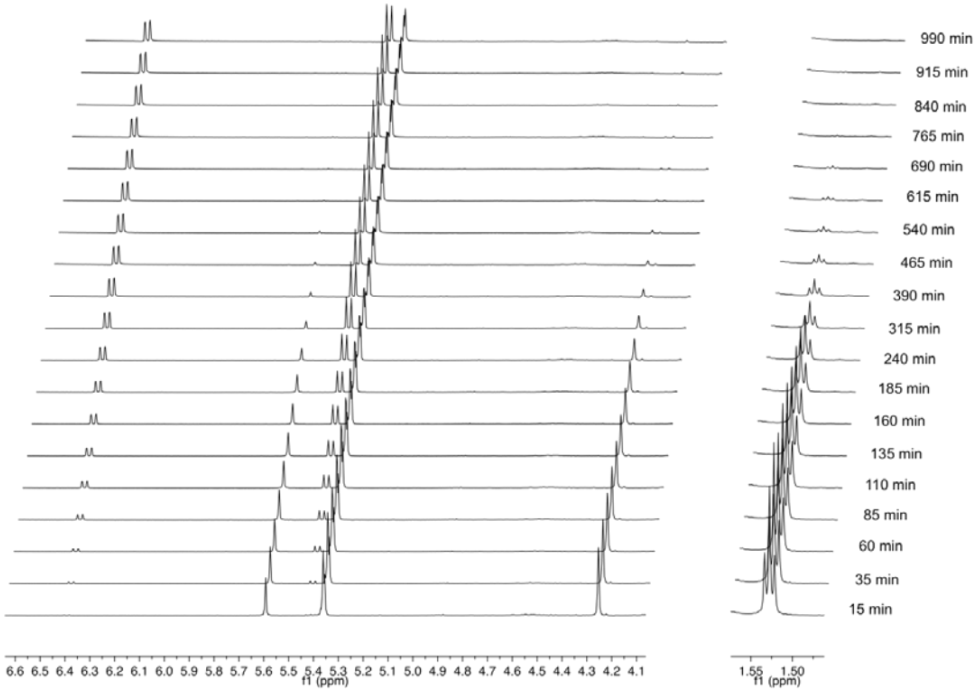

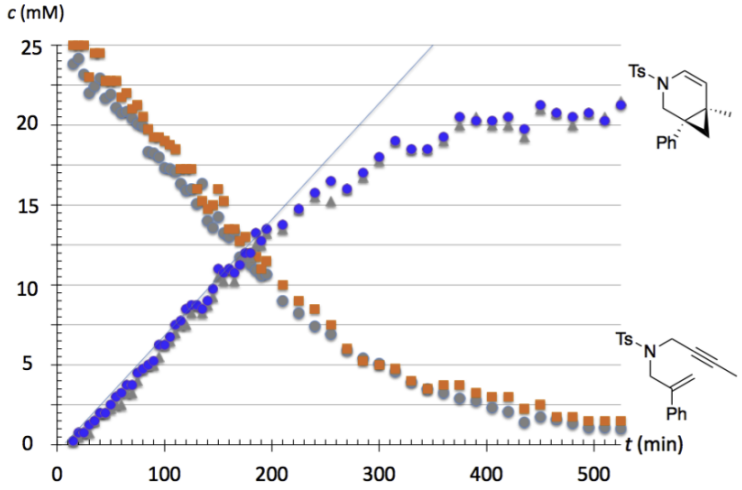

Figure 2.1 : Cycloisomerization catalyzed by β-ICyDAuCl at 300K in CD 2Cl2: a) Stacking of ^{1}H NMR spectra at different reaction times; b) Plot of the concentration as a function of time. The concentrations were determined by integration of different signals of the enyne and of the cyclized product. The internal reference was used for calibration. The slope at c = 0 for the cyclized product (blue line) gives r_0 of ca. 1.2 10^{-6} mol L^{-1} s Adapted with permission from Sollogoub and coworkers,[106] Copyright © 2017 Elsevier Inc.

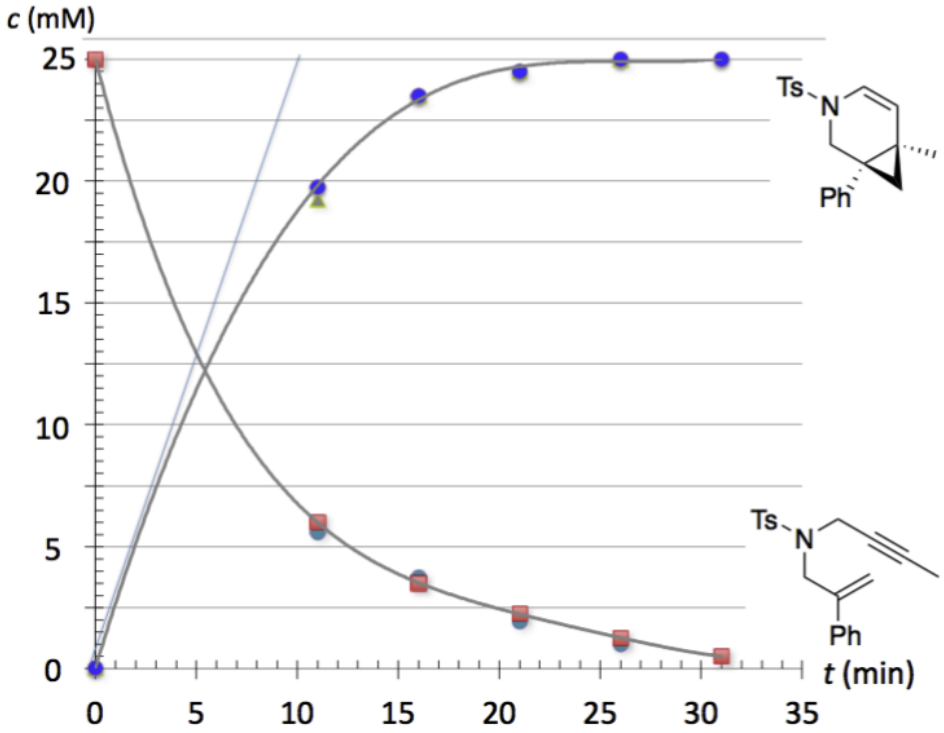

Figure 2.2: Cycloisomerization catalyzed by (IPr)AuCl at 300K in CD 2Cl2. Plot of the concentrations as a function of time. The slope at c = 0 for the cyclized product (blue line) gives an initial rate r_0 of ca. 41.6 10^{-6} mol L^{-1} s^{-1}. Adapted with permission from Sollogoub and coworkers,[106]Copyright © 2017 Elsevier Inc.

Leutzsch and co-workers[108] have used benchtop NMR to monitor a hydrogenation reaction on 1-octane, catalyzed with a porous material, using ^{1}H 1D NMR and T_1/T_2 measurement.[108] While the analysis of solid catalysts requires solid-state NMR methods, liquid-state NMR methods can provide extensive information on their reactivity for heterogeneous catalysis. In Ref.[105] , a rather exotic setting is used, as the NMR tube is filled with pellets and monitored under a flow of hydrogen gas. This is made possible because the solid has no proton (Pd/TiO_2), as well as the reduced magnetic susceptibility line broadening coming from the homogenous orientation of the pellet in the 5mm tube. The way to have an acceptable line broadening is to have the same orientation of the solid catalyst, that can be seen as well-ordered in the 5 mm tube, see figure 2.3. The coupling constant in ppm are expected to differ vastly from low field to high field yet this effect is compensated by the less important broadening effect from anisotropy at low field. Thus, the two sites of interest 1 and 2 despite being relatively close can still be separated and integrated at low field in those exotic conditions. It can be seen that the spectra at high and low fields are not as different as one could expect in normal condition because of those effects.

^{1}H 1D spectra are used to monitor the isomerization/reduction. Interestingly, the relaxation information is used to distinguish two different environments for the same molecule. Unreactive alkanes indeed tend to have longer relaxation time than those at the surface of the catalyst, which have shorter relaxation time. This is illustrated in Figure 2.4 where one can see the two populations of differently relaxing molecules. Before the reaction two populations are observed showing that the

surface alkenes and the free alkene are not in a fast exchange system. Then only one peak can be seen hinting at a fast exchange rate between free and surface. At about 50 % of the conversion two peaks can be seen once again. The peak with T_2 = 192 ms could be the alkene that has yet to react and is adsorbed on the surface, whilst the other peak shows the reacted alkenes that lost their affinity with the catalyst surface. Overall, this information makes it possible to monitor the reaction and access the turnover rate of the catalyser. It shows an interesting example of using NMR in unusual and challenging conditions by taking advantage of what is often considered a drawback (low field).

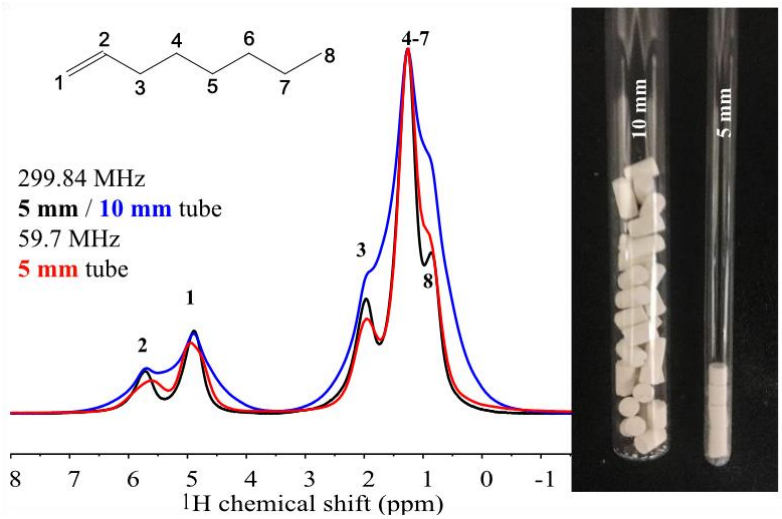

Figure 2.3 : ^{1}H NMR spectra of 1-octene in a heterogeneous TiO_2 support acquired at 59.7 MHz (1.4 T) (−) and 299.84 MHz (7 T) in a 5 mm (−) and 10 mm NMR tube (−). The chemical structure of 1-octene is shown on the top left and the corresponding assignments are shown above the peaks in the spectra. The right image shows the respective 5 mm and 10 mm sample used for the acquisition of the data. Adapted with permission from Leutzsch et al,[108] Copyright © 2018 Published by Elsevier Inc.

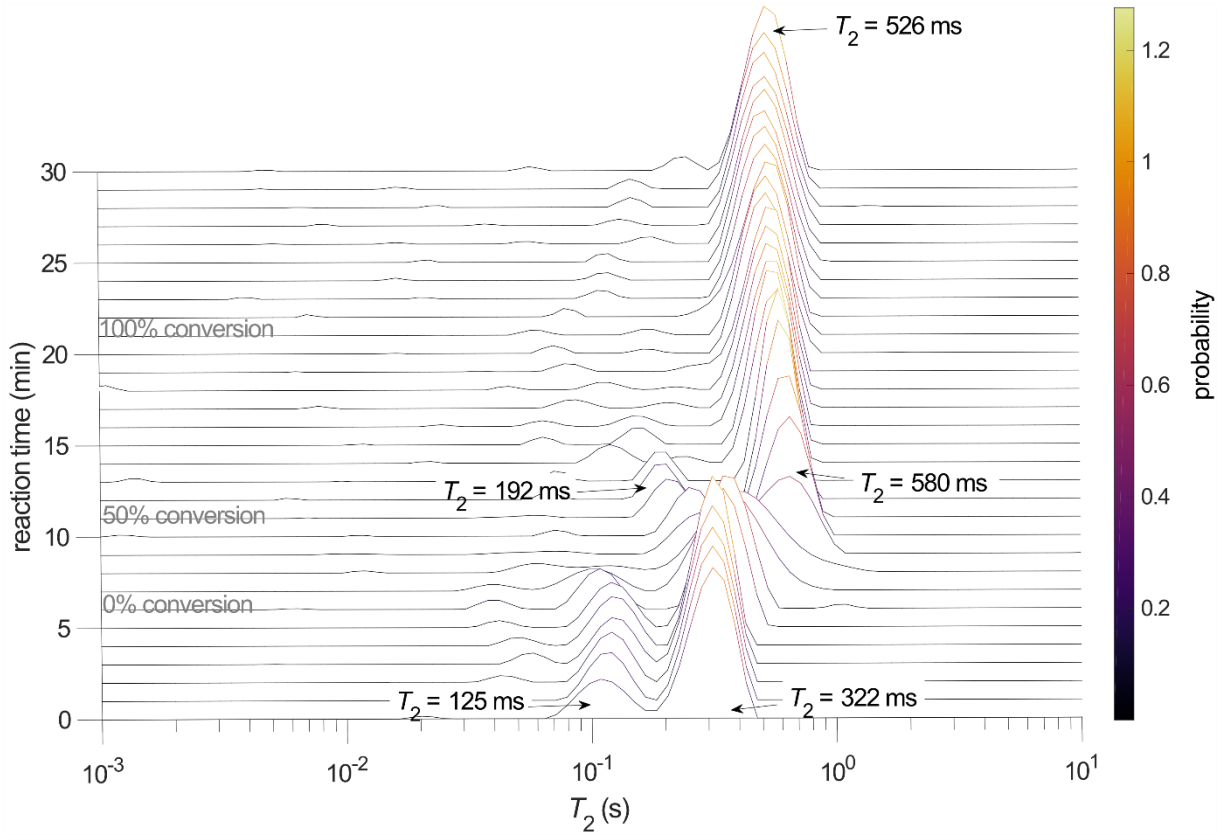

Figure 2.4 T_2 distributions obtained after Laplace inversion at different time points during the hydrogenation of 1-octene in 0.3 wt% Pd/TiO_2. Adapted with permission from Leutzsch et al[108] Copyright © 2018 Published by Elsevier Inc.

Reacting mixtures are often complex. Starting materials can go through multiple changes before becoming the final product. Secondary products can also be formed. NMR, being a very powerful tool for structural analysis, can be used to identify and monitor the formation of the different species of interest and sub-products. This will most of the time be critical in understanding the mechanism of the reaction. In Ref.[109] Kallman *et al*. proposed to study a reaction that may seem simple at first glance but that involves a complex mixture of species and equilibria (see Figure 2.5 a). For this application, they chose to use ^{19}F NMR, for two main reasons. First, ^{19}F NMR is highly sensitive and this makes it possible to acquire spectra in a short time. Second, ^{19}F has a large chemical shift range. Since multiple species that come from the same reaction condition can be closely related in their structure, ^{1}H NMR spectra can be plagued with overlapping problems.[110]

The authors also used the capability of NMR probes to reach high temperature levels. In order to have good monitoring condition, they raise the temperature up to 75 °C. In this work, monitoring is key to better optimize the reaction and understanding the reaction condition that will favour one product over another. The proposed mechanism is seen on figure 2.5b and shows a great extent of different species evolving throughout times. The capability of NMR to study mixtures is here the key point, all those equilibria and species present can be analysed at the same time to give a complete picture of the ongoing reaction. If the reaction were to be left unmonitored only two species could be

seen the aminopyrazol and the hydrazinylpyrazole (see figure 2.5). Here 3 more transient species can be seen, which is a great way to propose and understand the mechanism. This reaction is stated as useful but "underutilized",[109] the main reason being probably the difficulty to resolve such a complex mixture resulting in a lack of recent studies.[109] The articles show a very good example of what a classic *in situ* studies with relatively simple technic (1D NMR) can yield, deep insight into the chemical pathway and intermediate species of a complex reaction.

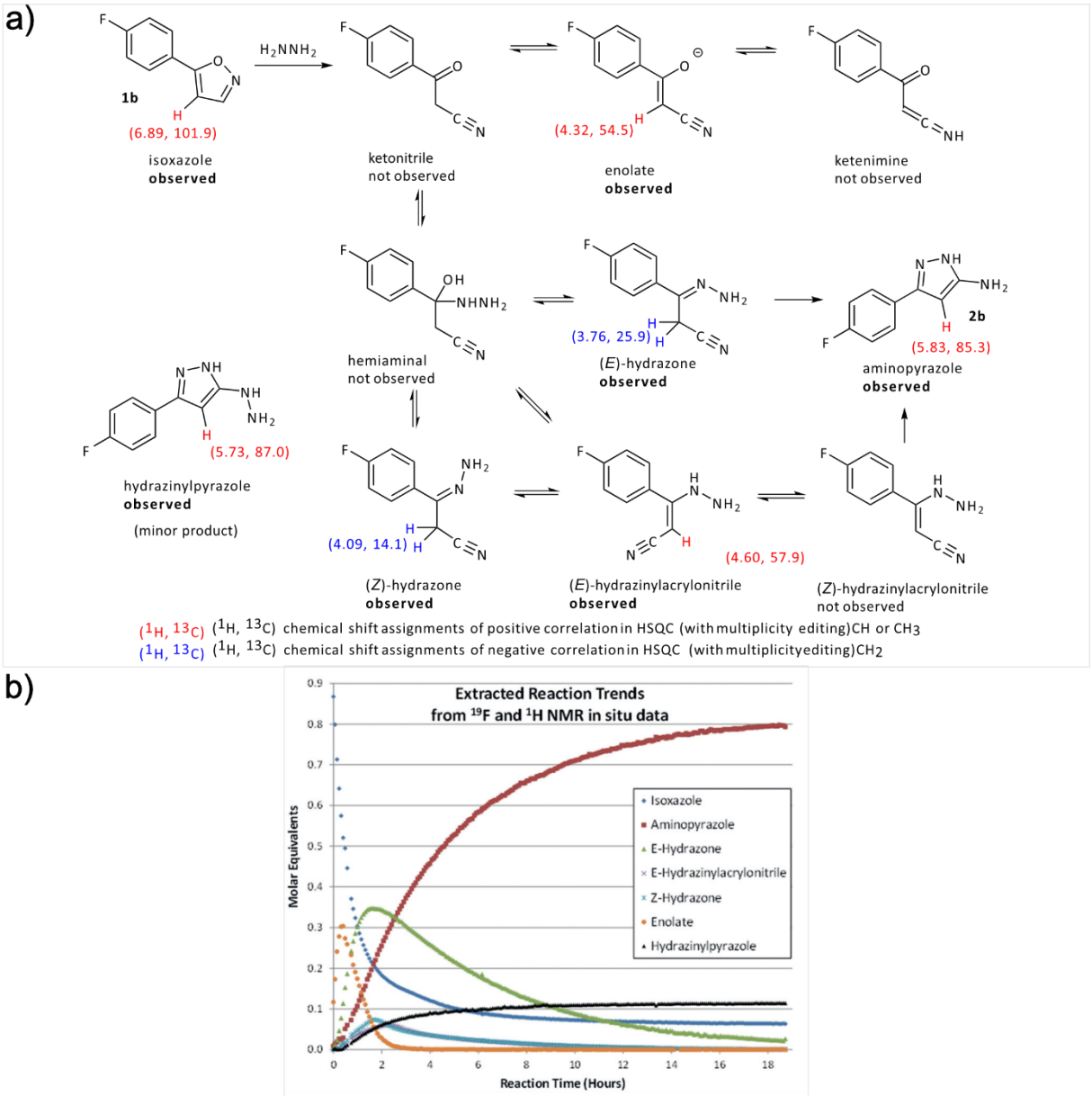

Figure 2.5 a) proposed mechanism for the conversion of 5-(4-fluorophenyl)isoxazole (**1b**) into 3-(4-fluorophenyl)-1H-pyrazol-5-amine (**2b**). b) Reaction profile of **1b** with hydrazine. Adapted with permission from Kallman et al.[109] Copyright © 2016, Rights Managed by Georg Thieme Verlag KG Stuttgart • New York

Thus far we have chosen examples that show the capability of NMR to study, in a simple setup, complex phenomenon, which is the general idea of *in situ* monitoring. Nonetheless some solutions exist for reactions that could not be monitored with such simple setups. Ideally those setups should remain compatible with classic NMR experiments, so that they can be used by non-NMR specialists. In

Ref. [111], Dolinski *et al.* propose to study photoreaction with *in situ* monitoring, for that they need a light to shine onto the sample. It seems a bit unreliable to shine a powerful light down the NMR shim cannon, they actually tried and record lack of repeatability, probably coming from the difficulty to aim precisely at the sample and the distance with the LED. To overcome this the team made the apparatus presented in figure 2.6a. They used an optically dense medium (opaque) that turns into a clear medium upon illumination, as it contains a "photoswitch" that photoisomerizes. With this approach, they can know which slice of the tube is getting shined on, thus they have a good understanding of the amount of light received by the reactants. The idea is that the light-impacted portion of the tube will go down as the reaction progress in a linear pattern (see figure 2.6c). This also allow precise control of the reaction of interest, here the team chose a light driven polymerization.[111,112] As seen above, polymerization can be a quick and sensitive reaction that is unsuitable to conventional means of monitoring. The use of a photoswitch allows to reduce the rate as well as to better control the reaction and the amount of light received. This peculiar method allows to gather the kinetic of reaction as well as its quantum yield which is a very important data for photochemistry. Adding this photoswitch to other light-catalysed reactions could allow to gather the same kind of information. The setup here makes the NMR capability shine as there is no need for NMR specialist in order to have information rich experiments while having very controlled condition. It pushes the boundaries of *in situ* monitoring by allowing to control the trigger of the reaction (light) within the spectrometer without compromise for the analysis.

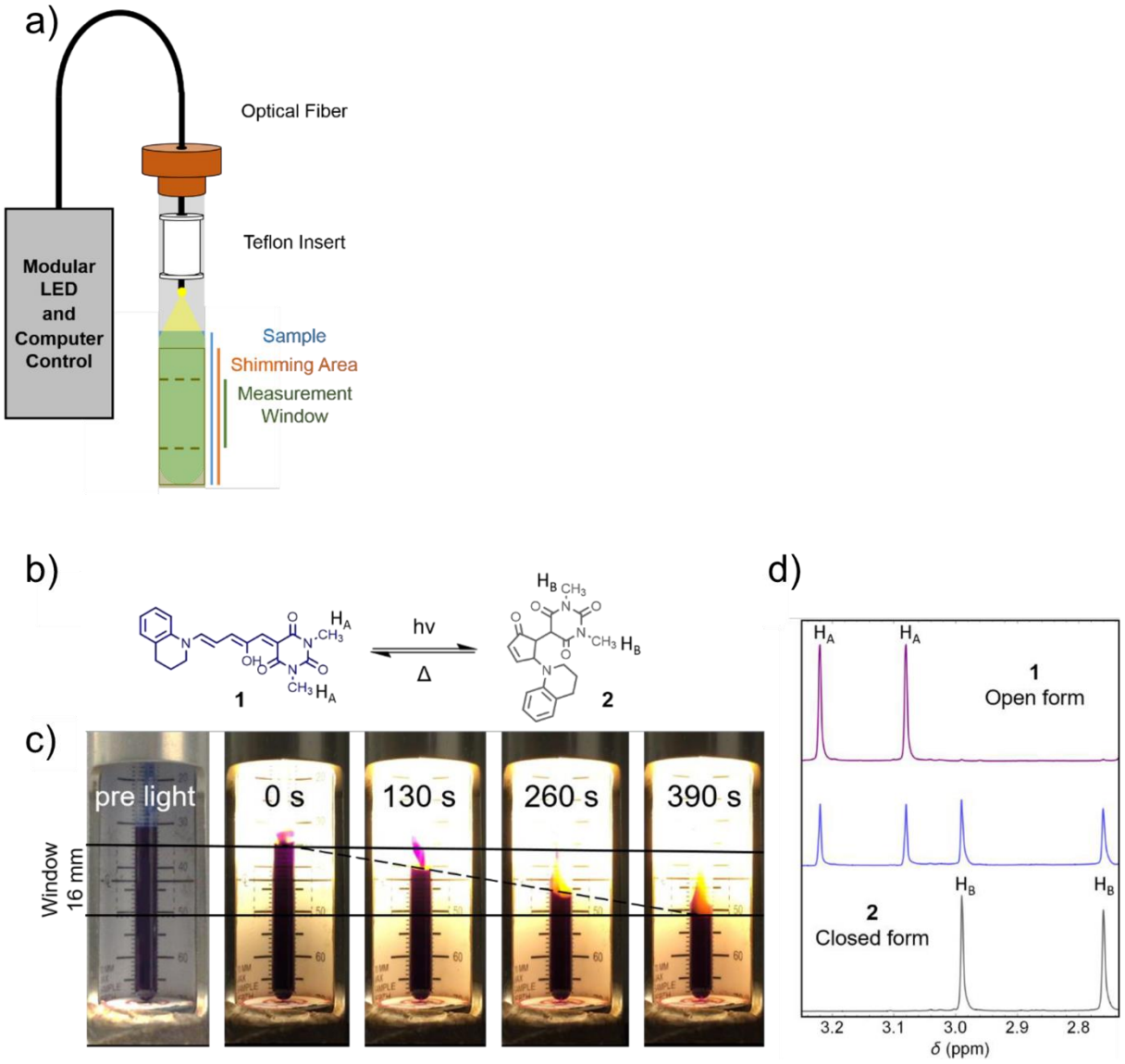

Figure 2.6. a) the NMR tube setup, note that they state that in reality there is only a small gap of air between the tube and the insert. DASA photoswitching in an NMR tube B) Chemical structures for tetrahydroquinoline barbituric acid DASA in the open, colored triene form (**1**) and the closed, colorless cyclopentenone form (2). c) An optically dense sample of **1** in toluene (10 mM) forming a switching front upon exposure. Adapted with permission from Dolinski et al.[111] Copyright © 2017 Wiley-VCH Verlag GmbH & Co. KGaA, Weinheim

Those examples do not show the average setup of *in situ* NMR monitoring, that is usually doing the reaction in the tube while monitoring the rise and fall of peaks in 1D NMR. It shows that it can be available in a wide range of setups, reaction conditions or NMR experiments while being relatively simple especially for chemists who specialize in synthesis. The main advantages of *in situ* monitoring is its simplicity and availability. Yet several drawbacks exist. Some are common to all the setups for NMR monitoring, such as spectral resolution and time resolution. Others are specific to *in situ* monitoring, such as the lack of stirring and the scale. Reaction monitoring and kinetic are usually very dependent of good homogeneity and of stirring/mixing. The lack of stirring/mixing in the NMR tube can be a problem especially coupled with the thin nature of the NMR tube.[98] The scale of reaction is important, it is well known that scaling up of reaction can be a real challenge but a worthy one as

industrial scale is well above benchwork scale. What happens is that often reactions are instead scaled down in order to fit the tube volume. *In situ* monitoring is also more difficult to combine with the use of specific reaction methods such as light illumination.

2.2. Flow methods

We have seen that there are different ways to monitor reactions using NMR in a static way. Yet those methods have a few drawbacks. The lack of access to the reacting medium is one, as it does not allow to act on the medium during the reaction, by adding reagents or solvent for example. The lack of clear correspondence between a thin volume without stirring, as in an NMR tube, and the benchwork condition is a problem that could lead to misconception.[98] In general the low volumes that have to be used are a major drawback for everything related to scaling-up the reaction and thus a severe drag on any industrialization process. Finally, we have seen several setups where the team developed their own specific apparatus for a kind of reaction, which may be difficult to reproduce in other labs. A common methodology that allows for adjustment during reaction or prior to it would be much preferable.

In this work we are particularly interested by flow-monitoring NMR, it seems a good alternative to *in situ* monitoring. It allows to have all the benchwork advantages with the NMR analysis at hand. Different ways of using flow for monitoring exist and are easy to implement once the apparatus is installed. The possibility to have a general setup that could work on multiple benchwork-like conditions was our main goal. We decided to lean toward flow to be able to be under the fumehood while analysing our medium at the same time using flow as a way to have insight into the reactive medium.

There are many different definitions for flow methods and the type of monitoring used, they can get rapidly confusing. It seems that definitions may slightly vary from authors to authors. In this section we will describe a range of flow methods, trying to use a consistent nomenclature.

2.2.1. Online monitoring

Online monitoring is the main method we have used during this work to monitor reactions. Generally, online monitoring refers to a continuous observation of the medium (here reactive medium) without interruption and as much as possible in a non-invasive way. In chemistry, it often refers to flow methods. Online monitoring can refer to virtually any analytical method, and here we will focus on its use with NMR. In NMR specifically, it can be defined as a flow of the studied medium in a loop-like system where the medium, whole or part of it, is flowed back and forth from the benchwork to the magnet.

2.2.1.1. Flowtubes, historical aspects

In this work we mostly used an apparatus known as the flowtube made and sold by Bruker in their InsightMR package. This flowtube is mostly inspired by the work of Foley *et al*.[98] Before going into an in-length description we will briefly review older apparatus, that could be considered the ancestor of our flowtube. To our knowledge one of the first attempt to achieve online monitoring with NMR dates from 1982.[113] The apparatus is already quite mature, as they use big reactor (up to 6 L) to mimic the big tank that are used in industrial plants. The sequence along with pump usage is summarized in figure 2.8. The apparatus consists of a by-pass pump that brings the liquid to the flowtube and back to the reactor. This by-pass pump is quite powerful in order to fill and empty the by-pass loop of 100 mL in 6 s and should be stopped during the NMR experiment. This time, needed for emptying and refilling the loop, defines the possible temporal resolution. Due to NMR limitations, mostly the need for a build-up magnetization and to wait for all flow effect to dissipate, they need to wait 10 s then the experiment is done with solvent suppression for both ^{31}P and proton for a duration of 95 s; then the medium is flown again back and forth for 30 s to have a good homogeneity. The true time resolution is then 135 s, and the result of the monitoring is shown in figure 2.7.

This apparatus is astonishingly modern for its time and even uses a computer to control another pump called the dosing pump, that control intake of reactant, hinting at a possible foreseen retroactive loop control. It uses ^{31}P and ^{1}H NMR to monitor an important industrial reaction,[114] the synthesis of retinoic acid (colloquially vitamin A) by a Wittig reaction, the reaction is figure 2.8 and the monitoring's result are shown in figure 2.9. If we refer to our first definition, the online monitoring should be as uninterrupted as possible. Here the need to stop the flow for 135 s for NMR experiment is a major drawback.

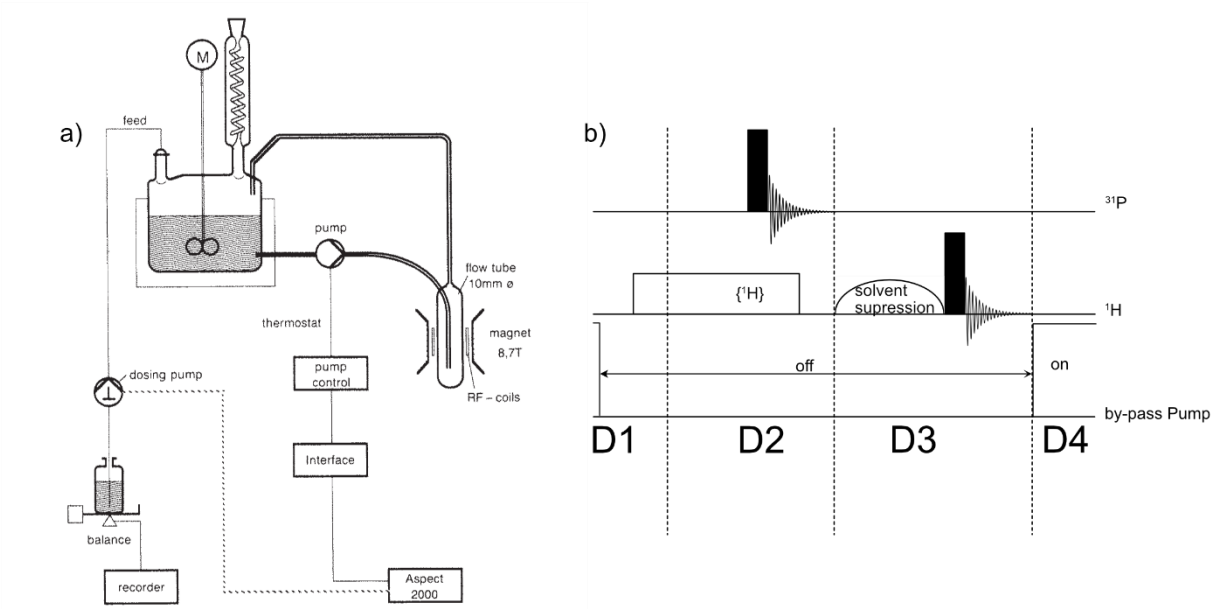

Figure 2.7 : A) Schematic diagram of a chemical reactor coupled to a 360 MHz Bruker NMR spectrometer. The dosing and by-pass pumps are controlled by the Aspect 2000 computer via interfaces. Reactor volumes between 0.5 and 6.0 l are available, large enough in comparison with the by-pass volume of approximately 0.1 l. A complete circulation of the reaction medium takes about 6 s. Commonly used control devices such as a thermocouple, pH electrode, gas-flow detectors and the corresponding chart recorders are installed but not shown in the diagram. B) Pulse sequence for ,$^{31}P/^{1}H$ measurements: D1, build-up time of the spin equilibrium, 10s; AQ, acquisition time for ,^{31}P and ^{1}H, 93 s; D3, solvent saturation, and D2, circulation time, 30 s. Adapted with permission from Neudert et al[113] Copyright © 1986 John Wiley & Sons, Ltd.

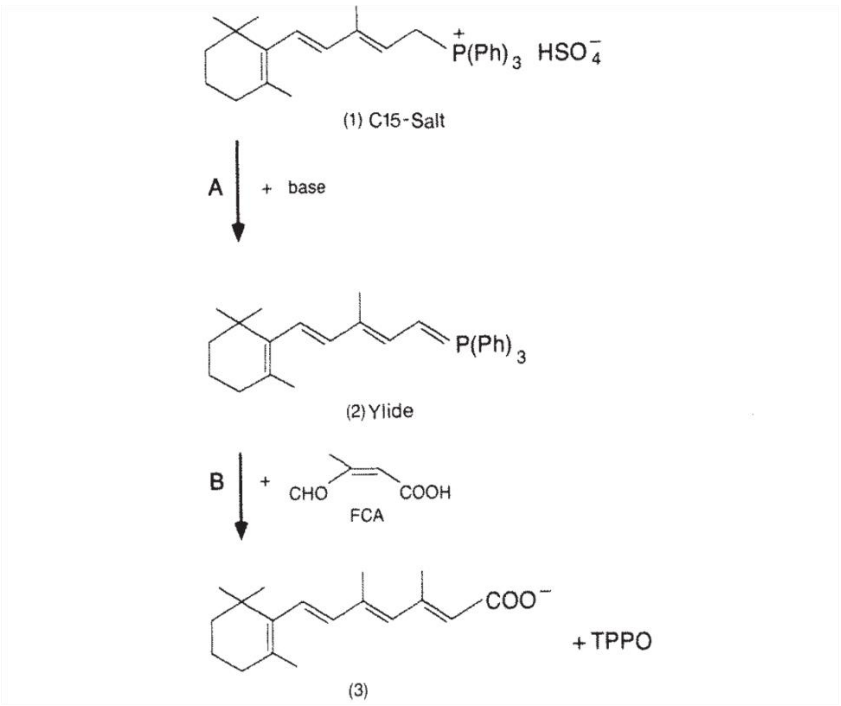

Figure 2.8. The last two steps of the retinoic acid synthesis. Step B, a semi-batch reaction, was investigated by ^{31}P NMR. Compounds 1 and 2 and TPPO are observable simultaneously. Adapted with permission from Neudert et al[113] Copyright © 1986 John Wiley & Sons, Ltd.

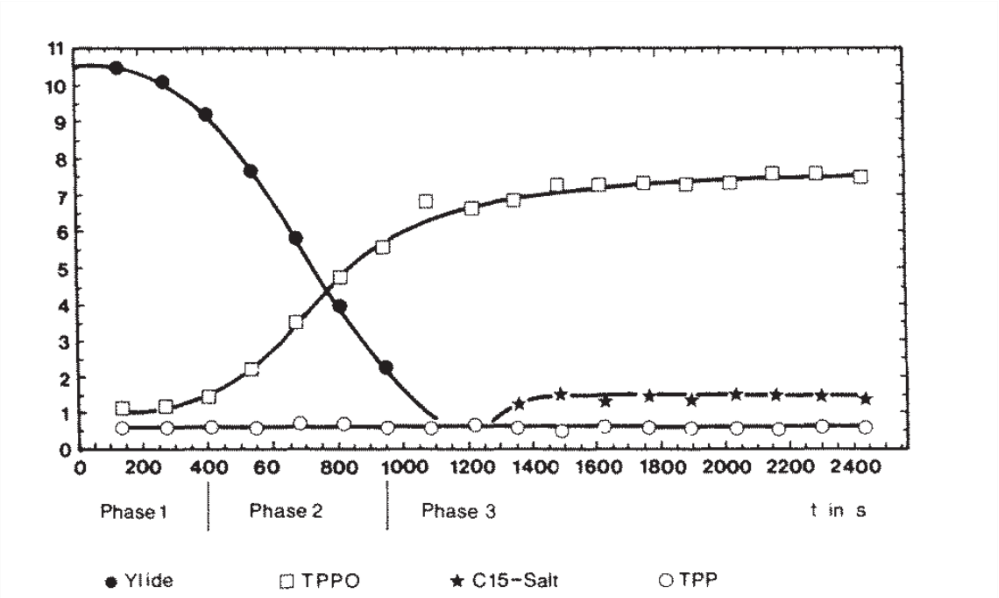

Figure 2.9. Areas of the ^{31}P resonance signals as a function of time. The integral values are given in arbitrary units and have not been corrected with the corresponding response factors. After correction, the sum of the 31P signal areas at the beginning is equal to the sum at the end of the reaction. Phases 1 and 3 belong to the region with non-linearity between the rate of FCA addition and the reaction rate, whereas during phase 2 the reaction rate is proportional to the addition of FCA. Adapted with permission from Neudert et al[113] Copyright © 1986 John Wiley & Sons, Ltd.

The work of Bernstein *et al*. described in Ref.[115] in 2007 also aimed at large-scale reactors. Their aim was to re-create large-scale conditions at the benchwork. This is useful in pharmaceutical companies, in order to closely monitor impurities and perform overall quality control. Large-scale reactors can be hard to sample, so doing the reaction at the benchwork scale on the same condition is a good way to analyse it in real time. To do that they create a benchwork-compatible reactor that can mimic and adjust the reaction condition, stirring, temperature, pressure, air exposition etc. The reactor is linked by PTFE capillaries to the NMR magnet. The apparatus, shown in figure 2.10, is used to monitor two kinds of reactions, one being in a classical setting but with a new green solvent,[112] the other being in heterogenous conditions. Scaling up is relevant for these two types of reactions.

The team chose a special flow-NMR probe usually employed for LC-NMR of supercritical fluid, the pressure and flow-speed they reach being incompatible with regular (and already specific) flow-probe. This can be considered as a drawback as those probes are not that readily available. The condition of pressure and temperature they want seems incompatible with more common NMR gears, which can be a huge drawback, not all labs have use for such specialized probes.

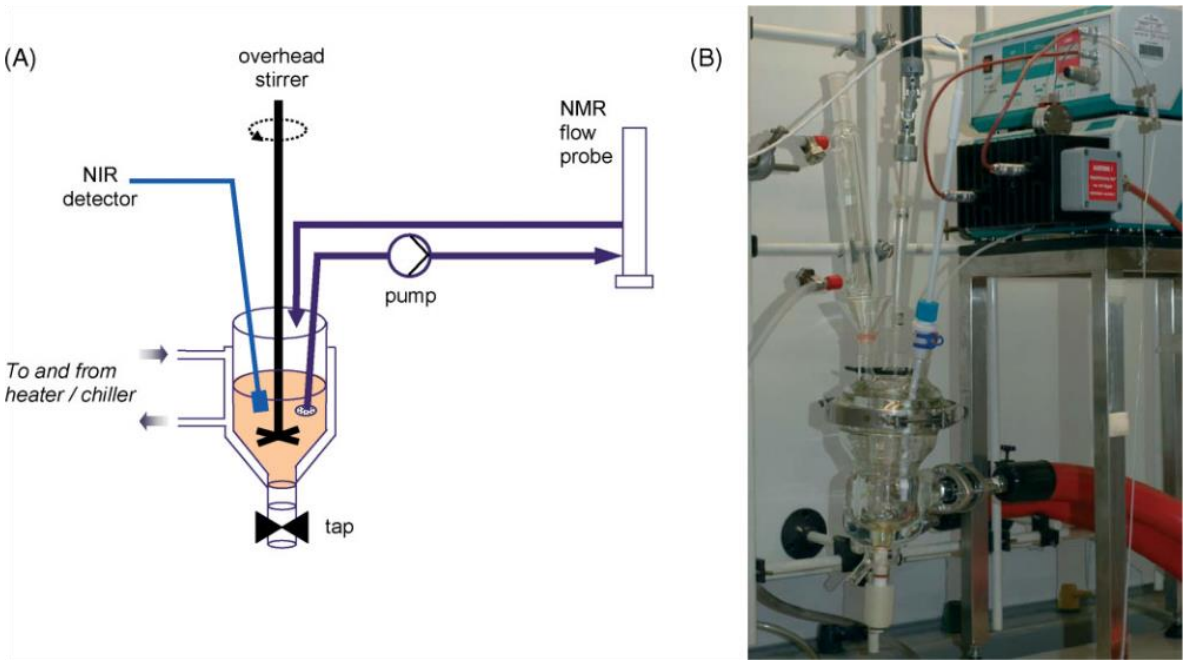

Figure 2.10. The flow-reactor apparatus shown (A) as a schematic and (B) a photograph. Adapted with permission from Bernstein et al[115] Copyright © 2007 John Wiley & Sons, Ltd.

Moving closer to the present in 2010 Khajeh et al.[116] did make an apparatus for flow NMR. Their focus is on the part that goes into the probes rather than the piping. They aim at making an apparatus that is compatible with various flow conditions, either stop-flow or continuous, in a relative simplicity for non-flow specialist. They call it the flowcell and the whole diagram of it is shown in figure 2.11. It consists of various capillaries that can be dipped into the reacting medium and bring the medium to the magnet. In the magnet lies a normal NMR tube that has the flowcell headpiece seen in figure 2.12, this headpiece has inlet and outlet capillaries as well as pieces to fit the top of the tube/spinner. The apparatus seems to aim at providing an easy access flow reaction monitoring. It includes anti-leak safety, a liquid sensor linked to a safety system that can cut the flow in case of leakage. It also includes spacers and stabilizers for the capillaries to stay still while the reaction happens, number 19-20 on the Figure 2.11. All those systems show a thoughtful process that seem to simplify or avoid lot of flow-related liquid handling challenges. The apparatus is tested in various condition including heterogenous reaction, done by using a filter to stop the solid to enter the flowcell. Interestingly it is one of the first system that is aiming to handle small volumes of liquid, excluding micro-fluidic approach, as the whole apparatus need a volume in the scale of millilitres. A problem may rise nonetheless since the capillaries that come from the medium to the magnet seems a bit bare. They might not be protected enough, especially in terms of temperature. Capillaries this size are known to change temperature very fast because of their small radius and the small volume per section.[117] Nonetheless the apparatus seems sturdy and well-thought enough to be aimed at non-NMR or non-flow chemists.

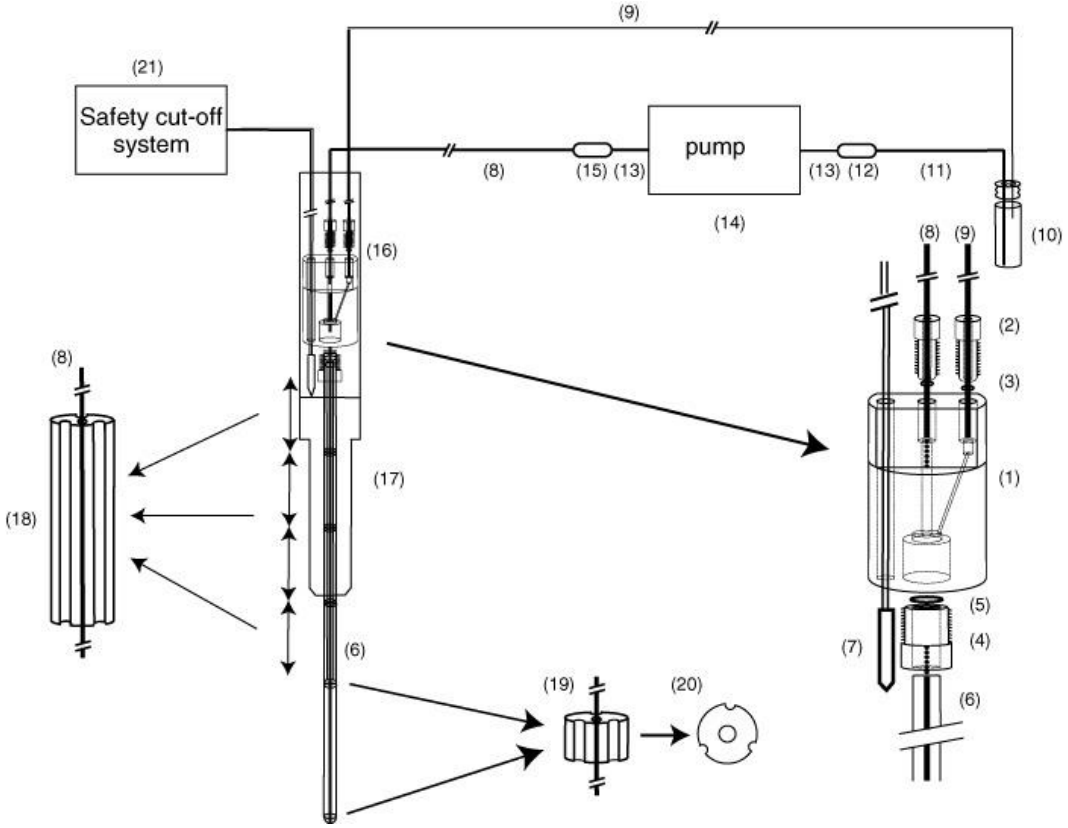

Figure 2.11 : Structure of the flow system used. (1) flowcell headpiece; (2) inlet and outlet pipe bushes; (3) and (5) O-rings; (4) NMR tube retaining bush; (6) NMR tube; (7) optical liquid sensor; (8) inlet pipe; (9) outlet pipe; (10) reaction vessel; (11) reaction vessel outlet pipe; (12) and (15) unions; (13) PTFE peristaltic tubing; (14) peristaltic pump; (16) glass tube, glued to turbine (17); (18) long grooved PTFE spacers; (19) short grooved PTFE spacers; (20) cross-section of spacers; (21) safety cutoff. Adapted with permission from Khajeh et al[116] Copyright © 2010 John Wiley & Sons, Ltd.

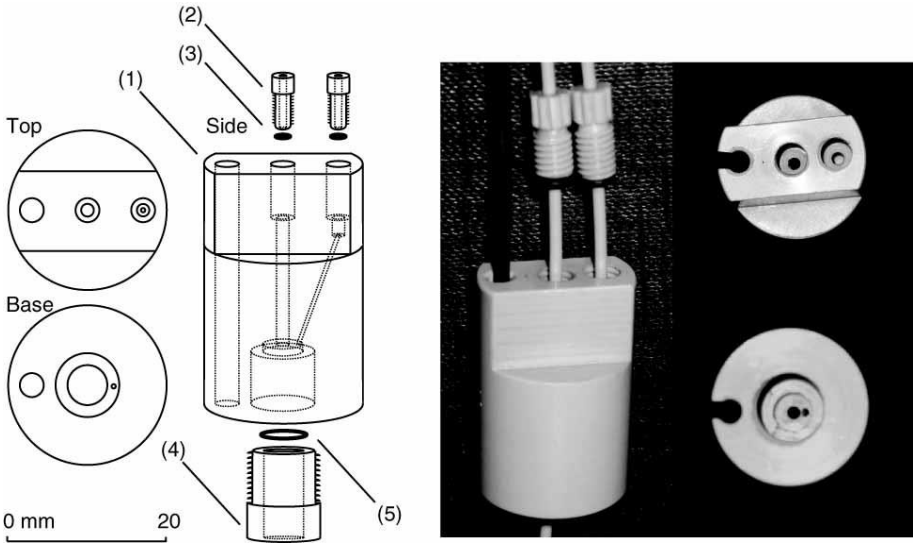

Figure 2.12: Scale drawing (left) and photographs (right) of the flowcell headpiece assembly. (1) headpiece; (2) inlet and outlet pipe bushes; (3) and (5) O-rings; (4) NMR tube retaining bush. The left part of the composite photograph shows the inlet and outlet pipes and their respective bushes and O-rings, together with the liquid sensor cable, the latter and the inlet pipe running continuously through the headpiece. The top right shows the top view, and the bottom right the bottom view, of the headpiece. Adapted with permission from Khajeh et al[116] Copyright © 2010 John Wiley & Sons, Ltd.

2.2.1.2. Rapid-injection and stop-flow

Stop-flow, in contrast to continuous flow, refers to methods where the flowing is not perfectly continuous throughout the line. Here we will refer to stop-flow only when done in a non-loop or in-line fashion and if it includes systems that are meant to stop actively the flow. This definition aims at differentiating stop-flow from turning off the pump briefly.

The rapid-injection strategy is a strategy where the medium injected from a suitable place and put in the NMR tube in a rapid fashion. It often has flow-related challenges like having to wait for homogenization of the solution. Those two methods, stop-flow and rapid injection, are often used to see or monitor species that are either short-lived. Note that so called stopped flow NMR methods are as old as 2D NMR.[118]

To illustrate the rapid injection NMR method we will use an example from one of its pioneers.[119] The goal is to see a particularly unstable intermediate known as a primary ozonide and see if the secondary ozonide is present, according to the scheme shown in figure 2.13. The apparatus is quite complex and consists of a syringe's-controlled piston that pours the liquid from pores that limit the motion of liquid and its inertia. The apparatus rests on the top of the shim-cannon, with the NMR tube already in the magnet. The part of the reaction that is supposed to be refrigerated lies already in the tube, here the ozone solution. The other reagent (tetramethylethylene) is injected quickly in a controlled way. As the solution is poured, an automatic switch starts the NMR experiment. The result is a reaction at -85°C within the spectrometer. Figure 2.14 shows a time series of spectra obtained during the monitoring experiments. The authors estimate that they need a minimum of 92 ms to make one spectrum and waiting time of 40 ms for the homogeneity within the solution. They estimate that they can obtain 16 spectra per injection and need 3 injections for their study. The volume and reagents being well controlled, several injections were done and their data regrouped to follow the kinetics of this reaction. The modest spectral resolution comes from the very short time of acquisition, 72 ms (2K point per spectra) and the homogeneity trouble due to fluid motion.

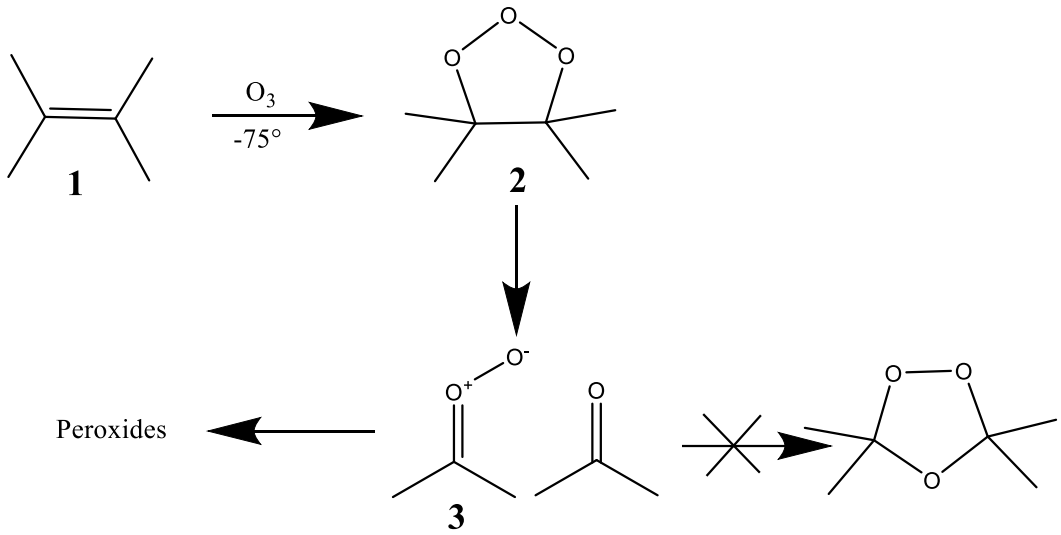

Figure 2.13 : the oxonolyse reaction. Adapted with permission from McGarrity et Prodolliet[119] Copyright © 1984 American Chemical Society

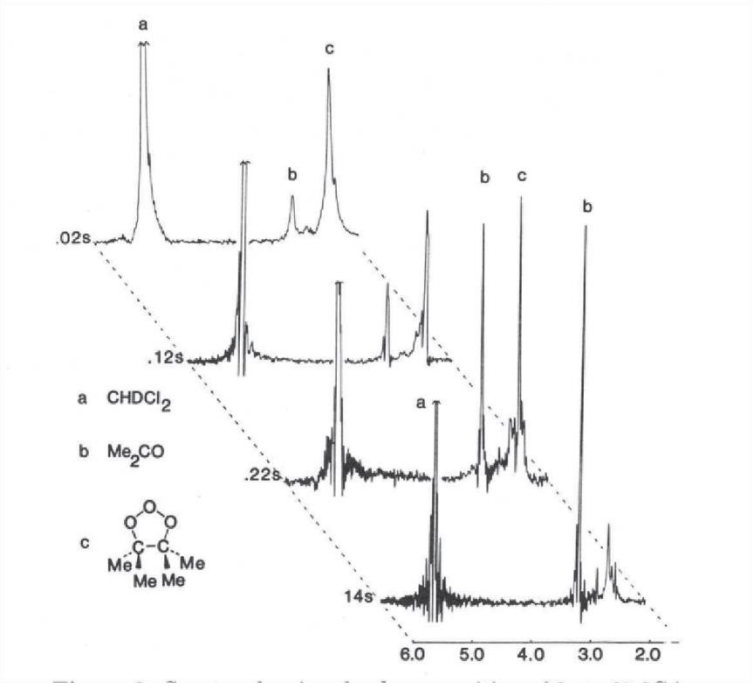

Figure 2.14 Spectra showing the decomposition of **2** at -85°C in CD_2Cl_2. Adapted with permission from McGarthy et Prodolliet[119] Copyright © 1984 American Chemical Society

The study has several features that could be considered unusual in kinetics, such as using multiple identical reactions to make one plot. The apparatus is heavy, and sits on top of the magnet, which may seem inconvenient, but this allows to have a pre-magnetized sample without waiting time. They are looking for new intermediate and species, using NMR as a qualitative rather than quantitative tool. From Figure 2.14 you can see the peak of the species labelled C, this peak rises quickly in the first seconds of the reaction and then becomes very faint. This indicates the formation of the first ozonide, however the rearrangement that can lead to secondary ozonide is not seen. This can be used as strong hint that it is not formed within those conditions, probably due to the lack of stabilizing effect from

the methyl substituent. Seeing the peak of such unstable intermediate that can only be spotted in such harsh conditions was an impressive feat and indeed to our knowledge one of the first-time short-lived intermediates were seen by high-field NMR.

The next example also uses stop-flow but it is a much more modern setup.[120,121] The general diagram of typical modern stop-flow device is showed in figure 2.15, where one can see that the reagents are stored in different syringes that allow a precise yet quick delivery. The flow is stopped quickly by the stopping syringe mitigating the motion of the fluid while the analysis is proceeding. The aim here is to illustrate the capability of a stop-flow cell to see the very beginning of a reaction while providing good temperature and mixing conditions. Dunn et Landis[120,121] use this device to study a polymerization reaction, that is sensitive to air and moisture, which also shows that the probe is air and moisture-free. The initial conditions of the reaction are important and can change the kinetic model. Using different techniques including stopped-flow, quenching the reaction at different point and retrieving the samples for other analyses (gel permeation chromatography mostly), they discuss a new model.

In figure 2.16 we see the epimerization of rac-lactide to meso-lactide in the first second of the reaction that play an important role on the mechanism. Indeed, they state that this epimerisation is in a kinetic competition with the polymer formation. This effect is only seen in the beginning of the reaction and will have a decisive importance on the rest of the mechanism and on the monomer availability during the reaction. This ability to see such rapid epimerization at the very beginning of the reaction, underlines the importance of stop-flow NMR.

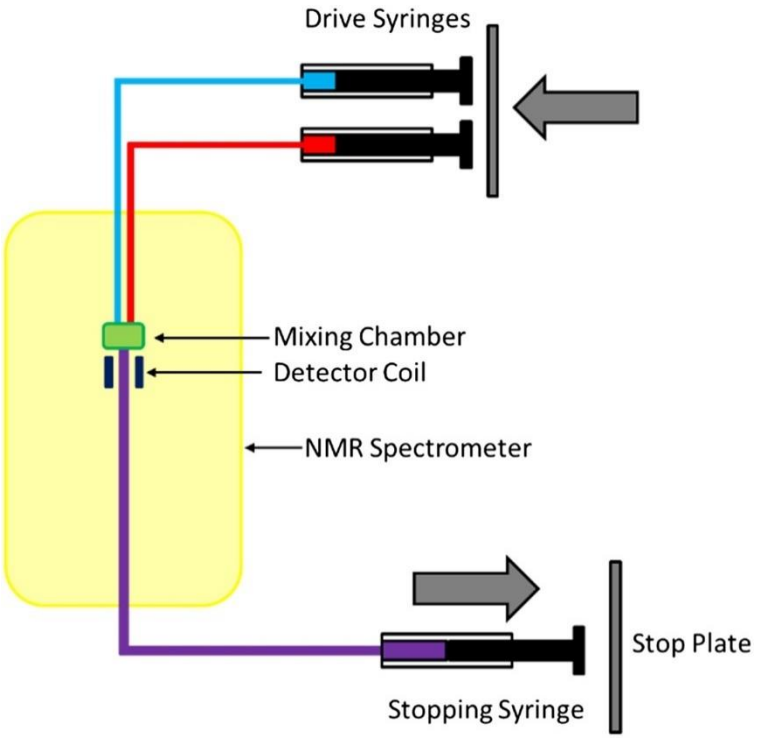

Figure 2.15 taken from Generalized diagram of typical stopped-flow NMR instrumentation. Adapted with permission from Dunn et Landis[120] Copyright © 2016 John Wiley & Sons, Ltd.

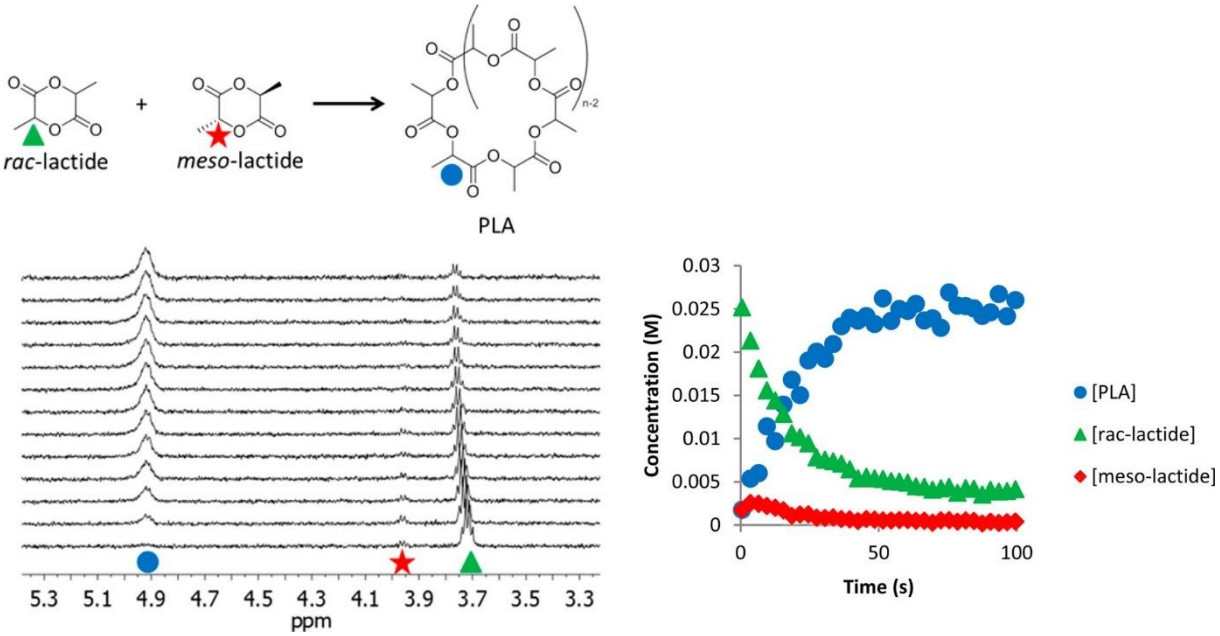

Figure 2.16 Direct, in situ [the author state in the text that it is "monitored using SF NMR spectroscopy" SF NMR being Stopped-Flow NMR] observation of meso-lactide growth and disappearance during time course of reaction in toluene at room temperature. The bottom spectrum is at reaction time 1 s, with each subsequent spectrum 9 s later. Concentrations plotted with reaction time clearly show growth of meso-lactide and its subsequent disappearance. Initial concentrations: 30 mM l-lactide; 6 mM IMes. All concentrations are calculated from integration of an unreactive internal standard, bis(trimethylsilyl)benzene (BTMSB). No meso-lactide is observable by NMR prior to addition of catalyst. Adapted with permission from Dunn et landis[121] Copyright © 2017 American Chemical Society

Finally, let us consider an example of stop-flow NMR that is a bit more exotic from the point of view of reaction monitoring. In the work of Keifer *et al.*[122] the goal is not to monitor a reaction as it

unravels, but rather to analyse quickly the outcome of a large number of reactions, using combinatorial organic synthesis of a chemical library. Different cyclic anhydrides were made to react with various primary amines in a combinatorial fashion. The result is placed in wells (one compound per well) with solvent. The content of each well is flowed in an automated way into the NMR magnet using a LC-NMR probe, analysed and handled back to its well. Figure 2.17 shows the apparatus, with the reaction and handling of the wells happening in the Gilson 215 liquid handler, and the flow regulated by N_2 gas (50-100 psi ≈ 3.4-6.9 bar). The flow stops during the acquisition and allow a very efficient handling of the samples. The mains advantages versus the classic NMR automation, with a robot that handle the NMR glass tubes, are less costly container, lesser volumes are needed and overall a better reliability as glass-tube NMR automatic-sampler are known to break tubes once in a while.[123]

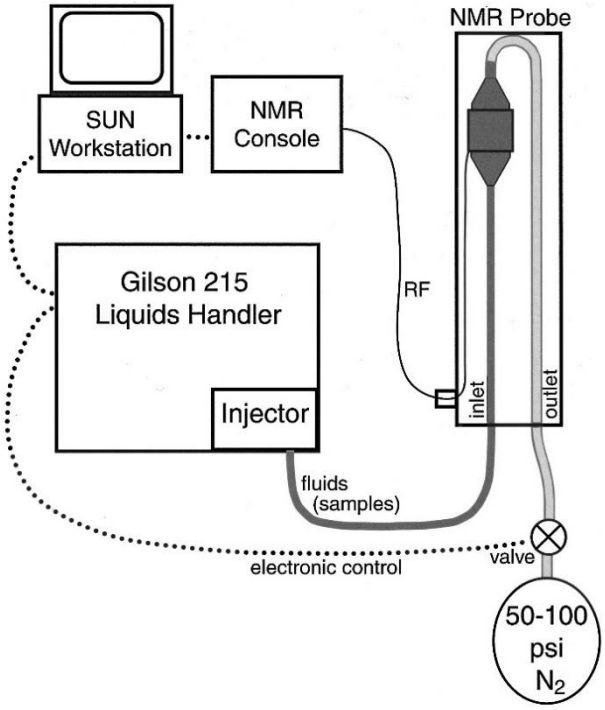

Figure 2.17: A block diagram of the VAST (versatile automated sample transport) DI-NMR (direct-injection NMR) system. II.1.3.2.1 Continuous-flow in-line monitoring. adapted with permission from Keifer et al.[122] Copyright © 2000 American Chemical Society.

2.2.1.3. Continuous flow in-line monitoring

In-line flow monitoring, like online monitoring, consists of monitoring a medium on flow, it differs from online monitoring in that the medium is not analysed in a loop-fashion. The sample once analysed might be discarded or retrieved for other purposes.

Continuous in-line monitoring is notably used to monitor the outcome of reactions that happen on flow. It is less common at high field but it has become a conventional NMR method at low field. Flow chemistry is a rapidly expanding area, and is particularly beneficial for reactions such as heterogenous catalysis where the supported catalyst is fixed in some part of the line, and reaction

triggered by a physical mean whether heat or light-wave and a combination of both. This is by no mean an exhaustive list but it corresponds to our knowledge to the most common cases.

Heterogenous catalysis in flow chemistry is an important topic, for applications that include chiral synthesis and hydrogenation. In this approach, a solid catalyst is put in the line, often supported on a resin/plastic or charcoal.[124–126] Tijssen et al.[124] have developed an in-line apparatus for NMR monitoring of hydrogenation reactions. The hydrogenation of alkynes can be a problem especially if there are multiple oxidation/reduction states (like alkyne to alkene to alkane) or sites that can be reduced. The hydrogen pressure, catalyst and other parameters should be adjusted to get the desired result. In this case in-line monitoring seems like an especially well fitted method. The principle, summarized in Fig. 2.18, is conceptually simple: a mix of liquid, the reaction medium, and gas, the di-hydrogen, is pumped through a solid catalyst cartridge then into an NMR probe, in the same line. The apparatus allows to monitor the quantity of dissolved hydrogen which is the important parameter regarding the hydrogenation. The authors tested it with 3 compounds having different possible states and confirm the importance and possibility to monitor the amount of hydrogen in the solvent in flow by NMR. This process allows the whole line to be under 5 bar of pressure on a flow speed of 80 µL/min in a specialized microfluidic NMR probe.[127] We are not going to review here the benefit of microfluidic but it is especially useful in in-line process because it allows very precise handling of small volumes at very well monitored pressure.

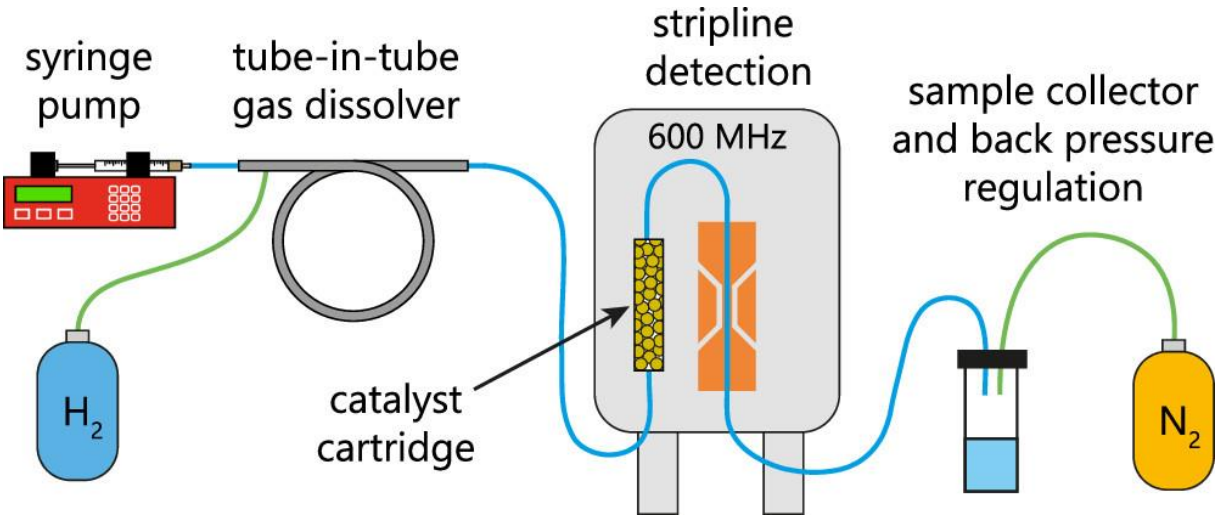

Figure 2.18 Schematic drawing of the stripline NMR reaction monitoring setup for heterogeneously catalyzed hydrogenation reactions. From Tijssen et al.[124] Anal. Chem. Licensed under CC-BY-NC-ND 4.0

Another use of continuous flow in-line monitoring is when the reaction is triggered or trigger a physical stimulus like heat or light. Reaction that are exothermic usually have complex kinetic as the heat created by the reaction accelerate it. To better control this having a small volume of reaction at once, as is the case in the capillaries used in flow chemistry, can allow for a better monitoring and control of the temperature. Schotten et al.[128] have shown such application, using the insightMR flow

tube in an in-line fashion. The exothermic reduction of $TMSCF_3$ to $TMSCF_2H$ was conducted in a capillary good for heat control and monitored using high ^{19}F field NMR.

The in-line monitoring is also quite popularized by new generation of medium-field benchtop spectrometers.[129] The relative portability of the spectrometer makes it highly useable under benchwork in a setup that does not require to be a flow expert or an NMR one which is highly valuable for synthesis chemist. Several benchtop spectrometers include flowing apparatus such as a flow-cell in their standard configuration. The main drawback of benchtop spectrometers is limited sensitivity and resolution, but this can be counter-balanced by the ease of analysis and the fact that reactive medium is often well concentrated.

2.2.1.4. The Bruker InsighMR flowtube

We have described the ancestor of our apparatus and we tried to highlight their advantages and disadvantages. The commercial Bruker InsightMR flowtube is a variation of the device described by Foley et al.[84] It aims to be as efficient and capable as earlier devices while being more accessible to chemists that are not flow specialists. It includes several features such as a special NMR-tube able to sustain up to 8 bar of pressure, other feature includes a thermoregulation that allow to thermostat the reaction within the capillaries, it is also very well fitted for the Bruker spectrometer, diverging little to a standard NMR analysis. One of the drawbacks is the lack of system to monitor pressure or leaks as the device is covered in a jacket any leak could be hard to detect before it became catastrophic (liquid in the probe).

We have already seen a few of its use in literature such as Dunn et Landis[108] and Foley et al[84,118] that developed the apparatus, Said et al.[117] also reviewed the engineering aspect of this flowtube, underlining the poor quality of the by default pump. Recently Hall et al.[130] used the flowtube to get chemical insight into the mechanism of a Noyori–Ikariya-like asymmetric hydrogenation. Their study focuses on the analysis of ruthenium catalyst that allow a transfer of hydrogen. They are able to see hydride species which are usually transient very reactive species through the use of the flowtube with 1D ^1H NMR. The same team previously worked on practical aspect of this device[131] for reaction monitoring, illustrating its usefulness and making it available for a broader audience. Recently the flowtube has been used in various study including important topic like C-H activation[132] or sulfonyl compounds.[133]

Another study using the flowtube is that of Hall et al.[134] in the conventional setting of this apparatus the flowtube is used as a way to observe continuously an ongoing reaction using flow. The study underlines one of the main advantages of this setup which is availability of the medium. If we look back at part 1 and the study of Dolinski *et al.*[111] they have photochemistry too and because the medium is not easily available they use a smart way to have illumination but also to control the reaction

with a photoswitch, while information rich it is not realistic benchwork condition. Here the goal is to have realistic condition NMR analysis with the medium available. The reaction is shown in scheme 2.1, compound **1** can give three products with the help of a catalyser that is light activated, Eosin Y.

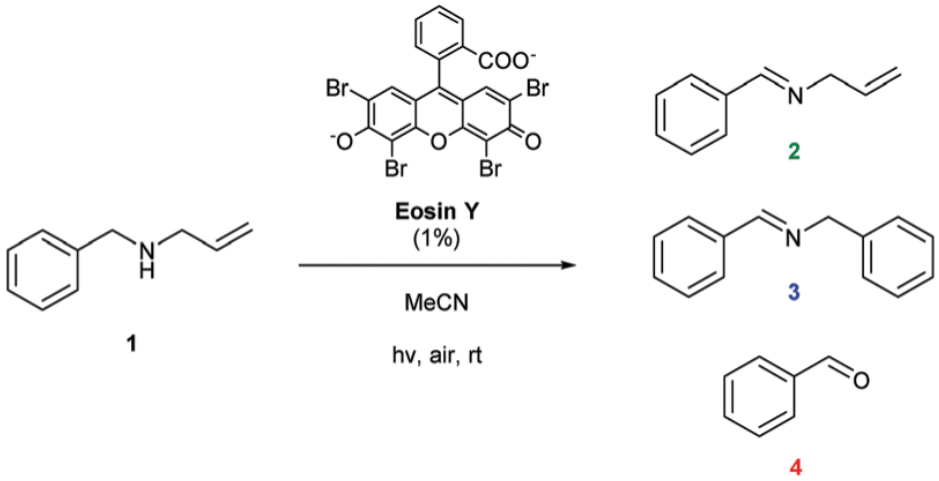

Scheme 2.1 Structure of Eosin Y and photocatalytic oxidation of allylic amines. From Hall et al.[134] Chem. Comm. Licensed under CC-BY-NC 3.0

They are interested in the reaction pathway that leads to the formation of the products. Eosin being known to form oxygen singlet under light they also question the importance of air and oxygen in this reaction. They test their hypothesis by using online monitoring and thus can monitor the impact of the condition on the reactivity live. To do so they try to activate light at some time in the reaction and observe that product seems to form, and reactant to disappear only at the interval where light is shined upon them. It indicates the importance of light for the making of any of the three products as seen in Figure 2.19, also that the active species that allow the reaction to happen is transient, short-live and only exist under the light.

Another interesting thing that highlights the advantages of having the medium accessible is to test the air condition. As they try casting light on the sample on anaerobic and aerobic condition and can monitor the result with no interruption, as seen in figure 2.20. This would have been complicated otherwise as aliquoting a medium in pure anaerobic condition may prove to be a hard task. They conclude that **2** and **3** are created in anaerobic condition but not **4** which make sense as **2** and **3** are hydrolysis resistant. Those manipulation of the reaction medium allow to propose a reaction network for this example that start by the formation of **2** that can react with the reactant to form **3** or get oxidized to form **4.**

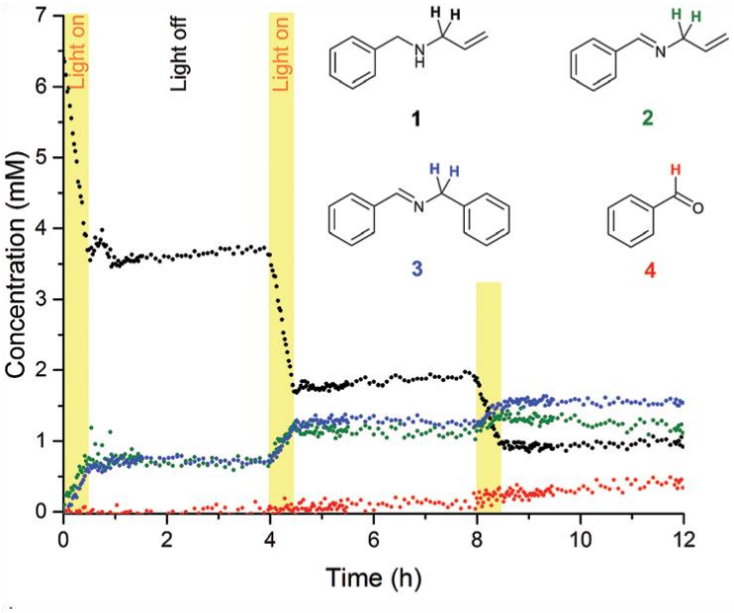

Figure 2.19 ^{1}H FlowNMR reaction profiles of N-allylbenzylamine (1) in MeCN (6.4 mM) at 20°C in the presence of Eosin Y catalyst (1 mol%) under chopped green LED illumination (633 mW) to form **2**, **3** and **4** (100 mL, 4 mL/min flowrate, WET solvent suppression, 1.46 s acquisition time, 3 s relaxation delay, 12 scans). From Hall et al.[134] Chem. Comm. Licensed under CC-BY-NC 3.0

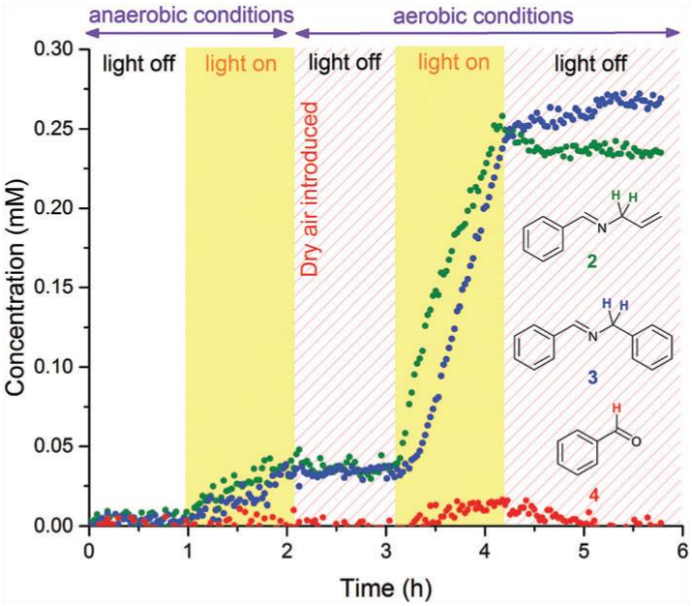

Figure 2.20, ^{1}H FlowNMR reaction profiles of N-allylbenzylamine (1) in MeCN (6.4 mM) at 20°C in the presence of Eosin Y catalyst (1 mol%) under chopped green LED illumination (633 mW) and different atmospheres (argon to dry air) to form **2**, **3** and **4** (50 mL, 4 mL/min flowrate, WET solvent suppression, 1.46 s acquisition time, 3 s relaxation delay, 16 scans). From Hall et al.[134] Chem. Comm. Licensed under CC-BY-NC 3.0

3. Fast DOSY NMR sequence

Reaction monitoring by NMR classically relies mainly on ^{1}H 1D experiments. The reasons for that are simplicity of acquisition and processing, speed, and straightforward access to concentrations and structural information. Yet 1D methods are limited and have known problems such as overlapping, especially with ^{1}H and usually does not allow efficient assignment of peaks especially in the case of mixture or complex molecule. To go beyond those limitations 2D NMR methods are used to gather more information. Yet they remain underused outside of their routine usage for the characterization of purified products, the main reason being their duration. Experiment duration is a key aspect for reaction monitoring, as it sets a limit on the range of kinetics that can be studied. A series of means to accelerate 2D NMR experiments have been described, with reaction monitoring as one of the motivations for their development. We will here propose a brief overview of those methods, focusing on DOSY NMR experiments.

3.1. Why do classic DOSY experiments take time?

Consider the simplest possible 1D NMR experiment: the pulse-acquire experiment. The parameters that define its duration are the number of scans, the acquisition time (which governs the resolution) and, if multiple scans are collected, the inter-scan delay needed for the recovery of longitudinal magnetization. The simplest 1D experiment, if sensitivity is sufficient, requires just 1 scan, with an acquisition time that can range from a few tens of milliseconds to a few seconds. Any conventional 2D NMR requires more time, because increments are needed to construct the so-called indirect dimension. Those increments are acquired consecutively, and separated by inter-scan delays. Another issue is that 2D experiments select complex coherence transfer pathway. Several methods can be used for this, and if phase cycling is used then multiple scans need to be acquired for each increment.

In classic DOSY experiments, several increments are collected in order to have enough points for the diffusion fitting, and phase cycling is used to select the desired coherence transfer pathways. In the STE experiment described in part 1, a minimum of 8 scans per increment is needed. As for the number of increments, it is highly dependent on the required accuracy and on the spread of diffusion coefficients within the sample. To our knowledge the number of increments usually varies from 8 to 32 for standard diffusion-NMR sequence such as the stimulated-echo (STE) sequence. Accurate fitting of the data also requires that diffusion only attenuates the signals. If inter-scan delays are too small, different consecutives scans can yield a decrease in intensity due to T_1 relaxation not being complete. This will lead to inaccurate diffusion coefficients. Different methods exist such as using dummy scans to reach an equilibrium with a smaller inter-scan delay but they are also time-consuming. Considering all of these criteria together, and assuming that the sample is sufficiently concentrated so that signal

averaging is unnecessary, a typical experiment will have 8 x 16 scans separated by an inter-scan delay of about 5 s, resulting in an experiment time of around 10 min. Realistically speaking DOSY experiment average around 15-20 min extra delay coming from acquisition, dummy scan and experiment time. When the DSTE pulse sequence is used, to compensate for convection effects, the minimum duration of the experiment is doubled, as 16 scans per increment are needed.

3.1.1. QNMR and flow effect

One of the most important ideas of quantitative NMR is to get a proportionality coefficient between the peaks and the spins they come from. The goal is to measure the relative quantity of molecules in a sample. It is an important concept to do kinetics by NMR as the goal is to see changes in those quantity indicatives of the species relative concentration. This can be written $I_x \propto N_x$ so $I_x = \mathrm{K}_x \times N_x$. Where K_x are parameters related to the spectrometer, I_x is the signal intensity (measured preferably in peak area), and N_x the number of nuclei.

For the relation of quantitativity to work a few conditions are necessary. The main condition that one will encounter usually is T_1 related. The relation between recycle time being $\approx 5 \times \mathrm{T}_1$ for the magnetization to be back to equilibrium is important especially if scans are done in sequence. Note that other problems may arise involving NoE effect, shaped pulse, decoupling etc. We are not in a setting where those will matter and the level of accuracy needed for relative concentration usually does not need to account for them.

The recycle time can be increased to meet the T_1 relation thus lengthening the experiment. Other way such as dummy scans can be used. The problem is that each site has its own T_1 value and sites with extreme T_1 may break the condition of quantitativity under rapid sequence of scans. This could explain why a lot of kinetics studies from the literature mostly focus on one site to access the concentration of a molecule. As a site well identified both in NMR terms (T_1, SNR…) and checked for being indicative of one compound only, is enough to access the molecule concentration.

Other parameters are important for the quantitativity of NMR such as a sufficient acquisition length and number of points. Good practice of gain, tunning and matching. Overall, a signal of good quality with sufficient SNR… Those parameters albeit important are usually relevant in our NMR condition anyway and the level of quantitativity wanted will not demand to look deep in those parameters.

These phenomena are relatively straightforward in normal condition and are usually responsible for the lengthy duration of most NMR experiment. Indeed, the waiting time need to be applied both between experiment but also between scans/increments in the case of a 2D NMR experiment. Hence, in the DOSY experiment the delay should be put between each scan. In general, for any 2D experiment or suite of experiment the spectrometer spend most of its time idle because of this waiting time.

The sample flow also has consequences for the recovery of the magnetisation. In a static NMR experiment, the sample is all the time at high magnetic field, and magnetisation relaxes towards its equilibrium value at high field, with a time constant T_1. In flow NMR, especially with shielded magnet, the time that the sample spends in a high-field region before excitation is more limited, and depends on the flow rate. Figure 3.1 show a schematic of an on-flow shielded spectrometer setup. Three area are there; area A before the magnetic field (B = 0); area B magnetic field is not the strongest (0 < B < B_0); area C magnetic field is B_0. The effective recovery delay, τ_B, becomes shorter when the flow rate increases. The condition that should be verified to acquire NMR spectra in quantitative conditions applies to τ_B rather that the recovery delay. For this reason, spectra that are acquired on flow are rarely acquired from fully relaxed magnetisation.

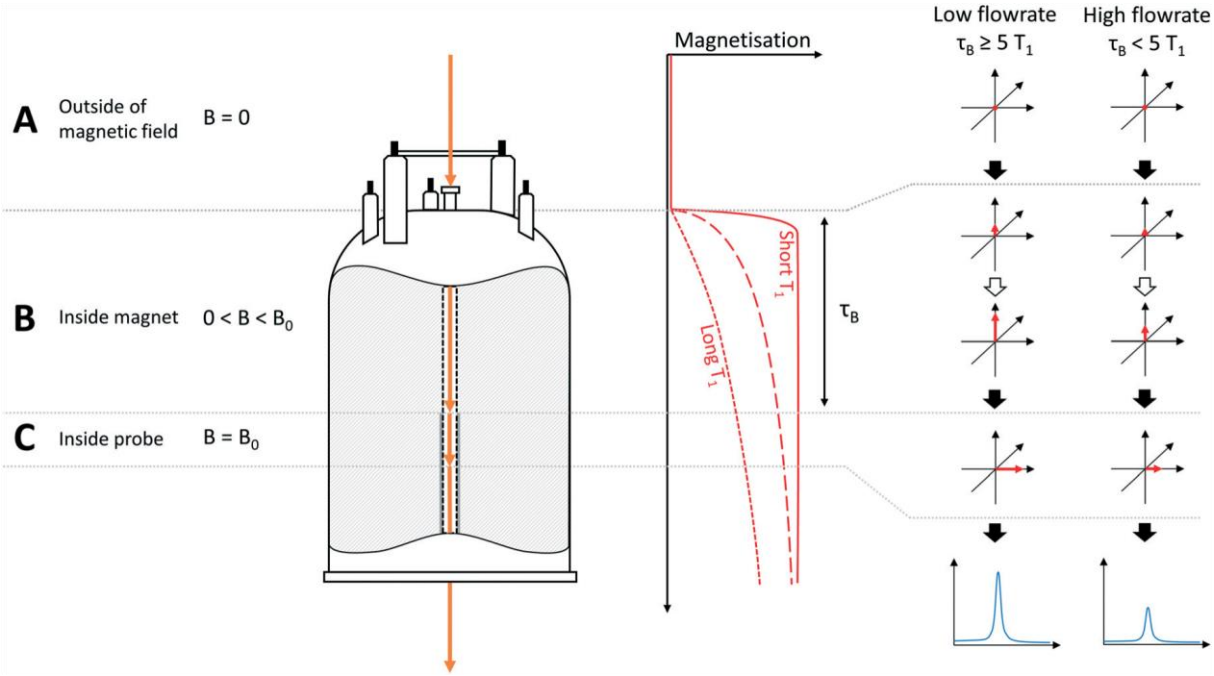

Figure 3.1 Schematic illustration of magnetization build-up effects in flow, resulting in non-quantitative results for nuclei with long T1 relaxation times or for high flow rates, where τB < 5 × T1. B = magnetic field strength, τB = residence time of sample in magnet prior to entering detector. Note: For the purpose of clarity, the sample is shown as exiting through the base of the instrument in this diagram, whereas in reality the sample returns by a path parallel to that it entered the instrument by (see Fig. 1). Stray field effects are ignored in this example. Hintermair and coworkers[135] propose a simple way to do so by using to formula one can straightaway correct the peak intensity as such. Reproduced from Ref. 135 with permission from the Royal Society of Chemistry.

The correction can be expressed as:

$$I_{corr} = CF \times I \qquad 3\text{-}1$$

$$\mathrm{CF} = \frac{\mathrm{I_{static}}}{\mathrm{I_{flow}}} \qquad 3\text{-}1'$$

With I the peak intensity/integral (depending on the case) and CF the correction factor. If needed one can also measure the apparent T1 on flow as such

$$\frac{1}{\mathrm{T^*_{1,flow}}} = \frac{1}{\mathrm{T^*_{1,static}}} + \frac{1}{\mathrm{Tb}} \qquad 3\text{-}2$$

Tb should be calculated as the residence time within the spectrometer (area B and C).

Note that on our case we take advantage of the unshielded nature of our magnet. Although it can be responsible for other trouble the unshielded magnet has a much larger area B that allow to have a build-up of magnetization akin to the one in static condition due to the elongated Tb.

To apply the correction a few things can be done. The author recommends to do analysis to measure static peaks integrals at the end of the reaction, the beginning and whenever intermediaries of interest form. This would allow to have a CF for every species and correct flow effect. Note that if those flow effect arise, it could be somehow beneficial. As the nuclei do not stay long enough to be fully magnetized, they also would leave too fast to suffer T_1 saturation. Applied correctly this correction would allow to increase the speed of experiment by reducing recycle time needed.

3.2. Methods to accelerate Diffusion experiment

Now that we have seen the factors that determine the duration of diffusion experiments, we are in a position to understand methods to reduce them and speed-up the process. We will describe the most commonly found and those that were considered (some only in theory) for this work.

3.2.1. Oneshot methods

The Oneshot (or one-shot) DOSY method was introduced by Pelta et al. in 2002.[136] It refers to a diffusion NMR sequence for which only 1 scan per increment is needed. This reduces the duration of an experiment from 10-20 min to ~1 min. The possibility to use just one scan per increment is achieved by getting rid of the phase cycling and using pulsed-field gradients instead for coherence transfer pathway selection. However, since PFGs are also used for diffusion encoding, CTP selection and diffusion attenuation can be inter-dependent and this needs to be accounted for.

In the work of Pelta et al. unbalanced gradient pairs are used to achieve simultaneously CTP selection and diffusion encoding. The sequence they used is shown in figure 3.2. It is based on a regular STE pulse sequence, in which the bipolar gradients that flank the 180° pulse are unbalanced by a factor called α. The bipolar gradients being unmatched, they will suppress any coherence that arise from the imperfect 180° pulse. Starting from this base, they later described several modifications of the pulse sequence. For example, in order to mitigate the effects of J-modulation they added a 45° pulse thus the name Oneshot45[137]. They also combined the Oneshot45 with the DISPEL (Destruction of Interfering Satellites by Perfect Echo Low-pass filtration) methods to suppress ^{13}C satellites without broadband decoupling[136]. Those methods show the good versatility and ease-of-use for this Oneshot method. it is interesting to mention that despite proof that it works better than conventional method in the same number of scans, to our knowledge few examples are reported using 1 scan per increment.

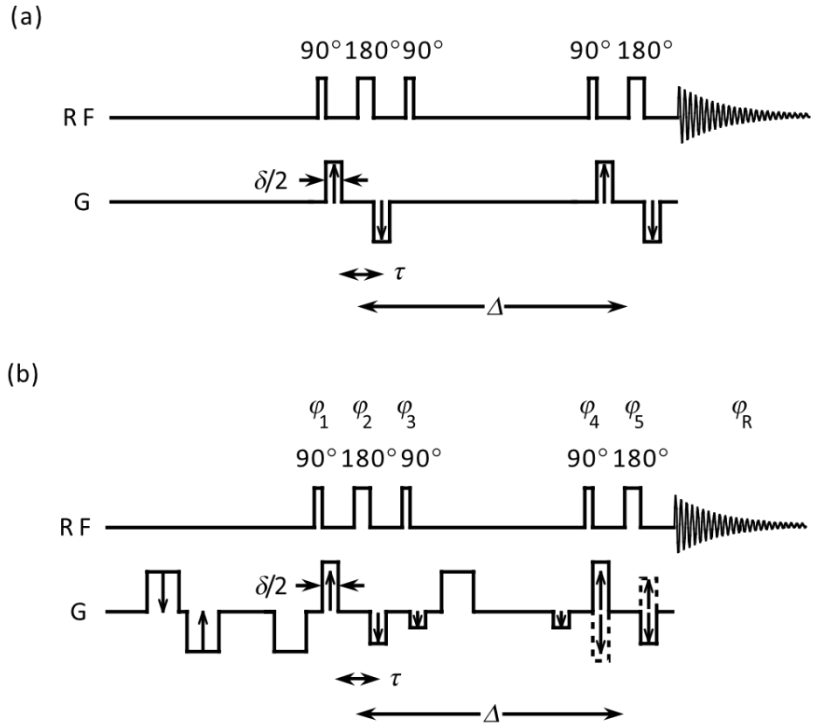

Figure 3.2. Radiofrequency (RF) and gradient (G) pulse sequences for DOSY. (a) Bipolar pulse pair stimulated echo (BPPSTE) sequence; (b) the proposed one-shot sequence using (solid line) the stimulated antiecho and (dotted line) the stimulated echo. The diffusion delay is the time between the mid points of the two diffusion-encoding periods and that between the midpoints of the antiphase field gradient pulses within a given diffusion-encoding period. The outward/inward facing arrows indicate gradient pulses which are incremented/decremented as the diffusion weighting is changed. The gradient prepulses in (b) are most conveniently given a duration of 2υ. Adapted with permission from Pelta et al.[136] Copyright © 2002 John Wiley & Sons, Ltd.

The use of PFGs for CTP selection in diffusion experiments becomes easier when more than 1 gradient axis is available. This was for example described by Sarkar et al,[138] who underlined the possibility to use other axes to have a better coherence selection/filter as well as different others possibility such as easy implementation of solvent suppression. It does not mention the possibility to use it in a oneshot fashion but it checks all the boxes for such use.

3.2.2. Spatial parallelization

Several methods have been reported for the single-scan acquisition of complete diffusion NMR data sets. They rely on spatial parallelization to replace the sequential acquisition of gradient increments. The spatial parallelization for DOSY follows two different close pathways. The first path starts in the UK with the work of Loening et al.[139] They described a STE experiment with a twist: the z^2 field from the shimming console is used in addition of the conventional z gradient. They relied on the fact that a field with a non-linear variation (such as z^2) causes the diffusion-dependent signal loss to vary along the different parts of the sample. Once the gradients are well mapped, for fitting purposes, the experiment can carry on. The principle is to do a simple STE with a z^2 gradient continuously active during the pulses and to read the data using a weak-readout gradient. The result although fast were not so good compared to the conventional version. The figure 3.3 show the 2D DOSY yielded by such

methods, also the use of a gradient during acquisition cause broadening of the peak. The method demands to use a lot of tools to fit the data or to map the gradients which makes it hard to implement yet it is very innovative and crafty. This can be defined as a first attend at 1 scan diffusion-NMR that will lead to further study and improvement.

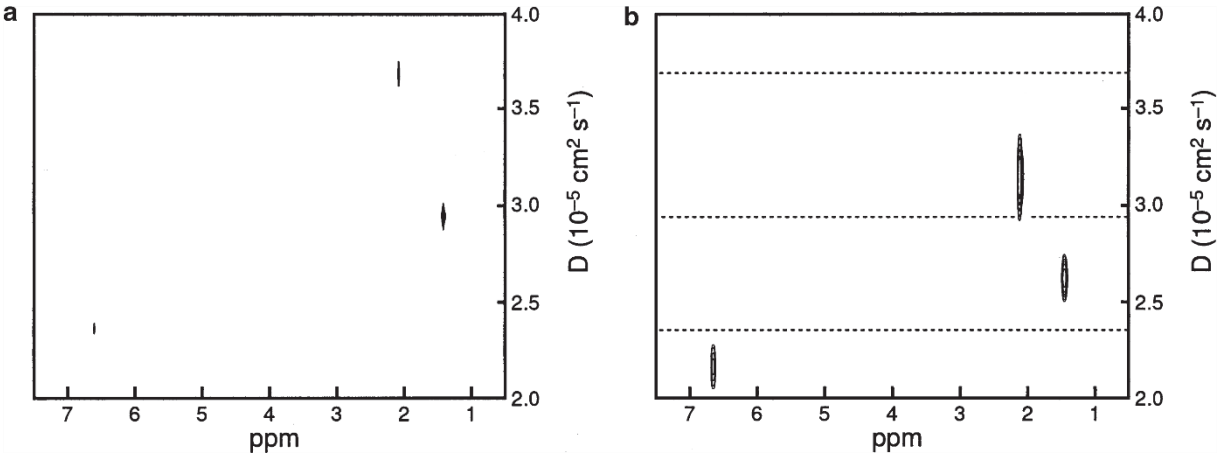

Figure 3.3, DOSY spectra constructed using data from (a) a conventional (stimulated-echo) two-dimensional DOSY experiment and (b) a one-dimensional DOSY experiment. The diffusion coefficients given in Table 1 are shown as dotted lines across (b); these values were used to construct (a). For the conventional DOSY spectrum, the intensities of the peaks correspond to the first increment of the DOSY experiment. For the one-dimensional DOSY spectrum, the intensities correspond to the one-dimensional spectrum shown in Fig. 7a. In the diffusion dimension, both spectra consist of Gaussians centered at the diffusion coefficient estimated by the fitting procedure and with widths corresponding to the standard deviations of the fits. For both spectra, the contour lines correspond to 1, 2, 5, 10, 20, and 50% of the maximum intensity of the spectrum. Adapted with permission from[139]. Copyright © 2001 Academic Press. All rights reserved.

Taking advantage of the rising use of swept pulse in NMR studies, the same team latter developed a new sequence aiming at the same one-scan goal. This was described by Thrippleton et al.[140], using the sequence shown in figure 3.4. The encoding step consists of the simultaneous application of a 180° CHIRP pulse and a magnetic-field gradient. The 180° CHIRP pulse purpose is to make the spin evolve under a gradient pulse for which the effective length varies linearly across the sample.[141] This replaces the needs for multiple gradient-increments or the need for non-linear gradients as the spins within the sample will experiment different effective gradients depending on their position. The diffusion-attenuated signal resulting from such pulses vary across the sample, the only thing left needed is a way to read it.

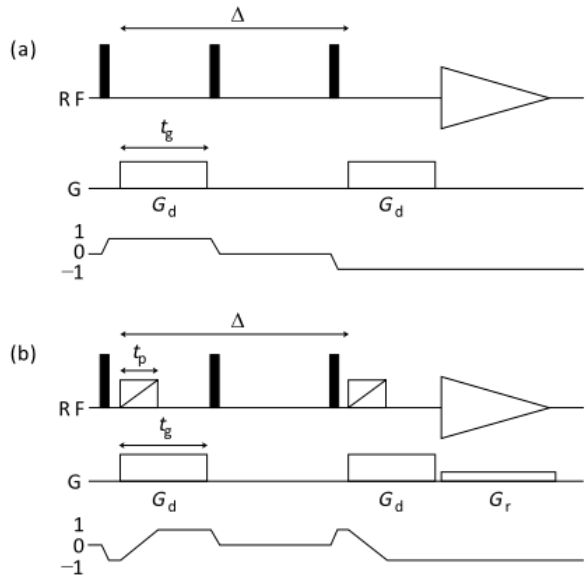

Figure 3.4: (a) The stimulated echo (STE) pulse sequence, commonly used for measuring diffusion coefficients. (b) The basic 1D DOSY pulse sequence, which permits the measurement of diffusion coefficients in a single scan. The required coherence transfer pathway is shown below each pulse sequence. The filled rectangles on the line marked RF represent 90° pulses and the hollow boxes with diagonal lines represent 180° CHIRP pulses. z-Gradients are displayed on the line marked G. Adapted with permission from Thrippleton et al[129] Copyright © 2003 John Wiley & Sons, Ltd.

In the work of Thrippleton et al., they kept the same acquisition method with a weak gradient-readout. The spectra yielded by such sequence is shown in figure 3.5. The principle is to record a 1D spectra with larger peaks; the line shape of which give a diffusion attenuation curve as seen in Figure 3.5c). This curve can be fitted to retrieve the diffusion coefficient like a normal DOSY but in 1 scan and no increments.

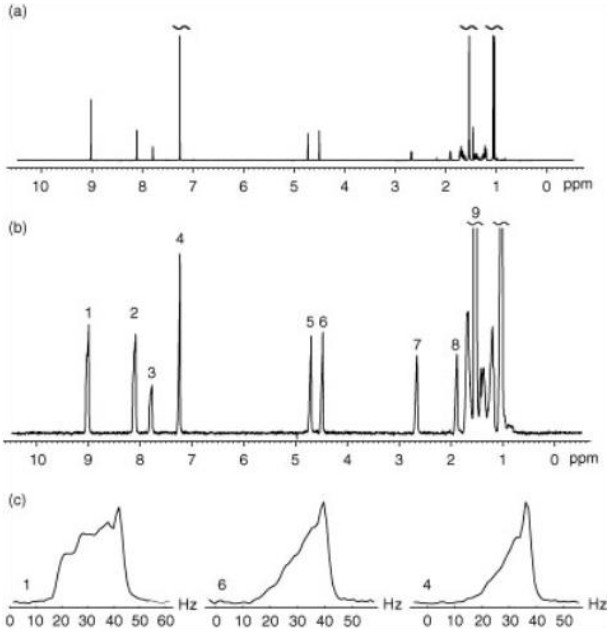

Figure 3.5 taken from[129]. (a) Conventional 1D proton spectrum of a sample containing camphene, a zinc(II) porphyrin and chloroform in $CDCl_3$. (b) 1D DOSY spectrum of the same sample; the diffusion coefficient for each resonance is encoded in its lineshape. (c) Expansions of the 1D DOSY spectrum, showing a zinc(II) porphyrin (1), camphene (6) and chloroform (4) peak. Visual inspection of the peaks gives a qualitative indication of the relative diffusion rates of the three molecules and a quantitative analysis of the lineshapes yields estimates of the diffusion coefficients. Adapted with permission from Thrippleton et al.[140] Copyright © 2003 John Wiley & Sons, Ltd.

The application of a weak gradient will broaden the peaks while making their diffusion-shape linewidth appear. This broadening depends on the gradient strength, a good balance must be reached between intensity, diffusion-lineshape and overlapping/resolution. Hence, using this method the peaks become a diffusion-weighted image of the sample. One must be careful with the gradient strength as it dictates the broadening of the linewidth. If it is too small, the curve cannot be resolved, if it is too large, the chemical-shift information and overall resolution of the spectra are lost.

The paper shows impressive result, with the possibility to acquire in 1 s > with result quality akin of a conventional STE experiment. A major drawback is the broadening of peaks as it does reduce the resolution, more caution should be taken for no overlapping as the diffusion attenuation curve would be unreadable. It is also interesting to note that linewidth analysis of a peak to fit for diffusion coefficient is not a straightforward operation, it calls for specialized software and knowledge in order to retrieve accurate values.

Another path for one-scan DOSY comes from Israel with the methodology reported by Frydman et al,[142] the so-called ultrafast (UF) NMR spectroscopy. In 2008 Frydman and coworkers[143] developed a one scan DOSY using this ultrafast methodology. Their UF DOSY sequence is illustrated in figure 3.6. The sequence is similar that one on the figure 3.4. The only difference is the acquisition scheme known as EPSI (echo planar spectroscopic imaging). The EPSI is a special scheme for acquisition first developed for MRI to have chemical insight in the MRI image by mapping the chemical shift,[144] and mostly used

to create voxel where the third dimension is of chemical shift.[145] In UF DOSY, EPSI is used to map the magnetization as a function of Z for each peak of the spectrum. The main advantage of EPSI over the weak gradient readout is that it increases the spatial resolution and thus the possible quality of the fit, yet it limits the time of the acquisition thus the possible spectral resolution attainable.

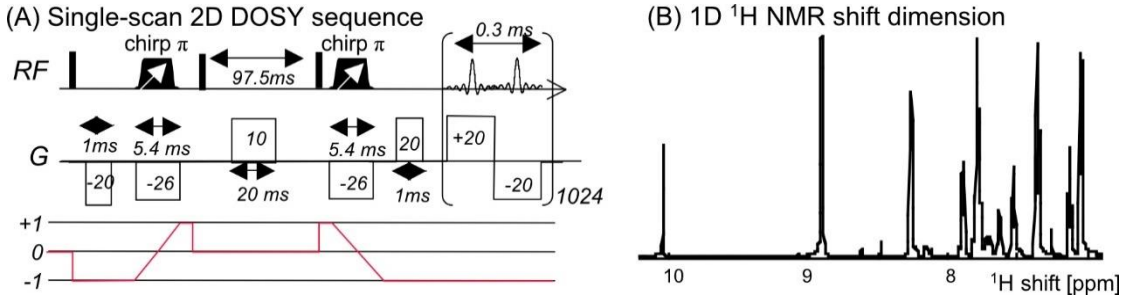

Figure 3.6 Results obtained for a TPP, Benzaldehyde and Diphenylether solution (≈50 mM each) in $CDCl_3$ at 25°C. (A) Pulse sequence and parameters employed in the ultrafast 2D DOSY implementation; notice that unlike the sequence in Fig. 3 (see original paper) this relies on an anti-echo coherence transfer pathway, associated now with equally-sensed p-frequency sweeps. (B) High-resolution spectrum afforded by this sequence along the ^1H shift dimension. Adapted from Frydman and coworker[142] with permission, Copyright © 2008 Elsevier Inc. All rights reserved.

In diffusion NMR experiments that involve spatial parallelization, the data is analysed with a modified Stejskal Tanner equation:

$$S(z) = S_0 \exp\left(-D\big(K(z)\big)^2 \Delta'\right) \qquad 3\text{-}1$$

Where Δ' is the corrected diffusion delay z is the position S the signal intensity and $K(z) = \frac{\partial \varphi}{\partial z}$ the spatial derivative of the spin's phase. The processing and analysis of UF DOSY data (also called SPEN DOSY) is summarized in figure 3.7 We can see that the data recorded are a train of sinc-shaped echoes rather than an FID this comes from the peculiar acquisition scheme. To process those data, they are reshaped to fit in the k-space, a concept often found in MRI. The idea is to have a space that depends on the time-dimension of the acquisition and one that depend on the gradient. The k dimension being a function of gradients area and gyromagnetic ratio[141] such as, $k = \int_0^t \gamma G(t')dt'$. The FT of such a space yields an image, where each peak is spread in a spectral dimension and diminish along the z (real-space) axis.

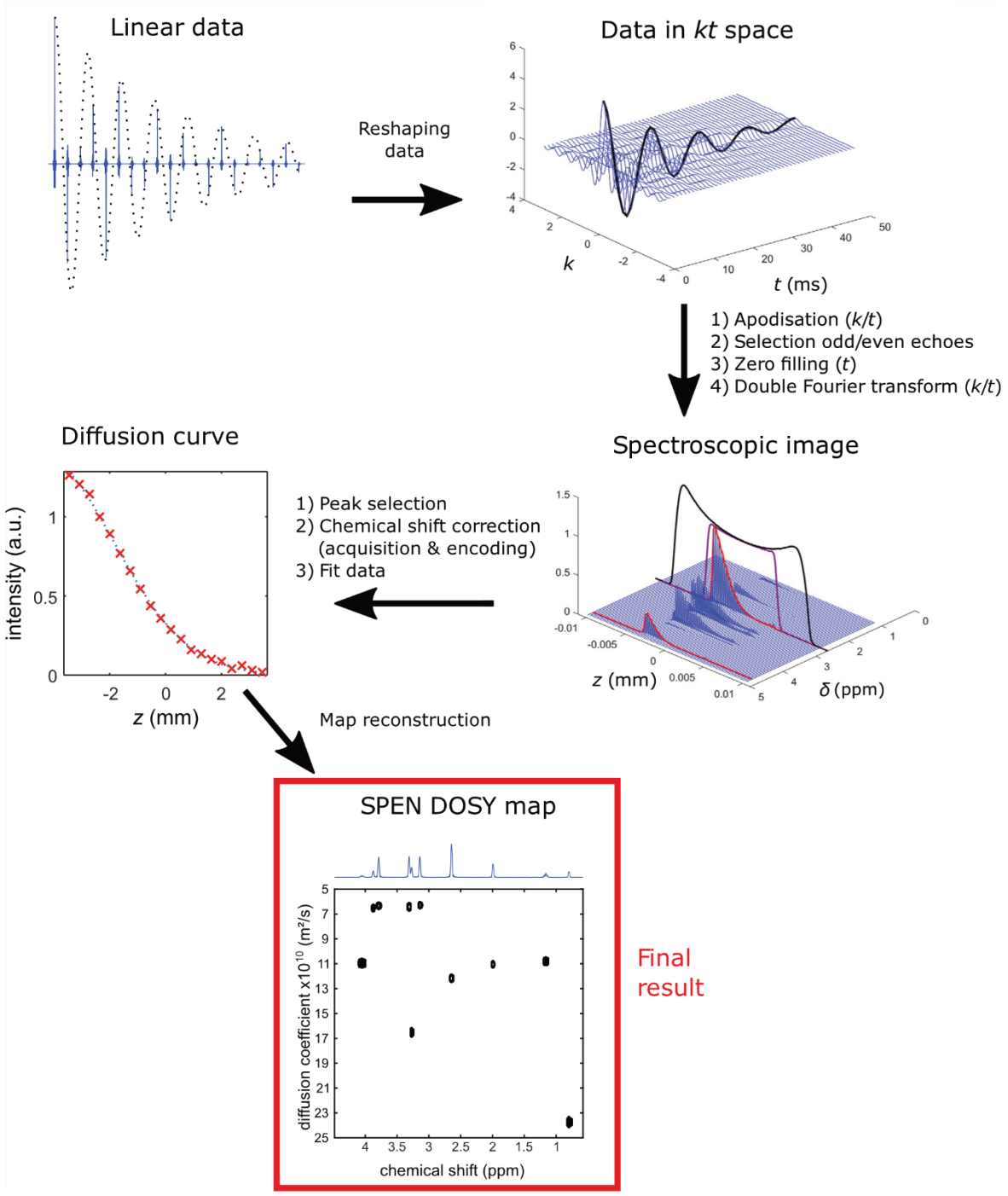

Figure 3.7: Principle of the SPEN DOSY processing. Adapted with permission from Lhoste et al.[146] under a license Creative Commons CC-BY-NC-ND, Published by Elsevier B.V.

This UF method for DOSY was used in a few different cases. The main disadvantage of having a one-scan experiment is often the sensitivity. It is thus a logical pathway for it to be used with hyperpolarization method especially if the hyperpolarization allows only one scan to be done. Two examples with different hyperpolarization methods exist.[147,148] It is also used to accelerate otherwise lengthy 3D experiment,[149] for monitoring of reaction,[150] and to accelerate restricted diffusion experiment.[151]

3.2.3. Sliding window and TR-DOSY

Non-uniform sampling (NUS) is a strategy that focuses on the reconstruction of a multidimensional NMR spectra from a reduced number of acquired increments. Instead of acquiring increments on a regular grid, only a subset is acquired, and non-Fourier reconstruction algorithms are used.[152–155] The validity of the approach relies on the fact that multidimensional NMR spectra are typically sparse. NUS can significantly shorten the time needed to obtain a full spectrum but may ask for careful optimization in the amount of sampling as a compromise between quality and rapidity.

2D DOSY experiments are not really compatible with such NUS strategies because they do not rely on the Fourier transform to process the indirect dimensions. NUS has been used to accelerate 3D DOSY experiments,[156,157] but we will not describe them in detail. We will focus here instead on 2D DOSY accelerated using NUS-like strategy

A NUS-like strategy was developed at first in the team of Urbańczyk et al.[158] It relies on an older work done by Oikonomou et al.[159], the permutated DOSY (p-DOSY) approach. It can be explained as using a list of randomly permutated gradient to remove the bias coming from changes of concentration within an out-of-equilibrium mixture. We have seen (part 1.1) that unwanted rise or fall of the peaks unlinked to diffusion-attenuation will compromise the accuracy of the fitting and lead to erroneous results. Rise and fall of the peaks can happen if concentration change such is expected in a reaction medium. The goal would be to separates those concentration changes from the diffusion-attenuation and thus having better DOSY results for the study of evolving medium. The team demonstrates that it can be done using random gradient ramps instead of monotonous ramp. The principle is to avoid any correlation between the experiment time, during which the system may evolve, and the gradient sampling.

Using the classical way, a decrease of signal while the gradient is increasing lead to a bias that increase the recorded diffusion coefficient. The impact of the gradient on the attenuation of the signal is exaggerated. If the gradient sampling goes from least to highest than the opposite happens, the coefficient is recorded inferior. The randomization of the gradient makes it so that the peak's time-variation is separated from the gradient evolution. With permutated DOSY, changes in concentration result in higher apparent noise, and the estimated error for the fit is larger, especially if the evolution is really too important at the scale of diffusion, but it will remove any bias, resulting in improved trueness for the estimated diffusion coefficient. In summary Using random gradients transforms the concentration change into a noise-like artefact rather than a bias.[159]

Knowing that p-DOSY approach we can go deeper into Time Resolved NUS (TR-NUS) strategy. Developed first by Urbańczyk et al.[158] in this approach the number of increments is not reduced, but rather increments are acquired using an uninterrupted series at randomly varying gradients. This series

can be analysed by creating a window that should encompass enough increments to allow for a good fit. It was used in the monitoring of polydispersity, using Laplace transformation in a combination of TR-NUS and technics seen in part 1.3.1. The same team also worked on an interesting comparison for restricted diffusion[140] (see part 1.1.1). Those restricted diffusion study can be quite long and so they tried different methods to accelerate them using the previously seen ultrafast approach and the TR-NUS methods. The implementation of both methods was successful as restricted diffusion is not the point of this work, we will simply explain their conclusion. The gain of time is around 1-2 order of magnitude using both methods, the UF methods seems completer and more accurate but is more demanding for the hardware and less easy to adapt to inhomogeneities in the sample compared to the TR-NUS.[151]

The principle of TR-NUS as we are interested in are illustrated in figure 3.8 from the work of MacDonald et al.[160] They study the variation of a single compound, methanol, during a rapid (5min) change of temperature from 304.5 to 306.5 K. One can see the different windows that allow the determination of diffusion coefficient along the continuum of scans (red crystal in figure 3.8a) using random gradient value (black boxes in figure 3.8a). Reporting the result of those windows in figure 3.8c, shows the increase of diffusion due to temperature shift in less than 2min. This process uses the same kind of fitting as conventional methods with here 8 random increments by fitted diffusion point.

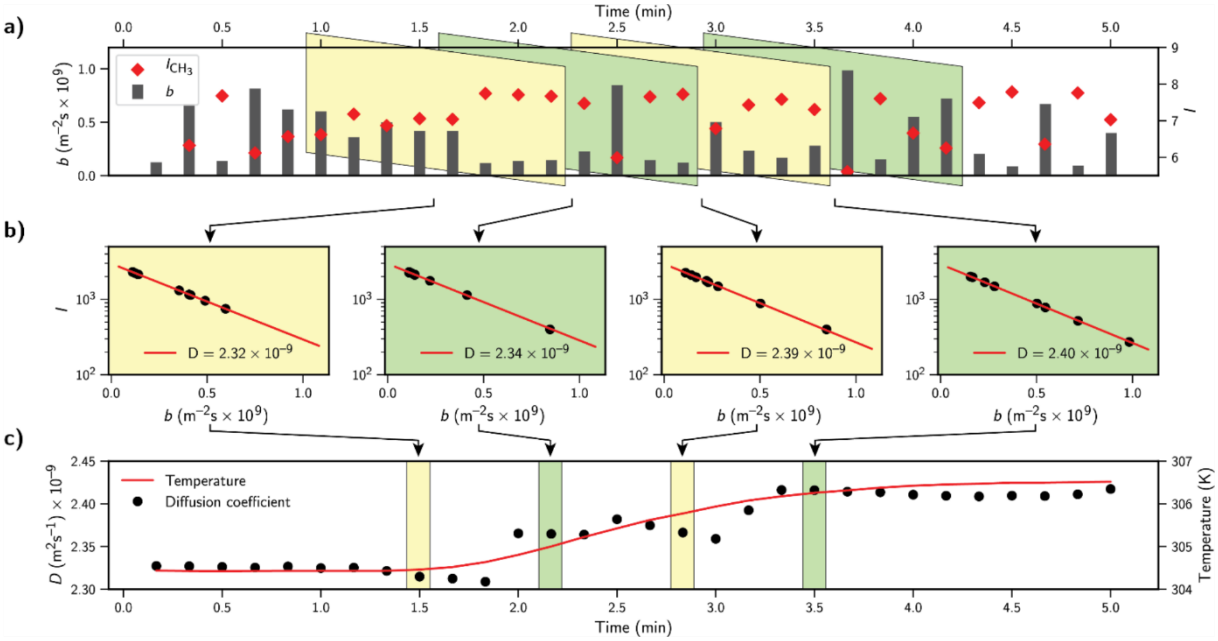

Figure 3.8 Moving average analysis of time-resolved diffusion NMR data. a) Continuous rapid acquisition of spectra using a random gradient list (grey bays) generates an array of NMR spectra over time from which peaks can be integrated (red). Diffusion coefficients are then obtained by fitting the Stejskal-Tanner equation to a subset of [integral, b] points (8 points here) centered about time t. b) Time-dependent diffusion information D(t) is found by advancing this fit over the dataset by a moving series of non-linear fits. c) Combining the fast PGSE experiment allows changes in diffusion (black) induced by temperature changes (red) to be followed over sub-minute timescales. 1H PGSE (δ = 1.2 ms, Δ = 45 ms, ns = 2, 5 s repetition time), methanol capillary placed in DMSO-d6, 304.5 – 306.5 K, 500 MHz. Adapted with permission from MacDonald et al.[160]

They also monitor a *in situ* polymerization, extracting concentration and the changes of diffusion coefficient of the resulting polymer with a time resolution of 40 s per gradient's value and 12 slices per fit so an average of 8 min per spectra/diffusion calculation. It is to be noted that they use a slightly unusual NMR experiment, they have a spin echoes with a spoiler gradient during the inter-scan delay that allow them an inter-scan delay of 1.5s. (see supplementary information of the paper[160]) thus explaining the very fast rate at which they record each increment.

Note that in the first article on tr-NUS DOSY by Urbańczyk et al.[158] they too studied polymer and polymerization. They looked at their capability to get the polydispersity index of standard samples. They also delved in the *in situ* polymerisation by looking at the depolymerisation of heparin by enzymes.

Part B Method

4. Methods for processing, analyzing and evaluating DOSY

4.1. The DOSY workflow

In the previous chapters we have described the basic principles of diffusion NMR and DOSY, as well as the associated challenges. In this chapter, we will describe the DOSY workflow, discuss the qualitative evaluation of DOSY results, and introduce quantitative metrics to assess and compare DOSY experiments.

4.1.1. Data acquisition

The first step of the workflow is to acquire the data. It is an important step as the quality of the acquired data strongly influences the subsequent steps. The key points are the attenuation of the signal that should go to around 1 to 5% of its initial strength. To reach this target, on multiple analytes that behave differently, we run the experiment with 2 steps/transients. The lightest gradient strength (most signal) and the strongest gradient (least signal). This helps us to check if the compound reaches the attenuation objective we have. In general, this is not done *ex nihilo* as knowledge of the solvent, viscous or not, and of the solute's nature will guide the parameters. Temperature should be known and as stable as possible, stirring/spinning or any kind of motion should be avoided.

The spectral width used for acquisition is also an important parameter. It often the case that the edge of the spectrum can be problematic. It is advisable not to have any peak in the edge of the spectrum. Notably, in Bruker systems the baseline at the extremities is known for going up or down due to digital filtering issues. DOSY being sensitive to baseline distortion/problems it is advisable to take a wide spectral width.

The spectra are acquired by repeating the same experiment multiple times with increasing gradient amplitudes. Gradient increase, in its simplest way, is done following a linear ramp. The list of gradient amplitudes increases linearly from the lowest value to the strongest value. Figure 4.1 shows the resulting FID from such experiment. The first increment gives the strongest signal and is very close to the 1D spectrum that would be obtained with a pulse-acquire sequence. On the other hand, the last increment is barely readable due to low SNR.

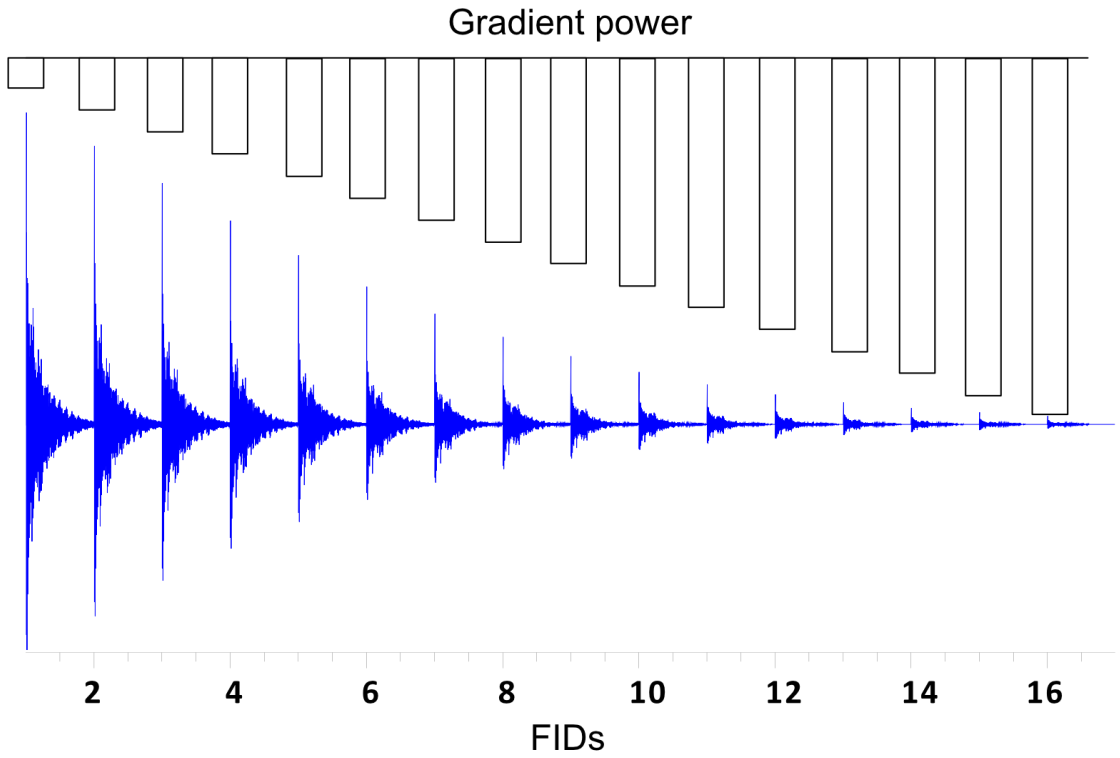

Figure 4.1, List of FIDs obtained in a DOSY experiment. Each Fid represent an acquisition with increasing gradient power. The gradient powers are illustrated by the area of each rectangle associated with its experiment.

4.1.2. Data processing

Once the data are acquired each data sets is a stack of *N* FIDs, *N* being the number of increments. In figure 4.1, one can see 16 FIDs for 16 increments. The Fourier transform is done only in the so-called direct dimension (F2), which means that every FID is converted into a spectrum but there is no 2D Fourier transform as for other 2D NMR experiments (like TOCSY, COSY, HMQC etc.). Apodization happens just like for 1D spectra, and is a balance between resolution, linewidth and lineshape. We tried a few apodization function at different weights but it does not appear to play a major role. Indeed, if the data are not good enough to be analyzed without apodization there is little to no chance that it will improve it for the rest of the DOSY analysis.

Here we chose to use the Topspin program for data processing. The reason why we decided to use Topspin, despite it not being made specially for DOSY, is because processing steps are also common in NMR. It therefore made more sense to use a software well known and robust while reserving the analysis part specific to DOSY data to a software made specially for such use.[161,162]

Another major point of importance for the processing is phase correction. The NMR signal can be written as: [163]

$$S(t) = S_0 \exp(i\Omega t) \exp\left(-\frac{t}{T_2}\right) \times \exp\left(i\phi'\right) \qquad 4\text{-}1$$

The term ϕ' corresponds to the phase, that can be adjusted in order to have good lineshape. After Fourier transform the signal $S(t)$ take the form:

$$S_0[A(\omega) + iD(\omega)] \times \exp(i\phi + \phi_{corrected}). \quad 4\text{-}2$$

Where $A(\omega)$ and $D(\omega)$ are absorption and dispersion part of the spectrum. We have to adjust the $\phi_{corrected}$ value to cancel the exponential and get a pure absorption lineshape in the real part of the spectrum, this is colloquially called “phasing the spectrum”.

In a 1D spectrum this is straightforward, and can be carried out using a graphical interface or by automated means. In a 2D data set (or pseudo 2D), it can be trickier, since a single value of $\phi_{corrected}$ might not be suitable for all the spectra simultaneously. For example, the first FID may have a good lineshape but as the gradient increase, due to hardware reasons the phase shift on the last increment might have a different value. This makes the phase correction step a double compromise, the peak should have a Lorentzian shape but also share this shape throughout the increments as much as possible. When the compromise gets difficult the decision is to phase as good as possible the first one (or least attenuated spectra) that carry the more signal strength and try to improve the following spectra without degrading it too much. Albeit this might seem complicated, we rarely if ever suffered from a problem or an inconsistency as long as the spectrum are correctly phased and phasable.

4.1.3. Data analysis

We have seen in part 1 (equation 1-13) the form and meaning of the Stejskal-Tanner equation, that describes signal attenuation in NMR due to translational diffusion and pulsed-field gradients. Once the DOSY data are processed, they are fitted with this equation. Least-squares methods are used to fit the signal strength as a function of the gradient amplitude, to yield the estimated diffusion coefficient for each peak that we choose to analyze. This option to choose peaks on the spectrum rather than taking the whole spectrum is the most easy and straightforward and is called univariate. There are others methods, called multivariate, that analyze the spectrum as a whole. They will be briefly described in part 6, here we will focus on univariate processing using least-squares methods.

There are two main methods of data selection that exist for univariate analysis of DOSY data: using integrals of selected spectral regions, or using intensities for all the peaks above a certain threshold. Those methods have different advantages and disadvantages that we are going to discuss in the context of complex mixtures.

The thresholding method relies on a peak picking tool, and then uses the intensity of the selected peaks. Peak picking can be of varying complexity depending on the software used. In the simplest case a threshold is set, anything above is a peak the rest is not accounted for. In most cases the peak-picking/thresholding will not consider a multiplet as a single peak, and instead picks each sub-peak separately. It can also miss-identify two close peaks as one or a slight lineshape distortions as a whole peak. Despite this it has many advantages, such as its speed (it is almost instantaneous), and the fact that it is less user dependent. Using thresholding may also be mandatory when the spectrum is too crowded.

The use of integrals of selected spectral regions is another option available to analyze the data. It does not depend on any peak-recognizer and is set by the experimenter by hand, which means that it is user-dependent.

Whatever the technic we use it will yield a set of numbers that can be referred as the signal (S in the Stejskal-Tanner equation) a function of the gradient strength. For each peak, whether decided by threshold or by the user, such values will be regrouped, creating a peak set for the DOSY experiment. With those values we can make the fit, each peak will be fitted and all the peaks of the set once fitted form the DOSY result.

Note that even if a spectrum is acquired in good conditions and well processed, some challenges still arise during analysis. Overcrowding of a spectrum, especially common for a mixture, could pose multiple problems. It is known[164] that two overlapped peaks will give an intermediate value of the two diffusion coefficients when single exponential fits are used. Bi-exponential fitting only gives correct values when SNR is very high.

Overlapping is often encountered in two different ways, some overlaps are complete and it is impossible to see or guess each peak, sometimes one can guess that there is two or more but not decipher them. Some are less straightforward; the peaks do mingle, yet they might be resolved, the peak only overlap at their extremities for example. This is the hard case as different way to process the spectra might or might not allow you to retrieve the right value, almost always with some drawback. Finally, another phenomenon is overlapping with smaller peaks, from impurities for example. Those small peaks can be invisible to the user but remain hidden under the peak of interest or close to it and thus hinder the analysis.

This fitting results in two numbers for each peak, the estimated value of the diffusion coefficient, and the associate estimated uncertainty. Figure 4.2 shows two DOSY displays with their respective fits, one being considered as good and one bad. The sample is the same in both cases. It is comprised of three different species. For the “good” example, one can see that the fitting curve for a same molecule almost superimpose both together and with the corresponding experimental points. While the other spectra considered bad is messier and even if some fitting curve slightly align, they do not match the experimental data point well.

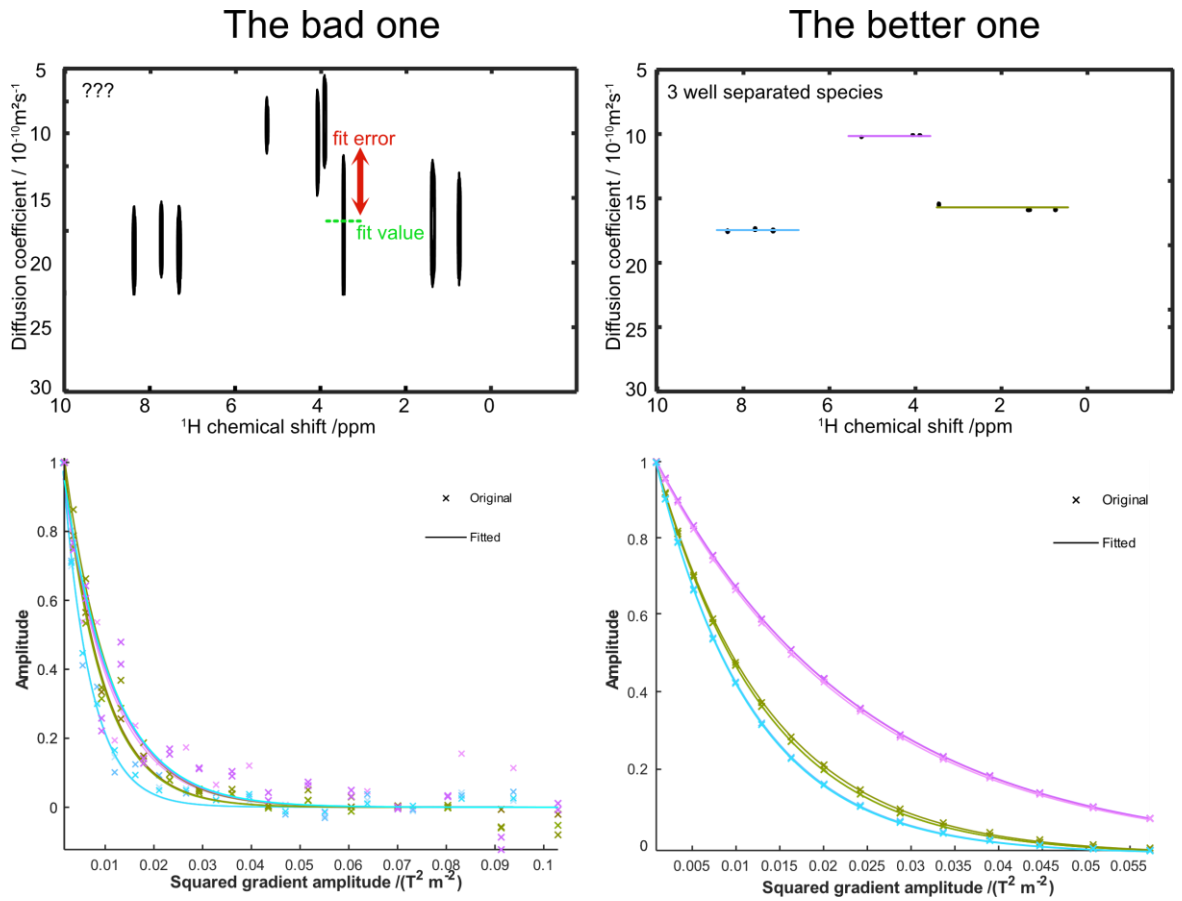

Figure 4.2 same sample with two different DOSY experiment and their display. Each species has its color and the fit's curve match the species color.

4.1.4. The DOSY display

The DOSY display has become a standard method to represent the result of diffusion NMR experiments on mixtures. In the context of mixture analysis, DOSY experiments should ideally give us information that makes it possible to associate peaks together as belonging to the same species, and hint on the size of the molecules relative to one another. As illustrated with the "bad spectrum" shown in figure 4.2, the peaks should not only be well aligned, but their widths (the uncertainty from the fit) should also be as small as possible; otherwise, it is difficult to know which molecule it belongs to. In this "bad" example it seems that there are 2 species instead of three, while the three species are well separated in the "good" example.

The display takes a form that is akin to the classic 2D NMR but it is only appearance as there is no spectral indirect dimension or 2D Fourier transform. Instead, the display shows peaks which value on the horizontal dimension match the frequency (in ppm) of the peak in the 1D spectra usually displayed on top of the map. The vertical value is then the value of the estimated diffusion coefficient belonging to the specific peak. Another important information that we retrieve from the fit is the uncertainty, derived from the differences between the experimental data points and the fitted ones.

This is represented as the vertical width of the peak. The horizontal width does not hold strong meaning except the size of the integration decided by the user or by the peak picking.

The display in itself is represented as a contour map, just like a map or most 2D NMR plot. Figure 4.2 shows two examples of this display. One of the main advantages of this display is that it is really simple to read, a simple look can help to determine where the fit worked well, and, if it did, which peak belongs to which species. It also provides the relative sizes of the different species. This is based on the reasonable assumption that translational diffusion happens for molecules as a whole, and therefore the estimated diffusion coefficient should be the same for all the peaks. One disadvantage is that it is easy to manipulate, as the choice of contour levels that show the topography, as well as the level of zoom, can give false impressions.

4.2. Methods

4.2.1. Sample

In order to assess existing and new DOSY methods, we worked mainly with a sample of sucrose, 2-butanol and pyridine in deuterated water. This sample was used for its convenience as it shows three species in three different area of the spectra. Figure 4.3 shows the 1D ^{1}H spectra of such a mixture. In this spectrum not all the peaks were considered. We decided to select well-resolved peaks, to limit the contributions of peak overlap and of the choice of integration region. We also chose to work with a concentrated sample, to limit the effect of sensitivity. This made it possible to focus on other sources of error in the DOSY experiments.

The three selected peaks of pyridine and sucrose are not overlapped and relatively well resolved. For butanol, the peak at 3.51 ppm may seem slightly overlapped with the sucrose but in practice it is easily separable from the sucrose. The multiplet at 1.25 ppm is of high multiplicity and the total SNR is a bit low this coupled with a slight overlap. This overlap with iPrOH, that is a solvent commonly found in the flowtube, because it is the storage solvent, being problematic we discarded this peak.

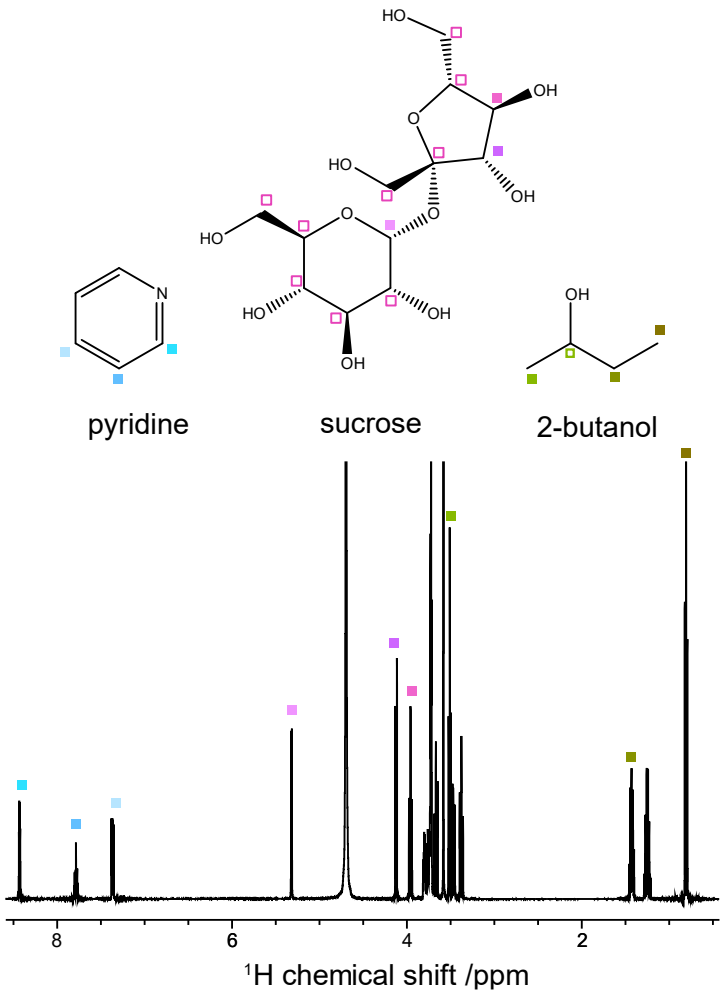

Figure 4.3, the 1D ^{1}H spectrum of the mixture most commonly used throughout this work. The wide peak at 4.7 is water mostly from the residual DOH and brought by both pyridine and sucrose that are not fully dry.

4.2.2. Processing software

The processing and analysis of DOSY data was done using multiple software. The Topspin software was used for the processing part, that is the same as for 1D NMR. Apodization was done often using very weak factor for the weighting functions. In general, we used the most classical exponential function, or no apodization at all. In this work all 2D data are shown without apodization except if specified and 1D data have a 0.5 Hz apodization using the exponential function.

For zero filling, all the 2D data sets were processed with 4 times their original number of points. This is because it was found to play a role in the analysis steps, when using peak picking. Zero filling is known to bring additional information when using 2 times the original number of points.[163] Beyond that, it simply acts as a form of interpolation. We observed empirically that, visually, the DOSY display was of higher quality when using zero-filling up to 4 time the points number rather than 2. This might be because peak picking with thresholding works better with a high degree of interpolation.

Baseline correction was performed with the default parameters of the automatic baseline correction functionality in topspin.

4.2.3. Analysis software

To analyze the data, we chose to use the General NMR Analysis Toolbox (GNAT).[161] It is a free toolbox developed with MATLAB, MATLAB being itself a commercial software. GNAT[161] is a software developed by the Manchester NMR methodology group to process and analyze all kinds of diffusion NMR experiments. It merges different analytical technics surrounding DOSY[165,166] or general NMR (baseline correction, apodization, reference shifting etc.). It also includes relaxation[167] NMR technics and analysis/processing tools for various special cases like a pure-shift chunks editor. It lacks detailed documentation but the code is fully available and well commented. Note that the InsightMR flow tube comes with software such as Dynamic Center but we found it not that convenient compared to GNAT, that is open-access version and that we could modify in various ways.

4.3. Qualitative comparison

In this section, we will discuss a few processing parameters and their impact on the general quality of the results of DOSY experiments, based on visual inspection of the DOSY display. Before doing so it is important to define what is expected from such a display in the context of complex mixture analysis. The measured diffusion coefficient is used as a mean to achieve a so-called virtual separation of the NMR spectra. Such separation is achieved only if the peaks are thin enough to not overlap in the diffusion dimension with those of others species. At the same time, the peaks of the same molecule should overlap in the diffusion dimension and not get scattered too far apart from each other.

4.3.1. Integration methods

To analyze the data, one needs a way to retrieve the signal *S* for the different peaks, so that it can be fitted. To do so, one can use the area under the peak by integrating the spectrum. In this case, the user chooses two points on the spectrum which determines the length of the integration region. Such integration regions can be stored and retrieved, allowing the user to re-use the area and hence use consistent integration regions across several experiments. It remains user-dependent, and the quality of the fit can be impacted heavily by the choice of integration region. One should remember that having peak with low error (small vertical width) that align with each other is unlikely to happen, if the user poorly integrates their data.

This method has some advantages. It can help untangle two peaks that happen to slightly-overlap by narrowing the integration region to fit the peak tightly. In theory the contribution of a noise region to an integral should not depend strongly on its size, so it is advisable to use large integration region if possible. In the real case low concentrated species or various phenomena can quickly lead to taking unwanted signal and thus heavily worsen the fit. In almost all cases the integration regions that we used remained tightly around the peak. This method also has the advantage of being straightforward.

The disadvantages of this method are mostly that it is difficult to perform well if small signals/peaks are present at the feet of the peak of interest. If those signals are impossible to separate or to disambiguate while integrating, they will play an adverse role in the fit. Also, a problem of this method is that is it time consuming: integration of a complex mixture with multiple species can take a long time. This is true when many species are present, but also if the peaks are close, as finding the right area that work throughout multiple spectra is not an easy task and may have to be redone multiple times.

Overall, this method was the most used during this work. It was our default method. When the analysis is done differently in this manuscript, it will be mentioned.

4.3.2. Thresholding/intensity methods

Another way to analyse data is to use the intensity rather than the integrals of the peaks. To do so a peak picking is necessary. Usually one chooses a threshold line, and everything above will be considered a peak, while anything below will be discarded as noise. It is less user dependent as the user does not decide for each peak, yet it can be tuned and will give different result depending on where the threshold is placed.

The main advantage of the method is that it is fast. It is virtually instantaneous, and the number of peaks or interesting area does not play a role in its length. Another advantage is that it is a good way to get rid of smaller uninteresting peaks those which may overlap with the peak of interest. This is another way to slightly bypass overlapping. Thresholding seems a better suited method if there is a crowd of smaller peaks at the feet of the interesting peaks. Conversely, Thresholding fails more often when the overlap happens between two peaks of similar intensity. A case that while difficult can often be solved by using integration regions, as long as the peaks can be distinguished. It happens that two peaks of similar intensity are easier to separate using integration than thresholding. Overall overlapping has no straightforward answer. To solve it, when possible, is often a trial and error between the different approach, regions… The use of thresholding/integration is not a solution to serious overlapping. When heavy or total overlap happens, one should look for other methods that increase resolution, such as pure-shift NMR.[168,169]

The main problem with peak picking is that it will not consider multiplets as a single entity, but rather consider each sub-peak on its own. It is a problem as multiplets suffer from lower SNR (relative to an equivalent singlet). This impact the fit negatively and also gives different values for a single peak. It increases the spread of the peak and thus the separation is less evident. We often found that, the actual diffusion value is the average of all sub-peaks. It also means that even if the average is right the peak might be very stretched in the whole spectrum, which worsen its readability.

To illustrate this discussion, figure 4.4, shows different DOSY displays obtained from the same experimental data set, using either intensity of integrals. The sample is made of quinine, geraniol and camphene, and the resulting spectrum is quite complex. For the purpose of this discussion, it can helpfully be split into two parts, from 4 to 9 ppm where there is barely any overlap, and from 0 to 3 ppm where there is a high degree of overlap. A situation often found in NMR with organic molecules, as aliphatic part often overlaps while more functionalized part does less so.

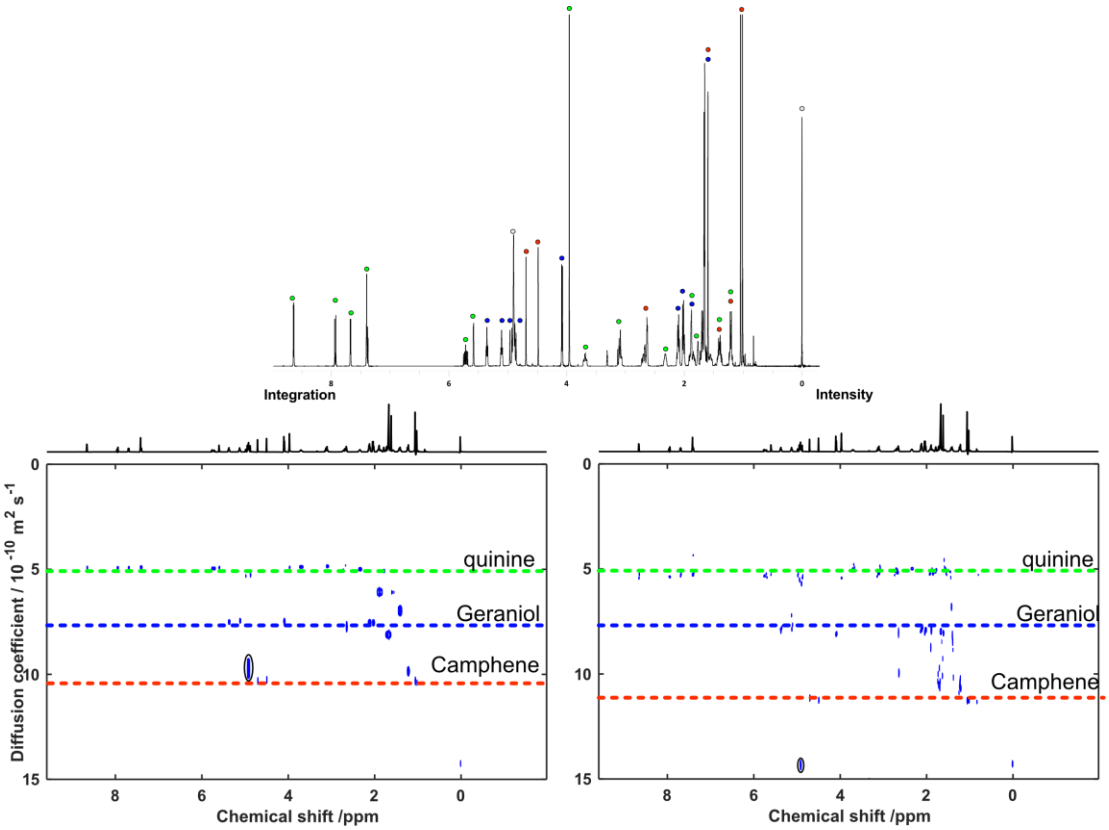

Figure 4.4, DOSY spectra of the mixture camphene, geraniol, quinine at 0.1M in MeOH. The attribution is done for the peaks that can be easily attributed. The method to analyze the mixture is either integration or intensity. The circled peak is for methanol.

In the 4–9 ppm region, using integrals gives good results, with well aligned peaks for the three compounds. One major mistake can be seen, for the peak of the solvent, methanol, that would be expected to be close to the peak of TMS. Here integration is clearly at fault, because of the overlap between the solvent signal and a peak of geraniol. The result is a peak in-between methanol and quinine in the diffusion dimension. Using finer integration area could give better result but the peaks never really separate from each other.

In that same region, using intensities gives clear separation between methanol and the rest but the results are not as good as with integrals when overlapping is weak. One can see that multiplets give multiple signals on the DOSY display that are slightly misaligned. There are even stronger glitches, such as the peak at 7.4 ppm and its estimated diffusion coefficient of 4.4×10^{-10} m²/s.

For the 0–3 ppm region, the differences between the two methods are subtler. The intensity method seems to gives lots of peaks. The quinine is almost perfect, the geraniol is readable but the camphene gets complicated with some cross talk with the other molecules. It is also interesting that even if the entanglement is not that strong, the spread simply coming from the multiplets make the display hard to read. The separation gives two molecules clearly but as for the camphene, it is not clear if it displays multiple species, a few bad instances of geraniol or a single species.

The integration method gives much clearer results, but they are in fact not better, as more peaks are visibly overlapping and give a value for the diffusion coefficient that is in-between two species. The uncertainty is also large for some regions, especially those that correspond to overlapping peaks. If the user is aware of the limitation of the thresholding, it gives slightly better results, as three lines can be guessed while integration give strong peaks in-between that one can doubt if they are true or artefact. The integration is very difficult in this case as the spectra is full of really small peak that are impossible to avoid when integrating bigger ones.

Overall, one method is not better than the other and it is about specific cases and time of analysis. We used the integration method during this work because our samples were not too hard to resolve nor too complex, and because user time was available. It also highlights that it is hard to anticipate what will work better. As there is no clear ruling that come out of this discussion rather a set of observations.

4.4. Quantitative comparison

In this part we are going to go deeper in the comparison of different DOSY spectra. We will now compare elements of the pulse sequence that may or may not modify the experimental result. We also are going to investigate some optimization methods and check at whether or not they are relevant.

4.4.1. Metrics

It is first helpful to define a few specific words. “Trueness” refers to how close a measurement’s value is to the true value, when such true value is conceivable. Precision, on the other hand, is a measure of how repeatable a measurement is. It indicates to which extent the same value is obtained or not if the measurement is repeated multiple times, irrespective of the trueness of that value. Accuracy is the combination of precision and trueness

It is important to note that, for diffusion NMR experiments, it is very difficult to evaluate the trueness of a result on an absolute scale, as there are many sources of systematic errors, that are difficult to evaluate. This is in most cases not a limitation, as most applications of diffusion NMR rely on the relative values of several diffusion coefficients, be it to separate the spectra of different compounds, or to estimate molecular sizes and shapes. What is then important is the trueness of

relative values of diffusion coefficients: are all the peaks for a given compound well aligned? Is the difference in diffusion coefficients for two compounds consistent?

Instead of the trueness of the estimated diffusion coefficients, we chose to use a metric that reflects how well the peaks for a given compound are aligned, in a given DOSY experiments. This "alignment" was calculated, for a given molecule, as the standard deviation for the set of values obtained from the different peaks of the molecule. In the following, the alignment will be expressed either in $m^2 \cdot s^{-1}$, or in percent (in which case it is divided by the average diffusion coefficient for the set). In order to summarize the results with a single number for a given experiments, the root mean square of the alignments for each of the molecules can also be calculated.

Concerning the precision of the estimated diffusion coefficients, in the case of DOSY experiments, it can in principle be estimated from the fit, using the residuals and the Jacobian that are output of the least-squares procedure. In practice, sources of systematic errors also contribute to the uncertainty as estimated in this way. For example, in the case of significant spatial non-uniformity of the gradient field, the Stejskal Tanner equation is not expected to describe the data perfectly.[170,171] This is illustrated in Table 1, where the uncertainty estimated from the fit is compared to the precision measured by repeating the same experiment three times, for selected peaks in three different pulse sequences. One can see that the uncertainty estimated from the fit is always larger than the actual repeatability. Here we chose to use this estimated uncertainty obtained from the fit, rather than the actual repeatability, as it corresponds to the number used for the peak width in the DOSY display. It is also a useful indicator, as we found out that experiment with large uncertainty and overall bad result, can still have good repeatability. It therefore makes more sense to use the uncertainty.

Table 4.1: value of repeatability/precision and uncertainty in percentage of coefficient diffusion. Values for precision are acquired by standard deviation of diffusion coefficient for three identical experiments. Values for uncertainty are acquired by summing with RMS each value of uncertainty for the three identical experiments. The STE/DSTE Bruker is the by default sequence while DSTE monitoring is the DSTE used for the monitoring in later part.

	STE bruker			DSTE bruker			DSTE monitoring		
	Pyr	Suc.	But.	Pyr	Suc.	But.	Pyr	Suc.	But.
% precision	0.40	0.16	0.38	1.77	0.34	0.32	0.72	0.32	1.16
% uncertainty	1.56	1.32	2.14	1.16	1.06	1.30	1.61	1.05	1.70

In order to provide a compact representation that helps to compare sequences, a single uncertainty value was calculated for each molecule, by calculating the root mean square of the uncertainties obtained for the different peaks of that molecule. An even more compact information was obtained by calculating a single uncertainty value for a complete display, as the root mean square of the uncertainties for all the analyzed peaks.

In summary, two quantitative metrics were used to assess the quality of the DOSY results at the level of a given compound, or a mixture of compound. They are the alignment and the uncertainty. These quantities are also referred to as “separation quality” and “fit quality” in our publication.

We are going to illustrate these concepts with an example, shown in figure 4.5. To do so we have created artificial displays, meaning they do not represent real sample and are born from a graphics software rather than data analysis. Consider three fictive experiments giving three sets of two peaks, for which the true value of the diffusion coefficient is not known. The only way to assess if the measured values are satisfactory is through the alignment of the two measured values. This is the case c) in figure 4.5. It represents the real situation of mixture analysis using DOSY and the challenge one can encounter.

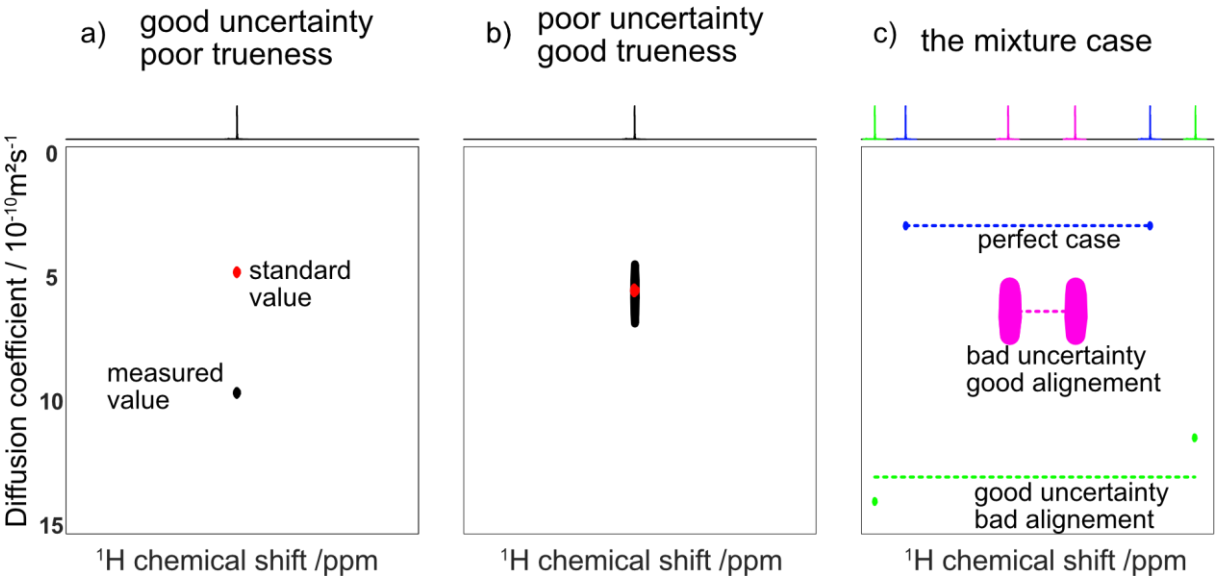

Figure 4.5, Three cases of DOSY spectra. The spectra here are fake and do not represent any mixture or chemical species. Case a) display a wrong coefficient value with no increase of uncertainty/error. The case b) show the right value with a large uncertainty. The case c) is a representation of the real case where a standard value is indeed improbable.

If we simplify the experiment by having a single species with single peak and a standard value that we know is true. In practice the case b) “poor uncertainty good trueness” is often found and can result from multiple problems, the most common being a bad optimization of the gradient strength, resulting in too slow or too fast signal attenuation. It can give some hints but 2D-peaks of the DOSY may overlap with others not part of the same molecule. It can also come from problem related to the NMR apparatus. Terrible gradient spatial homogeneity, motion within the sample, lack of temperature regulation… It often come from severe causes and while making the experiment less worthy, it is usually easy to diagnose.

The case a) “good uncertainty poor trueness” is more concerning and rarer. It often results from a problem within the experiment such as unwanted J-modulation, disturbance from the baseline, shimming qualities or problem with the fitting model. Those problems are usually subtler than case b).

To give a few examples that happened directly to us, a bad calculation of the delay for the fit model can give such kind of wrong value seemingly with good quality. It happened several times that we use wrong gradient list that is proportional to the real one, this give wrong D value but keep the error and alignment that would be the right ones. Distortion and glitches of the baseline can also cause this effect of having little to no effect on the error but change the value of the diffusion recorded. We are not sure why and this seems to be peak dependent so it will impar the alignment resulting in cases like the green one in case c).

This is for the causes unrelated to the chemistry of the system. Indeed, such modification of the measured values can come from non-user controllable causes. As said previously this change of the measured value could come from overlapping. It is reported[164,172] that upon overlapping the diffusion coefficient while be a midway between the overlapped species. Another case slightly related to overlapping is exchange. A peak in chemical exchange will also give erroneous diffusion coefficient value. In the same fashion as overlapping, the diffusion coefficient will be a midway between the exchange species. It could be useful as this value will be proportional to the ratio of the in-exchange species.[173] Overall this case a) is the most concerning because without a good *a priori* knowledge of the involved species/system it can be very misleading. Fortunately, it will also be rare as different effects that can create a wrong value of diffusion coefficient are likely to have an impact on the fit. The fitted model will be wrong and thus it is expected that the error increases. Nonetheless we have seen in this work case where the change of value is very large compared to a relatively benign increase of the error. This is particularly true on flow and will be discussed in the part 6.

4.4.2. Graphical representation

In order to compare the relative merits of different DOSY experiments, we propose to use a graphical 2D representation, in which each experiment appears as a single marker. The x coordinate is given by the uncertainty, and the y coordinate is given by the alignment, calculated over the whole set of selected peaks. The best experiment will thus have a marker close to the origin of the plot and as experiments worsen, they will move further away. This system is made for comparison of closely related experiment using the exact same sample, and the same kind of analysis. Here the sample of sucrose, butanol and pyridine was used with the integral's method for analysis. A selection of three spectra and the associated graphic is shown in Figure 4.6. The very bad DOSY was acquired with no coherence selection whatsoever, the bad spectra had an unsuited attenuation, the good was simply acquired in good condition. Each colored dot corresponds to a DOSY shown above. One can see that the "good" is close to origin as expected. The "bad" one is clearly unsatisfactory but could be exploited. The "very bad" one is chaotic and no information could really be extracted from it. In general, we

consider that anything that has 0.2 or more in any of its coordinate is failed, note that as previously said it depend on your system and goals.

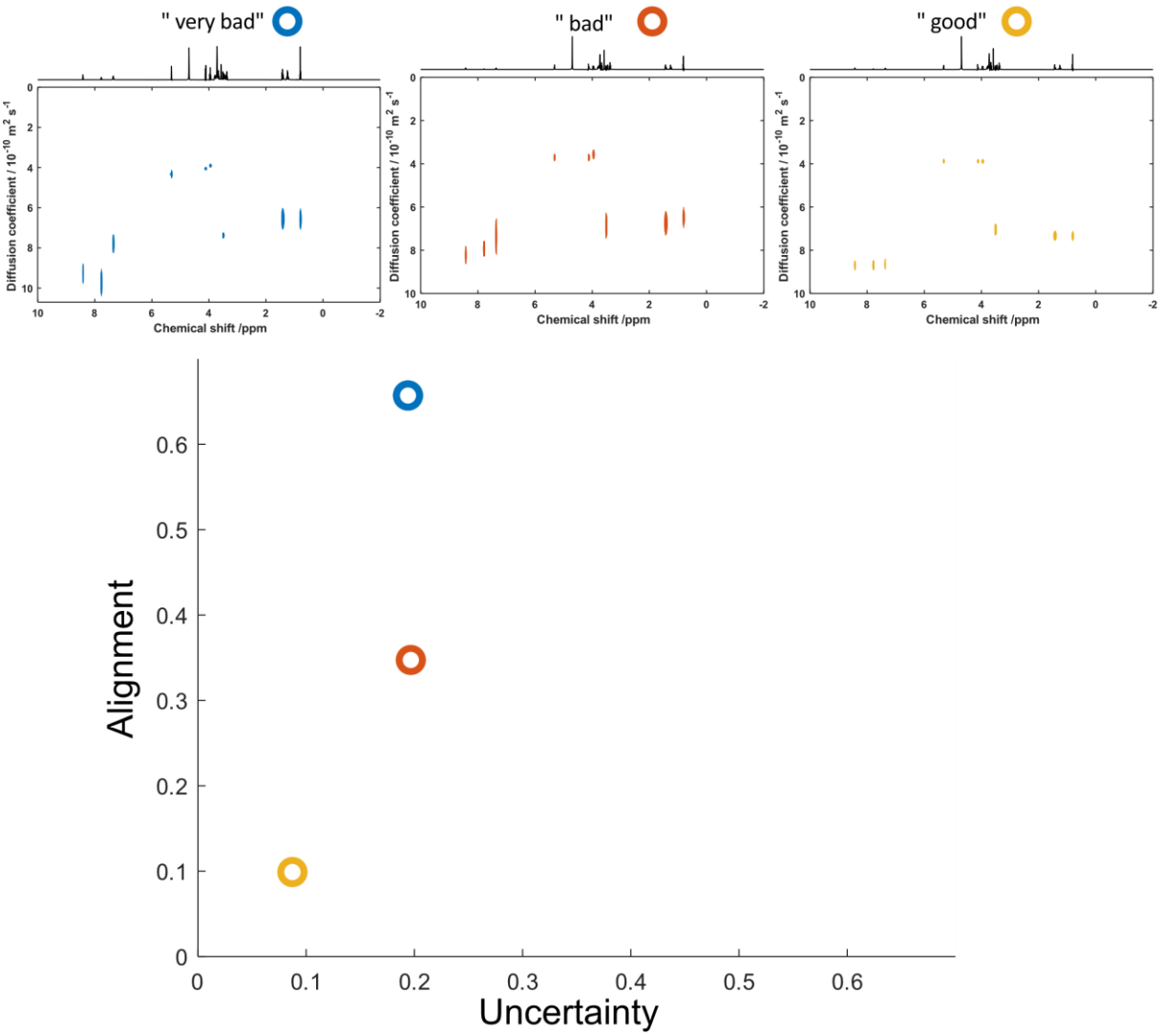

Figure 4.6, each correlation circle is representative of a single DOSY spectra matching its color. Both axis unit is that of diffusion coefficient ($\times 10^{-10} m^2/s$). Label are indicative related to the text.

4.5. Comparing DOSY pulse sequences

The quantitative metrics introduced above will be used in the rest of this manuscript to assess new developments. Before that, in this subsection we will illustrate their use to answer some of the questions that we had to address when searching for the "starting point" of our DOSY developments. Specifically, we will describe two examples, the choice to include an LED block or not, and the choice of the amplitude of the spoiler gradient.

Many pulse sequence elements have been introduced over the years for DOSY experiments, and not all of them are still relevant today. For example, the LED block[38,39] (see part I), while being relevant in the 90's, was said to be unnecessary thanks to the progress made in shielding of electronics and in general in FT-NMR.

To test this, we ran identical experiment with or without the LED. We tested it on both STE and DSTE pulse sequence as they use different numbers of gradient pulses. We also tested on different probes to see if our comparison made sense and converged toward same values.

The results of the w/wo LED comparison are displayed in figure 4.7. The difference observed is not very large but seems noteworthy. Eddy current are foretold as strong disruptor of the analysis[20] here nothing so obvious seems to happen. Indeed, in an unexpected turn of event the LED seems to worsen the analysis. Our main hypothesis is that introducing one more delay within the sequence worsen it; due to evolution or possible problem in the refocusing (imperfect spoiler, pulse calibration…). There is a difference between STE and DSTE; DSTE having better uncertainty but lower alignment and *vice versa*. This is something we have seen all throughout this work, it is possible that it is caused by the abundance of delay in DSTE that may cause unwanted evolution of the magnetization and J-modulation, sometimes visible in the spectra, lightly disturbing the integration process. On the other part convection is almost unavoidable[41] and even in water this could explain the better fit and improved uncertainty. This slight difference of alignment is deemed a small price to pay for the compensation of convection that will be a major issue in all organic solvent with low viscosity

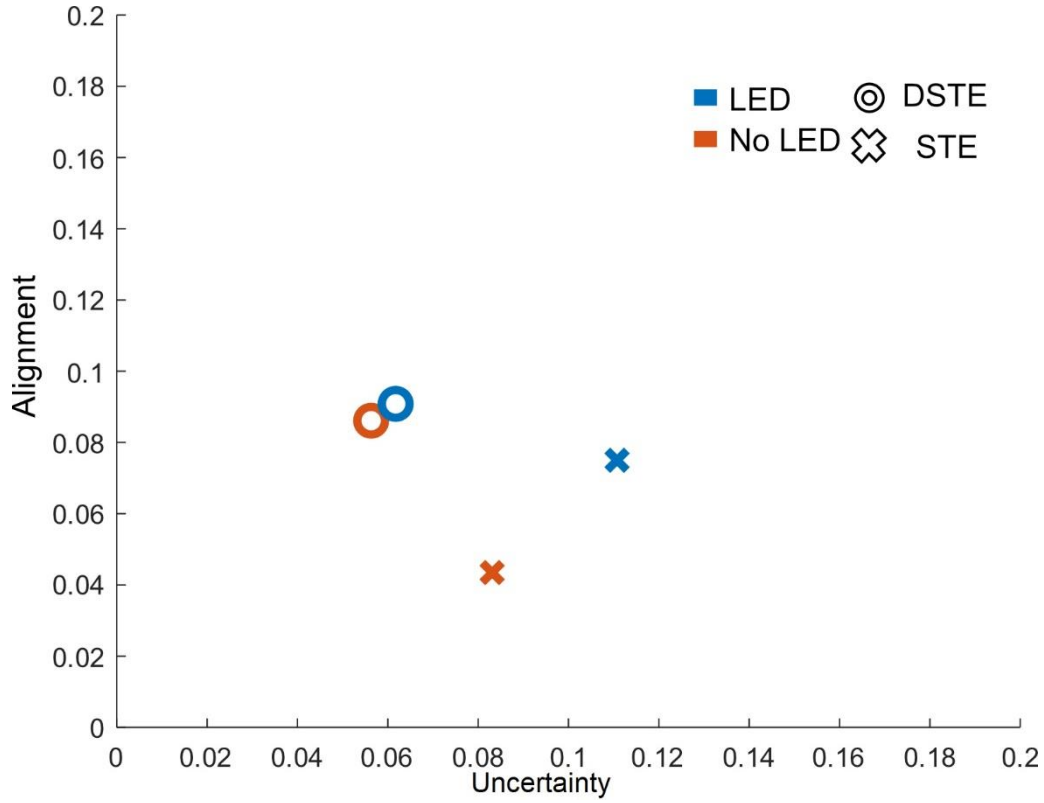

Figure 4.7. each correlation circle/cross is representative of a single DOSY spectra matching its color. Cross indicate STE ring DSTE, blue with led orange without. Both axis unit is that of diffusion coefficient ($\times 10^{-10} m^2/s$). Label are indicative related to the text.

Another aspect that we tested is the strength of the spoiler gradient. Without spoiler gradient the resulting spectra is barely readable and can be called non-working DOSY. Adding even a small value of spoiler seems to solve this but it is interesting to test it, as gradient and their behavior play a huge

role in DOSY. We tested the same sequence (without LED) with varying gradient power and the result is shown in figure 4.8. The test is also done on both DSTE and STE. The spoiler to be efficient should dephase the magnetization and never rephrases it, so they should have 2 different values for DSTE, in all cases it should never be the same as diffusion encoding or any other gradient value. The value in the figure 4.8 are just the order of magnitude of the gradient power (100% ≅ $60\ G/cm$). The result shows a lack of difference in gradient strength. It did not seem to play any meaningful role the difference observed are close to ~1%. We thus decided to use the value advised by the constructor around 10%(orange).

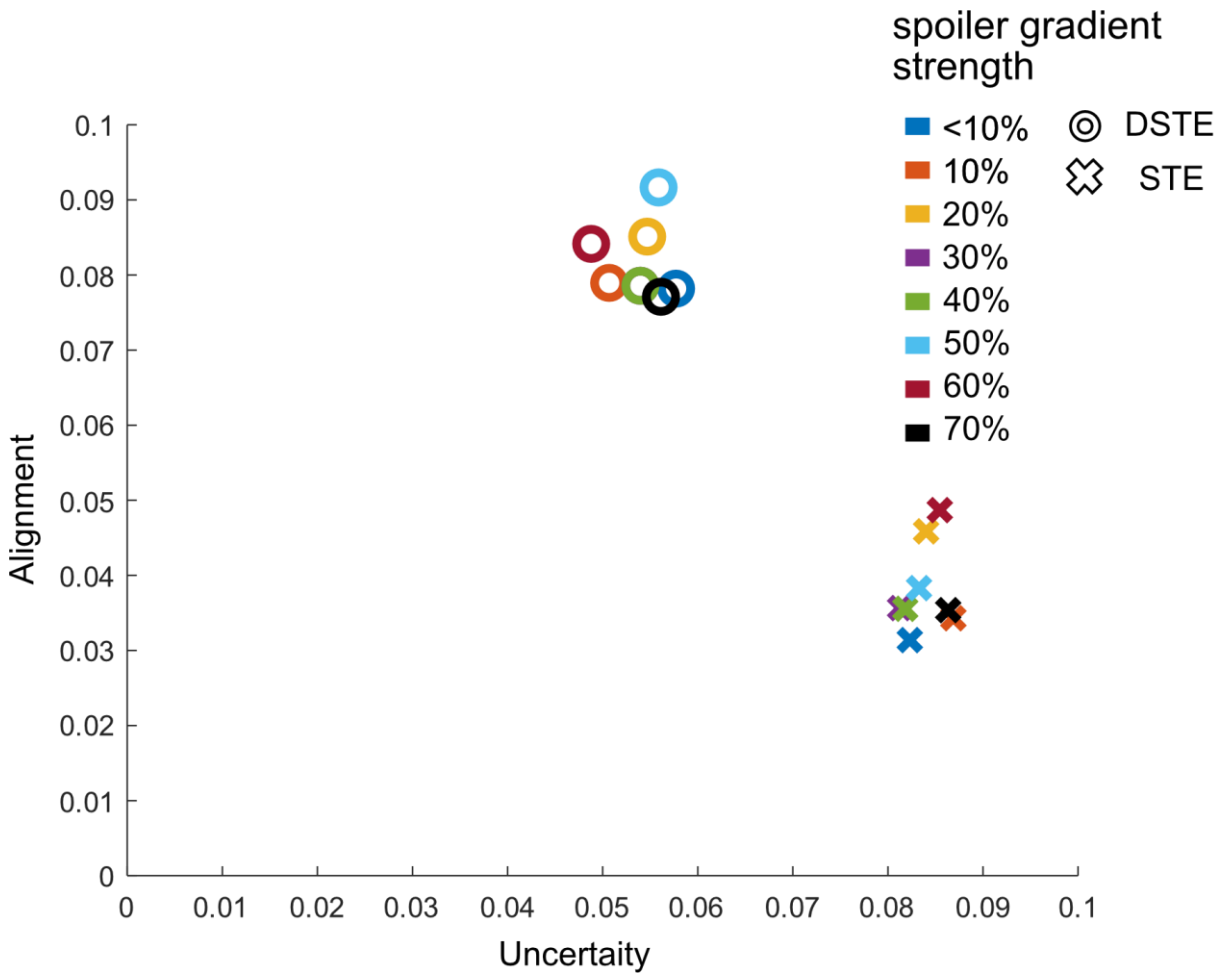

Figure 4.8. each correlation dot is representative of a single DOSY spectra matching its color. Cross indicate STE ring DSTE, gradient order of magnitude for spoiler are indicated in the legend. Both axis unit is that of diffusion coefficient ($\times\ 10^{-10} m^2/s$). Label are indicative related to the text.

5. Experimental part

In this part we will detail the experimental procedures for the rest of the thesis.

All experiments were done on a Bruker Avance III spectrometer, operating at a ^{1}H Larmor frequency of 500 Mhz, using a broadband inverse-detection triple-axis gradient probe (BBI) with a deuterium channel for locking. The NMR experiments are carried on a 5mm diameter NMR sample tube standard or with capillaries inside (flowtube).

The gradients were calibrated using a standard tube of doped water made by the vendor. "Doped water" by Bruker composition is 1% H_2O in D_2O doped with 0.1 mg/mL of $GdCl_3$ and containing 0.1% $^{13}CH_3OH$. Calibration of the gradients gave a value of 63.0 G/cm for the Z axis, 47.0 G/cm for the X axis, 48.2 G/cm for the Y axis. The gradient power is expressed as a percentage of this value.

The temperature was set at a nominal value of 298 K with an airflow 535 L/h and calibrated thanks to a standard methanol sample. No sample rotation was ever used.

All gradients for diffusion encoding are of sine shape (shape named SINE.100).

5.1. -Section 6 methods

5.1.1. Oneshot methodology

For this section the sample used was the same for all the experiments and was a solution in D_2O with a concentration at 0.1 M of three compounds: sucrose from edible sources, pyridine, and 2-butanol. The tube was standard NMR tube of 5 mm outer diameter filled with 600 μL of solution. The tube was closed with parafilm, and stored at room temperature.

5.1.1.1. Coherence selection using parallel gradients

The Oneshot parallel gradient sequence is described at ref XX and is named "Doneshot". It was used as it is, except for the version with no phase cycling. For this version the only modification is the removing of the phase cycling within the sequence program.

The diffusion time Δ was 160 ms for all the DOSY experiments and δ was 2.8 ms. Each experiment was started by 4 dummy scans and had a 3 s inter scan delay. The number of points is 16384 by spectra with a spectral width (SW) of 12 ppm leading to a total of 1.36 s of acquisition.

Each DOSY data set was acquired with 16 gradient increments, using a linear ramp of gradient power ranging from 10% to 70%, along the Z axis. For 1-scan experiments the total duration of the experiment was 90 s and for the 8 scans version 10 ~min. When not specified the α factor for coherence selection was 13%.

5.1.1.2. Coherence selection using orthogonal gradients

The oneshot orthogonal coherence selection gradient sequence was custom-written and is available in the appendix under the name "AMstebposgc_grad_v2".

The diffusion time Δ was 160 ms for all the DOSY experiments and δ was 2.8 ms. Each experiment was started by 4 dummy scans and had a 3 s inter scan delay. The number of points was 16384 by spectra with a spectral width (SW) of 12 ppm leading to a total of 1.36 s of acquisition.

Each DOSY data set was acquired with 16 gradient increments, using a linear ramp of gradient power ranging from 10% to 80%, along the Z axis. For 1 scan experiment the total duration of the experiment was 90 s and for the 8 scans 10 min. Coherence selection gradients (crushers) were on the the Y axis and spoilers were on the Z axis. There are two versions with and without phase cycling; phase cycling is noted "_phycy".

5.1.1.3. Comparison between the two

The condition for DSTE used in 5.1.1.2 and 5.1.1.1 were re-used. Δ was 160 ms, δ was 2.8 ms, the number of points is 16384 by spectra with a spectral width (SW) of 12 ppm leading to a total of 1.36 s of acquisition. The gradient ramp was 10% to 70% linear for all compared experiment.

5.2. Section 7 methods

For flow experiments the sample was made of a 25 mL solution in H_2O with three compounds concentrated at 0.1 M. The compounds were: sucrose from edible source, pyridine and 2-butanol. The reference data was acquired by using 600 μl of this solution in an NMR tube out-of-flow.

5.2.1.1. Methods for Diffusion-encoding with longitudinal gradients

For all experiments compared here the NMR setup was with flow on. The lock was off during the experiments. The NMR experiments were regular DSTE with bipolar pulses and 16 scans per increment and 16 increments with full phase cycling. The sequence used was "AMdsteosgc_grad_v2_phycy" with no crusher enabled and three spoiler gradients.

The diffusion time Δ was 160 ms for all the DOSY experiments and δ was 2.4 ms. Each experiment was started by 4 dummy scans and had a 3 s inter scan delay. The number of points was 16384 by spectra with a SW of 12 ppm leading to a total of 1.36 s of acquisition time. The gradient power for diffusion encoding is 10% to 80% linear ramp in the Z axis. The WET solvent suppression pulses powers were optimized each day as necessary and gradient pulse length was 2ms. The total duration for one experiment was 21 min.

5.2.1.2. Methods for Diffusion-encoding using transverse gradient

For all experiments compared here the NMR setup was with flow on. The lock was off during the experiment. The NMR experiment were either regular DSTE with 16 scans per increment and 16 total increments with full phase cycling or STE with 8 scan per increment with full phase cycling. The DSTE sequence was named "AMdsteosgc_gradX_phycy". The STE sequence was "AMwetstebposgc_gradX_ phycy _v2". Both were used with no crusher gradient.

Each experiment started with 4 dummy scans. The gradient power for diffusion encoding is 10% to 80% linear ramp in the X axis. The diffusion time Δ was 160 ms for all the DOSY experiments and δ was 2.4 ms. The number of points is 16384 by spectra with a SW of 12 ppm leading to a total of 1.36s of acquisition time. The WET solvent suppression pulses powers were optimized each day as necessary and gradient pulse length was 2ms. The total duration was 21min for DSTE experiments and 10 min for STE experiments.

5.3. Section 8 methods

5.3.1. Chemistry experiment setup

5.3.1.1. Sample preparation

The reaction was carried out in a glass flask with a special cap that allow capillaries to pass. The volume of solvent, acetonitrile HPLC-grad, was 20mL + the amount within the flowtube whole apparatus (~5 mL). In this volume dissolved 256 mg of the di-amine was dissolved. One has to be careful it oxidises quickly and form a black/brown dye. The solution was then put under magnetic stirring until full dissolution.

The flowtube apparatus was purged of the storing solvent, usually 2-propanol, by the reaction solvent acetonitrile. Once ready the capillaries were put on the glass flask containing the solution and the flow was set to 3 mL/min until pressure is constant and no bubbles appear. 1D NMR experiments and test DOSY experiments are done at this point. They are there to check the medium as well as the efficiency of solvent suppression.

When the solution containing acetonitrile and the di-amine loops continuously and properly, the aldehyde can be added. Using a glass syringe, 0.42 mL of aldehyde was added through the cap. The NMR monitoring experiments were then launched as fast as possible following this addition.

Throughout the reaction the medium will change colour, starting clear with a hint of yellow to orange/brown at the end, the pressure might slightly increase during the reaction (+0.5 bar maximum).

5.3.2. NMR experiment setup

DSTE experiments were interleaved with 1D experiments for the duration of the monitoring. 1D experiments were for safety/control and are not used here. The DSTE sequence name is "AMwetdsteosgc_gradX_phycy".

DSTE were 1 scan, 16 increments and 4 dummy scans with a diffusion encoding gradient in X with a linear randomly permutated ramp[159] of 10% to 80%. The diffusion time Δ was 100 ms for all the DOSY experiments and δ was 1.6 ms. Coherence selection gradient (crusher) were on the Y axis and spoilers were on Z axis.

DSTE were 16384 points, SW was 22 ppm for an acquisition time of 0.74 s and a recycle time (D1) of 3s, leading to a full experiment time of 80 s. The solvent suppression WET was on shaped pulses were aimed at the solvent peak (acetonitrile). Shimming routines were done when necessary, every ~20 min.

Part C

6. Accelerating DOSY experiments

This chapter describes two independent developments of fast DOSY experiments. The main goal of this Ph.D. work was to develop DOSY experiments for online reaction monitoring by flow NMR. For this to happen we needed an NMR experiment that is relatively fast, to be able to fit a lot of different situations that reflect the diversity of reaction monitoring. We aimed for an experiment duration of around one minute, which is an order of magnitude faster than classic DOSY experiments. This was achieved using the "oneshot" approach, as described in section 6.1. Independently from our main work on reaction monitoring, we also contributed to the development and implementation of multivariate processing methods for ultrafast diffusion-ordered NMR spectroscopy. This work is described in section 6.2.

6.1. The Oneshot approach

We will here call "oneshot" a sequence that allow to have only one scan per point in the indirect dimension. It means that coherence-transfer pathway selection cannot be achieved with phase cycling, and has to rely on pulsed field gradients. This is a general notion that could apply to any 2D NMR experiment. In DOSY it consists of using 1 scan per gradient value, greatly increasing the speed, by a factor of 8 or 16, corresponding to the minimum number of scans required for CTP selection in the STE and DSTE sequence. This approach also aims at being usable with traditional knowledge of routine diffusion NMR.

6.1.1. Coherence selection using parallel gradients

Probably the better documented method using such approach is the pulse sequence described by the Manchester NMR group in 2002.[136] Part 2 gives most of the detail needed to understand the sequence and its uses, we are here going to evaluate results obtained with this sequence, as well as modified sequences that we implemented.

Pelta et al.[136] aimed at finding a way to improve DOSY by reducing the number of scans for each gradient value. For that they use unbalanced bipolar gradient pulses around the 180° pulses, the goal is to dephase the magnetization that is not refocused by the 180° pulse. Their pulse sequence is a concatenation of works[164,174–176] on diffusion NMR. The work includes adding a spoiler, the bipolar pulses technic as well as the use of unbalanced gradients and a new phase cycling, overall having an updated diffusion NMR sequence. It is a "modern" sequence (from the late 90's), most of the improvement are the foundation of improved DOSY sequence, including this work.

The sequence is shown in Figure 3.1. The only new parameter one can really tune is the unbalancing factor α which makes the two gradient pulses of each pair in the ratio $1+\alpha : 1+\alpha$. The ideal value of α will depend on many factors such as the pulse calibration or any B_1 inhomogeneities. It is thus hard to tell which precise value will be the best, Pelta et al. advice a value between 10-20%. The gradient imbalance is achieved as a modification of the usual diffusion encoding gradient. We usually use a ramp of 10-80% of the maximum gradient amplitude, in order to avoid using the amplifier in a regime where it may be nonlinear. Using this we decided to run a test for each value between 10% and 20% imbalance by steps of 1 percentage point. The results are shown in Figure 5.1. It seems that all the results are very close to each other. One can see that there is already a noticeable error for the measured value of the diffusion coefficient, especially in the absence of phase cycling. For the rest of this work, we choose to use an experiment with 13% of alpha.

It is important to note that this approach requires a fit with a modified version of Stejskal-Tanner equation.[124] The equation used for the fit is therefore[124]

$$S = S_0 \exp\{-\gamma^2 g^2 \delta^2 \left[\Delta + \frac{\delta(\alpha^2-2)}{6} + \frac{\tau(\alpha^2-1)}{2}\right]\} \qquad 56\text{-}1$$

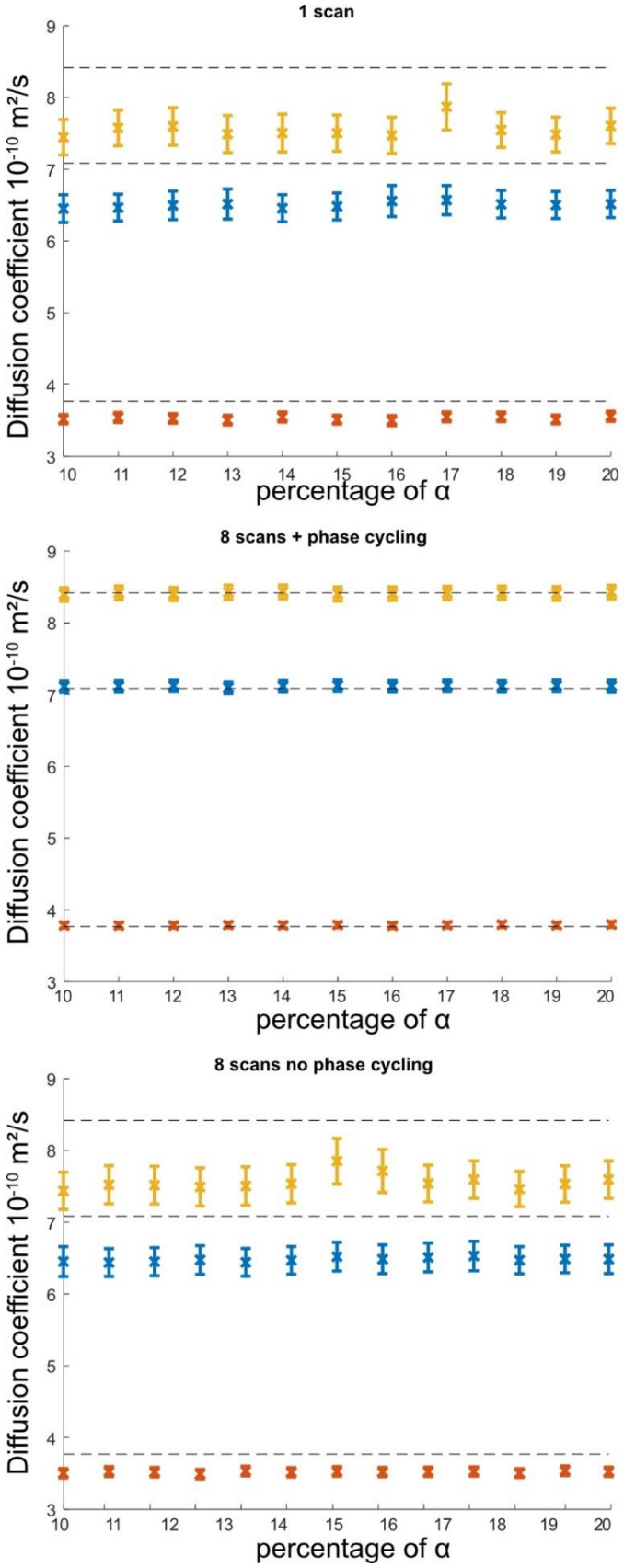

Figure 6.1 Optimization of the parameter α in the oneshot pulse sequence. The measured diffusion coefficients are shown for a series of values of α. The dotted line are references experiment from a STE in 8scans with full phase cycling.

6.1.2. Coherence selection using orthogonal gradients

Another method to achieve coherence selection with gradient pulses is to apply them on an axis that is orthogonal to the diffusion-encoding axis, rather than parallel. This method was for example described by Ferrage and co-workers in STE-DOSY NMR experiments.[138,177] Despite this early development it does not seems to have caught the attention of the community as we did not find much use of this method reported in the literature. The main probable reason being the need to implement it on a triple-axis gradient probe, which is not a common material in NMR lab and facilities. Having this kind of hardware in our lab (for the implementation or pulse sequences derived from MRI methods), we decided to use it.

To implement this method, we were inspired by the sequence X-STE of F. Ferrage et al.[177] Our implementation is shown in figure 6.2. It is important that the diffusion encoding and CTP selection happen at the same time. The diffusion channel is the axis on which the incremented diffusion-encoding pulse are. In this chapter it was the Z axis, to allow meaningful comparison with the other sequences. Each 180° pulse is flanked by a pair of identical gradient pulses. For this strategy to work as well as possible, the total area of the gradient pulses should be different for each pair, and for the spoiler gradient. If the total area is the same then we are at risk of defocusing the unwanted signal, then refocusing it with a latter pair (see part 1).

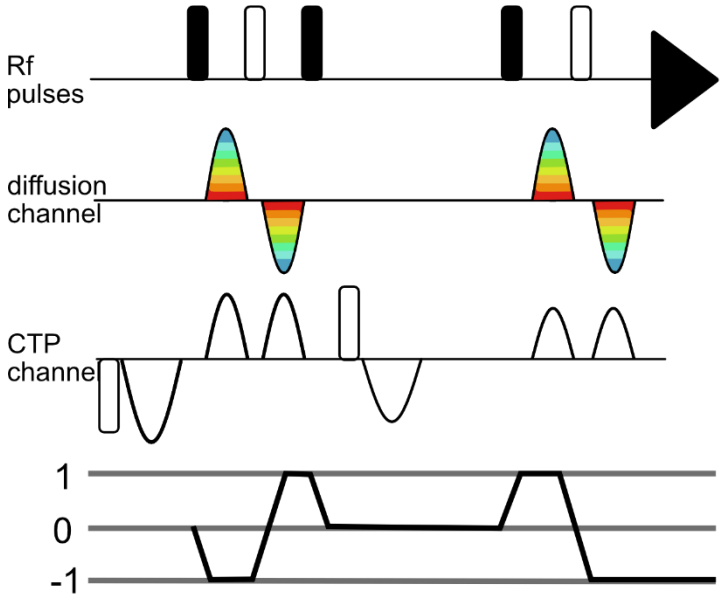

Figure 6.2. The STE orthogonal oneshot sequence. the rainbow-colored pattern pulses represent the incremented gradient for diffusion encoding. The black rectangle are 90° pulse and white ones are 180° on the Rf channel. The gradient pulse is either a sinusoid-like shape for CTP selection or a rounded-square for spoiler. The spoiler and CTP selection pulses are compensated to keep the lock working during the experiment.

As with the parallel encoding we did some tests to see what would be the best value for coherence selection gradient power. The results are displayed in figure 6.3. The method gave result that were satisfactory out-of-flow and allow for easy and rapid customization in the axes that can be used for the experiment. On figure 6.3 one can see that the relation between gradient power and

quality is not straightforward. There is no real trend one could confidently retrieve from this number of experiments. It seems that value between 10 % to 70 % are safe.

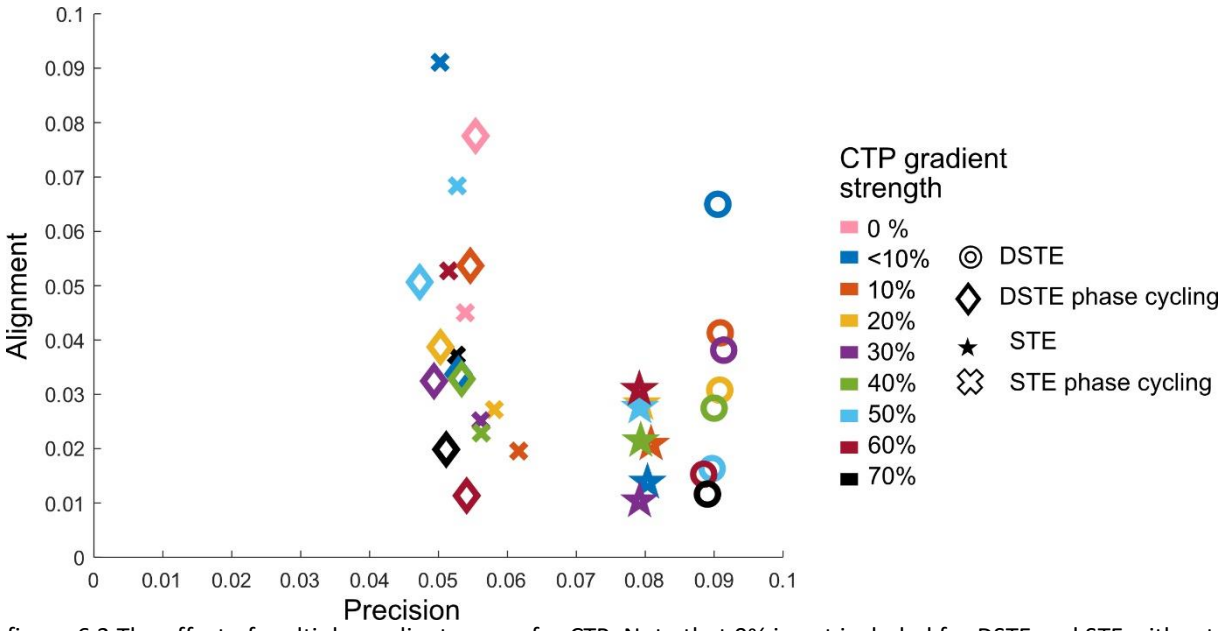

figure 6.3 The effect of multiple gradient power for CTP. Note that 0% is not included for DSTE and STE without phase cycling the result can be called non-working DOSY. The ramp was 10-80%.

6.1.3. Comparison between the two

Having characterized the two methods of oneshot we now want to compare them. We recorded DOSY experiments in a conventional fashion and with both parallel or orthogonal-coherence selection gradients, with and without the phase cycling in 8 scans for STE experiments and 16 for DSTE experiments. The experiments with multiple scans but not phase cycling were carried out to focus on the effect of CTP selection, rather than sensitivity. Experiments were also carried out with 1 scan to assess the results obtained with a fast implementation. For this part we choose a power for the CTP gradient to be around 10% for the orthogonal gradient and 13% for alpha in parallel gradient selection.

The results are displayed in figure 6.4, in the style of comparison that was described in part 4.4.2. As a reminder the closer a point is to the origin, the better the corresponding DOSY results are. For the STE case, we tried the two methods of gradient-based coherence selection (parallel and orthogonal) and we can see that, without the phase cycling, using parallel CTP selection gradients does not yield good results. In contrast, using orthogonal CTP selection gradients gives results that are in the middle. It is not easy to explain why the phase cycling does not yield better results in that case. Yet in the absence of phase cycling the orthogonal selection clearly works giving good result even in 1 scan and it seems to be the only coherence selection that allow 1 scan.

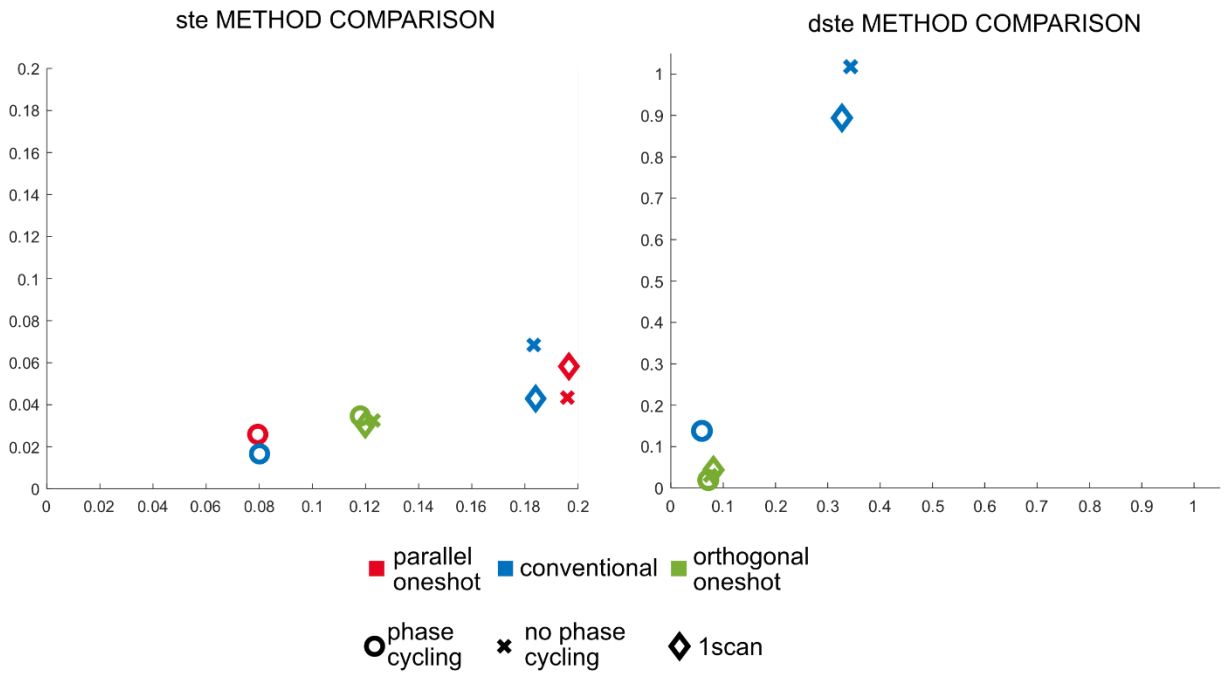

Figure 6.4, results of different comparison for coherence selection. STE are in 8 scan and 16 for DSTE as it is the minimum number of scans for a full phase cycling. Result seems to indicate that only orthogonal gradient and phase cycling give some coherence selection. DOSY spectra are available in annexe (figure 6-4s)

With those results in mind, we tried the DSTE sequence. Because there is no parallel oneshot reported in the literature, and because our result with STE sequences shows no improvement, we decided to skip this approach. We developed our own DSTE sequence using the same kind of instruction for orthogonal gradient. From our knowledge it is the first time a DSTE experiments in one scan per increment is reported. The sequence is showed in figure 6.5. The CTP gradients in the DSTE appear 3 times, one for each 180°and are identical within the same pair but slightly different between pairs (*vide supra*).

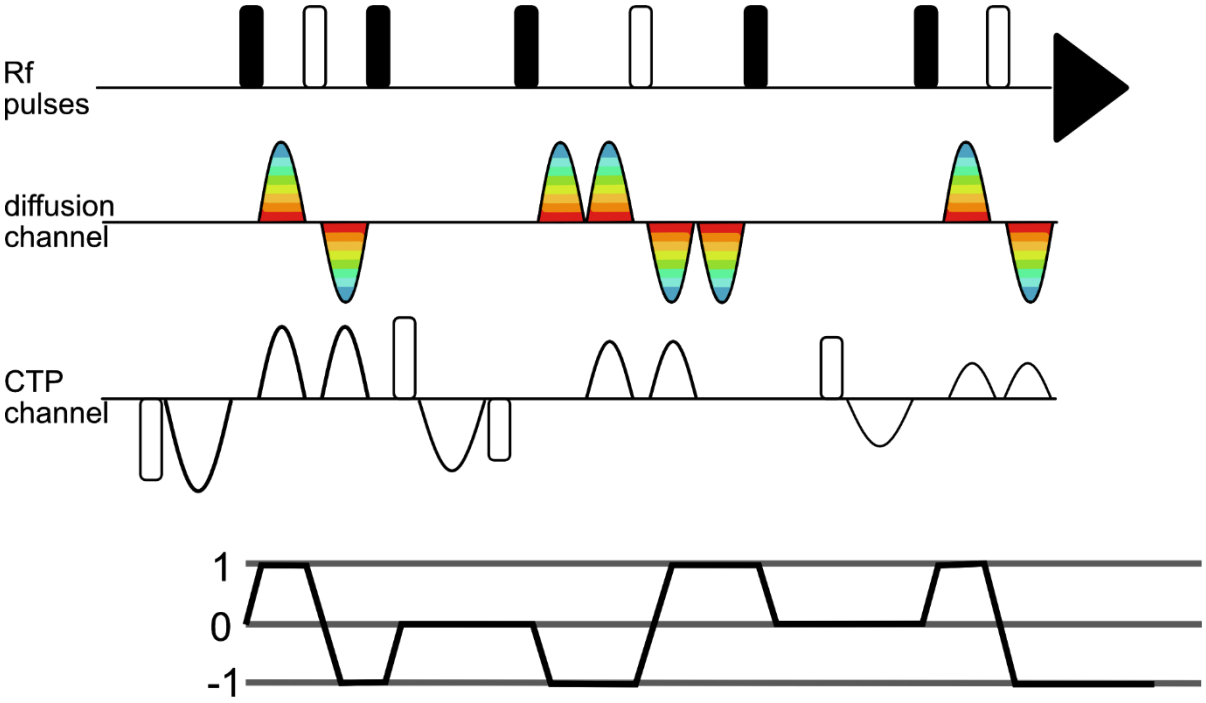

Figure 6.5. The DSTE orthogonal oneshot pulse sequence. The incremented diffusion encoding pulse are represented with the rainbow-colored pattern pulse. The black rectangle are 90° pulse and white ones are 180° on the Rf channel. The gradient pulse is either a sinusoid-like shape for CTP selection or a rounded-rectangle for spoiler. The spoiler and CTP selection pulses are compensated to keep the lock working during the experiment.

In the DSTE case, coherence-selection is even more important, because achieving it through phase cycling requires more scans than in the STE case. If no coherence selection is done, the errors accumulate and lead to much worse results. This is seen in Figure 6.6, where the error for the DSTE case without CTP selection is larger than for the STE case without CTP selection. The use of orthogonal gradients this time seems to give better result with or without phase cycling and in 1 scan.

6.2. Multivariate processing of ultrafast DOSY experiments

This section is largely independent from the rest of the thesis. It describes the design and implementation of multivariate processing methods for ultrafast DOSY experiments, to which I contributed in the early part of my Ph.D. work. The multivariate processing algorithms that we have used will first be briefly described in section 6.2.1., and their application of UF DOSY data will be described in section 6.2.2.

6.2.1. Multivariate processing methods for diffusion NMR

Up to this point, we have focused on the DOSY display as a way to analyse diffusion NMR data. This method used to construct a DOSY display is called univariate, because it accounts for one variable at a time, either an intensity or an integral. This approach while interesting has two major limitations: it is user dependent and it is very limited when it comes to overlapping peaks. Another approach, called multivariate processing, consists of processing the data set as a whole. These methods aim at solving the equation:

$$X = CP^T + E \quad \text{66-2}$$

where X Is the data set, C is a matrix of component decays, P is a matrix of component spectra, and E is the experimental error (noise). In practice, multivariate methods do not require setting a threshold and/or integration region. The parameters to apply are usually simple, and include the definition of the number of components within the mixture, and the possibility to disregard a region for the processing. This result in a set of 1D spectra with only the pure component, ideally one spectrum per molecule.

Multivariate methods rely on algorithms that are more user independent, and they can achieve better results for overlapping peaks, to the point of solving overlaps. They can also quicken the analysis as there is no need for manual integration, yet this can be balanced by the duration of the calculation. Also, the number of compounds that can be efficiently separated is somewhat limited. In the case of UF DOSY we tested two algorithms, Direct Exponential Curve Resolution Algorithm (DECRA), and Speedy Component Resolution (SCORE).

DECRA was introduced as a way to analyse diffusion NMR data by Antalek in 1996. It is one of the most straightforward methods of multivariate that exists, and also the fastest one.[166,178,179] It is available in the processing software Topspin, as well as in the GNAT package for MATLAB.[150] DECRA relies on the possibility to find the exact solution of Eq. 6-2 in the case of purely exponential decay of the data as a function of the row index. In the case of diffusion NMR data, this requires that the gradient ramp be quadratic, meaning that the values of G_i^2 are equally spaced, where G_i is the i^{th} gradient amplitude in the list. The benefits of using non-linear gradient ramps for univariate analysis have been debated in the literature,[180–182] but in the case of DECRA quadratic spacing is a requirement.

The SCORE algorithm was development by Nilsson and Morris,[183] and is an evolution of the CORE algorithm originally developed by Stilbs.[184–186] In contrast to DECRA, which relies on an exact solution, (S)CORE relies on an iterative fitting process, using a model for the data. The model is derived from the Stejskal-Tanner equation and can be defined for arbitrary gradient ramps. Initial guesses are made for the diffusion coefficients, and the component spectra and diffusion coefficients are then optimized in turns, until the convergence conditions are met. The improvement of SCORE over CORE arises from the realization that finding the best possible component spectra for a given set of diffusion coefficients is a linear rather than nonlinear optimization problem. In practice, in the implementation provided in GNAT,[150] the user simply has to provide the number of fitted components, and choose how the initial guesses of diffusion coefficients are made. Options are also available, such as the use of a non-negativity constraint within the algorithm.[183]

6.2.2. Methods[178]

6.2.2.1. Sample preparation

A sample composed of sucrose and propan-1-ol in D_2O was used to perform spatially encoded diffusion NMR experiments. 103 mg of sucrose is dissolved in a solution of 45 µL propanol and 555 µL D_2O to prepare approximate 500 mM concentration of both of the components in D_2O. The mixture was transferred to a standard 5 mm NMR tube for SPEN DNMR experiments.

6.2.2.2. NMR spectroscopy

All the experiments were carried out on a Bruker spectrometer operating at a Larmor frequency of 500.13 MHz, equipped with a triple-axis gradient, broadband inverse-detection probe. The temperature was set at a nominal value of 298 K and the diffusion time was 100 ms for all the DOSY experiments, except when specified.

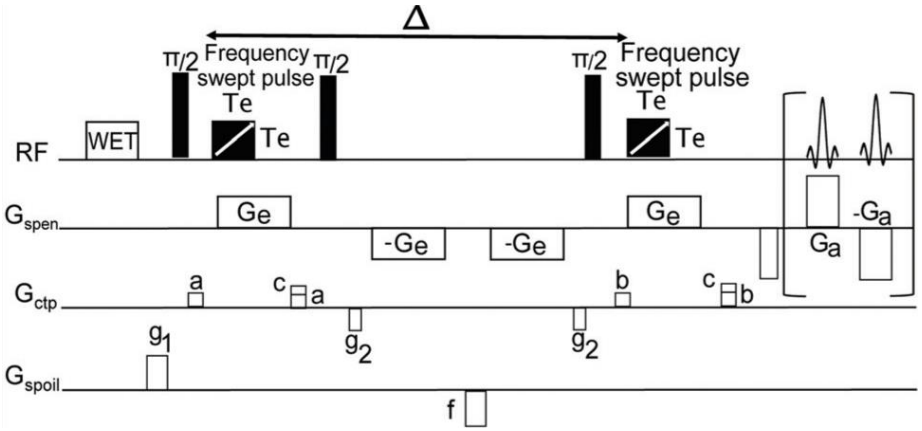

Figure 6.6, the pulse sequence for UF DOSY upper channel show the rf pulse. Medium channel shows the gradient pulses for encoding/acquisition. The bottom channel display coherence selection gradients. Reproduced from Mishra et al.[168] under a creative commons license (CC BY 3.0)

SPEN DOSY experiments were carried out using the pulse sequence shown in figure 6.6. The diffusion encoding parameters were chosen to sweep a 10.2 mm region of the sample with the frequency swept pulses (for both linear and quadratic sweep). The pulses had a bandwidth of 110 kHz, a duration of 1.5 ms, and were applied together with a rectangular gradient, with a short ramp of 25 µs placed symmetrically around the gradient, of 0.2538 T/m. The acquisition consisted of a train of bipolar gradient pulses, with an amplitude of ±0.29 T/m and a duration of 332.8 µs for each gradient pulse, resulting in a spectral width of 3 ppm. 256 loops were acquired, resulting in an acquisition time of 170.4 ms. Spatial encoding was performed along the Z axis. Coherence selection gradients were applied along the Y axis, with amplitude 0.041 T/m for a and 0.077 T/m for b, and a duration of 1000 µs. The spoiler gradient f was applied with 0.052 T/m on the X-axis and 0.061 T/m on the Y -axis, and a duration of 1000 µs. The compensation gradient was g1 = - f. The WET pulse sequence block was used for solvent suppression.

6.2.3. DECRA analysis of SPEN DOSY data

Before applying DECRA to SPEN DOSY data, we wanted to test it on conventional DOSY data. In order to do this, we worked with a simple mixture of sucrose and propan-1-ol. This mixture was prepared at a concentration of 0.1 M in D_2O. The 1D ^1H spectrum is shown in Fig 6.7 and it can be seen that peaks overlap in the 3.4–3.6 ppm region. Several conventional DOSY data set were acquired, using quadratic ramps, and different values of the diffusion delay (Δ). and of the duration of the diffusion-encoding gradient pulses (δ). We observed that the results are highly dependent on the choice of parameters. Also, unmixing was never perfect, with artefact visible in the new yielded spectra. On the other hand, field homogeneity was found to have little influence on the quality of the separation. Overall, the process was less straightforward than we thought. By using reduced fitting area in UF, shortening the spatial area that is the diffusion axis, we noticed, as reported[166], that linearity of gradients was very important.

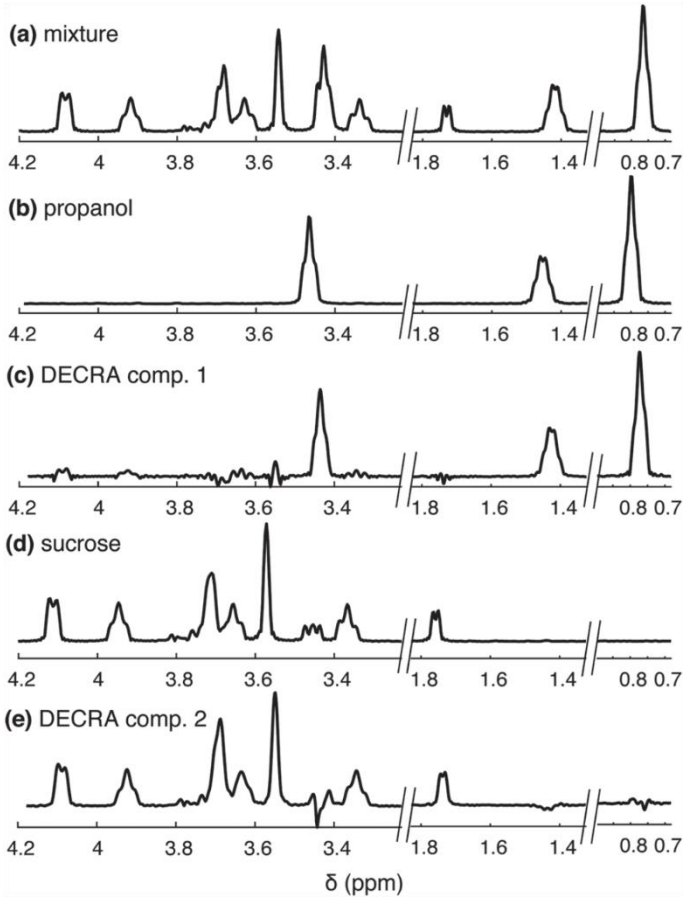

Figure 6.7, the UF spectra disentangled using DECRA procedure and the QS (Quadratic Sampling) pulse for spatial encoding. Reproduced from Mishra et al.[178] under a creative commons license (CC BY 3.0)

DECRA was initially not applicable to SPEN DOSY data. This is because the experiments are usually carried out with a linearly swept pulse, also called chirp pulses, that yields data with a linear ramp of effective gradient values:

$$K_n = n \times \mathrm{K}_1, \text{ for } n = 2, 3, \ldots \qquad 56\text{-}3$$

where K_n is the effective gradient area for slice n. This is in conflict with the requirement for DECRA, which is:

$$(\mathrm{K}_n)^2 = n \times K_1^2, \text{ for } n = 2, 3, \ldots \quad 56\text{-}4$$

A solution was found by R. Mishra and J.-N. Dumez having a swept pulse of the form[178]

$$v_{rf} = BW\left(\frac{(T_e - t)^2}{{T_e}^2} - \frac{1}{2}\right) \quad 56\text{-}5$$

Which give a gradient spacing that match the DECRA quadratic sampling condition.[178] Figure 6.8 shows the shape of the new pulse.

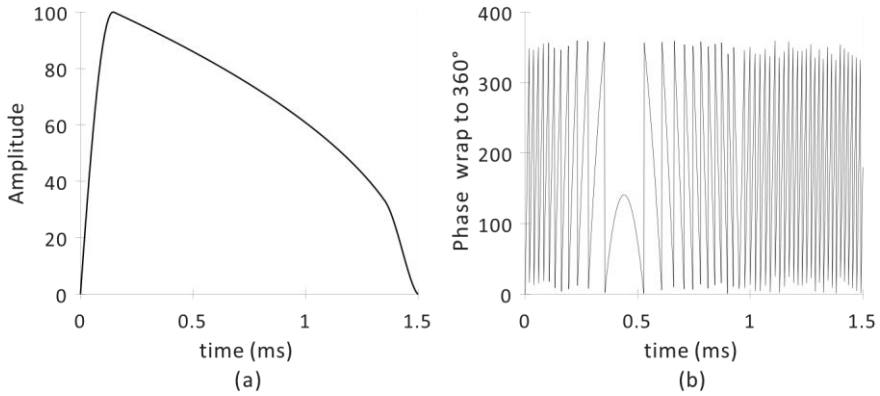

Figure 6.8, (a) Amplitude and (b) phase wrapped to 360° of the quadratic sampling (QS) chirp pulse of length 1:5 ms. Reproduced from Mishra et al.[178] under a creative commons license (CC BY 3.0)

This new swept pulse allowed to have unmixing of propanol and sucrose, after trial-and-error optimization of the spatial region used for the analysis. The algorithm, which is not based on a fitting process, required less than 1 second to run. At this stage, the analysis was found to fail for more than 2 spectra, for example when the residual HDO peak is kept in the analysis. For this reason, that signal was suppressed using the WET solvent-suppression block. The failure to separate 3 spectra might be because of insufficient sensitivity (multivariate methods will demand for more and more SNR as the number of compounds increase), and also because gradient non-uniformity is no accounted for in the analysis. Note that when carrying the experiment on conventional DOSY (non-uf) separation of more than 3 compounds was also very difficult.

6.2.4. SCORE UF

We also applied the SCORE algorithm to SPEN DOSY data. In this case the experiment does not need any adjustment, as SCORE does not have special requirements on the sampling scheme. However, the algorithm needs to be adapted to match the specific form of the Stejskal-found in SPEN DOSY. A general form of this equation with linear ramping can be written:

$$y = a_1 e^{-a_2 \Delta' K^2} \quad 56\text{-}6$$

With a_1 and a_2 adjustable parameters, those that the SCORE procedure will optimize. In the UF DOSY Δ′ and K are slightly different. Spatial encoding and parallelization that make the process possible is linked to a spatial axis z rather than incrementation in time. This gives:

$$y = a_1 e^{-a_2 \Delta' K(z)^2} \qquad 66\text{-}6$$

With $\Delta' = \Delta - \mathrm{Te}$ and $\mathrm{K(z)} = 2\gamma G[2Te - 2t_{flip}(z)]$. Note that $t_{flip}(z)$ is defined as the moment spins in z position undergo their flip due to the swept pulse. It is calculated in the classic CHIRP as:[141]

$$t_{flip}(z) = \frac{\Omega_i - \gamma G z - \omega_{rf}^i}{R} \qquad 56\text{-}7$$

With R the swept-rate, ω_{rf}^i the initial frequency-offset. The inner and outer loop can then do the SCORE routine and yield figure 5.8 upon successful separation of the compounds.

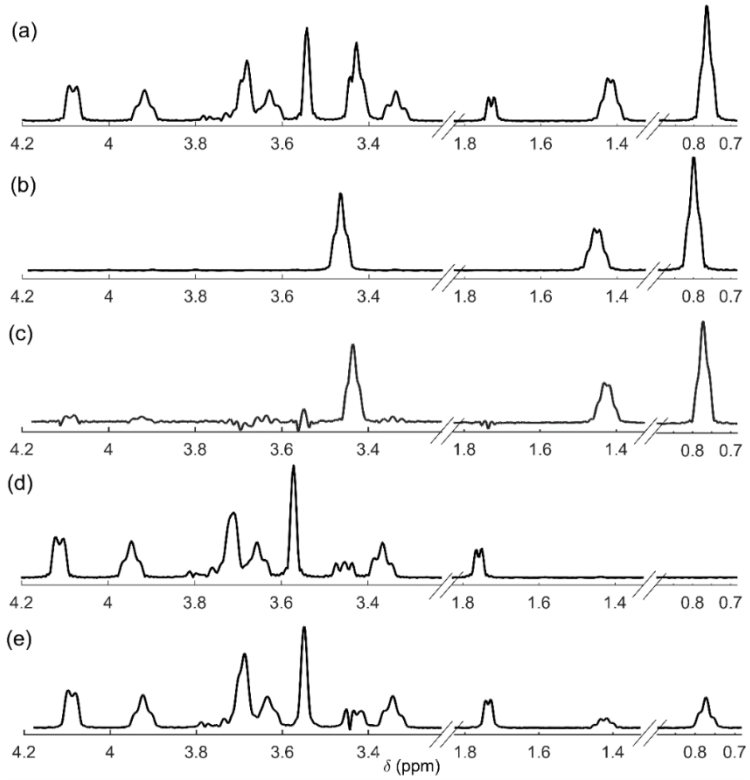

Figure 6.9 SCORE processing of SPEN DNMR data for a mixture of propan-1-ol and sucrose in D2O, compared to the spectra of the compounds acquired separately. The residual HDO peak is suppressed by a WET pulse sequence block. (a) 1D spectrum of a mixture of propan-1-ol and sucrose in D2O. (c, e) Components obtained by SCORE processing of SPEN DNMR data. (b, d) 1D spectra of (b) propan-1-ol and (d) sucrose alone in D2O. The 1D spectra are obtained as slices of EPSI data. Reproduced from Mishra et al. [178] under a creative commons license (CC BY 3.0)

SCORE and DECRA gave similar output and quality of separation, this is also true for conventional (non-UF) methods. The main difference between them is applicability and ease-of-use. SCORE as some parameters than can be changed and tunes which also implies that it will work on a trial-and-error fashion that can take time. The condition such as non-negative constrain will lengthen the analysis but can allow it to work. The main advantage versus DECRA is that it does not need special pulses or

modification of the experiments. In theory one could use or try SCORE on any DOSY data which is a huge advantage against DECRA that need a specific set of conditions.

6.2.5. UF DOSY for flow NMR monitoring

Since the main goal of this Ph.D. project was to achieve online reaction monitoring with fast DOSY methods that are flow compatible, one may wonder why spatially-encoded DOSY was not used further. The main interest of SPEN methods is the experiment duration, that is often under one second. However, this ultimate speed comes at the cost of several challenges, and it may also not be needed for the kind of applications targeted in this work. Here we will discuss these two points.

Several limitations of the SPEN DOSY method arise from the use of echo-planar spectroscopic imaging (EPSI) for detection. EPSI is very demanding for the gradient coils. The rapid change of polarity from the gradients put a physical constrain on the coils, making them heat, vibrate or even twisting them. This limits the minimum echo spacing that can be achieved, and as a result the spectral width, according to:

$$\mathrm{SW} = \frac{1}{2Ta'}, \qquad 56\text{-}8$$

Where $2\,Ta'$ is the echo spacing. The SW is often limited to ~4 ppm, aliasing possibly allowing to have all the peaks but in a crowded version with possible wrong chemical shifts.[187] This could probably be addressed with the used of “interleaved” acquisitions, as for ultrafast 2D spectroscopy experiments, but such strategy has not been implemented so far.

Another limitation results from the maximum duration during which the EPSI train can be sustained by the gradient coil. On high-resolution probes, the acquisition time is limited to about 150 ms, which limits the resolution that can be achieved in the spectral dimension. This could be addressed with the use of more robust gradients, for example those available on a micro-imaging probe, but it will require dedicated developments. These two limitations, together with the fact that setting up SPEN DOSY experiments is not straightforward, mean that specific motivations are needed to use spatial parallelization as a way to accelerate diffusion experiments.

Reaction monitoring by flow NMR, using devices such as the InsightMR flow tube, typically do not aim at monitoring reactions that occurs in time as short as a minute or less, since this is shorter than the transfer time from the reaction flask to the spectrometer. The ultimate speed that can be achieved with SPEN DOSY (acquiring all the data in one scan), is thus not mandatory. Since preliminary experiments suggested that mitigating flow effects in SPEN DOSY would be even more complicated than for conventional DOSY, we decided to leave that approach aside in the context of this Ph.D. work.

6.3. Conclusion

We have seen strategies to increase the speed of the DOSY experiment by doing coherence selection using gradients. This was done in two ways, with either parallel or orthogonal gradients. We found that

using orthogonal gradients was a functioning way to bypass the phase cycling. This new way of CTP selection enables diffusion experiment in 1 scan. We can now reach an experiment time of less than 2 min instead of 10 to 20 min. The methods are relatively easy to implement and has drawback associated with its 1 scan nature (sensitivity mostly) but seems a convenient way to accelerate the process. This will be useful for our aim of monitoring reaction as it will allow to study a larger array of reactions.

We have seen the so-called way of multivariate processing, instead of univariate processing. This way of processing the data make the analysis much more straightforward and less user-dependant. It even allows to go further and solve the problem of overlapping. We have seen two of those technics applied in Ultrafast-NMR SCORE and DECRA. Those technics while having peculiar need such as the choice of constrain for SCORE or the use of quadratic gradient sampling or ramp for DECRA have shown unmixing capabilities.

The implementation of SPEN UF (or UF DOSY) is not straightforward and give data that are not easy to process and could be dangerous for the spectrometer to acquire. Despite astonishing time scale reached, with experiment taking less than a second, we believe it would not be easy to use for non-NMR specialist. This coupled with the relatively good time scale (<2 min) reached by 1 scan diffusion NMR make us choose the latter option. It remains a very interesting technic and we believe that further development could make it closer to routine technics. Once this point reached it would make a very powerful tool for monitoring but the accessibility to non-NMR specialist is a bit too far at the moment.

7. DOSY NMR in continuous flow.

7.1. Presentation of the apparatus

To carry out flow NMR experiments we used a commercial device, called InsightMR, that we briefly described in part 2.2.1. We will here describe our experimental setup in details and its evolution throughout this work.

The InsightMR product contains several elements. The flow tube itself is a glass NMR-tube-like insert located within the probe like a regular NMR tube. Capillaries carry the solution to the magnet and back. They are surrounded by a jacket. In order to carry out flow NMR experiments, additional elements are needed, and in particular a pump that generates the flow. A “chiller” is also used to flow the thermoregulation liquid, we are not going to detail it as it does not play any major role. In this subsection we will describe our experience with the operation of these devices.

7.1.1. The tubbing

The exterior jacket is one large tube made of rigid polymer. It is not supposed to be in contact with any chemical/liquid. It consists of a black rigid and resistant polymer wrapped around the main line. It protects against light, and against possible aggression from the exterior like pinching or physical damage.

Inside the jacket is found the large tube. Made of a polymer, it carries the thermoregulation fluid. In this tube are located the two capillaries that carry the flowing medium. The temperature regulation happens within the large tube, with a flow of liquid that is circulated by the chiller. Temperature regulation is possible with fluids other than water, such as ethylene glycol or some specialized oil that have a greater range of temperature than water, but this was not tested. Most of our experiments were carried out at room temperature. For this reason, temperature regulation was not used, as testing showed no difference if the room is correctly air-conditioned. Furthermore, the probe temperature regulation was calibrated carefully by using a standard sample of methanol. Experiment onflow and out of flow showed repeatability of diffusion coefficient in this fashion, showing no need for more temperature regulation. The temperature regulation of the tubbing, is a source of both vibrations and possible leaks so after testing showed no difference it was mostly discarded despite the importance of temperature in diffusion measuring.

Finally, within the large tube are the two capillaries that carries the medium of interest. During this work we tested two main kind of capillaries PEEK and PTFE both with the same diameter of 0.5 mm. Those materials are known to resist to a wide range of solvents, and conditions, thus chemo-resistance was not a problem for either of them for this work. Interestingly the elasticity and behavior of those capillaries are not the same and PEEK is much more rigid and hard to use than the PTFE. We

settled for PTFE in the connection to the pump and back for simplicity of handling. The rest of the capillaries that are the main line are in PEEK.

The small inner diameter of the capillaries, 0.5 mm, raised some challenges, especially for concentrated solutions. Reaction monitoring applications in organic chemical synthesis can involve highly concentrated solutions. As such we aimed for a concentration of 100 mM in most of our mixtures, whether they are reacting or not. In those conditions, solubility can start to be a problem and what is not apparent in a large flask (50 to 100 mL) can become a problem in an 0.5 mm capillary. Our tests with sucrose showed that, despite excellent solubility of sucrose in water, if it happens that a co-solvent is found in the flowtube (as impurities most of the time), the solubility of sucrose is reduced and a solid can start to precipitate, blocking the capillaries. Fortunately, the problem is easy to solve as a cleared batch of solvent (water) will quickly solubilize the solid (sucrose). Such blockage can have two main consequences, the increase of the pressure in the tubbing and loss of homogeneity within the flowtube as a solid perturbs the analysis. Another problem is that the very small size of the capillaries makes it so that it changes temperature extremely fast. The capillaries themselves are unprotected for ~15cm when they go in and out of the reactor which allows the medium inside to change its temperature at the outside temperature.[117] Here we worked at room temperature so this was not an issue for most of the work. Figure 7.1 illustrates a schematic of the insightMR/flowtube, it re-use the lexicon we have used in the above paragraph (Jacket,large tube…).

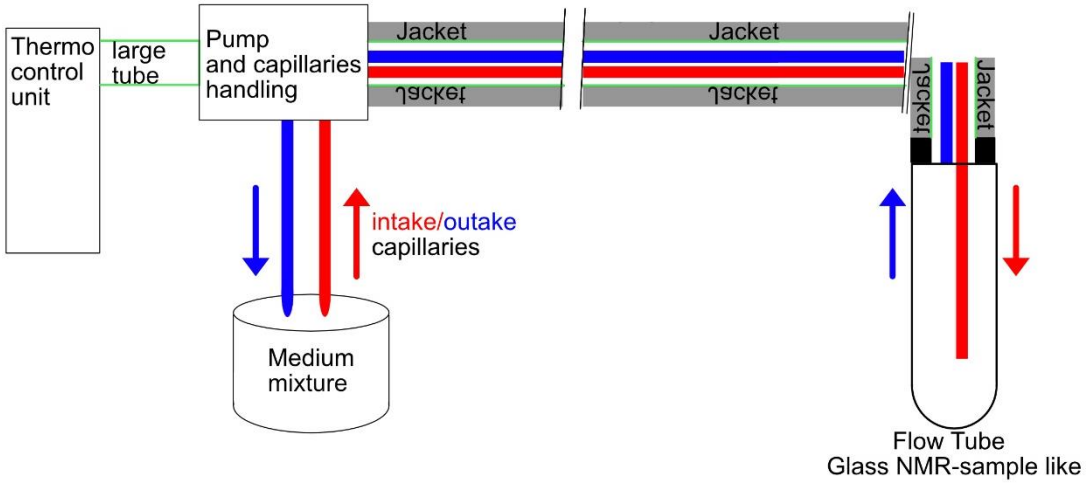

Figure 7.1 an illustration of the flowtube. The grey jacket represents the protective semi-rigid outside layer. The green “large tube” is the canal for thermoregulation fluid. The red capillary is the intake one that take out the medium and pour it into the NMR-sample flow tube. The blue one retake it and pour it back to the solution medium. The thermo control unit is both a pump for the thermoregulation fluid and a thermo-regulator. The unit “pump and capillaries handling” include a small plastic interface where the tubes are connected.

The increase of pressure is the main problem one could face and it should be acknowledged as fast as possible to avoid any catastrophic outcomes. The main sources of pressure increase are the nature of the flowing sample dictated mostly by the kind of solvent and its viscosity. Other sources include disruption of the line by the inside or outside. Inside disruptions are blockages, partial or total,

linked to solid formation. Fortunately, the ever-flowing nature of the medium made total long-lived blockage unlikely. The main problem will be blockage from insoluble (salt, dust…) compounds that will often be partial. The increase of pressure will thus be treacherous as it will be shallow and hard to decipher from the normal state. It is to be noted that the problem could be much more concerning if solid with low solubility find their way within the reaction, solid formation should be avoided if possible.[176] We decided to use a sinter filter (so-called "last-drop filter") to avoid absorption of solid from the medium as much as possible. All of our reagents were tested for solubility and our solvents were of HPLC grade to avoid any solid particle. Storage of the reactor and glassware are also made in a fashion that should avoid dust. It is to be noted that despite those efforts we have seen multiple unwanted and terrifying increase of pressure that were not always well explained.

Another possible source of pressure increase is outside disruption, the twisting and possible knotting of the capillaries or both capillaries and large tube. As the capillaries are not accessible from the outside, it is hard to know in which state they are. Pinching, knotting or twisting are known to increase the pressure and are not easy to see, just like precipitation of a solid in the middle of the line. The answer to those problems is a set of good practice recommendations, such as storing the flowtube in the same position. Avoiding twisting either on its axis (as it is cylindrical) or otherwise and any kind bending, seems to give good result.

The cleaning and storage of the line is an important point as we have seen in this work several instances of contaminations. The lack of access to the main-line as well as the lack of visibility makes the operation somewhat difficult. Our first protocol included rinsing with the solvent of the sample/reaction for 15 min then replacing it with water for 10 min. The pipeline was left in this state with water in it for storage. The water used was osmosed water to avoid any traces of minerals or salt that could precipitate. We did encounter some problems because of the water, mostly we feared the apparition of algae that could damage the apparatus. We then settled for another solvent much more common in storing and maintaining electronics, isopropanol. The protocol was also further modified with a cleaning and rinsing of 30 min. The isopropanol although good for storing is our most viscous solvent which restrict us from going above 1 mL/min for the filing/rinsing.

As a side note and despite this work containing mostly work in water, we discourage water use in the flowtube especially if one wants to also use organic solvent. Using water is a challenging condition both for its viscosity, solubilization properties and great abilities to support life, extra care should be used with it.

7.1.2. The pumps

7.1.2.1. Dual piston HPLC Azura

The HPLC Azura pump is the by-default pump sold by the manufacturer of the insighMR flowtube. It is a dual piston pump *a priori* designed for HPLC. This kind of pump is capable of handling strong pressure (up to 400 bar) and high temperature variation (-40 to 200°C) in the pumped liquid, as well as a fine regulation of the flow rate (0.001 to 10 mL/min).[117] It works with a set of two pistons that make inverse motion with one another so that it can provide a steady continuous flow. The pistons and fine moving parts are in direct contact with the flowing medium. One of the most critical parts of the machinery is the check-valves that control the motion of the fluid so that the piston action does not cancel out. The flowing medium pass through those check-valves.

In order to work, this kind of pump needs to be manually primed, meaning that the user should fill the pump head with the solvent of the medium, thus getting rid of all the air inside. This procedure can be done easily, but needs to be done very carefully and can be long depending on the solvent. If not done well, the pump can be impacted and give wrong flow rate or simply stop pumping while seemingly working. The piston being inside of a bubble of gas continue the pumping motion without being efficient at generating the flow.

Even if priming is done well some bubbles may appear in the system. The phenomena of cavitation can be attributed to degassing of the medium or by vaporization of the solvent due to suction pressure.[105] This can be damaging for the pump as solute may precipitate and hinder the valves and pistons. It can also slow the flow-rate, increase the pressure or send the bubble inside the NMR flow tube, which is disastrous for the field homogeneity and the overall quality of the analysis. For this reason, a careful degassing of the solvent or the medium was performed using 15 min of ultrasounds prior to priming. Even with that the vaporization of the solvent is still possible and will lead to bubbles.

The pump being well specialized in pumping exclusively fluids, it was impossible to use it to empty the flowtube. Such emptying was done using a simple syringe filled with air that needed to be pushed slowly and constantly to get rid of the liquid (manually). This operation was not very efficient and could be long depending on the fluid viscosity. It called for the use of another pump that could pump gas to empty the flowtube. It is also interesting to note that any increase of pressure while pumping gas would have been a clear sign of a blockage, which is useful for troubleshooting.

Because of those variables, and due to the different natures of the solvents that were tested, calibration of the pump was important as the indicated flow rate could be different from the actual flow rate. Calibration was done in a straightforward way using chronometer and measuring-glassware while monitoring the pressure indicated by the pump. If not successful the rate had to be adapted and if the difference was deemed too important, we would empty the pump and re-prime it.

The direct contact of check-valves and piston with the solvent was a problem as it limits the compatibility of the pump with the medium. The parts being ceramic and metal they are not at risk when in contact with most organic solvent. Yet, the parts are very sensitive to gas and solids, it often happened that the valves were blocked by something, to clean them was half a day long in a mixture of methanol and water under ultrasound. Those valves were considered as consumable needing change quite often. It is thought, from reading literature, that such kind of pump are not meant to work at those low-pressure with high-flowrate (relative to HPLC).

In conclusion despite seemingly good capability the Azura pump was not deemed a good starting pump for our use. It might come handy in more advanced situation if harsher condition or medium are necessary. As it stands the rest of the apparatus is not able to withstand high temperature or pressure the NMR flowtube being limited to 10 bars. The lack of compatibility with a variety of medium as well as its long needs for priming, cleaning and high cost of maintenance due to the valves, made it difficult to use.

7.1.2.2. Vapourtec Peristatic pump

The peristatic pump by Vapourtec is a pump that was brought to our attention by the work of Hall[188], and which seemed more convenient to monitor reactions. It is a pump aimed at pumping reaction medium. The peristaltic motion consists of the pinching of a flexible tube called peristatic tube. This pinching is slid along the tube by the rotors in a controlled way thus creating the flow. It is convenient as it allows to pump a large variety of medium from liquid to slurry or gas. Peristaltic pumps are the by default pumping option for many NMR setup especially for benchwork/low-field NMR. Despite the large array of possible medium it can handle, it is less efficient in providing very accurate flow and handling strong pressure or temperature.

We have peristatic pumps in the lab used for NMR at low field. From the past experience of our coworker, we validated that it is good at handling different media, including challenging ones.[189] Yet the pump we had at hand or traditionally available does not always have good or well-document chemical compatibility. The handling of pressure was also a problem, and the pump we tested were not able to pump the liquid in the flow tube. The pressure was too intense due to capillaries being long and thin. In contrast, the Vapourtec peristatic pump is designed for continuous flow reaction[190,191] and is well suited for our purpose.

The part of the pump handling the reaction medium is made of a polymer that comes with a comprehensive list of what reagents it can handle. This peristatic tube is the most critical point in the setup. It has to resist any chemical aggression, either by dissolution from the solvent or of other kind such as acidic/basic. Chemical compatibility is crucial as the tube is always under stress by the rotor and its plastic abilities and resilience should not be impaired otherwise the peristatic flow will not work

well. A major problem was that we believe it may be able to absorb some solvent without looking damaged and release it within the pumped medium. The peristatic tube has a limited life duration and should be changed regularly.

The peristatic motion does not need for priming as it can handle fluid and gas and create little to no bubble on its own. Despite that to test both the state of the peristatic tube and the accuracy of the flow, the pump includes a calibration routine much like the Azura that allow to compensate for flow-rate inaccuracy. The time needed for this is approximately 10 min.

The critical factor being the peristatic tube it needs to be inspected and checked regularly as well as stored in the right conditions. There is a variety of tubes to handle different pressures and solvents. It is interesting to notice that constructor advise the use of a back pressure to ensure better result, we did not use it. This could be the cause of reduced lifetime for the tubes although unlikely, as back-pressure are more often advised to avoid cavitation and improve flow regularity. Despite this, it seems that the cost of maintenance was less than with the Azura pump as the valves are too costly and fragile.

The Vapourtec pump is less prone to handle complex situations in regard of flow physics (high or low pressure, temperature etc.) but more efficient at handling a variety of media. This seems appropriate for reaction monitoring. Even if reactions are tested before flow NMR experiments, unexpected problems may happen and the possibility to pump even slurry is welcomed. It also allows to empty and clean the flowtube using the same pump instead of manually which is more reliable.

It asks the question, have we switched the critical point from the pump to the capillaries. The capillaries themselves are not made to handle slurry or solid and due to their thin nature may block quickly. A blockage of the capillaries could be much worse than a blockage of the pump and cause damage to system or even to the probe. For this reason, we decided to take more precaution with the last droplet filter on the receiving end of the capillaries to allow for filtration of solids. We deemed the peristatic motion and pump more useful for our use with its polyvalence. It is still not the perfect systems as flow quality using such pump is sub-optimal.[117] We are working on installing a new kind of pump that use quaternary pistons which should have the combined advantage of the two pumps. It is a less user-friendly so we take more time to made it work as the two pumps discussed here were very user-friendly.

7.2. Flow compensation and effect

We are here going to discuss the effect of flow in diffusion NMR experiments. It is interesting to note that we use an unshielded magnet and a flow rate of 3 mL/min max to spare the flowtube of pressure-related problems. In those conditions we did not see much difference between on-flow and out-of-

flow 1D ^{1}H spectra, except possible shimming/locking effects more related to the use of non-deuterated solvent.

7.2.1. Methods

The sample is made of pyridine, sucrose and butanol at 0.1 M in 30 mL of H_2O. The medium was flowed using the Vapourtec pump (peristatic motion) at 3 mL/min. All the experiments were carried out on a Bruker spectrometer operating at a Larmor frequency of 500.13 MHz, equipped with a triple-axis gradient, broadband inverse-detection probe. The temperature was set at a nominal value of 298 K and the diffusion time Δ was 160 ms for all the DOSY experiments, and δ was 1.4 ms. Spoiler gradients were on the Z axis. All the experiments used their full phase cycling, STE experiments thus had 8 scans are were ~12 min long, while DSTE experiments had 16 scans and were ~25min long.

7.2.2. flow effect on diffusion

The effect of flow on diffusion experiments has been characterized already. Consider the magnetization helix from by diffusion-encoding gradient pulses, as described in section 1.1.2. In the absence of diffusion or other motion, refocusing of the helix would be perfect. In the presence of diffusion, refocusing is unperfect due to the individual displacement of spins, and this results in an attenuation of the signal. In the presence of flow, assuming uniform motion of the spins, the helix is displaced and this result, after the refocusing gradient, into an additional phase, which is independent of position.[5] This phenomenon is illustrated in figure 7.2 taken from the work of Sinnaeve[21]

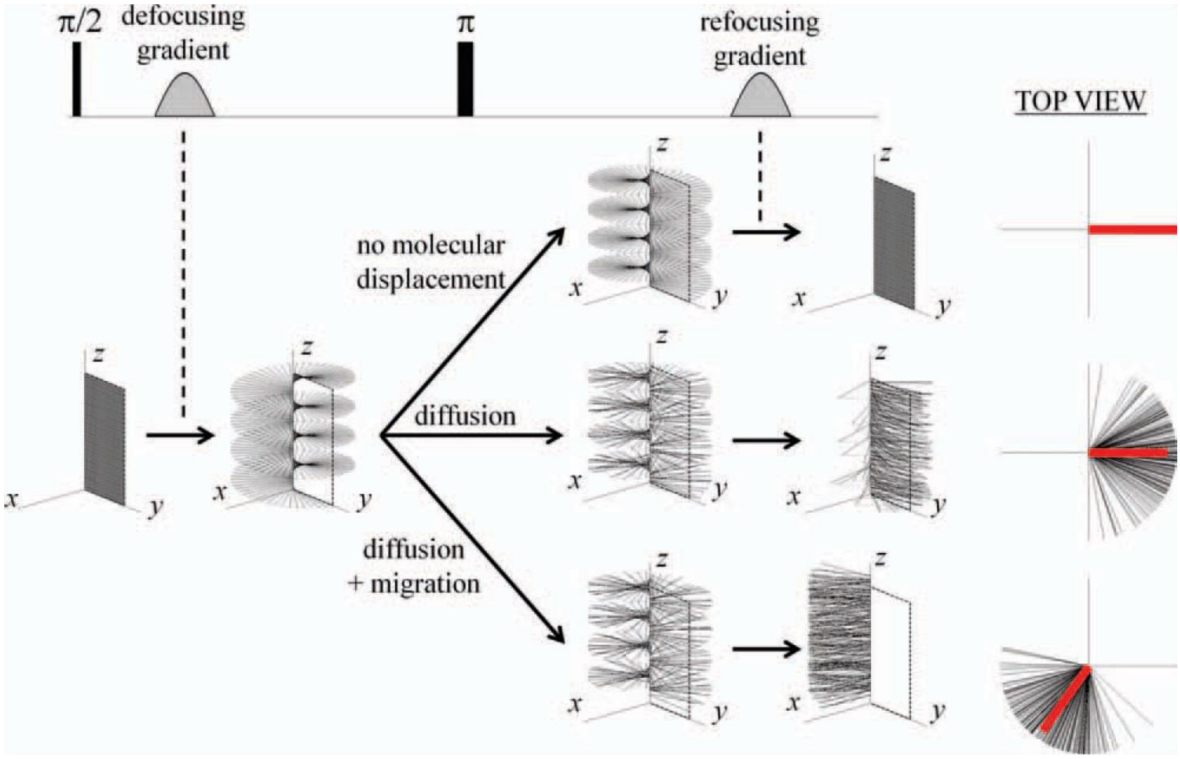

Figure 7.2, Simulation of the effects of diffusion and unidirectional translation on the magnetization during a PFG spin echo. The transverse magnetization, with initial position along the y-axis, is assumed here to be on resonance. Here every line represents a single randomly selected spin at each position along the z-axis, as opposed to Fig. where each line represents the magnetization, i.e., an ensemble of spins. The spins are dephased by a first, defocusing constant gradient pulse with 1.25 G/cm strength and 500 ms duration. The 180°$_y$ pulse inverts the phase of the spins, so a second, refocusing gradient pulse with the same gradient strength, polarity, and duration will realign the spins to the y-axis, concluding the spin echo. The diffusion delay of the spin echo in this simulation was 10 s, chosen so long for the purpose of illustration. If during the spin-echo diffusion takes place (with a diffusion coefficient D of 4×10^{9} m^2/s), the molecules displace randomly across the z-axis, causing the helix pattern to disintegrate. When each line would have represented the magnetization instead of a single selected spin, the visual effect would be that the helix diameter attenuates due to diffusion, as is illustrated and explained in the Figure 80 on page 80 in the book by Price[192]. The refocusing of the second gradient pulse is now no longer ideal, leaving a stochastic, irreversible dephasing of the spins along the z-axis. The red line in the top view represents the vector sum of all spins. When additionally, unidirectional translation takes place (here simulated with a velocity v_z of 8.7 cm/s, chosen so high for the purpose of illustration), the molecules and thus the helix pattern will experience a constant shift in position along the z-axis, causing a constant phase shift for all spins after the refocusing gradient. Note that since the magnetic field gradient is constant, the helix pitch is constant along the z-axis and therefore diffusion and unidirectional translation induce a z-position independent loss of coherence or phase shift, respectively. Reproduced from Sinnaeve[21] with permission Copyright © 2012 Wiley Periodicals, Inc.

7.2.2.1. Diffusion-encoding with longitudinal gradients

We evaluate different diffusion NMR pulses sequences in continuous flow, starting with the use of the Z axis for diffusion encoding. Since the mail direction of the flow is also along Z, flow effects are expected to be stronger in this configuration. However, NMR probes equipped with a Z-only gradient are more common.

Since we chose to work with a model mixture in water, our flowrate was limited to 3 mL/min. Indeed, water is a relatively viscous solvent compared to organic solvent (Acetonitrile, chloroform, DCM…). As the flowrate increase so does the pressure inside the flowtube, and this is linked to viscosity.[105] The guidelines for the maximum pressure for the flowtube state that it is resistant "up to 10 bars". As we relied on the pressure sensor of the pump only, which may not be accurate for the pressure at various critical point of the apparatus, we used conservative values of the flow rates.[117] A flow rate of 3 mL/min is both relevant for monitoring application and sufficient to observe significant flow effects. Note that the choice of water as a solvent date from early investigation, when the fumehood was not available and toxic solvents had to be avoided.

Unsurprisingly, STE experiments in flow using longitudinal gradients gave nonsensical results. They are not represented here as DOSY displays, which would have little meaning but the size of the error along with the recorded diffusion coefficient were very large. The results obtained with DSTE experiments are more relevant and are displayed in figure 7.3. It is interesting to note that the relation between the measured diffusion coefficient and the flow rate seems almost linear. Indeed, the difference between coefficient stay the same. The flow seems to also increase the uncertainty.

Independently from our work, Hintermair and coworkers[193] also investigated diffusion NMR in continuous flow.[182] They worked with an InsightMR flow tube and a single-axis gradient probe. They found that with the same peristatic apparatus and suitable parameter choices for the DSTE sequence they indeed get a linear relation between flow-rates and measured diffusion coefficients. In order to have a linear dependence, they notably used a small diffusion delay, Δ, that is counterbalanced by longer durations of the diffusion-encoding gradient pulses, δ. The dependence as a function of the flow rate was otherwise more complex. They also observed that the uncertainty also increases at significant flow-rate, making separation more and more difficult. Interestingly, they also observed that, using a rotary tetra-piston pump that delivers a steady flow rate,[117,134] the estimated diffusion coefficients were approximately constant as a function of the flow rate. It would be interesting to compare the accuracy of this approach, and of the method described in the following.

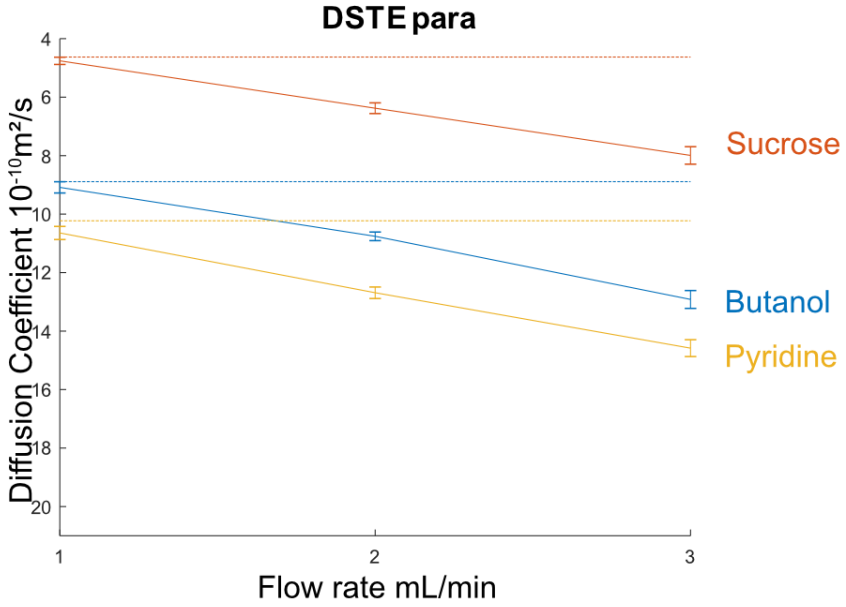

Figure 7.3, The DSTE parallel to the flow diffusion encoding gradient. The dotted line represents the reference experiments in the same setup with no flow. Error bar come from the uncertainty calculated from the fitting. The diffusion coefficient come from the average of three sites belonging to same molecule see part 4.

7.2.2.2. Using transverse gradient

With our lack of success to deliver accurate diffusion coefficient using diffusion-encoding gradients that are parallel to the main direction of the flow, we decided to try to use transverse gradients for diffusion-encoding. Since the flow is expected to be mainly laminar and longitudinal, it should have much less influence on diffusion experiments in that case. The experimental results are displayed in figure 7.4 In the case of STE experiments, a clear effect of the flow is observed. Both the estimated diffusion coefficients and the corresponding uncertainties increase when the flow rate increases, in a non-linear fashion. Spectral separation is thus very poor at 3 mL/min, especially between butanol and pyridine.

In contrast, in the case of DSTE experiments, flow effects appear to be very small. The flow-rate and the measured diffusion coefficients do not seem to be correlated, and the results are very close whatever the flowrate. Even the uncertainty does not appear to move significantly. There is a slight deviation from the reference value, which is difficult to explain, but which is also much smaller than any of the errors observed with the other methods. It is good to remind that because of the lack of locking on flow a wide array of causes could explain this relatively small deviation. On average the deviation from the reference is 1.9% with a maximum at 4.2%.

It is interesting to note that double-diffusion encoding is still needed when using transverse encoding. This implies that their flow has a transverse component, which is consistent with the fact that the flow tube does not have perfect cylindrical symmetry. In the case of transverse encoding, double diffusion encoding works very well while it fails for longitudinal encoding. This may simply be

due to the relative magnitude of flow effects in the two cases, which make flow fluctuations negligible in the transverse encoding case.

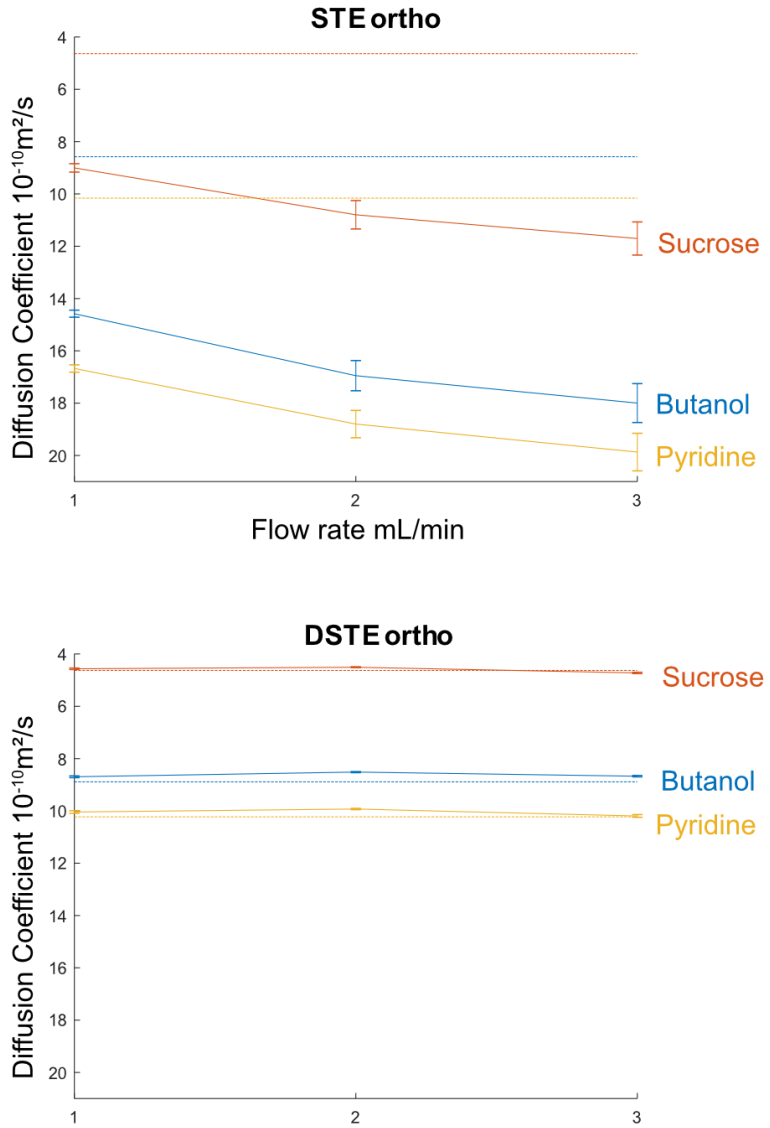

Figure 7.4, diffusion coefficient at different flowrate. The dotted lines are conventional experiment out-of-flow. The error bars represent the uncertainty from the DOSY plot.

Figure 7.5 summarizes the results obtained in this chapter, using the representation presented in part 4.4.2. This gives a good idea of the experiment's usability and of the impact of the flow. One can see that DSTE experiments using longitudinal encoding at 1 mL/min is only slightly degraded. This worsens when the flow rate increases, although with a simple relationship between estimated diffusion coefficient and flow rate. This is relevant for experiments carried out with a single-axis gradient probe. Along the same line, we can see that the STE experiment with transverse encoding seems good at 1 mL/min but fails at higher flow rates. In this case the dependence of the estimated diffusion coefficients on the flow rate is more complex. Then, DSTE experiments using transverse encoding gave results that are very close to those of the conventional experiment, no matter the flowrate. This makes it a very interesting option for reaction monitoring applications.

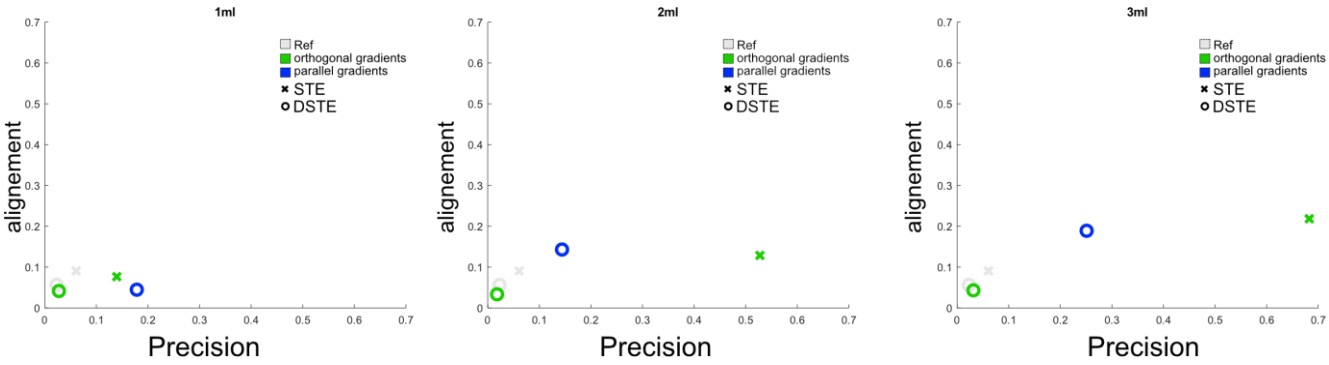

Figure 7.5 quality of the experiment at 1,2,3 mL/min flowrate. The grey experiments are references out-of-flow. green experiments use orthogonal gradients, blue use parallel no other modification were made to those experiments.

Finally, as a proof of concept for the reaction monitoring, that was our goal and that will be discussed in the next part, we decide to use the orthogonal gradient coherence selection method (see part 5) with the orthogonal diffusion encoding to record a 1 scan spectra on flow at 3 mL/min. The DOSY display is show in figure 7.6. It is very satisfactory knowing we go from ~25 min for the conventional method to 90 s.

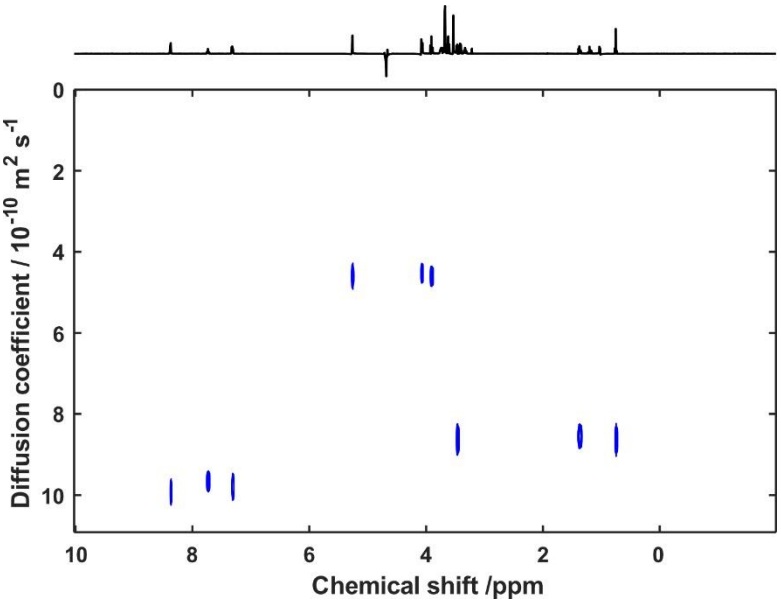

Figure 7.6 The DOSY display for a 1 scan DSTE DOSY on flow (3 mL/min) total experiment duration was 90s.

8. Monitoring a flowing reaction with DOSY

8.1. Prerequisite for Reaction monitoring

8.1.1. Solvent suppression

Throughout this work we have used non-deuterated solvent. There are several reasons for this, one of which is the cost of deuterated solvents in large quantities. Indeed, to fill the reaction vessel and the flowtube, and have realistic conditions the sample volume has to be increased from the usual ~500 μL to ~30 mL. Another problem is that deuterated solvents are known to have different viscosities. This change of viscosity can impact diffusion heavily, as we have seen. Also, it can modify the kinetic properties of the reaction, especially if proton/deuteron motion is involved[194,195] but possibly also in other cases. To have realistic conditions we have to use non-deuterated solvent, as such we need a way to suppress its signal and work without the spectrometer lock. Solvent suppression technics are widespread in NMR. There is no universally best method, and they have to be compared in an application-specific way. Here we compared three methods that were already used with flow NMR in the past: pre-saturation[196], excitation sculpting[197], and finally WET[198].

8.1.2. Presaturation

Presaturation is one of the oldest[196] and easiest methods for solvent suppression. The principle is simple and relies on using a long, low-power pulse at the solvent frequency to saturate it. The longer the pulse the more frequency selective is its saturation profile. The method consists of putting this long low-power pulse just before the excitation pulse in order to suppress the solvent signal.

This method, while straightforward, does not always give best performance. From a practical point-of-view it seems to be very sample dependent. Furthermore, in our experience we found it hard to predict which combination of power/duration would be the right one to efficiently suppress the signal. This resulted in rather long time for pulse calibration/optimization. It also requires some care, very long pulse with excessive power can damage the transmitter or at least reduce the lifetime of the hardware.

As for flow effects and monitoring, presaturation have the issue of needing rather long dead-time during the long pulse, up to seconds. This could make the experiment notably longer, in our case we use the recovery delay so it is less impactful. Related to this duration, a strong apparent relaxation is reported due to the influx of solvent, lessening the effectiveness of the suppression.[199] Indeed, the long pulse duration allows medium to flow in and out, lessening the effect of the saturation.

It is also known that presaturation influences the signals for protons that are in exchange with solvent protons, which can be a problem. It is not a direct problem for us but in the case of a chemical reaction, interactions with the solvent are common and it could be an issue. Finally, methods exist to

improve the presaturation,[200,201] especially to provide answers for suppressing multiple frequencies, but we chose to use instead gradient-based methods.[200,202]

One of our attempts at presaturation is displayed in figure 8.1, it shows a sample of sucrose and DMSO in water on-flow (3 mL/min). The presaturation was 3 s long to match the relaxation recovery delay that we typically use. The spectra have the same level of receiver gain and are displayed such that the whole peak is in the frame. The decrease of the water peak intensity is of ~10 folds with presaturation. Note that it is not a very good result if we compare to other results in the literature. This is attributed to a sub-optimal optimization of the pulse and delay. This could come from flow effect but our experiments out-of-flow showed a rather weak solvent suppression by 10 to 60 folds.

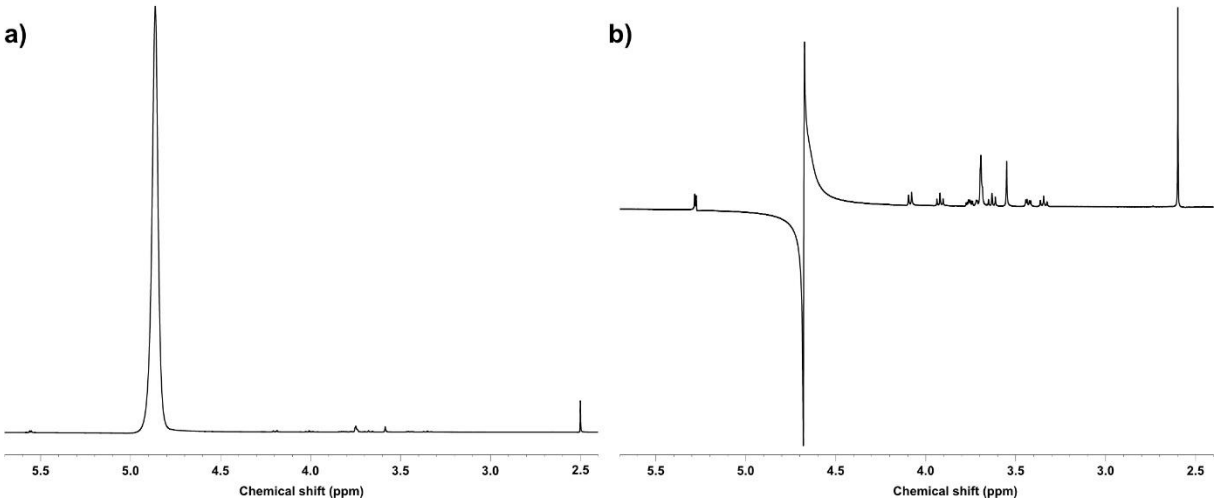

Figure 8.1, sample of 0.1 M of DMSO and sucrose in H2O at 3 mL/min. a) no solvent suppression is used. b) spectrum presaturation is used on water for a duration of 3 s. The zoom level is chosen in both cases so that all the peaks appear whole within the frame. The approximate reduction of intensity for water is 10-fold.

8.1.2.1. Excitation sculpting

Excitation sculpting is a solvent suppression technic first named and published in 1995, nicknamed "Water Suppression That Work".[197] The technic is relatively simple and relies on a block consisting of a selective 180° pulse at the solvent's signal and a non-selective 180° pulse, flanked by two identical gradients pulses. The net result is that the excited solvent magnetisation will be dephased by the gradient pulses and the corresponding signal removed, while the rest will be untouched. This block is doubled for better result and placed at the end of the sequence of interest. The sequence and typical results are shown in figure 8.2.

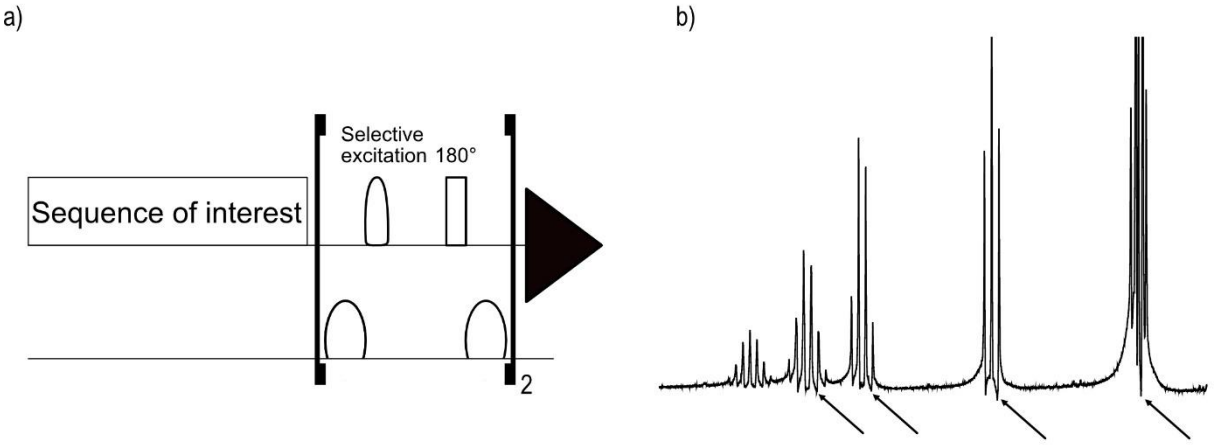

Figure 8.2 a) typical block for excitation sculpting, the bottom axe represent gradient. b) typical DOSY transient spectrum given with excitation sculpting. The arrows underline the baseline distortion (J-modulation).

This technic has been the topic of a number of developments, and it is often found associated with DOSY.[20,203] The solvent suppression is impressively efficient and quick to obtain in our experience and as reported. Yet it is known to cause J-modulation effects, that result in the distortion of multiplets.[195] In our attempts, the J-modulation effects that appeared from the use of excitation sculpting were often visible, and distorted the baseline, thus making integration difficult or hazardous. This compounds with the fact that multiplets can already be difficult to integrate accurately because of their lower intensity. While improved versions of excitation sculpting exist, which compensate to some extent for J-modulation effects, we decided to set aside this approach for a more robust and easily accessible one.

Figure 8.3 shown an example of spectrum obtained with excitation sculpting under flow (3 ml/min). The sample is made of a mixture of alcohols (iPrOH, n-PrOH and EtOH) in water. One can clearly see that the solvent peak almost disappears entirely.

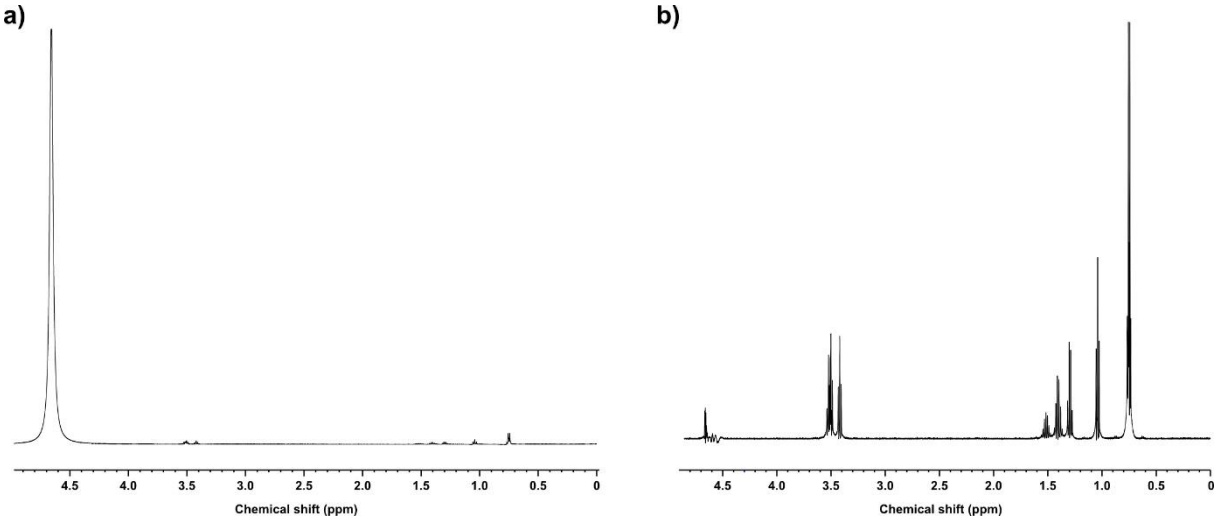

Figure 8.3. 1D ^{1}H spectra of an 0.1 M alcohol mixture. a) no solvent suppression. b) solvent suppression with excitation sculpting, solvent suppression on water for a duration of 3 s. The zoom level is chosen in both cases so that all the peaks appear whole within the frame. The approximate reduction of intensity for water is more than 600 folds.

8.1.2.2. WET - Water suppression Enhanced through T1 effects

WET is a solvent suppression technic that was first published in 1993[198] and that was designed for MRI applications. The principles of WET are to use selective shaped pulses to selectively excite the magnetization of the solvent protons and then to dephase their signal using gradient pulses. This is repeated 4 times to suppress the magnetization, and then the sequence of interest proceeds. The pulses angles are calculated using simulations to be optimal in difficult situations such as field inhomogeneities, and different T_1 values for the solvent spins, both issues being common in MRI.[198] This makes the sequence rather useful as it will be effective in a large array of situations. The duration of the whole block is usually around 100 ms, much faster than presaturation. The WET solvent suppression bloc is illustrated in figure 7.4. It is nowadays the default method used on flow NMR especially with LC-NMR.[199,204–206]

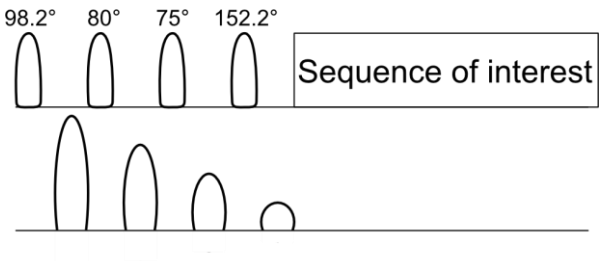

Figure 8.4. The WET sequence. The pulses are on the top axis. They are selective pulses on the signal of the solvent. The bottom axis represents gradient pulses.

WET relies on RF pulses that are about 20 ms. The overall rapid nature of the WET suppression-block makes it more suitable for flow than presaturation. It will be better to handle the refreshment of the solvent spins due to the flow.[204] The selective pulses may be problematic as their selective excitation profile is limited and it may also suppress part of the signal in close vicinity of the solvent.

This can be a problem as it will prevent any successful fitting of peaks too close, for diffusion analysis purposes.

WET is being advised for flow and compatible with a large array of conditions. It is also automatically implemented in Bruker's spectrometers. This implementation includes a routine to calculate of the angles and that can also modify the pulses to have multiple signals suppression, for solvents with multiple peaks. The optimization is made on the last angle and the others are readjusted to follow the ratio of power to respect the sequence. It is therefore the most straightforward and simple sequence to use, for us. The only drawback is that one has to be careful and may sacrifice the peaks close to the suppressed peak, its efficiency while being sufficient is often less than excitation sculpting.

Figure 8.5, display the result of WET solvent suppression in the same sample as before (alcohol mixture), at the same flow rate (3 mL/min). The result shows that the peak of the solvent while still there, has decrease by approximately 140 folds.

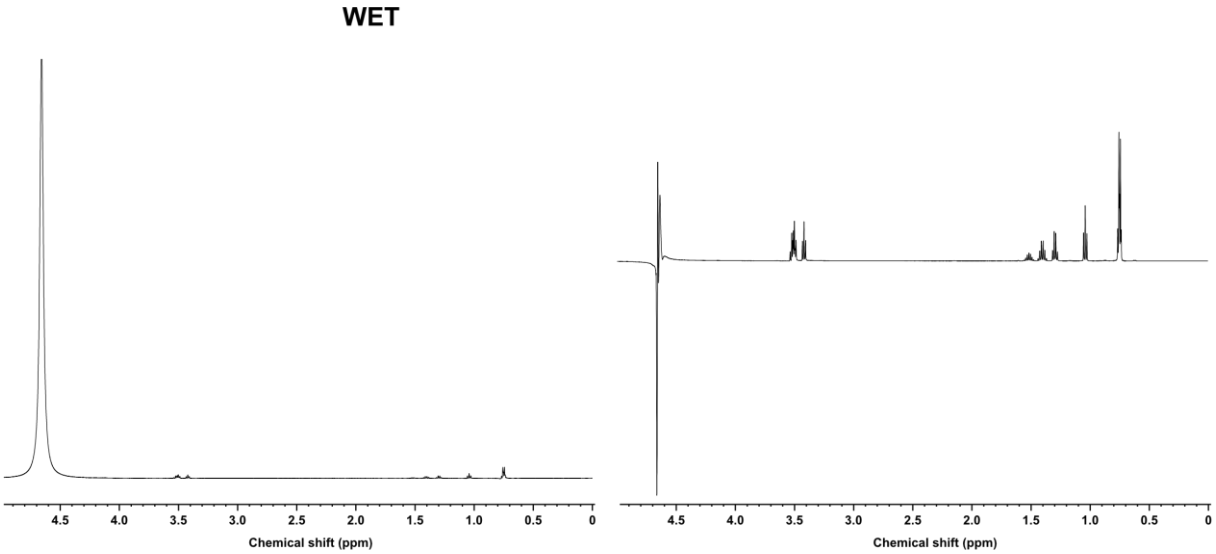

Figure 8.5, sample of 0.1M alcohol mixture. A) show no solvent suppression. b) WET, solvent suppression on water. The zoom level is chosen in both cases so that all the peaks appear whole within the frame. The approximate reduction of intensity for water is 140 folds.

8.1.3. Spectral and diffusion resolution

To assess the possibility to monitor reactions with our methods, we have to choose a relevant and appropriate test reaction. While we have already described the key parameters of the experiment, we will summarize them here for the case of reaction monitoring.

Spectral resolution plays an important role, as the peaks should be well separated and if possible, not subject to effects such as widening from exchange, or to T_1-T_2 effect (possibly caused by metals in the medium).[17] This in itself can be considered as a challenge, since some reactions use paramagnetic metals for catalysis, sometimes in transient states. Changes of viscosity in the medium, possibly due to polymerization for example or complexation, could also disturb the diffusion analysis.

It also happens that reactants and products might be close in terms of chemical structure and therefore also in chemical shift, thus causing some form of overlapping. This proximity may hinder the processing of the spectra. This is an important and hard-to-avoid fact. It underlines the needs for means to separate the overlapping peaks. Such mean includes multivariate processing as seen in part 6. Especially a multivariate method known as PARAFAC[207] which allow to retrieve concentration profiles, diffusion curve and pure component spectra untangled.

The differences between reactants and products will be a key point for reaction monitoring with DOSY. Reaction such as reduction will often have a small impact on the molecular weight, and if we have seen that this is not the relevant parameters (the molecular radius is) the two remain linked. Therefore adding 1 or 2 hydrogens to a possibly bigger molecule may not be sufficient to change its diffusion coefficient enough to virtual separate them. Overall, many reactions that add few atoms in a bigger molecule will not be well suited for DOSY monitoring. This still left a large array of reaction, as coupling reaction are common and those changes will be impactful on smaller molecule. If we take the example of drug design adding different block to a molecule to add different effects is a common practice that will often make the molecule bigger.[208]

8.2. The model reaction

In order to evaluate the methods that we have developed, we chose to monitor the double imination reaction described in Figure 8.6. This reaction was already monitored by flow NMR in the past,[150] and by diffusion NMR on a static (non-flowing) sample.

There are several interesting aspects of this reaction, especially to provide a test for our monitoring methods. The reaction occurs in two steps, each increasing the molecular weight noticeably, with an additional isobutyraldehyde moieties. This suggests that it should be possible to separate the compounds with DOSY. There are five molecules of different molecular weights to follow, the reactants, the intermediate, and the final product. This is displayed in Figure 8.6.

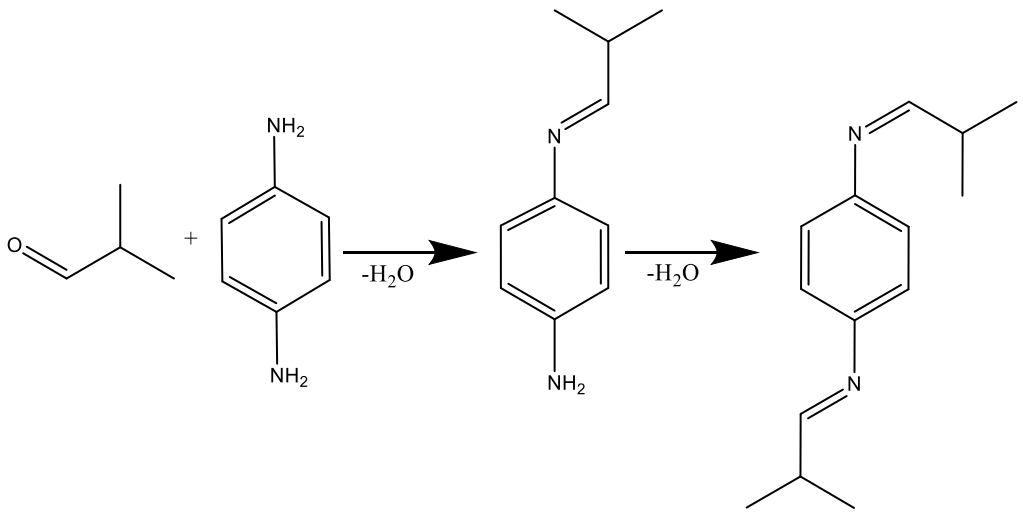

Figure 8.6 reaction scheme for the reaction of interest. Note that the isobutyraldehyde is present in twice the equivalents of the amine. The reaction creates water and the imine are actually in equilibrium with their dissociated forms.

This reaction, while it was not primarily chosen for its relevance in synthetic chemistry, yields a Schiff base that can be of interest in biological and coordination chemistry.[209–211] It was chosen for its simplicity as the known mechanism and relative ease of manipulation make it safe for our apparatus. Indeed, the reaction involve little to no precipitation or risk of solid formation which is a very important point for the safety. It also does not involve ions or species that could become salt, even less so metallic species.

Interesting information on this reaction is available in the literature[150,212]. The kinetics depend strongly on the ratio of aldehyde/amine and can therefore happen quickly ~20 min[150] or very slowly ~47 h.[212] Due to its equilibrium nature, it is not straightforward when the reaction reach completion, yet it can be estimated that after ~4h a plateau is reached in our conditions. Working on a well-known reaction also helped to be able to confirm our observation by comparing with the literature.

The reaction also displays some challenges that make it a relevant example for online monitoring. Neither the reactant, the aldehyde, nor the product, an imine, are very stable. This means that once in solution they can be hard to extract, separate or characterize. The reaction is indeed in equilibrium with water and water can be the main reason why the reaction would not work. The fact that it reacts accordingly to our plan with a slowly rising water peak indicate that the apparatus is protected enough against ambient water. Those imines would be challenging to separate and isolate, indeed they are sensible to oxidation by air and water. Imine are often used as intermediaries, mean to react *in-situ* rather than be separated/isolated.[213]

Interestingly, the handling of the amine reactant was not easy. Indeed, it is a very potent pigment that get more coloured with time and oxidation by air.[214] This property while forcing us to

handle with extreme care, especially due to the toxicity of the compound, also showed us where leaks or exchange with the exterior might happen. It challenged deeply our belief, and our methods for cleaning and storing of the whole flowtube apparatus.

8.3. Methods

8.3.1. The pulse sequence

For reaction monitoring to happen we had to merge all the different strategies introduced from part 4 to part 7. The resulting pulse sequence is shown in figure 8.7. Note that the $\Delta/2$ delay starts precisely with the first encoding gradient pulse and end precisely right before the second pair,[5] while $\delta/2$ is the length of the diffusion encoding pulse.

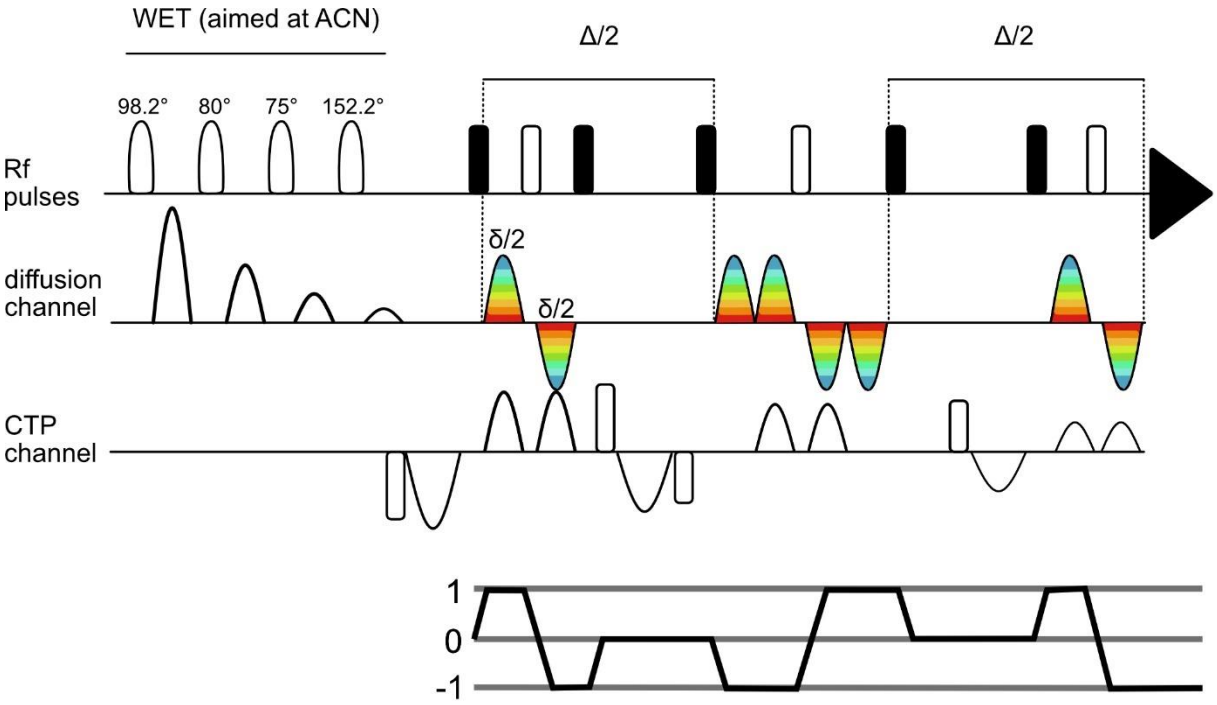

figure 8.7 the reaction monitoring sequence. Ellipse-shaped pulse represent selective pulse for the WET that select the peak of acetonitrile. Black rectangles pulses are 90° while white ones are 180°.Rainbow ellipse are the diffusion encoding gradient pulses. On the CTP channel white rectangle represent spoiler pulses, note that they can be put on any axis. The wider ellipse inverted pulse on CTP channel are compensation pulse. $\Delta/2$ length start exactly after or before the diffusion encoding pulse as illustrated.

The compatibility with flow is ensured by using the DSTE approach with diffusion encoding gradients along the X axis, an axis orthogonal to the flow direction. We have seen in part 6 that it allows to measure accurate diffusion coefficients while on flow up to 3 mL/min, which will be the flow rate here. The incremented diffusion encoding pulse are shown as rainbow-colored ellipses on the so-called diffusion channel (X-axis).

The improvement of the time resolution is achieved by the strategy described in part 6, which consists of using gradient pulses around the 180° RF pulses for coherence pathway selection. This allows to have accurate experiment in 1 scan, effectively replacing the phase cycling. This is true if the

concentration allows to have enough sensitivity in 1 scan. Those pulses are simultaneous to the diffusion encoding pulse, and on another axis, here Y orthogonal to the flow.

In part 4 we have seen that to calibrate DOSY experiments one should do the experiment with 2 transients with maximum and minimum gradient. This is done to evaluate that the signal of all compound attenuates to ~5% of its original strength. It was not straightforward for the reaction. The first time we did the reaction (figure 8.6) it was done on the benchwork with monitoring done on thin layer chromatography. Once every product visible we sampled the medium put it into an NMR tube, added a bit of water and ACN to quench the reaction. The tube was submitted to the DOSY process and it was found that 0.1 s of Δ with 1.6ms of δ was sufficient for all species. Note that adding water was not the cleverest idea as it quickly degraded the species in the sample and it was not useable after 1 hour ahead of sampling.

8.3.2. Experimental

For all the reactions studied here, the flowtube apparatus was used as described in part 4. Thermoregulation was off, as using it did not yield any difference at room temperature. In a flask closed by a holed cap 25 mL of acetonitrile HPLC grade was added, 256 mg of solid p-phenylenediamine (white slightly pink) was added with magnetic stirring. The solution was left until complete dissolution. The flowtube apparatus was washed of isopropanol (the storage solvent) with acetonitrile and filled with it. The capillaries linked to the apparatus were then inserted into the flask and the flow was settled at 3 mL/min for 10 min. Solvent suppression and the NMR sequence were checked and corrected if necessary due to field drifting. An extensive shimming was made during 10 to 15 min using both the vendor's routine and manual options. On flow while continuously stirring the isobutyraldehyde was added (0.42 mL), with a Hamilton glass syringe. The cascade of NMR experiments was launched as the user promptly went from the fumehood to the computer (~5 m apart). The reaction medium turns slightly yellow up to red-brownish at the end of the reaction.

The NMR experiment consisted of a DSTE with 16 increments and 1 scan per increment. The duration of it was ~80 s. It was interleaved with 1D ^{1}H experiment using WET for diagnostic and to check the ongoing process that were ~20 s long. The repetition delay between experiment was 3 s. For 1D experiment the acquisition time was 0.43 s for DSTE it was 0.74 s.

In order to face and overcome the trouble of changing concentration (and linked intensity) the p-DOSY[159] strategy was used. It consists of taking the conventional linear ramp of gradient and permutate the gradients order in a random way. The same randomized list was used for all experiments.

8.4. Results and discussion

8.4.1. Monitoring's data and processing

The monitoring data for the reaction takes the form of ~140 DOSY data sets and the same number of 1D spectra. An example of DOSY display that corresponds to 120min of monitoring is shown in figure 7.8. In Figure 7.8a), all the peaks were integrated. In figure 8.8b), only the peaks that can be reliably integrated are shown. These peaks were considered in the following.

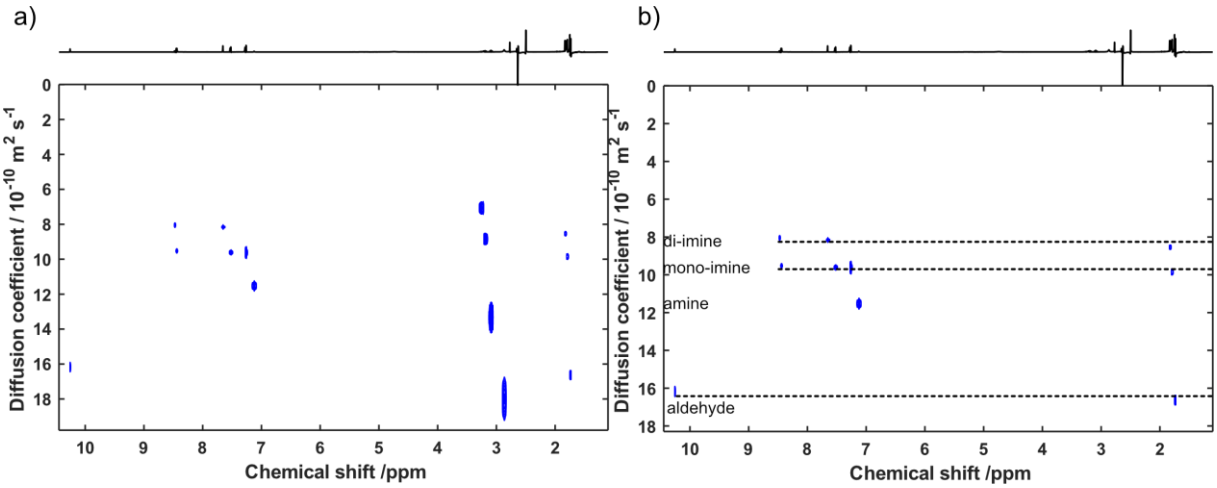

Figure 8.8 the DOSY map for the monitoring. This represent a DOSY experiment done at the middle of the monitoring (~140min). A) The full map with every relevant peak integrated including water, the large peaks of mono-imine and amine N-H proton was not integrated (barely visible). The area 3.6-2.3 ppm has multiplet that have very low SNR and overlap. They were discarded for the final display b).

The excluded peaks include multiplets in the in the 3.6-2.3 ppm region. These give erroneous and inconsistent values of the diffusion coefficients. This can be explained by their high multiplicity and low SNR. The multiplicity also causes the peaks to spread facilitating the overlap making the processing of integration complex. Indeed, those give non-conclusive answer their diffusion coefficient seems to fluctuate, sometimes depending on the shim, sometimes in more mysterious way.

To process each experiment, a list of the integration regions is needed, with one integration region for each peak of interest. The problem is that the spectrum moves slightly throughout the reaction. The exact cause is not well known, it could be field drifting, temperature, chemical environment changes such as pH… This change is relatively slow, and this makes it possible to create integration regions that can be reused on average for 20 spectra (~40 min) before requiring recalibration. This reduces the time needed for processing and reduce the impact of the experimenter. The recalibration is very light and is in the order of 0.1 ppm or less. It is to be noted that usually it also depends on the shimming as better shimming give more intensity and SNR, and peaks with higher SNR are easier to integrate.

The DOSY display is useful as a virtual separation tool but is a bit less convenient when one wants to do monitoring. Indeed, overlapping a great number of DOSY map to show all the points is not

especially information rich. We decided to do another way of processing the data that use the DOSY display but in another form. GNAT[161] provide detailed non-graphic report of each DOSY map. In it are found the value of each diffusion coefficient (at the chemical shift value) along with its associated uncertainty. This can be extracted to get the core information and use it for monitoring.

Along this process that is specific to DOSY, we were interested to retrieve information that is commonly retrieved in reaction monitoring. The least attenuated transient of a DOSY is very akin to a normal 1D ^{1}H spectra. We decided to use those transients to integrate the peaks and have a monitoring of the peaks area that give us information on the relative concentration. This was done by very conventional manner by selecting the areas to integrate and processing all the least attenuated transient. In this case the same integral regions were used for the entire set of spectra. This is because no visual difference was observed when using integral regions that change from spectra to spectra, as was done for DOSY. If the data were analysed quantitatively, then such recalibration may be needed.

The result of all those processing steps is displayed in figure 8.9, which can be considered the final product of our effort to make online reaction monitoring by diffusion NMR

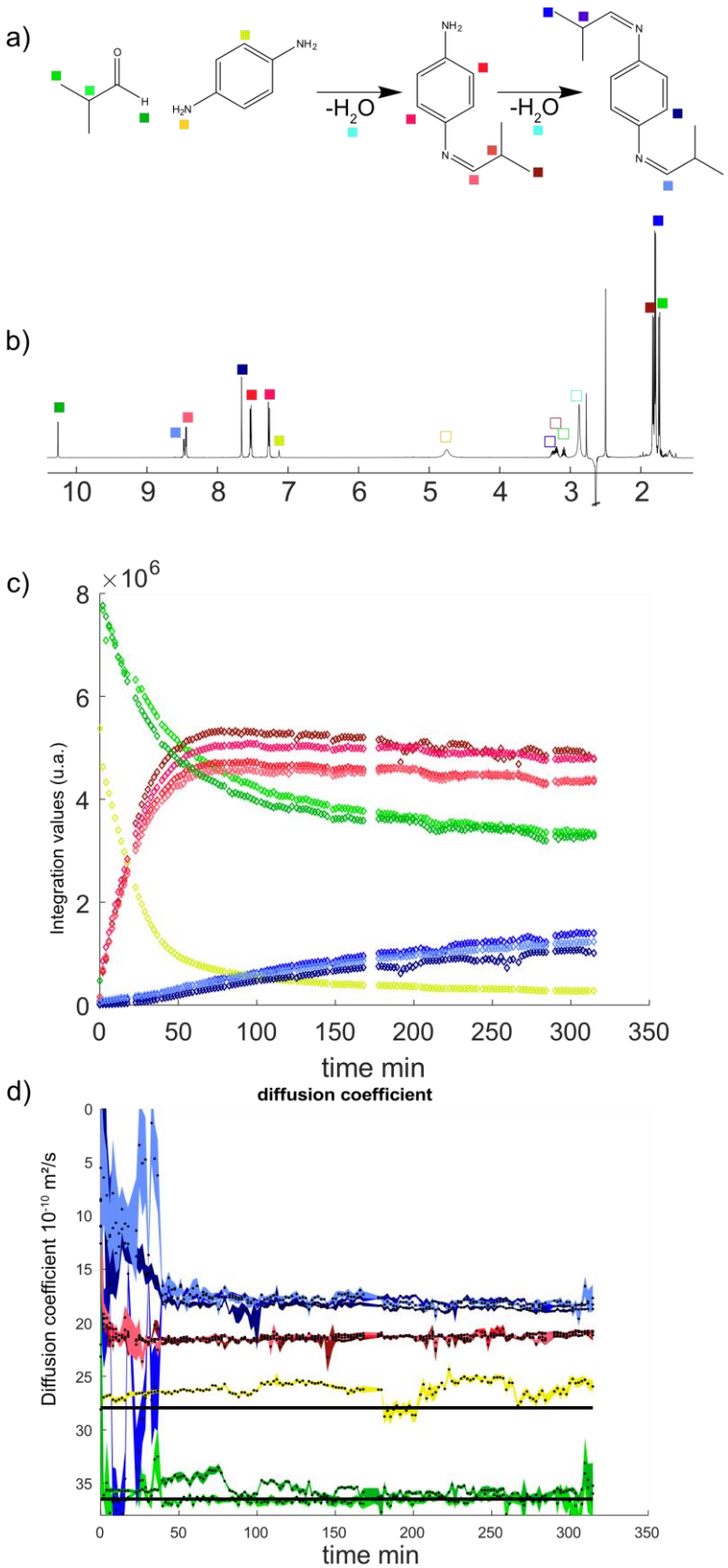

Figure 8.9 Monitoring of a di-imination reaction by flow DOSY NMR. a) Reaction scheme. b) Representative 1D spectrum from a DOSY transient, chosen here at ~250 min of the reaction's monitoring to display all species. c) Integration of the least attenuated spectra in the time series of DOSY data sets. d) Diffusion coefficient measured by DOSY throughout the reaction. The width of the curve represents the uncertainty for each site. The black line represents the reference values measured in a NMR sample tube in pure CAN, for reactant separately.

8.4.2. Estimated diffusion coefficients

One can see at first glance in Figure 8.9d that the estimated diffusion coefficients are fluctuating over time, while no changes in size or shape are expected for the different molecules during the reaction. This can be explained by considering the concentration of the compounds as a function of time. Figure 8.9d) shows the fitting results at every time point in the reaction, but looking at Figure 8.9c) one can see for example that the di-imine is barely present before 50 min of reaction. The diffusion fitting curve thus yield non-sensical diffusion coefficient as there is in reality no peak to integrate and fit. The same is true for the mono-imine (red) that seems to give bad result in the first points and improve quickly after that. The amine shows the opposite behaviour. This is correlated to its concentration that drops fast as seen in figure 8.9c).

These phenomena are finally the consequence of something already known and observed in this work. Relatively high SNR is needed to get a good fit and reliable measurements of diffusion coefficients. This allows us to make some estimate about the SNR threshold needed to retrieve a good fit. We estimated that SNR should be above ~200 for the fit to work reliably. It is to be noted that the amine site gets quickly depleted therefore only the first dozens of points are usually useable with this condition. We decided to keep the amine site nonetheless as it seemed an interesting information, but note that it almost never validates the SNR condition. This SNR threshold also explains the exclusion of the multiplets that indeed never reach the condition, and also overlap.

To assess the reliability of the estimated diffusion coefficients, we compared them, for the reactants, to values measured on the compounds alone and at equilibrium. The products are not very stable and thus it is difficult to use conventionally accepted method to record their diffusion coefficients. The reactants, on the other hand, are reasonably stable, which allows to record diffusion NMR experiments in a straightforward manner, in an NMR tube using non-deuterated acetonitrile, using the DSTE pulse sequence. This yields the reference values shown by the black line in figure 8.9d). There is a difference of about 6 % for the amine and 2 % for aldehyde, on average the maximum reached difference is 12 %, if we only consider points with enough SNR (*vide-supra*) it falls at ~8 %.

The estimated diffusion coefficient stays relatively constant as expected throughout the whole experiment. The Mono-imine case is particularly interesting as one can see a slight increase of the error from 5 to 40 min, it can be explained by the great increase of concentration at the same time. Using non-permutated random gradient ramp, this increase of concentration would change the measured diffusion coefficient. Indeed, the increase of concentration creates an increase of intensity that perturbs the fitted attenuation. Using p-DOSY allows to have those variation in a random way rather than a systematic one, making it akin to noise-related error.[159] The mono-imine can be seen rising extremely fast up to 44% in between two point in its fastest segment, reaching a maximum

concentration around 92 min. The increase of concentration of the amine is in average ~30% during the first 40 min of monitoring. Despite this impressive rate, the error only slightly increases during the fastest growth segment. This is rather impressive as the error increase is visible but stay in very acceptable margin which show that the use of fast DOSY and shuffled gradient work well for monitoring.

8.4.3. Some challenges of reaction monitoring

Flow NMR and the use of non-deuterated solvent raises some challenges concerning the homogeneity and stability of the magnetic field. They were described in previous sections already, but their consequences are more of a concern in the case of reaction monitoring. When the reaction proceeds it cannot be stopped to improve field homogeneity.

Figure 8.9 presents one of the best results obtained for reaction monitoring. Figure 8.10 shows the result of a monitoring session during which several issues were met. It corresponds to the data published in Ref[215]. One can see that the main difference is the lack of several points in the beginning. There is a point at 0 then 15 min, and the points in between are lost because of a severe loss of field homogeneity. This was found to be quite common across different attempts. Lineshapes become terrible a few minutes after the introduction of the aldehyde. We are not sure why this happens, and it could be a change of nature of the medium, viscosity or otherwise, maybe the presence of very transient solid formation. It is even hard to tell if it comes from the studied system or if it is something that is bound to happen from time to time because of the hardware or environment. As figure 7.9 demonstrate, such issues are not systematic.

One can also see especially when comparing figure 8.9c) and 8.10a) that the gaps between the points are not always at the same position or of the same length. Those gaps correspond to shimming events during which the flow is stopped and a shimming routine is performed. This routine is usually very fast (~30s) and barely visible. It is an automatic feature and it can be longer in the case when it did not reach its linewidth goal and should be prolonged, or if it completely fails and the operator has to shim manually. Those gaps are very visible albeit small in the figure 8.10 and barely visible in figure 8.9 except for a bigger one in the middle. This bigger gap is a shimming routine failure that demanded operator intervention and was longer. It just shows that despite the care taken in the NMR room and the prevention of exterior disruption, some differences are bound to happen.

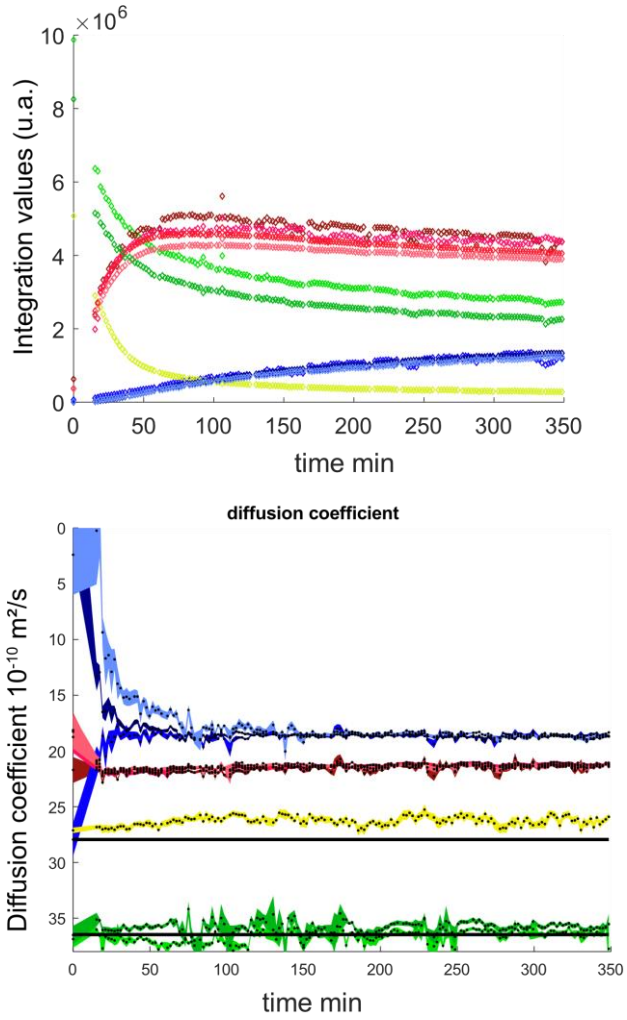

Figure 8.10 another earlier occurrence of the monitoring. Everything experimentally wise was done the same way as figure 8.9 as well as analyze processing etc.

The loss of those few points at the beginning is a real trouble. Indeed, one could argue that the whole point of the flowing apparatus is to have those first, very important points that can be keypoint in the monitoring. This effect is problematic but can be overcome by knowing the system well and doing multiple tries, it is also worth noting that even in the figure 8.10 the time resolution of the 3 firsts points is above the capability of conventional DSTE (0-15-17 min vs 20 min for a conventional DSTE experiment).

Another problem is the field drift. While it is usually negligible during one, it can be significant across a series of experiments. This can require recalibration of the solvent-suppression block. It is also the case that the solvent suppression become less effective from the beginning to the end of the experiment because the solvent signal has moved. This did not have enough effect on the baseline to corrupt the DOSY data mostly due to the double effect of solvent suppression and diffusion attenuation on the solvent, that make the solvent peak rather small anyway. It could be a problem for the integration of peak close to the solvent peak. In practice the need to adjust the frequency was only present beforehand and not during the monitoring.

8.4.4. Repeatability

The reaction monitoring experiment was repeated multiples times. After two initial runs to set up the parameters, five independent runs were performed. Out of these two were unsuccessful, giving three repetitions that can be analysed. The two failed experiment come from a problem of field homogeneity and a problem with the solvent suppression. The shimming was deemed ok for the experiment but was in fact bad and did not allow a good integration and fitting. A problem of solvent suppression as the WET strategy failed in the middle of the monitoring also made the processing difficult and not comparable to the already analysed points. The reason of this failing is unclear.

In order to assess the repeatability of the experiments, the average estimated diffusion coefficient was calculated for each compound, keeping only points that verify the SNR > ~200 conditions. The results are shown in Table 1 for the three reaction runs. One can see that the diffusion coefficient values are comparable even between different runs. The associated uncertainties are estimate in two different ways: (a) as the root mean square, over a reaction run, (b) as the standard deviation of the diffusion coefficient values over a reaction run of the uncertainties estimated from the fits.

The aldehyde has a surprisingly high uncertainty, probably coming from its hard to integrate nature and the fact that it stays for a rather long-time near the threshold level. One can see that the estimated uncertainty is, for three compounds, larger with method (b) then with method (a), which is consistent with the fact that the latter also accounts for variations during the reaction. The results for the amine are an exception, but the corresponding data set is in fact smaller, the SNR condition is verified only for about ~20 min for that compound. In those condition the apparatus instability, field shift and other inconveniences have no time to develop and thus give very repeatable experiment.

Table 8.1 Average estimated diffusion coefficient over different reaction runs, for the compounds involved in the di-imination reaction. The average is calculated, for each reaction run, over all of the data points for which SNR >~200. The associated uncertainty is calculated in two ways: (a) as the root mean square, over a reaction run, of the uncertainties estimated from the fits, (b) as the standard deviation of the diffusion coefficient values over a reaction run. The standard deviation for the average diffusion coefficients over the three reaction runs is also reported.

Exp no°	Amine (1 site)			Aldehyde (2 site)			Imine (4 sites)			Dimine (3 sites)		
	D	Uncertainty		D	Uncertainty		D	Uncertainty		D	Uncertainty	
		(a)	(b)		(a)	(b)		(a)	(b)		(a)	(b)
1	27.36	0.31	0.23	35.86	0.37	0.61	21.63	0.21	0.25	18.30	0.28	0.76
2	26.72	0.30	0.29	36.03	0.62	0.74	21.35	0.32	0.34	18.16	0.31	0.53
3	26.67	0.30	0.30	36.25	0.50	0.73	21.48	0.20	0.28	18.49	0.21	0.47
Standard deviation	0.38			0.19			0.15			0.16		

Doing the experiment 3 times in a row allow us to appreciate the differences with the reference compound for the reagents. Interestingly despite different behaviour the maximum deviation is ~10 % and the average is around 4 % for all experiment, on reasonable condition (SNR > 200.). It shows that, the change of behaviour one can sees comparing figure 8.9 and 8.10 are little and the impact of the shimming and other possible bad influences average over the time of the experiment. Those influences may worsen in the case of a much shorter monitoring but do not make it impossible just challenging. It is very interesting to see that the deviations in between experiment are very close to the deviations seen inside the same experiment.

8.5. Conclusion and perspective

We have shown that DOSY NMR in continuous flow can be used for the monitoring of an organic chemical reaction. Besides some preliminary experiments to select the parameters of the diffusion NMR pulses sequences, the approach is not more complicated or time consuming than a typical NMR monitoring, provided that a triple-axis gradient probe is available.

The experimental errors that we have reported are consistent across all of this work. Indeed, the error is of ~4 % in average and rarely goes above ~8 %. These results are obtained when sensitivity is sufficient and there is little to no overlapping, which is not always easy to obtain. Nonetheless, a chemical reaction is often a good medium as concentration are often quite high.

We believe that this method can be extended to a broad range of application, and in particular more complex reactions, or reactions or which the diffusion information itself if of interest. The most obvious for us would be polymerization or reactions where mass/size should be monitored such as coupling reactions. Reaction like this can be prone to mishaps, the coupling happening in multiple site or multiple times thus creating mixture that could use virtual separation. The monitoring of such kind of reactions in an online way with diffusion NMR could be very useful, as is could allow to have a finer understanding but also to have a finer control of the medium and the outcome. Reaction of coupling and polymerization indeed often yield multiple species of various length. NMR could be the insight to finely tune the system by using retro-loops and automated optimization.[129,216]

It is interesting to note that other reactions such as complexation, supramolecular assemblies also could use this technic to separate the component of the mixture and link which part are indeed bounded together. The interest being the change of size and well as the possibility to identify the possible outcome using its size. This is an interesting thing in the field of designing/understanding catalysts, that are often metallic complexes of varying nature. The catalyst being by definition present in low concentration in actual catalytic reactions, and often invisible for NMR, reactions in which it may be monitored by NMR most often concern specific steps, sometimes modified for analytical purpose, in the catalytic reaction.[81,106,217]

Different complementary paths may be taken to further improve the method. The improvement and change made to the flowing apparatus and flow quality could solve much problems.[117,193] One other way could be to improve or change the analysis methods. In this work we focused much of our attention on univariate methods but multivariate methods presented in part 5 could be interesting. Especially we found that PARAFAC[207,218] is a very good tool for the chemist as it gives as output concentration profiles, diffusion curves and the spectral component of each molecule. PARAFAC can disentangle spectra and get rid of the overlap which would allow to study more system with less *a priori* knowledge. It is also less user dependant and if one has enough calculation power it is faster. We tried our hand on this but the results are not right yet. Such methods being very sensitive to inhomogeneities and other problems they probably suffer from the harsh NMR conditions. Those methods also seem to require rather high SNR, and the required SNR increases with the number of compounds to solve. Nonetheless having this to work would mean a very simple method both for NMR experiments and to fully analyse the data. This would open it to more systems that overlap and to user that would need less NMR knowledge, ultimately the method could spread to a much wider audience of chemists.

Conclusion

In the bibliographical sections of the manuscript, we have highlighted the principles and features of diffusion NMR, as well as its usefulness for mixture analysis. We have also illustrated the relevance of reaction monitoring by NMR, and the usefulness of flow NMR for that purpose. Since reaction monitoring can require speed, we also described the acceleration strategies that are available for diffusion NMR. All of these considerations pointed out to the relevance of having diffusion NMR methods available for reaction monitoring by online flow NMR.

A first requirement was to have a way to evaluate the "virtual separation" provided by DOSY NMR methods. To do so we studied the processing and analysis of diffusion NMR, and proposed quantitative metrics to compare different methods. We then used methods to accelerate the NMR experiment while avoiding any drawback from this acceleration. The use of another axis for pulsed gradients around the 180° radiofrequency pulses turned out to be an excellent way of accelerating the experiments, even for DSTE pulse sequences, where, it allowed to accelerate the experiment by a factor 16 with not significant drawback.

We then evaluated methods to compensate for flow effect in diffusion NMR, and thus obtained accurate experiments for a continuously flowing sample. The best results were obtained with the combination of DSTE and the use of an axis orthogonal to the flow direction. Flow effects are very well suppressed with this approach, even for pulsatile flow.

Using what we learned and merging the methods of flow-compensation and acceleration we obtained a powerful sequence for monitoring. We illustrated its capability with the monitoring of a model organic chemical reaction. We expect this methodology to be useful to a broad community of chemists, and hope that it will be used by non-NMR specialist to get relevant information on interesting and complex chemical reactions.

References

(1) Brown, R. XXVII. A Brief Account of Microscopical Observations Made in the Months of June, July and August 1827, on the Particles Contained in the Pollen of Plants; and on the General Existence of Active Molecules in Organic and Inorganic Bodies. Philos. Mag. 1828, 4 (21), 161–173. https://doi.org/10.1080/14786442808674769.

(2) Brown, R. XXIV. Additional Remarks on Active Molecules. Philos. Mag. 1829, 6 (33), 161–166. https://doi.org/10.1080/14786442908675115.

(3) Einstein, A. Über die von der molekularkinetischen Theorie der Wärme geforderte Bewegung von in ruhenden Flüssigkeiten suspendierten Teilchen. Ann. Phys. 1905, 322 (8), 549–560. https://doi.org/10.1002/andp.19053220806.

(4) Adamczyk, Z.; Sadlej, K.; Wajnryb, E.; Ekiel-Jeżewska, M. L.; Warszyński, P. Hydrodynamic Radii and Diffusion Coefficients of Particle Aggregates Derived from the Bead Model. J. Colloid Interface Sci. 2010, 347 (2), 192–201. https://doi.org/10.1016/j.jcis.2010.03.066.

(5) Wilke, C. R.; Chang, P. Correlation of Diffusion Coefficients in Dilute Solutions. AIChE J. 1955, 1 (2), 264–270. https://doi.org/10.1002/aic.690010222.

(6) Fick, A. Ueber Diffusion. Ann. Phys. Chem. 1855, 170 (1), 59–86. https://doi.org/10.1002/andp.18551700105.

(7) Vink, H. Mutual Diffusion and Self-Diffusion in the Frictional Formalism of Non-Equilibrium Thermodynamics. J. Chem. Soc. Faraday Trans. 1 Phys. Chem. Condens. Phases 1985, 81 (7), 1725. https://doi.org/10.1039/f19858101725.

(8) Kanematsu, T.; Sato, T.; Imai, Y.; Ute, K.; Kitayama, T. Mutual- and Self-Diffusion Coefficients of a Semiflexible Polymer in Solution. Polym. J. 2005, 37 (2), 65–73. https://doi.org/10.1295/polymj.37.65.

(9) Scalettar, B. A.; Hearst, J. E.; Klein, M. P. FRAP and FCS Studies of Self-Diffusion and Mutual Diffusion in Entangled DNA Solutions. Macromolecules 1989, 22 (12), 4550–4559. https://doi.org/10.1021/ma00202a030.

(10) Balinov, B.; Jonsson, B.; Linse, P.; Soderman, O. The NMR Self-Diffusion Method Applied to Restricted Diffusion. Simulation of Echo Attenuation from Molecules in Spheres and between Planes. J. Magn. Reson. A 1993, 104 (1), 17–25. https://doi.org/10.1006/jmra.1993.1184.

(11) Tanner, J. E.; Stejskal, E. O. Restricted Self-Diffusion of Protons in Colloidal Systems by the Pulsed-Gradient, Spin-Echo Method. J. Chem. Phys. 1968, 49 (4), 1768–1777. https://doi.org/10.1063/1.1670306.

(12) Lipsicas, M.; Banavar, J. R.; Willemsen, J. Surface Relaxation and Pore Sizes in Rocks—a Nuclear Magnetic Resonance Analysis. Appl. Phys. Lett. 1986, 48 (22), 1544–1546. https://doi.org/10.1063/1.96864.

(13) Van As, H.; Lens, P. Use of 1 H NMR to Study Transport Processes in Porous Biosystems. J. Ind. Microbiol. Biotechnol. 2001, 26 (1–2), 43–52. https://doi.org/10.1038/sj.jim.7000087.

(14) Sotak, C. H. Nuclear Magnetic Resonance (NMR) Measurement of the Apparent Diffusion Coefficient (ADC) of Tissue Water and Its Relationship to Cell Volume Changes in Pathological States. Neurochem. Int. 2004, 45 (4), 569–582. https://doi.org/10.1016/j.neuint.2003.11.010.

(15) Damadian, R. Tumor Detection by Nuclear Magnetic Resonance. Science 1971, 171 (3976), 1151–1153. https://doi.org/10.1126/science.171.3976.1151.

(16) Wang, H.; Park, M.; Dong, R.; Kim, J.; Cho, Y.-K.; Tlusty, T.; Granick, S. Boosted Molecular Mobility during Common Chemical Reactions. Science 2020, 369 (6503), 537–541. https://doi.org/10.1126/science.aba8425.

(17) Günther, J.-P.; Fillbrook, L. L.; MacDonald, T. S. C.; Majer, G.; Price, W. S.; Fischer, P.; Beves, J. E. Comment on “Boosted Molecular Mobility during Common Chemical Reactions.” Science 2021, 371 (6526), eabe8322. https://doi.org/10.1126/science.abe8322.

(18) MacDonald, T. S. C.; Price, W. S.; Astumian, R. D.; Beves, J. E. Enhanced Diffusion of Molecular Catalysts Is Due to Convection. Angew. Chem. Int. Ed. 2019, 58 (52), 18864–18867. https://doi.org/10.1002/anie.201910968.
(19) Huang, T.; Granick, S. Comment on "Following Molecular Mobility during Chemical Reactions: No Evidence for Active Propulsion" and "Molecular Diffusivity of Click Reaction Components: The Diffusion Enhancement Question." J. Am. Chem. Soc. 2022, 144 (30), 13431–13435. https://doi.org/10.1021/jacs.2c02965.
(20) Sinnaeve, D. Simultaneous Solvent and J-Modulation Suppression in PGSTE-Based Diffusion Experiments. J. Magn. Reson. 2014, 245, 24–30. https://doi.org/10.1016/j.jmr.2014.05.007.
(21) Sinnaeve, D. The Stejskal-Tanner Equation Generalized for Any Gradient Shape-an Overview of Most Pulse Sequences Measuring Free Diffusion. Concepts Magn. Reson. Part A 2012, 40A (2), 39–65. https://doi.org/10.1002/cmr.a.21223.
(22) Torrey, H. C. Bloch Equations with Diffusion Terms. Phys. Rev. 1956, 104 (3), 563–565. https://doi.org/10.1103/PhysRev.104.563.
(23) Stejskal, E. O.; Tanner, J. E. Spin Diffusion Measurements: Spin Echoes in the Presence of a Time-Dependent Field Gradient. J. Chem. Phys. 1965, 42 (1), 288–292. https://doi.org/10.1063/1.1695690.
(24) Tanner, J. E. Use of the Stimulated Echo in NMR Diffusion Studies. J. Chem. Phys. 1970, 52 (5), 2523–2526. https://doi.org/10.1063/1.1673336.
(25) Blümich, B. P. T. Callaghan. Principles of Nuclear Magnetic Resonance Microscopy. Oxford University Press, Oxford, 1993, 492 Pp, £25. ISBN 0 198 53997 5. Magn. Reson. Chem. 1995, 33 (4), 322–322. https://doi.org/10.1002/mrc.1260330417.
(26) Zheng, G.; Price, W. S. Simultaneous Convection Compensation and Solvent Suppression in Biomolecular NMR Diffusion Experiments. J. Biomol. NMR 2009, 45 (3), 295–299. https://doi.org/10.1007/s10858-009-9367-2.
(27) Liu, M.; Nicholson, J. K.; Lindon, J. C. High-Resolution Diffusion and Relaxation Edited One- and Two-Dimensional 1 H NMR Spectroscopy of Biological Fluids. Anal. Chem. 1996, 68 (19), 3370–3376. https://doi.org/10.1021/ac960426p.
(28) Liu, M.; Tang, H.; Nicholson, J. K.; Lindon, J. C. Use Of1H NMR-Determined Diffusion Coefficients to Characterize Lipoprotein Fractions in Human Blood Plasma. Magn. Reson. Chem. 2002, 40 (13), S83–S88. https://doi.org/10.1002/mrc.1121.
(29) Esturau, N.; Espinosa, J. F. Optimization of Diffusion-Filtered NMR Experiments for Selective Suppression of Residual Nondeuterated Solvent and Water Signals from 1 H NMR Spectra of Organic Compounds. J. Org. Chem. 2006, 71 (11), 4103–4110. https://doi.org/10.1021/jo060229i.
(30) Prieto, J. M.; Mellinas-Gomez, M.; Zloh, M. Application of Diffusion-Edited and Solvent Suppression 1 H-NMR to the Direct Analysis of Markers in Valerian-Hop Liquid Herbal Products: Direct NMR of Valerian-Hop Liquid Herbal Products. Phytochem. Anal. 2016, 27 (2), 100–106. https://doi.org/10.1002/pca.2603.
(31) Bliziotis, N. G.; Engelke, U. F. H.; Aspers, R. L. E. G.; Engel, J.; Deinum, J.; Timmers, H. J. L. M.; Wevers, R. A.; Kluijtmans, L. A. J. A Comparison of High-Throughput Plasma NMR Protocols for Comparative Untargeted Metabolomics. Metabolomics 2020, 16 (5), 64. https://doi.org/10.1007/s11306-020-01686-y.
(32) Bleicher, K.; Lin, M.; Shapiro, M. J.; Wareing, J. R. Diffusion Edited NMR: Screening Compound Mixtures by Affinity NMR to Detect Binding Ligands to Vancomycin. J. Org. Chem. 1998, 63 (23), 8486–8490. https://doi.org/10.1021/jo9817366.
(33) Hajduk, P. J.; Olejniczak, E. T.; Fesik, S. W. One-Dimensional Relaxation- and Diffusion-Edited NMR Methods for Screening Compounds That Bind to Macromolecules. J. Am. Chem. Soc. 1997, 119 (50), 12257–12261. https://doi.org/10.1021/ja9715962.
(34) Lucas, L. H.; Larive, C. K. Measuring Ligand-Protein Binding Using NMR Diffusion Experiments. Concepts Magn. Reson. 2004, 20A (1), 24–41. https://doi.org/10.1002/cmr.a.10094.

(35) Lin, M.; Shapiro, M. J.; Wareing, J. R. Diffusion-Edited NMR−Affinity NMR for Direct Observation of Molecular Interactions. J. Am. Chem. Soc. 1997, 119 (22), 5249–5250. https://doi.org/10.1021/ja963654+.
(36) Gu, K.; Onorato, J.; Xiao, S. S.; Luscombe, C. K.; Loo, Y.-L. Determination of the Molecular Weight of Conjugated Polymers with Diffusion-Ordered NMR Spectroscopy. Chem. Mater. 2018, 30 (3), 570–576. https://doi.org/10.1021/acs.chemmater.7b05063.
(37) Voorter, P.; McKay, A.; Dai, J.; Paravagna, O.; Cameron, N. R.; Junkers, T. Solvent-Independent Molecular Weight Determination of Polymers Based on a Truly Universal Calibration. Angew. Chem. 2022, 134 (5). https://doi.org/10.1002/ange.202114536.
(38) Gibbs, S. J.; Johnson, C. S. A PFG NMR Experiment for Accurate Diffusion and Flow Studies in the Presence of Eddy Currents. J. Magn. Reson. 1969 1991, 93 (2), 395–402. https://doi.org/10.1016/0022-2364(91)90014-K.
(39) Hrovat, M. I.; Wade, C. G. NMR Pulsed Gradient Diffusion Measurements. II. Residual Gradients and Lineshape Distortions. J. Magn. Reson. 1969 1981, 45 (1), 67–80. https://doi.org/10.1016/0022-2364(81)90100-1.
(40) Loening, N. M.; Keeler, J. Measurement of Convection and Temperature Profiles in Liquid Samples. J. Magn. Reson. 1999, 139 (2), 334–341. https://doi.org/10.1006/jmre.1999.1777.
(41) Barbosa, T. M.; Rittner, R.; Tormena, C. F.; Morris, G. A.; Nilsson, M. Convection in Liquid-State NMR: Expect the Unexpected. RSC Adv. 2016, 6 (97), 95173–95176. https://doi.org/10.1039/C6RA23427E.
(42) Jerschow, A.; Müller, N. Suppression of Convection Artifacts in Stimulated-Echo Diffusion Experiments. Double-Stimulated-Echo Experiments. J. Magn. Reson. 1997, 125 (2), 372–375. https://doi.org/10.1006/jmre.1997.1123.
(43) Fleischer, G. The Effect of Polydispersity on Measuring Polymer Self-Diffusion with the n.m.r. Pulsed Field Gradient Technique. Polymer 1985, 26 (11), 1677–1682. https://doi.org/10.1016/0032-3861(85)90285-X.
(44) Gu, K.; Onorato, J.; Xiao, S. S.; Luscombe, C. K.; Loo, Y.-L. Determination of the Molecular Weight of Conjugated Polymers with Diffusion-Ordered NMR Spectroscopy. Chem. Mater. 2018, 30 (3), 570–576. https://doi.org/10.1021/acs.chemmater.7b05063.
(45) Provencher, S. W. A Constrained Regularization Method for Inverting Data Represented by Linear Algebraic or Integral Equations. Comput. Phys. Commun. 1982, 27 (3), 213–227. https://doi.org/10.1016/0010-4655(82)90173-4.
(46) Jerschow, A.; Müller, N. Diffusion-Separated Nuclear Magnetic Resonance Spectroscopy of Polymer Mixtures. Macromolecules 1998, 31 (19), 6573–6578. https://doi.org/10.1021/ma9801772.
(47) Honerkamp, J.; Weese, J. A Nonlinear Regularization Method for the Calculation of Relaxation Spectra. Rheol. Acta 1993, 32 (1), 65–73. https://doi.org/10.1007/BF00396678.
(48) Monteiro, M. J. Fitting Molecular Weight Distributions Using a Log-Normal Distribution Model. Eur. Polym. J. 2015, 65, 197–201. https://doi.org/10.1016/j.eurpolymj.2015.01.009.
(49) Röding, M.; Bernin, D.; Jonasson, J.; Särkkä, A.; Topgaard, D.; Rudemo, M.; Nydén, M. The Gamma Distribution Model for Pulsed-Field Gradient NMR Studies of Molecular-Weight Distributions of Polymers. J. Magn. Reson. 2012, 222, 105–111. https://doi.org/10.1016/j.jmr.2012.07.005.
(50) Williamson, N. H.; Nydén, M.; Röding, M. The Lognormal and Gamma Distribution Models for Estimating Molecular Weight Distributions of Polymers Using PGSE NMR. J. Magn. Reson. 2016, 267, 54–62. https://doi.org/10.1016/j.jmr.2016.04.007.
(51) Guo, X.; Laryea, E.; Wilhelm, M.; Luy, B.; Nirschl, H.; Guthausen, G. Diffusion in Polymer Solutions: Molecular Weight Distribution by PFG-NMR and Relation to SEC. Macromol. Chem. Phys. 2017, 218 (1), 1600440. https://doi.org/10.1002/macp.201600440.
(52) Urbańczyk, M.; Bernin, D.; Koźmiński, W.; Kazimierczuk, K. Iterative Thresholding Algorithm for Multiexponential Decay Applied to PGSE NMR Data. Anal. Chem. 2013, 85 (3), 1828–1833. https://doi.org/10.1021/ac3032004.

(53) Hou, J.; Pearce, E. Characterization of Polymer Molecular Weight Distribution by NMR Diffusometry: Experimental Criteria and Findings. Anal. Chem. 2021, 93 (22), 7958–7964. https://doi.org/10.1021/acs.analchem.1c00793.
(54) Viéville, J.; Tanty, M.; Delsuc, M.-A. Polydispersity Index of Polymers Revealed by DOSY NMR. J. Magn. Reson. 2011, 212 (1), 169–173. https://doi.org/10.1016/j.jmr.2011.06.020.
(55) Chen, X.; Cheng, Y.; Matsuba, M.; Wang, X.; Han, S.; Mowbray, J.; Zhu, Q. EXPRESS: In Situ Monitoring of Heterogeneous Hydrosilylation Reactions Using Infrared and Raman Spectroscopy: Normalization by Phase-Specific Internal Standards. Appl. Spectrosc. 2019, 000370281985891. https://doi.org/10.1177/0003702819858916.
(56) Augé, S.; Schmit, P.-O.; Crutchfield, C. A.; Islam, M. T.; Harris, D. J.; Durand, E.; Clemancey, M.; Quoineaud, A.-A.; Lancelin, J.-M.; Prigent, Y.; Taulelle, F.; Delsuc, M.-A. NMR Measure of Translational Diffusion and Fractal Dimension. Application to Molecular Mass Measurement. J. Phys. Chem. B 2009, 113 (7), 1914–1918. https://doi.org/10.1021/jp8094424.
(57) Wackerly, J. Wm.; Dunne, J. F. Synthesis of Polystyrene and Molecular Weight Determination by 1 H NMR End-Group Analysis. J. Chem. Educ. 2017, 94 (11), 1790–1793. https://doi.org/10.1021/acs.jchemed.6b00814.
(58) Kavakka, J. S.; Kilpeläinen, I.; Heikkinen, S. General Chromatographic NMR Method in Liquid State for Synthetic Chemistry: Polyvinylpyrrolidone Assisted DOSY Experiments. Org. Lett. 2009, 11 (6), 1349–1352. https://doi.org/10.1021/ol9001398.
(59) Ernst, R. R.; Anderson, W. A. Application of Fourier Transform Spectroscopy to Magnetic Resonance. Rev. Sci. Instrum. 1966, 37 (1), 93–102. https://doi.org/10.1063/1.1719961.
(60) Rodrigues, E. D.; da Silva, D. B.; de Oliveira, D. C. R.; da Silva, G. V. J. DOSY NMR Applied to Analysis of Flavonoid Glycosides from Bidens Sulphurea. Magn. Reson. Chem. 2009, 47 (12), 1095–1100. https://doi.org/10.1002/mrc.2516.
(61) Kleks, G.; Holland, D. C.; Porter, J.; Carroll, A. R. Natural Products Dereplication by Diffusion Ordered NMR Spectroscopy (DOSY). Chem. Sci. 2021, 12 (32), 10930–10943. https://doi.org/10.1039/D1SC02940A.
(62) Halabalaki, M.; Vougogiannopoulou, K.; Mikros, E.; Skaltsounis, A. L. Recent Advances and New Strategies in the NMR-Based Identification of Natural Products. Curr. Opin. Biotechnol. 2014, 25, 1–7. https://doi.org/10.1016/j.copbio.2013.08.005.
(63) You, Y.-L.; Li, F.-F.; Wang, N.; Wang, S.-Q. Matrix-Assisted DOSY for Analysis of Indole Alkaloid Mixtures. Molecules 2021, 26 (6). https://doi.org/10.3390/molecules26061751.
(64) Li, Y.; Li, J.; Ding, H.; Li, A. Recent Advances on the Total Synthesis of Alkaloids in Mainland China. Natl. Sci. Rev. 2017, 4 (3), 397–425. https://doi.org/10.1093/nsr/nwx050.
(65) Evans, R.; Hernandez-Cid, A.; Dal Poggetto, G.; Vesty, A.; Haiber, S.; Morris, G. A.; Nilsson, M. Matrix-Assisted Diffusion-Ordered NMR Spectroscopy with an Invisible Matrix: A Vanishing Surfactant. RSC Adv. 2017, 7 (1), 449–452. https://doi.org/10.1039/C6RA26144B.
(66) Vieira, M. G. S.; Gramosa, N. V.; Ricardo, N. M. P. S.; Morris, G. A.; Adams, R. W.; Nilsson, M. Natural Product Mixture Analysis by Matrix-Assisted DOSY Using Brij Surfactants in Mixed Solvents. RSC Adv 2014, 4 (79), 42029–42034. https://doi.org/10.1039/C4RA04433A.
(67) Voda, M. A.; van Duynhoven, J. Characterization of Food Emulsions by PFG NMR. Trends Food Sci. Technol. 2009, 20 (11–12), 533–543. https://doi.org/10.1016/j.tifs.2009.07.001.
(68) Balinov, B.; Jonsson, B.; Linse, P.; Soderman, O. The NMR Self-Diffusion Method Applied to Restricted Diffusion. Simulation of Echo Attenuation from Molecules in Spheres and between Planes. J. Magn. Reson. A 1993, 104 (1), 17–25. https://doi.org/10.1006/jmra.1993.1184.
(69) Lu, Y.; Hu, F.; Miyakawa, T.; Tanokura, M. Complex Mixture Analysis of Organic Compounds in Yogurt by NMR Spectroscopy. Metabolites 2016, 6 (2), 19. https://doi.org/10.3390/metabo6020019.
(70) Trefi, S.; Gilard, V.; Balayssac, S.; Malet-Martino, M.; Martino, R. The Usefulness of 2D DOSY and 3D DOSY-COSY 1H NMR for Mixture Analysis: Application to Genuine and Fake Formulations of Sildenafil (Viagra). Magn. Reson. Chem. 2009, 47 (S1), S163–S173. https://doi.org/10.1002/mrc.2490.

(71) Vaysse, J.; Balayssac, S.; Gilard, V.; Desoubdzanne, D.; Malet-Martino, M.; Martino, R. Analysis of Adulterated Herbal Medicines and Dietary Supplements Marketed for Weight Loss by DOSY 1 H-NMR. Food Addit. Contam. Part A 2010, 27 (7), 903–916. https://doi.org/10.1080/19440041003705821.
(72) Barbosa, T. M.; Morris, G. A.; Nilsson, M.; Rittner, R.; Tormena, C. F. 1 H and 19 F NMR in Drug Stress Testing: The Case of Voriconazole. RSC Adv. 2017, 7 (54), 34000–34004. https://doi.org/10.1039/C7RA03822D.
(73) Avram, L.; Cohen, Y. Diffusion NMR of Molecular Cages and Capsules. Chem. Soc. Rev. 2015, 44 (2), 586–602. https://doi.org/10.1039/C4CS00197D.
(74) Cohen, Y.; Slovak, S.; Avram, L. Solution NMR of Synthetic Cavity Containing Supramolecular Systems: What Have We Learned on and From? Chem. Commun. 2021, 57 (71), 8856–8884. https://doi.org/10.1039/D1CC02906A.
(75) McConnell, A. J. Metallosupramolecular Cages: From Design Principles and Characterisation Techniques to Applications. Chem. Soc. Rev. 2022, 51 (8), 2957–2971. https://doi.org/10.1039/D1CS01143J.
(76) Pluth, M. D.; Tiedemann, B. E. F.; van Halbeek, H.; Nunlist, R.; Raymond, K. N. Diffusion of a Highly Charged Supramolecular Assembly: Direct Observation of Ion Association in Water 1. Inorg. Chem. 2008, 47 (5), 1411–1413. https://doi.org/10.1021/ic7020885.
(77) Merget, S.; Catti, L.; Zev, S.; Major, D. T.; Trapp, N.; Tiefenbacher, K. Concentration-Dependent Self-Assembly of an Unusually Large Hexameric Hydrogen-Bonded Molecular Cage. Chem. – Eur. J. 2021, 27 (13), 4447–4453. https://doi.org/10.1002/chem.202005046.
(78) Pastor, A.; Martínez-Viviente, E. NMR Spectroscopy in Coordination Supramolecular Chemistry: A Unique and Powerful Methodology. Coord. Chem. Rev. 2008, 252 (21–22), 2314–2345. https://doi.org/10.1016/j.ccr.2008.01.025.
(79) Qiao, Y.; Ge, W.; Jia, L.; Hou, X.; Wang, Y.; Pedersen, C. M. Glycosylation Intermediates Studied Using Low Temperature 1 H- and 19 F-DOSY NMR: New Insight into the Activation of Trichloroacetimidates. Chem. Commun. 2016, 52 (76), 11418–11421. https://doi.org/10.1039/C6CC05272J.
(80) Boyle, T. J.; Guerrero, F.; Alam, T. M.; Dunnigan, K. A.; Sears, J. M.; Wheeler, D. R. Trapped Intermediate of a Meerwein–Pondorf–Verley Reduction of Hydroxy Benzaldehyde to a Dialkoxide by Titanium Alkoxides. Inorg. Chem. 2020, 59 (1), 880–890. https://doi.org/10.1021/acs.inorgchem.9b03134.
(81) Matador, E.; Retamosa, M. de G.; Rohal'ová, D.; Iglesias-Sigüenza, J.; Merino, P.; Fernández, R.; Lassaletta, J. M.; Monge, D. α-Keto Hydrazones in Asymmetric Aminocatalysis: Reactivity through β-Amino Aza-Dienamine Intermediates. Org. Chem. Front. 2021, 8 (13), 3446–3456. https://doi.org/10.1039/D1QO00384D.
(82) Yamaguchi, S.; Ichikawa, T.; Wang, Y.; Nakagawa, Y.; Isobe, S.; Kojima, Y.; Miyaoka, H. Nitrogen Dissociation via Reaction with Lithium Alloys. ACS Omega 2017, 2 (3), 1081–1088. https://doi.org/10.1021/acsomega.6b00498.
(83) Keresztes, I.; Williard, P. G. Diffusion-Ordered NMR Spectroscopy (DOSY) of THF Solvated n -Butyllithium Aggregates. J. Am. Chem. Soc. 2000, 122 (41), 10228–10229. https://doi.org/10.1021/ja002278x.
(84) Jones, A. C.; Sanders, A. W.; Bevan, M. J.; Reich, H. J. Reactivity of Individual Organolithium Aggregates: A RINMR Study of n -Butyllithium and 2-Methoxy-6-(Methoxymethyl)Phenyllithium. J. Am. Chem. Soc. 2007, 129 (12), 3492–3493. https://doi.org/10.1021/ja0689334.
(85) Li, D.; Sun, C.; Liu, J.; Hopson, R.; Li, W.; Williard, P. G. Aggregation Studies of Complexes Containing a Chiral Lithium Amide and n -Butyllithium. J. Org. Chem. 2008, 73 (6), 2373–2381. https://doi.org/10.1021/jo702655m.
(86) Li, D.; Keresztes, I.; Hopson, R.; Williard, P. G. Characterization of Reactive Intermediates by Multinuclear Diffusion-Ordered NMR Spectroscopy (DOSY). Acc. Chem. Res. 2009, 42 (2), 270–280. https://doi.org/10.1021/ar800127e.

(87) Wang, Z.; Gobet, M.; Sarou-Kanian, V.; Massiot, D.; Bessada, C.; Deschamps, M. Lithium Diffusion in Lithium Nitride by Pulsed-Field Gradient NMR. Phys. Chem. Chem. Phys. 2012, 14 (39), 13535. https://doi.org/10.1039/c2cp42391j.
(88) Kao, H.-M.; Chang, P.-C.; Chao, S.-W.; Lee, C.-H. 7Li NMR, Ionic Conductivity and Self-Diffusion Coefficients of Lithium Ion and Solvent of Plasticized Organic–Inorganic Hybrid Electrolyte Based on PPG-PEG-PPG Diamine and Alkoxysilanes. Electrochimica Acta 2006, 52 (3), 1015–1027. https://doi.org/10.1016/j.electacta.2006.06.042.
(89) Aliakbari, F.; Mohammad-Beigi, H.; Rezaei-Ghaleh, N.; Becker, S.; Dehghani Esmatabad, F.; Eslampanah Seyedi, H. A.; Bardania, H.; Tayaranian Marvian, A.; Collingwood, J. F.; Christiansen, G.; Zweckstetter, M.; Otzen, D. E.; Morshedi, D. The Potential of Zwitterionic Nanoliposomes against Neurotoxic Alpha-Synuclein Aggregates in Parkinson's Disease. Nanoscale 2018, 10 (19), 9174–9185. https://doi.org/10.1039/C8NR00632F.
(90) Kumar, J.; Sreeramulu, S.; Schmidt, T. L.; Richter, C.; Vonck, J.; Heckel, A.; Glaubitz, C.; Schwalbe, H. Prion Protein Amyloid Formation Involves Structural Rearrangements in the C-Terminal Domain. ChemBioChem 2010, 11 (9), 1208–1213. https://doi.org/10.1002/cbic.201000076.
(91) Svane, A. S. P.; Jahn, K.; Deva, T.; Malmendal, A.; Otzen, D. E.; Dittmer, J.; Nielsen, N. Chr. Early Stages of Amyloid Fibril Formation Studied by Liquid-State NMR: The Peptide Hormone Glucagon. Biophys. J. 2008, 95 (1), 366–377. https://doi.org/10.1529/biophysj.107.122895.
(92) Suzuki, Y.; Brender, J. R.; Soper, M. T.; Krishnamoorthy, J.; Zhou, Y.; Ruotolo, B. T.; Kotov, N. A.; Ramamoorthy, A.; Marsh, E. N. G. Resolution of Oligomeric Species during the Aggregation of Aβ 1–40 Using 19 F NMR. Biochemistry 2013, 52 (11), 1903–1912. https://doi.org/10.1021/bi400027y.
(93) Kandiyal, P. S.; Kim, J. Y.; Fortunati, D. L.; Mok, K. H. Size Determination of Protein Oligomers/Aggregates Using Diffusion NMR Spectroscopy. In Protein Self-Assembly; McManus, J. J., Ed.; Methods in Molecular Biology; Springer New York: New York, NY, 2019; Vol. 2039, pp 173–183. https://doi.org/10.1007/978-1-4939-9678-0_13.
(94) Dehner, A.; Kessler, H. Diffusion NMR Spectroscopy: Folding and Aggregation of Domains in P53. ChemBioChem 2005, 6 (9), 1550–1565. https://doi.org/10.1002/cbic.200500093.
(95) Lee, M.-K.; Kim, H.-S.; Rhee, H.-J.; 주재범. Reaction Monitoring of Imine Synthesis Using Raman Spectroscopy. Bull. Korean Chem. Soc. 2003, 24 (2), 205–208. https://doi.org/10.5012/BKCS.2003.24.2.205.
(96) Arpino, P. J.; Dawkins, B. G.; McLafferty, F. W. A Liquid Chromatography/Mass Spectrometry System Providing Continuous Monitoring with Nanogram Sensitivity. J. Chromatogr. Sci. 1974, 12 (10), 574–578. https://doi.org/10.1093/chromsci/12.10.574.
(97) Ben-Tal, Y.; Boaler, P. J.; J. A. Dale, H.; Dooley, R. E.; Fohn, N. A.; Gao, Y.; García-Domínguez, A.; Grant, K. M.; M. R. Hall, A.; Hayes, H. L. D.; Kucharski, M. M.; Wei, R.; Lloyd-Jones, G. C. Mechanistic Analysis by NMR Spectroscopy: A Users Guide. Prog. Nucl. Magn. Reson. Spectrosc. 2022, S0079656522000073. https://doi.org/10.1016/j.pnmrs.2022.01.001.
(98) Foley, D. A.; Dunn, A. L.; Zell, M. T. Reaction Monitoring Using Online vs Tube NMR Spectroscopy: Seriously Different Results: Online vs Tube NMR: A Kinetic Evaluation of NMR Reaction Monitoring Approaches. Magn. Reson. Chem. 2016, 54 (6), 451–456. https://doi.org/10.1002/mrc.4259.
(99) Knöös, P.; Topgaard, D.; Wahlgren, M.; Ulvenlund, S.; Piculell, L. Using NMR Chemical Shift Imaging To Monitor Swelling and Molecular Transport in Drug-Loaded Tablets of Hydrophobically Modified Poly(Acrylic Acid): Methodology and Effects of Polymer (In)Solubility. Langmuir 2013, 29 (45), 13898–13908. https://doi.org/10.1021/la4024458.
(100) Deus, W. B.; Ventura, M.; Silva, J. R.; Andrade, L. H. C.; Catunda, T.; Lima, S. M. Monitoring of the Ester Production by Near-near Infrared Thermal Lens Spectroscopy. Fuel 2019, 253, 1090–1096. https://doi.org/10.1016/j.fuel.2019.05.097.

(101) Pang, K.; Kotek, R.; Tonelli, A. Review of Conventional and Novel Polymerization Processes for Polyesters. Prog. Polym. Sci. 2006, 31 (11), 1009–1037. https://doi.org/10.1016/j.progpolymsci.2006.08.008.
(102) Yan, Q.-Z.; Zhang, W.-F.; Lu, G.-D.; Su, X.-T.; Ge, C.-C. Frontal Polymerization Synthesis of Starch-Grafted Hydrogels: Effect of Temperature and Tube Size on Propagating Front and Properties of Hydrogels. Chem. - Eur. J. 2006, 12 (12), 3303–3309. https://doi.org/10.1002/chem.200500970.
(103) Britton, D.; Heatley, F.; Lovell, P. A. Chain Transfer to Polymer in Free-Radical Bulk and Emulsion Polymerization of Vinyl Acetate Studied by NMR Spectroscopy. Macromolecules 1998, 31 (9), 2828–2837. https://doi.org/10.1021/ma971284j.
(104) Tillman, E. S.; Contrella, N. D.; Leasure, J. G. Monitoring the Nitroxide-Mediated Polymerization of Styrene Using Gel Permeation Chromatography and Proton NMR. J. Chem. Educ. 2009, 86 (12), 1424. https://doi.org/10.1021/ed086p1424.
(105) Liu, P.; Pearce, C. M.; Anastasiadi, R.-M.; Resmini, M.; Castilla, A. M. Covalently Crosslinked Nanogels: An NMR Study of the Effect of Monomer Reactivity on Composition and Structure. Polymers 2019, 11 (2), 353. https://doi.org/10.3390/polym11020353.
(106) Zhang, P.; Tugny, C.; Meijide Suárez, J.; Guitet, M.; Derat, E.; Vanthuyne, N.; Zhang, Y.; Bistri, O.; Mouriès-Mansuy, V.; Ménand, M.; Roland, S.; Fensterbank, L.; Sollogoub, M. Artificial Chiral Metallo-Pockets Including a Single Metal Serving as Structural Probe and Catalytic Center. Chem 2017, 3 (1), 174–191. https://doi.org/10.1016/j.chempr.2017.05.009.
(107) Rebilly, J.-N.; Colasson, B.; Bistri, O.; Over, D.; Reinaud, O. Biomimetic Cavity-Based Metal Complexes. Chem. Soc. Rev. 2015, 44 (2), 467–489. https://doi.org/10.1039/C4CS00211C.
(108) Leutzsch, M.; Sederman, A. J.; Gladden, L. F.; Mantle, M. D. In Situ Reaction Monitoring in Heterogeneous Catalysts by a Benchtop NMR Spectrometer. Magn. Reson. Imaging 2019, 56, 138–143. https://doi.org/10.1016/j.mri.2018.09.006.
(109) Kallman, N.; Cole, K.; Koenig, T.; Buser, J.; McFarland, A.; McNulty, L.; Mitchell, D. Synthesis of Aminopyrazoles from Isoxazoles: Comparison of Preparative Methods by in Situ NMR Analysis. Synthesis 2016, 48 (20), 3537–3543. https://doi.org/10.1055/s-0035-1561861.
(110) Rosenau, C. P.; Jelier, B. J.; Gossert, A. D.; Togni, A. Exposing the Origins of Irreproducibility in Fluorine NMR Spectroscopy. Angew. Chem. Int. Ed. 2018, 57 (30), 9528–9533. https://doi.org/10.1002/anie.201802620.
(111) Dolinski, N. D.; Page, Z. A.; Eisenreich, F.; Niu, J.; Hecht, S.; Read de Alaniz, J.; Hawker, C. J. A Versatile Approach for In Situ Monitoring of Photoswitches and Photopolymerizations. ChemPhotoChem 2017, 1 (4), 125–131. https://doi.org/10.1002/cptc.201600045.
(112) Xu, J.; Jung, K.; Boyer, C. Oxygen Tolerance Study of Photoinduced Electron Transfer–Reversible Addition–Fragmentation Chain Transfer (PET-RAFT) Polymerization Mediated by Ru(Bpy) 3 Cl 2. Macromolecules 2014, 47 (13), 4217–4229. https://doi.org/10.1021/ma500883y.
(113) Neudert, R.; Ströfer, E.; Bremser, W. On-Line NMR in Process Engineering. Magn. Reson. Chem. 1986, 24 (12), 1089–1092. https://doi.org/10.1002/mrc.1260241214.
(114) Nicolaou, K. C.; Härter, M. W.; Gunzner, J. L.; Nadin, A. The Wittig and Related Reactions in Natural Product Synthesis. Liebigs Ann. 1997, 1997 (7), 1283–1301. https://doi.org/10.1002/jlac.199719970704.
(115) Bernstein, M. A.; Štefinović, M.; Sleigh, C. J. Optimising Reaction Performance in the Pharmaceutical Industry by Monitoring with NMR. Magn. Reson. Chem. 2007, 45 (7), 564–571. https://doi.org/10.1002/mrc.2007.
(116) Khajeh, M.; Bernstein, M. A.; Morris, G. A. A Simple Flowcell for Reaction Monitoring by NMR. Magn. Reson. Chem. 2010, 48 (7), 516–522. https://doi.org/10.1002/mrc.2610.
(117) Saib, A.; Bara-Estaún, A.; Harper, O. J.; Berry, D. B. G.; Thomlinson, I. A.; Broomfield-Tagg, R.; Lowe, J. P.; Lyall, C. L.; Hintermair, U. Engineering Aspects of FlowNMR Spectroscopy Setups for Online Analysis of Solution-Phase Processes. React. Chem. Eng. 2021, 6 (9), 1548–1573. https://doi.org/10.1039/D1RE00217A.

(118) Kühne, R. O.; Schaffhauser, T.; Wokaun, A.; Ernst, R. R. Study of Transient Chemical Reactions by NMR. Fast Stopped-Flow Fourier Transform Experiments. J. Magn. Reson. 1969 1979, 35 (1), 39–67. https://doi.org/10.1016/0022-2364(79)90077-5.
(119) McGarrity, J. F.; Prodolliet, J. High-Field Rapid Injection NMR: Observation of Unstable Primary Ozonide Intermediates. J. Org. Chem. 1984, 49 (23), 4465–4470. https://doi.org/10.1021/jo00197a027.
(120) Dunn, A. L.; Landis, C. R. Progress toward Reaction Monitoring at Variable Temperatures: A New Stopped-Flow NMR Probe Design: Progress toward Reaction Monitoring at Variable Temperatures: A New Stopped-Flow NMR Probe Design. Magn. Reson. Chem. 2017, 55 (4), 329–336. https://doi.org/10.1002/mrc.4538.
(121) Dunn, A. L.; Landis, C. R. Stopped-Flow NMR and Quantitative GPC Reveal Unexpected Complexities for the Mechanism of NHC-Catalyzed Lactide Polymerization. Macromolecules 2017, 50 (6), 2267–2275. https://doi.org/10.1021/acs.macromol.6b02139.
(122) Keifer, P. A.; Smallcombe, S. H.; Williams, E. H.; Salomon, K. E.; Mendez, G.; Belletire, J. L.; Moore, C. D. Direct-Injection NMR (DI-NMR): A Flow NMR Technique for the Analysis of Combinatorial Chemistry Libraries 1. J. Comb. Chem. 2000, 2 (2), 151–171. https://doi.org/10.1021/cc990066u.
(123) Ask Your Local NMR Engineer.
(124) Tijssen, K. C. H.; van Weerdenburg, B. J. A.; Zhang, H.; Janssen, J. W. G.; Feiters, M. C.; van Bentum, P. J. M.; Kentgens, A. P. M. Monitoring Heterogeneously Catalyzed Hydrogenation Reactions at Elevated Pressures Using In-Line Flow NMR. Anal. Chem. 2019, 91 (20), 12636–12643. https://doi.org/10.1021/acs.analchem.9b00895.
(125) Yu, T.; Ding, Z.; Nie, W.; Jiao, J.; Zhang, H.; Zhang, Q.; Xue, C.; Duan, X.; Yamada, Y. M. A.; Li, P. Recent Advances in Continuous-Flow Enantioselective Catalysis. Chem. – Eur. J. 2020, 26 (26), 5729–5747. https://doi.org/10.1002/chem.201905151.
(126) Irfan, M.; Glasnov, T. N.; Kappe, C. O. Heterogeneous Catalytic Hydrogenation Reactions in Continuous-Flow Reactors. ChemSusChem 2011, 4 (3), 300–316. https://doi.org/10.1002/cssc.201000354.
(127) Oosthoek-de Vries, A. J.; Bart, J.; Tiggelaar, R. M.; Janssen, J. W. G.; van Bentum, P. J. M.; Gardeniers, H. J. G. E.; Kentgens, A. P. M. Continuous Flow 1 H and 13 C NMR Spectroscopy in Microfluidic Stripline NMR Chips. Anal. Chem. 2017, 89 (4), 2296–2303. https://doi.org/10.1021/acs.analchem.6b03784.
(128) Schotten, C.; Howard, J. L.; Jenkins, R. L.; Codina, A.; Browne, D. L. A Continuous Flow-Batch Hybrid Reactor for Commodity Chemical Synthesis Enabled by Inline NMR and Temperature Monitoring. Tetrahedron 2018, 74 (38), 5503–5509. https://doi.org/10.1016/j.tet.2018.05.070.
(129) Giraudeau, P.; Felpin, F.-X. Flow Reactors Integrated with In-Line Monitoring Using Benchtop NMR Spectroscopy. React. Chem. Eng. 2018, 3 (4), 399–413. https://doi.org/10.1039/C8RE00083B.
(130) Hall, A. M. R.; Dong, P.; Codina, A.; Lowe, J. P.; Hintermair, U. Kinetics of Asymmetric Transfer Hydrogenation, Catalyst Deactivation, and Inhibition with Noyori Complexes As Revealed by Real-Time High-Resolution FlowNMR Spectroscopy. ACS Catal. 2019, 9 (3), 2079–2090. https://doi.org/10.1021/acscatal.8b03530.
(131) Hall, A. M. R.; Chouler, J. C.; Codina, A.; Gierth, P. T.; Lowe, J. P.; Hintermair, U. Practical Aspects of Real-Time Reaction Monitoring Using Multi-Nuclear High Resolution FlowNMR Spectroscopy. Catal. Sci. Technol. 2016, 6 (24), 8406–8417. https://doi.org/10.1039/C6CY01754A.
(132) Ryder, A. S. H.; Cunningham, W. B.; Ballantyne, G.; Mules, T.; Kinsella, A. G.; Turner-Dore, J.; Alder, C. M.; Edwards, L. J.; McKay, B. S. J.; Grayson, M. N.; Cresswell, A. J. Photocatalytic A-Tertiary Amine Synthesis via C−H Alkylation of Unmasked Primary Amines. Angew. Chem. Int. Ed. 2020, 59 (35), 14986–14991. https://doi.org/10.1002/anie.202005294.
(133) Lynch, D.; O'Mahony, R. M.; McCarthy, D. G.; Bateman, L. M.; Collins, S. G.; Maguire, A. R. Mechanistic Study of In Situ Generation and Use of Methanesulfonyl Azide as a Diazo Transfer Reagent with Real-Time Monitoring by FlowNMR: Mechanistic Study of In Situ Generation and

Use of Methanesulfonyl Azide as a Diazo Transfer Reagent with Real-Time Monitoring by FlowNMR. Eur. J. Org. Chem. 2019, 2019 (22), 3575–3580. https://doi.org/10.1002/ejoc.201900184.

(134) Hall, A. M. R.; Broomfield-Tagg, R.; Camilleri, M.; Carbery, D. R.; Codina, A.; Whittaker, D. T. E.; Coombes, S.; Lowe, J. P.; Hintermair, U. Online Monitoring of a Photocatalytic Reaction by Real-Time High Resolution FlowNMR Spectroscopy. Chem. Commun. 2018, 54 (1), 30–33. https://doi.org/10.1039/C7CC07059D.

(135) Hall, A. M. R.; Chouler, J. C.; Codina, A.; Gierth, P. T.; Lowe, J. P.; Hintermair, U. Practical Aspects of Real-Time Reaction Monitoring Using Multi-Nuclear High Resolution FlowNMR Spectroscopy. Catal. Sci. Technol. 2016, 6 (24), 8406–8417. https://doi.org/10.1039/C6CY01754A.

(136) Pelta, M. D.; Morris, G. A.; Stchedroff, M. J.; Hammond, S. J. A One-Shot Sequence for High-Resolution Diffusion-Ordered Spectroscopy. Magn. Reson. Chem. 2002, 40 (13), S147–S152. https://doi.org/10.1002/mrc.1107.

(137) Botana, A.; Aguilar, J. A.; Nilsson, M.; Morris, G. A. J-Modulation Effects in DOSY Experiments and Their Suppression: The Oneshot45 Experiment. J. Magn. Reson. 2011, 208 (2), 270–278. https://doi.org/10.1016/j.jmr.2010.11.012.

(138) Sarkar, R.; Moskau, D.; Ferrage, F.; Vasos, P. R.; Bodenhausen, G. Single or Triple Gradients? J. Magn. Reson. 2008, 193 (1), 110–118. https://doi.org/10.1016/j.jmr.2008.04.029.

(139) Loening, N. M.; Keeler, J.; Morris, G. A. One-Dimensional DOSY. J. Magn. Reson. 2001, 153 (1), 103–112. https://doi.org/10.1006/jmre.2001.2423.

(140) Thrippleton, M. J.; Loening, N. M.; Keeler, J. A Fast Method for the Measurement of Diffusion Coefficients: One-Dimensional DOSY. Magn. Reson. Chem. 2003, 41 (6), 441–447. https://doi.org/10.1002/mrc.1195.

(141) Dumez, J.-N. Spatial Encoding and Spatial Selection Methods in High-Resolution NMR Spectroscopy. Prog. Nucl. Magn. Reson. Spectrosc. 2018, 109, 101–134. https://doi.org/10.1016/j.pnmrs.2018.08.001.

(142) Frydman, L.; Lupulescu, A.; Scherf, T. Principles and Features of Single-Scan Two-Dimensional NMR Spectroscopy. J. Am. Chem. Soc. 2003, 125 (30), 9204–9217. https://doi.org/10.1021/ja030055b.

(143) Shrot, Y.; Frydman, L. Single-Scan 2D DOSY NMR Spectroscopy. J. Magn. Reson. 2008, 195 (2), 226–231. https://doi.org/10.1016/j.jmr.2008.09.011.

(144) Mansfield, P. Spatial Mapping of the Chemical Shift in NMR. Magn. Reson. Med. 1984, 1 (3), 370–386. https://doi.org/10.1002/mrm.1910010308.

(145) Posse, S.; Otazo, R.; Dager, S. R.; Alger, J. MR Spectroscopic Imaging: Principles and Recent Advances. J. Magn. Reson. Imaging 2013, 37 (6), 1301–1325. https://doi.org/10.1002/jmri.23945.

(146) Lhoste, C.; Lorandel, B.; Praud, C.; Marchand, A.; Mishra, R.; Dey, A.; Bernard, A.; Dumez, J.-N.; Giraudeau, P. Ultrafast 2D NMR for the Analysis of Complex Mixtures. Prog. Nucl. Magn. Reson. Spectrosc. 2022, 130–131, 1–46. https://doi.org/10.1016/j.pnmrs.2022.01.002.

(147) Guduff, L.; Kurzbach, D.; van Heijenoort, C.; Abergel, D.; Dumez, J.-N. Single-Scan 13 C Diffusion-Ordered NMR Spectroscopy of DNP-Hyperpolarised Substrates. Chem. - Eur. J. 2017, 23 (66), 16722–16727. https://doi.org/10.1002/chem.201703300.

(148) Guduff, L.; Berthault, P.; van Heijenoort, C.; Dumez, J.-N.; Huber, G. Single-Scan Diffusion-Ordered NMR Spectroscopy of SABRE-Hyperpolarized Mixtures. Chemphyschem Eur. J. Chem. Phys. Phys. Chem. 2019, 20 (3), 392–398. https://doi.org/10.1002/cphc.201800983.

(149) Guduff, L.; Kuprov, I.; van Heijenoort, C.; Dumez, J.-N. Spatially Encoded 2D and 3D Diffusion-Ordered NMR Spectroscopy. Chem. Commun. 2017, 53 (4), 701–704. https://doi.org/10.1039/C6CC09028A.

(150) Hamdoun, G.; Guduff, L.; van Heijenoort, C.; Bour, C.; Gandon, V.; Dumez, J.-N. Spatially Encoded Diffusion-Ordered NMR Spectroscopy of Reaction Mixtures in Organic Solvents. The Analyst 2018, 143 (14), 3458–3464. https://doi.org/10.1039/C8AN00434J.

(151) Urbańczyk, M.; Kharbanda, Y.; Mankinen, O.; Telkki, V.-V. Accelerating Restricted Diffusion NMR Studies with Time-Resolved and Ultrafast Methods. Anal. Chem. 2020, 92 (14), 9948–9955. https://doi.org/10.1021/acs.analchem.0c01523.
(152) Gołowicz, D.; Kasprzak, P.; Orekhov, V.; Kazimierczuk, K. Fast Time-Resolved NMR with Non-Uniform Sampling. Prog. Nucl. Magn. Reson. Spectrosc. 2020, 116, 40–55. https://doi.org/10.1016/j.pnmrs.2019.09.003.
(153) Delaglio, F.; Walker, G. S.; Farley, K. A.; Sharma, R.; Hoch, J. C.; Arbogast, L. W.; Brinson, R. G.; Marino, J. P. Non-Uniform Sampling for All: More NMR Spectral Quality, Less Measurement Time. Am. Pharm. Rev. 2017, 20 (4), 339681.
(154) Hyberts, S. G.; Arthanari, H.; Robson, S. A.; Wagner, G. Perspectives in Magnetic Resonance: NMR in the Post-FFT Era. Spec. "JMR Perspect. Issue Foresights Biomol. Solut.-State NMR Spectrosc. – Spin Gymnast. Struct. Dyn. 2014, 241, 60–73. https://doi.org/10.1016/j.jmr.2013.11.014.
(155) Mobli, M.; Hoch, J. C. Nonuniform Sampling and Non-Fourier Signal Processing Methods in Multidimensional NMR. Prog. Nucl. Magn. Reson. Spectrosc. 2014, 83, 21–41. https://doi.org/10.1016/j.pnmrs.2014.09.002.
(156) Urbańczyk, M.; Kazimierczuk, K. A Method for Joint Sparse Sampling of Time and Gradient Domains in Diffusion-Ordered NMR Spectroscopy; 2013; p 6. https://doi.org/10.1109/SPS.2013.6623587.
(157) Pudakalakatti, S. M.; Chandra, K.; Thirupathi, R.; Atreya, H. S. Rapid Characterization of Molecular Diffusion by NMR Spectroscopy. Chem. - Eur. J. 2014, 20 (48), 15719–15722. https://doi.org/10.1002/chem.201404038.
(158) Urbańczyk, M.; Bernin, D.; Czuroń, A.; Kazimierczuk, K. Monitoring Polydispersity by NMR Diffusometry with Tailored Norm Regularisation and Moving-Frame Processing. The Analyst 2016, 141 (5), 1745–1752. https://doi.org/10.1039/C5AN02304A.
(159) Oikonomou, M.; Asencio-Hernández, J.; Velders, A. H.; Delsuc, M.-A. Accurate DOSY Measure for Out-of-Equilibrium Systems Using Permutated DOSY (p-DOSY). J. Magn. Reson. 2015, 258, 12–16. https://doi.org/10.1016/j.jmr.2015.06.002.
(160) MacDonald, T. S. C.; Price, W. S.; Beves, J. E. Time-Resolved Diffusion NMR Measurements for Transient Processes. ChemPhysChem 2019, 20 (7), 926–930. https://doi.org/10.1002/cphc.201900150.
(161) Castañar, L.; Poggetto, G. D.; Colbourne, A. A.; Morris, G. A.; Nilsson, M. The GNAT: A New Tool for Processing NMR Data. Magn. Reson. Chem. 2018, 56 (6), 546–558. https://doi.org/10.1002/mrc.4717.
(162) Nilsson, M. The DOSY Toolbox: A New Tool for Processing PFG NMR Diffusion Data. J. Magn. Reson. 2009, 200 (2), 296–302. https://doi.org/10.1016/j.jmr.2009.07.022.
(163) Keeler, J. J. Understanding NMR Spectroscopy, 2nd ed., repr.; Wiley: Chichester, West Sussex, 2011.
(164) Pelta, M. D.; Barjat, H.; Morris, G. A.; Davis, A. L.; Hammond, S. J. Pulse Sequences for High-Resolution Diffusion-Ordered Spectroscopy (HR-DOSY). Magn. Reson. Chem. 1998, 36 (10), 706–714. https://doi.org/10.1002/(SICI)1097-458X(199810)36:10<706::AID-OMR363>3.0.CO;2-W.
(165) Colbourne, A. A.; Morris, G. A.; Nilsson, M. Local Covariance Order Diffusion-Ordered Spectroscopy: A Powerful Tool for Mixture Analysis. J. Am. Chem. Soc. 2011, 133 (20), 7640–7643. https://doi.org/10.1021/ja2004895.
(166) Nilsson, M.; Morris, G. A. Improved DECRA Processing of DOSY Data: Correcting for Non-Uniform Field Gradients. Magn. Reson. Chem. 2007, 45 (8), 656–660. https://doi.org/10.1002/mrc.2023.
(167) Dal Poggetto, G.; Castañar, L.; Adams, R. W.; Morris, G. A.; Nilsson, M. Relaxation-Encoded NMR Experiments for Mixture Analysis: REST and Beer. Chem. Commun. 2017, 53 (54), 7461–7464. https://doi.org/10.1039/C7CC03150E.

(168) Foroozandeh, M.; Castañar, L.; Martins, L. G.; Sinnaeve, D.; Poggetto, G. D.; Tormena, C. F.; Adams, R. W.; Morris, G. A.; Nilsson, M. Ultrahigh-Resolution Diffusion-Ordered Spectroscopy. Angew. Chem. Int. Ed. 2016, 55 (50), 15579–15582. https://doi.org/10.1002/anie.201609676.
(169) Zhao, Q.; Pedersen, C. M.; Wang, J.; Liu, R.; Zhang, Y.; Yan, X.; Zhang, Z.; Hou, X.; Wang, Y. NMR Diffusion Analysis of Catalytic Conversion Mixtures from Lignocellulose Biomass Using PSYCHE-IDOSY. Green Energy Environ. 2022, S246802572200019X. https://doi.org/10.1016/j.gee.2022.02.003.
(170) Kiraly, P.; Swan, I.; Nilsson, M.; Morris, G. A. Improving Accuracy in DOSY and Diffusion Measurements Using Triaxial Field Gradients. J. Magn. Reson. 2016, 270, 24–30. https://doi.org/10.1016/j.jmr.2016.06.011.
(171) Connell, M. A.; Bowyer, P. J.; Adam Bone, P.; Davis, A. L.; Swanson, A. G.; Nilsson, M.; Morris, G. A. Improving the Accuracy of Pulsed Field Gradient NMR Diffusion Experiments: Correction for Gradient Non-Uniformity. J. Magn. Reson. 2009, 198 (1), 121–131. https://doi.org/10.1016/j.jmr.2009.01.025.
(172) Bradley, S. A.; Krishnamurthy, K.; Hu, H. Simplifying DOSY Spectra with Selective TOCSY Edited Preparation. J. Magn. Reson. 2005, 172 (1), 110–117. https://doi.org/10.1016/j.jmr.2004.10.004.
(173) Johnson, C. S. Effects of Chemical Exchange in Diffusion-Ordered 2D NMR Spectra. J. Magn. Reson. A 1993, 102 (2), 214–218. https://doi.org/10.1006/jmra.1993.1093.
(174) Sørland, G. H.; Hafskjold, B.; Herstad, O. A Stimulated-Echo Method for Diffusion Measurements in Heterogeneous Media Using Pulsed Field Gradients. J. Magn. Reson. 1997, 124 (1), 172–176. https://doi.org/10.1006/jmre.1996.1029.
(175) Bodenhausen, G.; Freeman, R.; Turner, D. L. Suppression of Artifacts in Two-Dimensional J Spectroscopy. J. Magn. Reson. 1969 1977, 27 (3), 511–514. https://doi.org/10.1016/0022-2364(77)90016-6.
(176) Cotts, R. M.; Hoch, M. J. R.; Sun, T.; Markert, J. T. Pulsed Field Gradient Stimulated Echo Methods for Improved NMR Diffusion Measurements in Heterogeneous Systems. J. Magn. Reson. 1969 1989, 83 (2), 252–266. https://doi.org/10.1016/0022-2364(89)90189-3.
(177) Ferrage, F.; Zoonens, M.; Warschawski, D. E.; Popot, J.-L.; Bodenhausen, G. Slow Diffusion of Macromolecular Assemblies by a New Pulsed Field Gradient NMR Method. J. Am. Chem. Soc. 2003, 125 (9), 2541–2545. https://doi.org/10.1021/ja0211407.
(178) Mishra, R.; Marchand, A.; Jacquemmoz, C.; Dumez, J.-N. Ultrafast Diffusion-Based Unmixing of 1H NMR Spectra. Chem Commun 2021, 57 (19), 2384–2387. https://doi.org/10.1039/D0CC07757G.
(179) Windig, W.; Antalek, B. Direct Exponential Curve Resolution Algorithm (DECRA): A Novel Application of the Generalized Rank Annihilation Method for a Single Spectral Mixture Data Set with Exponentially Decaying Contribution Profiles. Chemom. Intell. Lab. Syst. 1997, 37 (2), 241–254. https://doi.org/10.1016/S0169-7439(97)00028-2.
(180) Pagès, G.; Gilard, V.; Martino, R.; Malet-Martino, M. Pulsed-Field Gradient Nuclear Magnetic Resonance Measurements (PFG NMR) for Diffusion Ordered Spectroscopy (DOSY) Mapping. The Analyst 2017, 142 (20), 3771–3796. https://doi.org/10.1039/C7AN01031A.
(181) Specht, A.; Ziarelli, F.; Bernard, P.; Goeldner, M.; Peng, L. Para-Sulfonated Calixarenes Used as Synthetic Receptors for Complexing Photolabile Cholinergic Ligand. Helv. Chim. Acta 2005, 88 (10), 2641–2653. https://doi.org/10.1002/hlca.200590205.
(182) Pagès, G.; Bonny, A.; Gilard, V.; Malet-Martino, M. Pulsed Field Gradient NMR with Sigmoid Shape Gradient Sampling To Produce More Detailed Diffusion Ordered Spectroscopy Maps of Real Complex Mixtures: Examples with Medicine Analysis. Anal. Chem. 2016, 88 (6), 3304–3309. https://doi.org/10.1021/acs.analchem.5b04781.
(183) Nilsson, M.; Morris, G. A. Speedy Component Resolution: An Improved Tool for Processing Diffusion-Ordered Spectroscopy Data. Anal. Chem. 2008, 80 (10), 3777–3782. https://doi.org/10.1021/ac7025833.

(184) Stilbs, P.; Paulsen, K.; Griffiths, P. C. Global Least-Squares Analysis of Large, Correlated Spectral Data Sets: Application to Component-Resolved FT-PGSE NMR Spectroscopy. J. Phys. Chem. 1996, 100 (20), 8180–8189. https://doi.org/10.1021/jp9535607.
(185) Stilbs, P. Automated CORE, RECORD, and GRECORD Processing of Multi-Component PGSE NMR Diffusometry Data. Eur. Biophys. J. 2013, 42 (1), 25–32. https://doi.org/10.1007/s00249-012-0794-8.
(186) Stilbs, P.; Paulsen, K. Global Least-squares Analysis of Large, Correlated Spectral Data Sets and Application to Chemical Kinetics and Time-resolved Fluorescence. Rev. Sci. Instrum. 1996, 67 (12), 4380–4386. https://doi.org/10.1063/1.1147539.
(187) Jacquemmoz, C.; Giraud, F.; Dumez, J.-N. Online Reaction Monitoring by Single-Scan 2D NMR under Flow Conditions. The Analyst 2020, 145 (2), 478–485. https://doi.org/10.1039/C9AN01758E.
(188) Hall, A. A Combined Spectroscopic and Theoretical Approach to the Development of Homogeneous Catalysts for Hydrogen Transfer Chemistry, Bath, university.
(189) Bouillaud, D.; Drouin, D.; Charrier, B.; Jacquemmoz, C.; Farjon, J.; Giraudeau, P.; Gonçalves, O. Using Benchtop NMR Spectroscopy as an Online Non-Invasive in Vivo Lipid Sensor for Microalgae Cultivated in Photobioreactors. Process Biochem. 2020, 93, 63–68. https://doi.org/10.1016/j.procbio.2020.03.016.
(190) Britton, J.; Majumdar, S.; Weiss, G. A. Continuous Flow Biocatalysis. Chem. Soc. Rev. 2018, 47 (15), 5891–5918. https://doi.org/10.1039/C7CS00906B.
(191) Sugisawa, N.-N., HiroyukiAU-Fuse, ShinichiroTI. Recent Advances in Continuous-Flow Reactions Using Metal-Free Homogeneous Catalysts. Catalysts 2020, 10 (11). https://doi.org/10.3390/catal10111321.
(192) Price, W. S. NMR Studies of Translational Motion: Principles and Applications, 1. publ.; Cambridge molecular science; Cambridge University Press: Cambridge, 2009.
(193) Thomlinson, I. A.; Davidson, M. G.; Lyall, C. L.; Lowe, J. P.; Hintermair, U. Fast and Accurate Diffusion NMR Acquisition in Continuous Flow. Chem. Commun. 2022, 58 (59), 8242–8245. https://doi.org/10.1039/D2CC03054C.
(194) Gold, V.; Grist, S. Deuterium Solvent Isotope Effects on Reactions Involving the Aqueous Hydroxide Ion. J. Chem. Soc. Perkin Trans. 2 1972, No. 1, 89. https://doi.org/10.1039/p29720000089.
(195) Shiner, V. J.; Rapp, M. W.; Pinnick, H. R. ..Alpha.-Deuterium Effects in SN2 Reactions with Solvent. J. Am. Chem. Soc. 1970, 92 (1), 232–233. https://doi.org/10.1021/ja00704a056.
(196) Hoult, D. I. Solvent Peak Saturation with Single Phase and Quadrature Fourier Transformation. J. Magn. Reson. 1969 1976, 21 (2), 337–347. https://doi.org/10.1016/0022-2364(76)90081-0.
(197) Hwang, T. L.; Shaka, A. J. Water Suppression That Works. Excitation Sculpting Using Arbitrary Wave-Forms and Pulsed-Field Gradients. J. Magn. Reson. A 1995, 112 (2), 275–279. https://doi.org/10.1006/jmra.1995.1047.
(198) Ogg, R. J.; Kingsley, R. B.; Taylor, J. S. WET, a T1- and B1-Insensitive Water-Suppression Method for in Vivo Localized 1H NMR Spectroscopy. J. Magn. Reson. B 1994, 104 (1), 1–10. https://doi.org/10.1006/jmrb.1994.1048.
(199) Höpfner, J.; Mayerhöfer, B.; Botha, C.; Bouillaud, D.; Farjon, J.; Giraudeau, P.; Wilhelm, M. Solvent Suppression Techniques for Coupling of Size Exclusion Chromatography and 1H NMR Using Benchtop Spectrometers at 43 and 62 MHz. J. Magn. Reson. 2021, 323, 106889. https://doi.org/10.1016/j.jmr.2020.106889.
(200) Canton, M.; Roe, R.; Poigny, S.; Renault, J.-H.; Nuzillard, J.-M. Multiple Solvent Signal Presaturation and Decoupling Artifact Removal in 13C{1H} Nuclear Magnetic Resonance. Magn. Reson. 2020, 1 (2), 155–164. https://doi.org/10.5194/mr-1-155-2020.
(201) Mo, H.; Raftery, D. Pre-SAT180, a Simple and Effective Method for Residual Water Suppression. J. Magn. Reson. 2008, 190 (1), 1–6. https://doi.org/10.1016/j.jmr.2007.09.016.

(202) Kew, W.; Bell, N. G. A.; Goodall, I.; Uhrín, D. Advanced Solvent Signal Suppression for the Acquisition of 1D and 2D NMR Spectra of Scotch Whisky. Magn. Reson. Chem. 2017, 55 (9), 785–796. https://doi.org/10.1002/mrc.4621.
(203) Balayssac, S.; Delsuc, M.-A.; Gilard, V.; Prigent, Y.; Malet-Martino, M. Two-Dimensional DOSY Experiment with Excitation Sculpting Water Suppression for the Analysis of Natural and Biological Media. J. Magn. Reson. 2009, 196 (1), 78–83. https://doi.org/10.1016/j.jmr.2008.09.022.
(204) Gouilleux, B.; Charrier, B.; Akoka, S.; Giraudeau, P. Gradient-Based Solvent Suppression Methods on a Benchtop Spectrometer: Gradient-Based Solvent Suppression Methods on a Benchtop Spectrometer. Magn. Reson. Chem. 2017, 55 (2), 91–98. https://doi.org/10.1002/mrc.4493.
(205) Bobzin, S. C.; Yang, S.; Kasten, T. P. LC-NMR: A New Tool to Expedite the Dereplication and Identification of Natural Products. J. Ind. Microbiol. Biotechnol. 2000, 25 (6), 342–345. https://doi.org/10.1038/sj.jim.7000057.
(206) Wolfender, J.-L.; Terreaux, C.; Hostettmann, K. The Importance Of LC-MS And LC-NMR In The Discovery Of New Lead Compounds From Plants. Pharm. Biol. 2000, 38 (sup1), 41–54. https://doi.org/10.1076/phbi.38.6.41.5957.
(207) Bro, R. PARAFAC. Tutorial and Applications. Chemom. Intell. Lab. Syst. 1997, 38 (2), 149–171. https://doi.org/10.1016/S0169-7439(97)00032-4.
(208) Leeson, P. D.; Young, R. J. Molecular Property Design: Does Everyone Get It? ACS Med. Chem. Lett. 2015, 6 (7), 722–725. https://doi.org/10.1021/acsmedchemlett.5b00157.
(209) Abu-Dief, A. M.; Mohamed, I. M. A. A Review on Versatile Applications of Transition Metal Complexes Incorporating Schiff Bases. Beni-Suef Univ. J. Basic Appl. Sci. 2015, 4 (2), 119–133. https://doi.org/10.1016/j.bjbas.2015.05.004.
(210) García-Valle, F. M.; Tabernero, V.; Cuenca, T.; Mosquera, M. E. G.; Cano, J. Intramolecular C–F Activation in Schiff-Base Alkali Metal Complexes. Organometallics 2019, 38 (4), 894–904. https://doi.org/10.1021/acs.organomet.8b00868.
(211) Iacopetta, D.; Ceramella, J.; Catalano, A.; Saturnino, C.; Bonomo, M. G.; Franchini, C.; Sinicropi, M. S. Schiff Bases: Interesting Scaffolds with Promising Antitumoral Properties. Appl. Sci. 2021, 11 (4), 1877. https://doi.org/10.3390/app11041877.
(212) Gomez, M. V.; de la Hoz, A. NMR Reaction Monitoring in Flow Synthesis. Beilstein J. Org. Chem. 2017, 13, 285–300. https://doi.org/10.3762/bjoc.13.31.
(213) Srimani, D.; Feller, M.; Ben-David, Y.; Milstein, D. Catalytic Coupling of Nitriles with Amines to Selectively Form Imines under Mild Hydrogen Pressure. Chem. Commun. 2012, 48 (97), 11853. https://doi.org/10.1039/c2cc36639h.
(214) DeLeo, V. A. P-Phenylenediamine. Dermatitis® 2006, 17 (2). https://doi.org/10.2310/6620.2006.05054.
(215) Marchand, A.; Mishra, R.; Bernard, A.; Dumez, J. Online Reaction Monitoring with Fast and Flow-Compatible Diffusion NMR Spectroscopy. Chem. – Eur. J. 2022, 28 (52). https://doi.org/10.1002/chem.202201175.
(216) Cortés-Borda, D.; Wimmer, E.; Gouilleux, B.; Barré, E.; Oger, N.; Goulamaly, L.; Peault, L.; Charrier, B.; Truchet, C.; Giraudeau, P.; Rodriguez-Zubiri, M.; Le Grognec, E.; Felpin, F.-X. An Autonomous Self-Optimizing Flow Reactor for the Synthesis of Natural Product Carpanone. J. Org. Chem. 2018, 83 (23), 14286–14299. https://doi.org/10.1021/acs.joc.8b01821.
(217) Boudart, M. Model Catalysts: Reductionism for Understanding. Top. Catal. 2000, 13 (1), 147. https://doi.org/10.1023/A:1009080821550.
(218) Harshman. FOUNDATIONS OF THE PARAFAC PROCEDURE: MODELS AND CONDITIONS FOR AN "EXPLANATORY" MULTIMODAL FACTOR ANALYSIS. Harshman, R.. UCLA Working Papers in Phonetics. Volume: 16 (1970) ISSN: 1067-9030.

Appendix

A-1 DOSY plot

The figure is labelled function of where its spectra are used. Such as S7-5 is linked to figure 7-5.

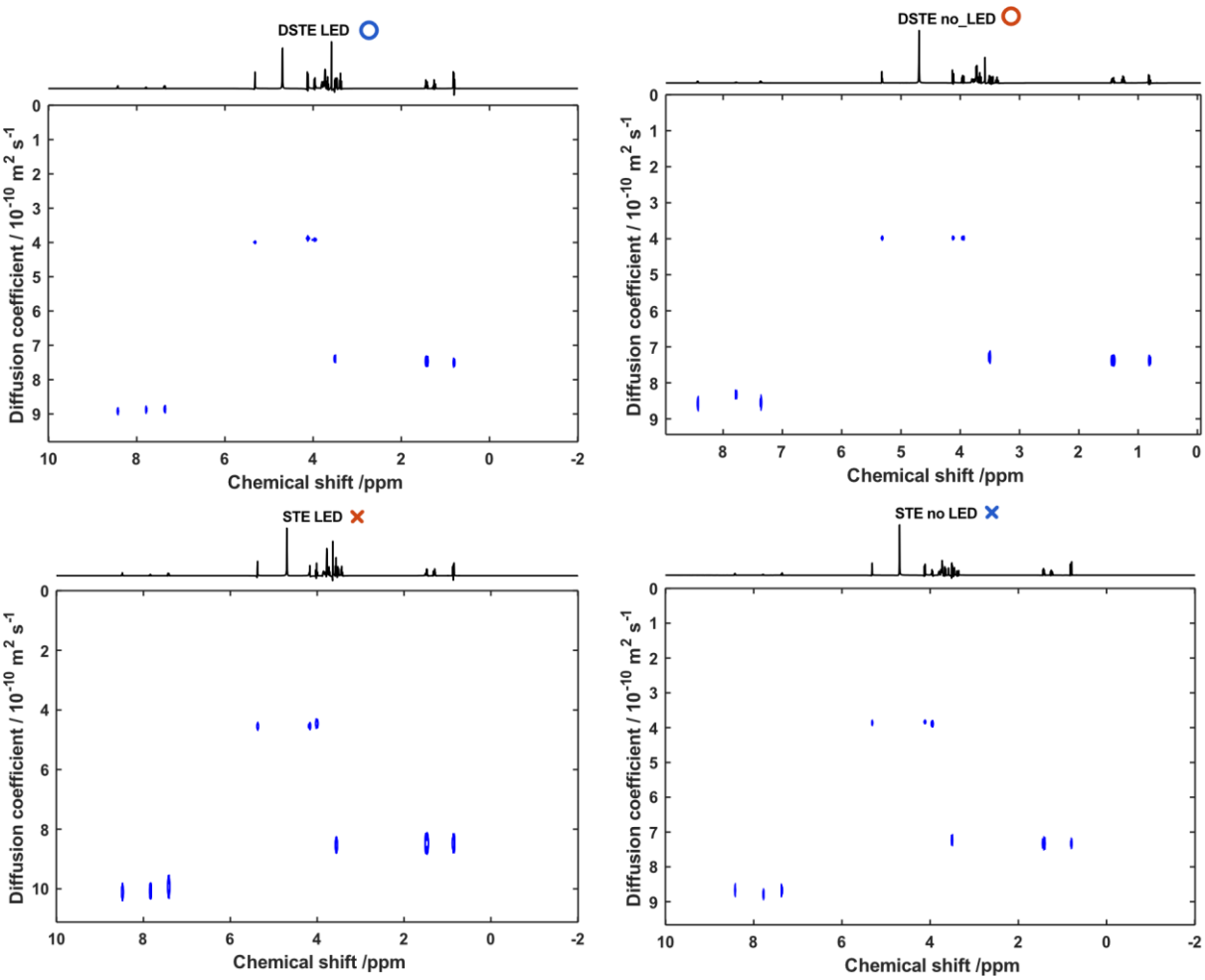

Figure S4.7 Corresponding DOSY spectra.

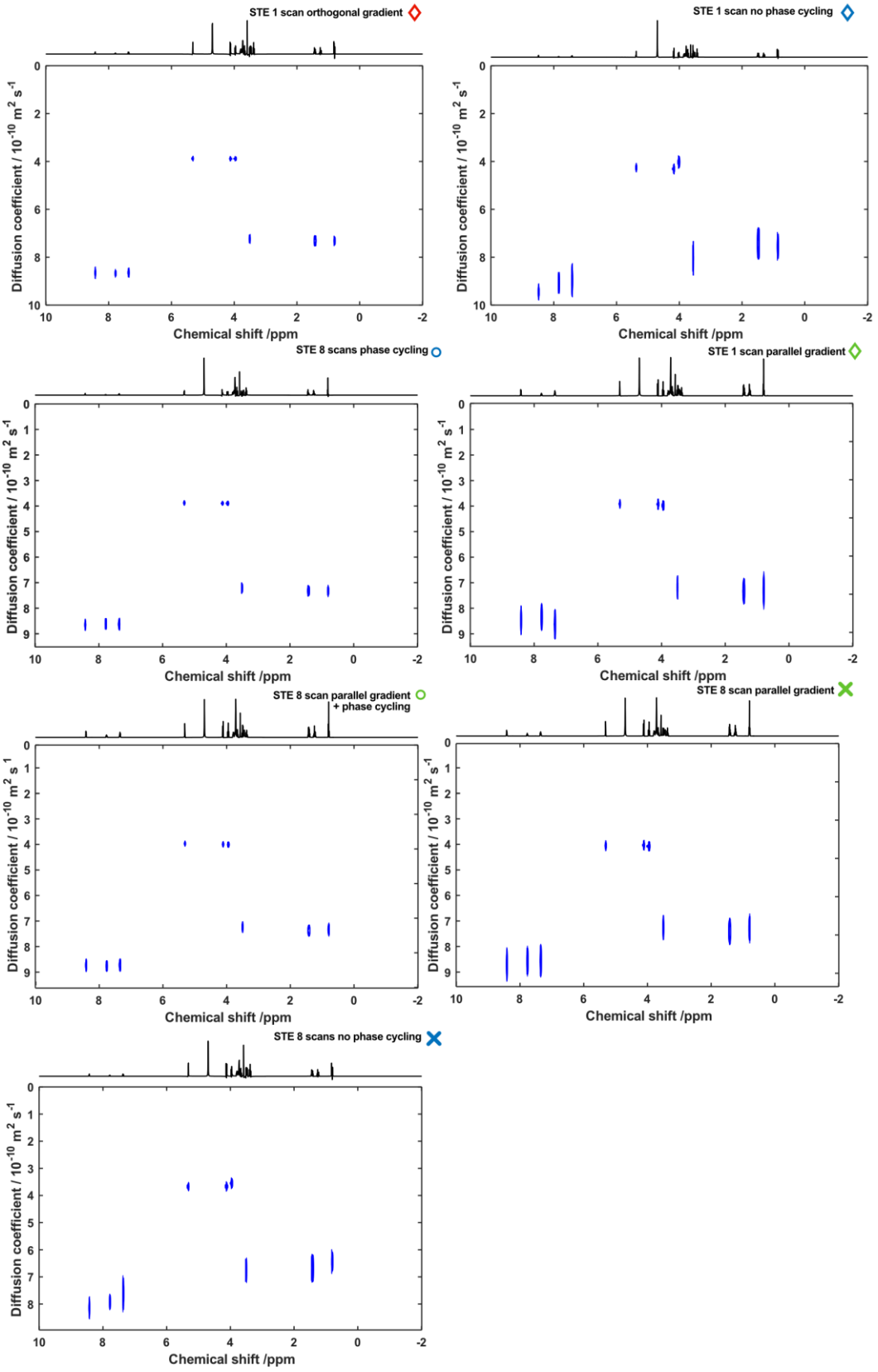
STE 1 scan orthogonal gradient
STE 1 scan no phase cycling
STE 8 scans phase cycling
STE 1 scan parallel gradient
STE 8 scan parallel gradient + phase cycling
STE 8 scan parallel gradient
STE 8 scans no phase cycling
Diffusion coefficient / 10^-10 m^2 s^-1
Chemical shift /ppm

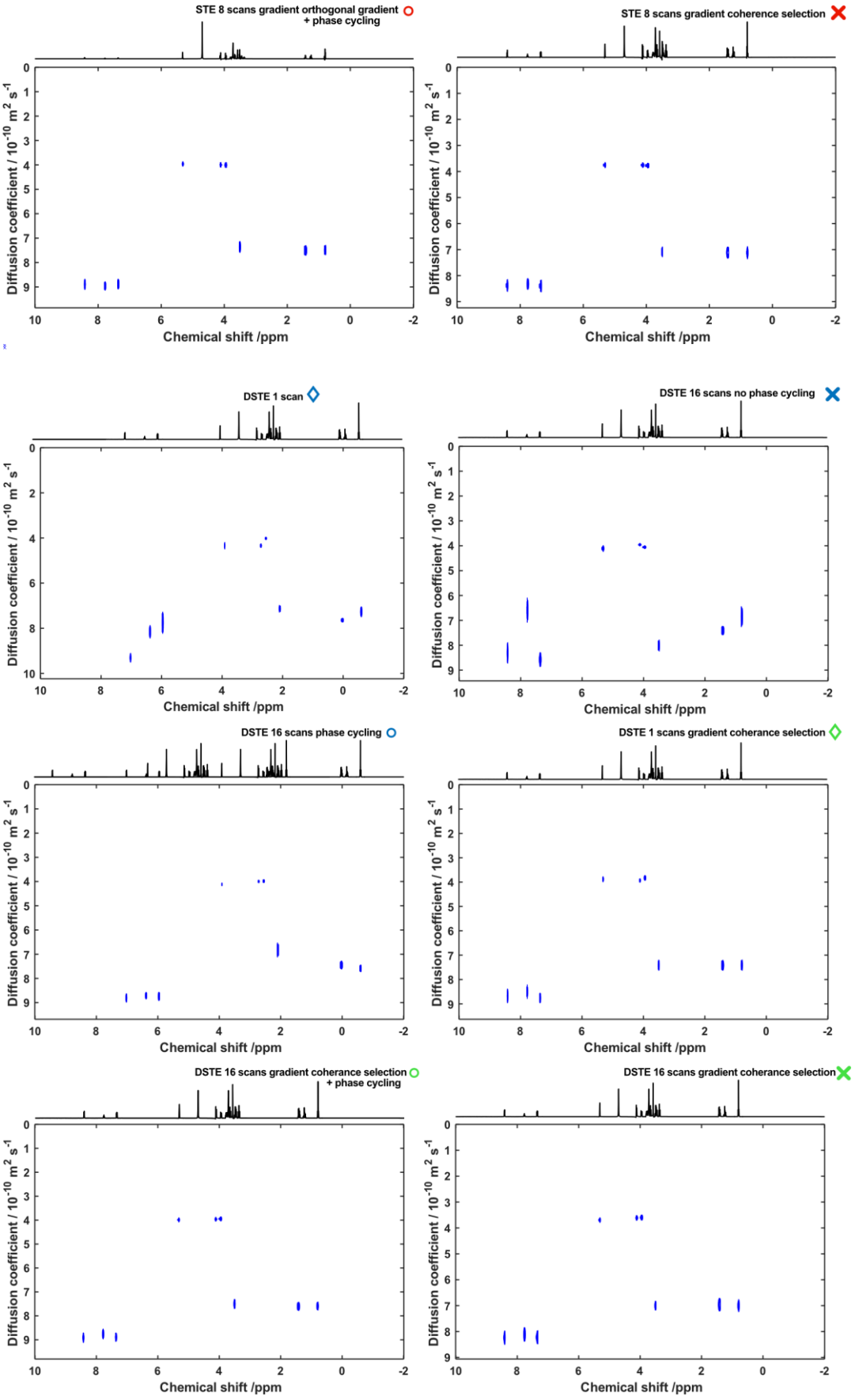

Figure S6-4 DOSY spectra with their matching symbols in the figure.

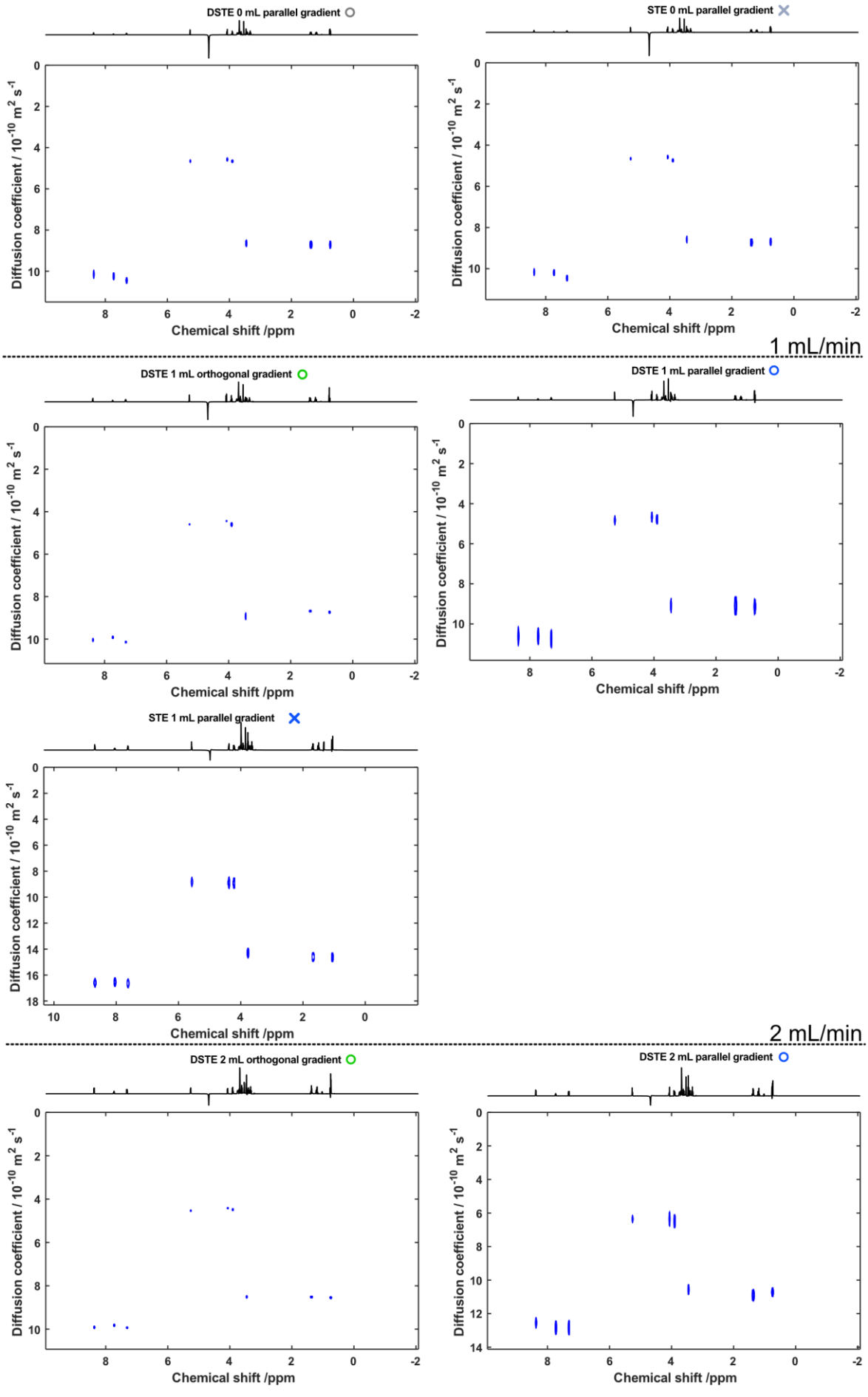
DSTE 0 mL parallel gradient
STE 0 mL parallel gradient
Diffusion coefficient / 10^-10 m^2 s^-1
Chemical shift /ppm
1 mL/min
DSTE 1 mL orthogonal gradient
DSTE 1 mL parallel gradient
STE 1 mL parallel gradient
2 mL/min
DSTE 2 mL orthogonal gradient
DSTE 2 mL parallel gradient

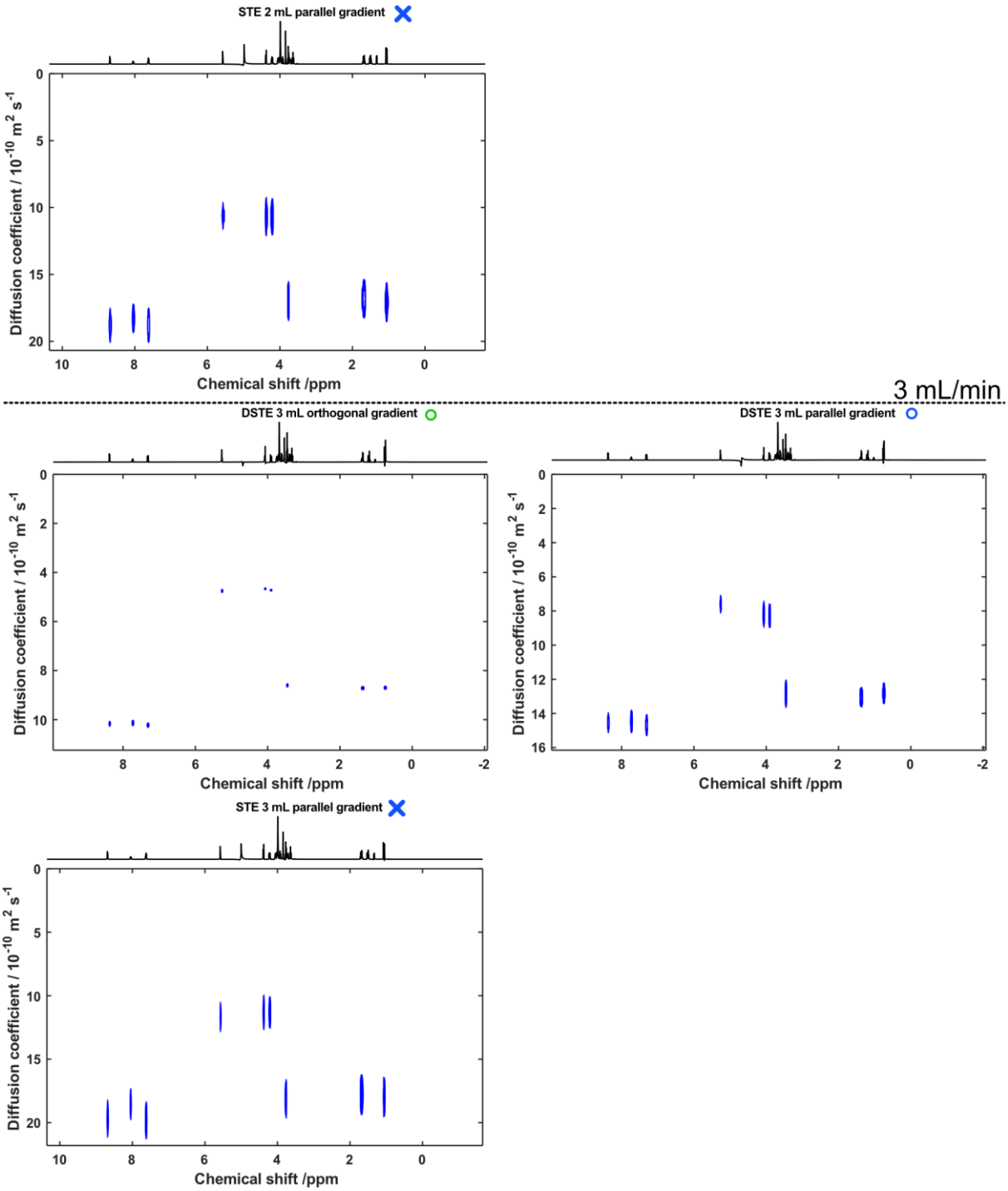

Figure S7-5, DOSY plot that are used to make figure 7.5.

Sequence

"AMstebposgc_grad_phycy_v2"

;by achille Marchand CEISAM nantes 29/04/21 under direction by J.-N. Dumez

;STE diffusion with CTP gradient in non-diffusion axis (simultaneous)

```
;reasonnable doubt for l2 is it working

#include <Avance.incl>

#include <Grad.incl>

#include <Delay.incl>



define list<gradient> diff=<Difframp>



"p2=p1*2"

"d24=0*abs(cnst1)*abs(cnst11)"

"GPX8=abs(cnst1*0.01)"

"d25=0u*abs(cnst2)*abs(cnst13)"

"GPY9=abs(cnst2*0.01)"

"d26=1u*abs(cnst3)"

"d27=1u*abs(l2)"

"d31=d30*2"

"DELTA1=d20-d30-10u-d16-p2-d30-10u-d16-p1-p19-d31-10u-d16-p1"

"p21=2*p20"



1 ze

2 d1
```

```
 50u UNBLKGRAD


 p19:gp7*-1
        d16
        d31 grad{ sin(cnst1*-1,l2) | sin(cnst2*-1,l2) | sin(0,l2)}
        10u groff
        d16


; excitation
 p1 ph1
; diffusion encoding with xy ctp gradients
        d30 grad{ sin(cnst1,l2) | sin(cnst2,l2) | sin(cnst3,l2)*diff}
        10u groff
        d16
 p2 ph2
        d30 grad{ sin(cnst1,l2)| sin(cnst2,l2) | sin(cnst3*-1,l2)*diff}
 10u groff
        d16


; storage
```

```
  p1 ph3
  p19:gp7
  DELTA1
        d31 grad{ sin(cnst11*-1,l2) | sin(cnst13*-1,l2) | sin(0,l2)}
        10u groff
        d16
; excitation
  p1 ph4

; diffusion decoding with xy ctp gradients
        d30 grad{ sin(cnst11,l2) | sin(cnst13,l2) | sin(cnst3,l2)*diff}
        10u groff
  d16
  p2 ph2
  d30 grad{sin(cnst11,l2)| sin(cnst13,l2) | sin(cnst3*-1,l2)*diff }
        10u groff
  d16

; acquisition
  4u BLKGRAD
```

```
 go=2 ph31
 d1 mc #0 to 2 F1QF(calgrad (diff))
 d24*0
        d25*0
        d26*0
        d27*0
        exit


ph1= 0
ph2= 0 0 0 0  2 2 2 2
ph3= 0 0 0 0  0 0 0 0  2 2 2 2  2 2 2 2
ph4= 0 1 2 3
ph31=0 3 2 1  0 3 2 1  2 1 0 3  2 1 0 3


;p1 : f1 channel -  90 degree high power pulse
;p2 : f1 channel - 180 degree high power pulse
;p19: gradient pulse 2 (spoil gradient)
;d31: gradient pulse (little DELTA * 0.5)
;d1 : relaxation delay; 1-5 * T1
;d16: delay for gradient recovery 200u
```

;d20: diffusion time (big DELTA)

;cnst1 value of x gradient constant

;cnst11 value X grad 2nd

;cnst13 value y grad 2nd

;cnst2 value of ygradient constant

;cnst3 value of z gradient incremented by diff 100

;cnst11 for 2nd 180 value of x gradient constant

;l2 number of point for sin grad

;NS : 8 * n

;DS : 4 * m

;td1: number of experiments

;FnMODE: QF

; use xf2 and DOSY processing

;use gradient ratio: gp 6* : gp 7

; 100 : -17.13

;*not included anymore

;for z-only gradients:

;gpz7: -17.13% (spoil)

;use gradient files:

;gpnam6: SINE.100

;gpnam7: SINE.100

;use AU-program dosy to calculate gradient-file Difframp

"AMdsteosgc_gradZ_phycy"

;avance-version (08/01/16)

;2D sequence for diffusion measurement using double stimulated

; echo for convection compensation and LED

;using bipolar gradient pulses for diffusion

;using 3 spoil gradients

;A. Jerschow & N. Mueller, J. Magn. Reson. A 123, 222-225 (1996)

;A. Jerschow & N. Mueller, J. Magn. Reson. A 125, 372-375 (1997)

;$CLASS=HighRes

;$DIM=2D

;$TYPE=

```
;$SUBTYPE=

;$COMMENT=




#include <Avance.incl>

#include <Grad.incl>

#include <Delay.incl>


define list<gradient> diff=<Difframp>


"d24=0u*abs(cnst1)*abs(cnst11)*abs(cnst12)*abs(l2)*abs(cnst13)*abs(cnst14)"

"d12=20u"

"d13=4u"

"d17=2m"

"d31=2*d30"

"p2=p1*2"

"d3=p2"

"p7=2*p6"

"DELTA1=d20*0.5-d30-10u-d16-p2-d30-10u-d16-p1-p19-d16-d31-10u-d16-p19-d16-p1"

"DELTA3=d21-p19-d16-4u" ;led
```

;"WETWAIT=10m-d16"

"acqt0=-p1*2/3.1416"

1 ze

2 30m

d1

50u UNBLKGRAD

d12 pl0:f1

d13

(p11:sp7 ph15):f1

4u

p16:gp21

d17 pl0:f1

(p11:sp8 ph16):f1

4u

p16:gp22

```
 d17 pl0:f1
 (p11:sp9 ph16):f1
4u
p16:gp23

 d17 pl0:f1
 (p11:sp10 ph16):f1
 4u
 p16:gp24
        d16


; compensation grad
        p19:gp7*-1
        d16
        d31 grad{ sin(1*-1,l2) | sin(cnst2*-1,l2) | sin(0,l2)}
        10u groff
 d16 pl1:f1
; excitation
 p1 ph1
```

```
  d30 grad{ sin(cnst1,l2) | sin(cnst2,l2) | sin(cnst3,l2)*diff}
          10u groff
  d16
  p2 ph2
  d30 grad{ sin(cnst1,l2) | sin(cnst2,l2) | sin(cnst3*-1,l2)*diff}
          10u groff
  d16
;storage
  p1 ph3
  p19:gp7
  d16
  DELTA1
  d31 grad{ sin(cnst16*-1,l2) | sin(cnst13*-1,l2) | sin(0,l2)}
          10u groff
  d16
  p19:gp8*-1
  d16
;transplannation
  p1 ph4
  d30 grad{ sin(0,l2) | sin(0,l2) | sin(cnst3,l2)*diff}
```

```
        10u groff
d16
d30 grad{ sin(cnst16,l2) | sin(cnst13,l2) | sin(cnst3,l2)*diff}
        10u groff
d16
p2 ph5
d30 grad{ sin(cnst16,l2) | sin(cnst13,l2) | sin(cnst3*-1,l2)*diff}
        10u groff
d16
d30 grad{ sin(0,l2) | sin(0,l2) | sin(cnst3*-1,l2)*diff}
        10u groff
d16
        d3 ;symmetrization
p1 ph6


p19:gp8
d16
DELTA1
p19:gp9*0
d16
```

```
        d31 grad{ sin(17*-1,l2) | sin(cnst14*-1,l2) | sin(0,l2)}
        10u groff
d16


p1 ph3
d30 grad{ sin(cnst17,l2) | sin(cnst14,l2) | sin(cnst3,l2)*diff}
        10u groff
d16
p2 ph8
d30 grad{ sin(cnst17,l2) | sin(cnst14,l2) | sin(cnst3*-1,l2)*diff}
        10u groff
d16


4u BLKGRAD
go=2 ph31
30m mc #0 to 2 F1QF(calgrad(diff))
d24*0
exit
```

ph1= 0 0 1 1 2 2 3 3

ph2= 1 2 2 3 3 0 0 1

ph3= 0

ph4= 2 2 3 3

ph5= 3 3 0 0 3 3 0 0 0 0 1 1 0 0 1 1

ph6= 2

ph8= 0 0 0 0 0 0 0 0 0 0 0 0 0 0 0 0

2 2 2 2 2 2 2 2 2 2 2 2 2 2 2 2

ph31=0 2 0 2 2 0 2 0 2 0 2 0 0 2 0 2

ph15= 0

ph16= 1

;pl1 : f1 channel - power level for pulse (default)

;cnst1 ctp grad x

;cnst2 ctp grad y

;cnst3 diff grad 100

;cnst11 ctp grad x 2ng 180

;cnst12 ctp grad x 3th 180

;cnst13 ctp grad y 2th 180

;cnst14 ctp grad y 3th 180

;l2 number point ctp and diff grad

;p1 : f1 channel - high power pulse

;p2 : f1 channel - 180 degree high power pulse

;p19: gradient pulse 2 (spoil gradient)

;d30: gradient pulse (little DELTA * 0.5)

;d1 : relaxation delay; 1-5 * T1

;d16: delay for gradient recovery

;d20: diffusion time (big DELTA)

;d21: eddy current delay (Te) [5 ms]

;NS: 16 * n

;DS: 4 * m

;td1: number of experiments

;FnMODE: QF

; use xf2 and DOSY processing

;use gradient ratio: gp 6 : gp 7 : gp 8 : gp 9

; 100 : -13.17 : -17.13 : -15.37

```
;for z-only gradients:

;gpz6: 100%

;gpz7: -13.17% (spoil)

;gpz8: -17.13% (spoil)

;gpz9: -15.37% (spoil)



;use gradient files:

;gpnam6: SINE.100

;gpnam7: SINE.100

;gpnam8: SINE.100

;gpnam9: SINE.100



;use AU-program dosy to calculate gradient ramp-file Difframp



;the gradients serve the following purpose:

;   d30

;   d30             first STE dephase bipolar pulse pair

;   p19             spoiler

;   d30
```

; d30 first STE rephase bipolar pulse pair

; d30 and second STE dephase bipolar pulse pair

; d30

; p19 spoiler

; d30

; d30 second STE rephase bipolar pulse pair

; p19 LED with spoiler

“AMwetstebposgc_gradX_ phycy _v2”

;by achille Marchand CEISAM nantes 29/04/21 under direction by J.-N. Dumez

;STE diffusion with CTP gradient in non-diffusion axis (simultaneous)

;reasonnable doubt for l2 is it working

#include <Avance.incl>

#include <Grad.incl>

#include <Delay.incl>

define list<gradient> diff=<Difframp>

"d12=20u"

"d13=4u"

"d17=2m"

"p2=p1*2"

"d24=0*abs(cnst1)*abs(cnst11)"

"d25=0u*abs(cnst2)*abs(cnst13)"

"GPY9=abs(cnst2*0.01)"

"d26=1u*abs(cnst3)"

```
"d27=1u*abs(l2)"
"d31=d30*2"
"DELTA1=d20-d30-10u-d16-p2-d30-10u-d16-p1-p19-d31-10u-d16-p1"
"p21=2*p20"

1 ze
2 30m
        d1
 50u UNBLKGRAD

 d12 pl0:f1
 d13
 (p11:sp7 ph15):f1
 4u
 p16:gp21

d17 pl0:f1
(p11:sp8 ph16):f1
4u
p16:gp22

 d17 pl0:f1
 (p11:sp9 ph16):f1
4u
p16:gp23

 d17 pl0:f1
 (p11:sp10 ph16):f1
 4u
 p16:gp24
        d16 pl1:f1
```

```
  p19:gp7*-1
        d16
        d31 grad{ sin(cnst1*-1,l2) | sin(cnst2*-1,l2) | sin(0,l2)}
        10u groff
        d16

; excitation
  p1 ph1
; diffusion encoding with xy ctp gradients
        d30 grad{ sin(cnst1,l2) | sin(cnst2,l2) | sin(cnst3,l2)*diff}
        10u groff
        d16
  p2 ph2
        d30 grad{ sin(cnst1,l2)| sin(cnst2,l2) | sin(cnst3*-1,l2)*diff}
  10u groff
        d16

; storage
  p1 ph3
  p19:gp7
  DELTA1
        d31 grad{ sin(cnst11*-1,l2) | sin(cnst13*-1,l2) | sin(0,l2)}
        10u groff
        d16
; excitation
  p1 ph4

; diffusion decoding with xy ctp gradients
        d30 grad{ sin(cnst11,l2) | sin(cnst13,l2) | sin(cnst3,l2)*diff}
        10u groff
```

```
  d16
  p2 ph2
  d30 grad{sin(cnst11,l2)| sin(cnst13,l2) | sin(cnst3*-1,l2)*diff }
          10u groff
  d16

; acquisition
  4u BLKGRAD
  go=2 ph31
  30m mc #0 to 2 F1QF(calgrad (diff))
  d24*0
          d25*0
          d26*0
          d27*0
          exit

ph1= 0
ph2= 0 0 0 0  2 2 2 2
ph3= 0 0 0 0  0 0 0 0  2 2 2 2  2 2 2 2
ph4= 0 1 2 3
ph15= 0
ph16= 1
ph31=0 3 2 1  0 3 2 1  2 1 0 3  2 1 0 3

;p1 : f1 channel -  90 degree high power pulse
;p2 : f1 channel - 180 degree high power pulse
;p19: gradient pulse 2 (spoil gradient)
;d31: gradient pulse (little DELTA * 0.5)
;d1 : relaxation delay; 1-5 * T1
;d16: delay for gradient recovery 200u
;d20: diffusion time (big DELTA)
```

;cnst1 value of x gradient constant

;cnst11 value X grad 2nd

;cnst13 value y grad 2nd

;cnst2 value of ygradient constant

;cnst3 value of z gradient incremented by diff 100

;cnst11 for 2nd 180 value of x gradient constant

;l2 number of point for sin grad

;NS : 8 * n

;DS : 4 * m

;td1: number of experiments

;FnMODE: QF

; use xf2 and DOSY processing

;use gradient ratio: gp 6* : gp 7

; 100 : -17.13

;*not included anymore

;for z-only gradients:

;gpz7: -17.13% (spoil)

;use gradient files:

;gpnam6: SINE.100

;gpnam7: SINE.100

;use AU-program dosy to calculate gradient-file Difframp

"AMwetdsteosgc_gradX_phycy"

;avance-version (08/01/16)

;2D sequence for diffusion measurement using double stimulated

```
;   echo for convection compensation and LED

;using bipolar gradient pulses for diffusion

;using 3 spoil gradients



;A. Jerschow & N. Mueller, J. Magn. Reson. A 123, 222-225 (1996)

;A. Jerschow & N. Mueller, J. Magn. Reson. A 125, 372-375 (1997)

;

;$CLASS=HighRes

;$DIM=2D

;$TYPE=

;$SUBTYPE=

;$COMMENT=



#include <Avance.incl>

#include <Grad.incl>

#include <Delay.incl>



define list<gradient> diff=<Difframp>

"d16=20u"
```

"d24=0u*abs(cnst1)*abs(cnst11)*abs(cnst12)*abs(l2)*abs(cnst13)*abs(cnst14)*abs(cnst2)*abs(cnst3)*abs(cnst15)*abs(cnst16)"

"d12=20u"

"d13=4u"

"d17=2m"

"d31=2*d30"

"p2=p1*2"

"d3=p2"

"p7=2*p6"

"DELTA1=d20*0.5-d30-10u-d16-p2-d30-10u-d16-p1-p19-d16-d31-10u-d16-p19-d16-p1"

"DELTA3=d21-p19-d16-4u" ;led

;"WETWAIT=10m-d16"

"acqt0=-p1*2/3.1416"

1 ze

2 30m

d1

50u UNBLKGRAD

d12 pl0:f1

d13

(p11:sp7 ph15):f1

4u

p16:gp21

d17 pl0:f1

(p11:sp8 ph16):f1

4u

p16:gp22

d17 pl0:f1

(p11:sp9 ph16):f1

4u

p16:gp23

d17 pl0:f1

(p11:sp10 ph16):f1

4u

```
  p16:gp24
          d16



; compensation grad
          p19:gp7*-1
          d16
          d31 grad{  sin(0,l2) | sin(cnst2*-1,l2) | sin(cnst3*-1,l2)}
          10u groff
  d16 pl1:f1
; excitation
  p1 ph1
  d30 grad{ sin(cnst1,l2)*diff| sin(cnst2,l2) | sin(cnst3,l2)}
          10u groff
  d16
  p2 ph2
  d30 grad{ sin(cnst1*-1,l2)*diff | sin(cnst2,l2) | sin(cnst3,l2)}
          10u groff
  d16
;storage
```

```
  p1 ph3
  p19:gp7
  d16
  DELTA1
  d31 grad{ sin(0,l2) | sin(cnst13*-1,l2) | sin(cnst15*-1,l2)}
          10u groff
  d16
  p19:gp8*-1
  d16
;transplannation
  p1 ph4
  d30 grad{ sin(cnst1,l2)*diff | sin(0,l2) | sin(0,l2)}
          10u groff
  d16
  d30 grad{ sin(cnst1,l2)*diff | sin(cnst13,l2) | sin(cnst15,l2)}
          10u groff
  d16
  p2 ph5
  d30 grad{ sin(cnst1*-1,l2)*diff | sin(cnst13,l2) | sin(cnst15,l2)}
          10u groff
```

```
d16
d30 grad{ sin(cnst1*-1,l2)*diff | sin(0,l2) | sin(0,l2)}
        10u groff
d16
        d3 ;symmetrization
p1 ph6


p19:gp8
d16
DELTA1
p19:gp9*0
d16
        d31 grad{ sin(0*-1,l2) | sin(cnst14*-1,l2) | sin(cnst16*-1,l2)}
        10u groff
d16


p1 ph3
d30 grad{ sin(cnst1,l2)*diff | sin(cnst14,l2) | sin(cnst16,l2)}
        10u groff
d16
```

```
 p2 ph8
 d30 grad{ sin(cnst1*-1,l2)*diff | sin(cnst14,l2) | sin(cnst16,l2)}
          10u groff
 d16


 4u BLKGRAD
 go=2 ph31
 30m mc #0 to 2 F1QF(calgrad(diff))
 d24*0
exit


ph1= 0 0 1 1 2 2 3 3
ph2= 1 2 2 3 3 0 0 1
ph3= 0
ph4= 2 2 3 3
ph5= 3 3 0 0 3 3 0 0  0 0 1 1 0 0 1 1
ph6= 2
ph8= 0 0 0 0 0 0 0 0  0 0 0 0 0 0 0 0
    2 2 2 2 2 2 2 2  2 2 2 2 2 2 2 2
ph31=0 2 0 2 2 0 2 0  2 0 2 0 0 2 0 2
```

ph15= 0

ph16= 1

;pl1 : f1 channel - power level for pulse (default)

;cnst1 diffusion x 100

;cnst2 ctp grad y

;cnst3 ctp grad z

;cnst11 ctp grad x 2ng 180

;cnst12 ctp grad x 3th 180

;cnst13 ctp grad y 2th 180

;cnst14 ctp grad y 3th 180

;cnst15 ctp grad z 2th

;cnst16 ctp grad z 3rd

;l2 number point ctp and diff grad

;p1 : f1 channel - high power pulse

;p2 : f1 channel - 180 degree high power pulse

;p19: gradient pulse 2 (spoil gradient)

;d30: gradient pulse (little DELTA * 0.5)

;d1 : relaxation delay; 1-5 * T1

;d16: delay for gradient recovery

;d20: diffusion time (big DELTA)

;d21: eddy current delay (Te) [5 ms]

;NS: 16 * n

;DS: 4 * m

;td1: number of experiments

;FnMODE: QF

; use xf2 and DOSY processing

;use gradient ratio: gp 6 : gp 7 : gp 8 : gp 9

; 100 : -13.17 : -17.13 : -15.37

;for z-only gradients:

;gpz6: 100%

;gpz7: -13.17% (spoil)

;gpz8: -17.13% (spoil)

;gpz9: -15.37% (spoil)

;use gradient files:

;gpnam6: SINE.100

;gpnam7: SINE.100

;gpnam8: SINE.100

;gpnam9: SINE.100

;use AU-program dosy to calculate gradient ramp-file Difframp

;the gradients serve the following purpose:

; d30

; d30 first STE dephase bipolar pulse pair

; p19 spoiler

; d30

; d30 first STE rephase bipolar pulse pair

; d30 and second STE dephase bipolar pulse pair

; d30

; p19 spoiler

; d30

; d30 second STE rephase bipolar pulse pair

; p19 LED with spoiler

DOCTORAT MATIERE BRETAGNE MOLECULES LOIRE ET MATERIAUX

Nantes Université

Titre : développement de méthodes RMN diffusionnel rapide et compatible avec le flux pour le suivi de réaction en ligne

Mots clés : : RMN, suivi de réaction, flux, réaction en ligne, DOSY

Résumé : La RMN est un outil d'analyse puissant qui a plusieurs usages. Parmi ces usages nous pouvons citer l'analyse de composé organique, leur structure et diverse propriété associé et le suivi de réaction. Nous nous intéressons particulièrement à une méthode particulière de la RMN, la RMN DOSY (Diffusion Ordered SpectroscopY). Cette méthode s'intéresse particulièrement à la diffusion des molécules et utilise ces propriétés de diffusion afin de crée un spectre qui permet la séparation virtuelle des composant. Cette séparation est très utile afin d'identifié les composés dans un mélange potentiellement complexe et donne quelques informations possiblement utiles lié à la taille des composés. Nous aimerions coupler cette expérience RMN avec la possibilité de faire du suive de réaction en flux. Le suivis de réaction par NMR existe sous diverse forme mais souvent l'échantillonnage du milieu de réaction pose problème. Il semblerait qu'utilisé le flux afin de permettre cet échantillonnage serait une manière appropriée et peu dérangeante pour le système étudié. Nous nous proposons ici d'étudier l'impact du flux sur la RMN diffusionnel. De voir comment en compensé ces effets en utilisant un axe d'encodage de la diffusion orthogonal à la direction du flux et une séquence appelée DSTE. Puis nous nous intéressons à des méthodes pour accélérer l'expérience RMN afin de pouvoir analyser un grand nombre de réactions possiblement courte. Pour ce faire nous utilisons des pulse de gradients qui permettent une sélection de cohérence alternative en un seul scan, accélérant ainsi le processus par un facteur 16. Finalement en fusionnant ces deux approches nous démontrons la possibilité de faire du monitoring de réaction en utilisant la RMN DOSY en flux.

Title : Development of fast and flow-compatible NMR diffusion methods for online reaction monitoring.

Keywords : NMR, Reaction monitoring, flow, Online reaction, DOSY

Abstract : NMR is a powerful analysis tool with multiple usages. Among those uses, one can cite the analysis of organic compound and molecules, especially their structure and other properties, there is also the reaction monitoring. We are interested in a special kind of NMR method called DOSY (Diffusion Ordered SpectroscopY). This method is focused on molecular diffusion and use those properties to create display. Those display are often referred as a virtual separation method. This separation is then useful to identify compounds within a complex mixture and give some hint linked to their molecular size. We would like to use this with the possibility to do reaction monitoring by NMR. We would like to use this with the possibility to do reaction monitoring by NMR. NMR reaction monitoring exist on various form, we here ask the question of the medium sampling. It appears to us that using flow as a sampling method for the reacting medium would be a rightful and non-disruptive way to do so. We herein study the impact of flow on diffusion NMR as well as compensating the flow effects thanks to a sequence called DSTE. We are interested in methods to accelerate the diffusion NMR experiment. In order to have the possibilities of monitoring a large array of reaction, some potentially fast. To do so we use pulsed gradient for coherence selection which allow to do the NMR experiment in one scan instead of 16. Finally, by merging the two approach we show the possibility to do reaction monitoring using such DOSY NMR for online monitoring.